MINERAL INCLUSIONS IN RUBY AND SAPPHIRE FROM BO WELU AND BO RAI DEPOSITS, EASTERN THAILAND

Miss Supparat Promwongnan

A Thesis Submitted in Partial Fulfillment of the Requirements
for the Degree of Master of Science in Geology
Department of Geology
Faculty of Science
Chulalongkorn University
Academic Year 2018

มลทินแร่ในพลอยทับทิมและแซปไฟร์จากแหล่งบ่อเวฬุและบ่อไร่ ภาคตะวันออกของประเทศไทย

น.ส.ศุภรัตน์ พรหมวงศ์นันท

วิทยานิพนธ์นี้เป็นส่วนหนึ่งของการศึกษาตามหลักสูตรปริญญาวิทยาศาสตรมหาบัณฑิต
สาขาวิชาธรณีวิทยา ภาควิชาธรณีวิทยา
คณะวิทยาศาสตร์ จุฬาลงกรณ์มหาวิทยาลัย
ปีการศึกษา 2561

Thesis Title	MINERAL INCLUSIONS IN RUBY AND SAPPHIRE FROM BO WELU AND BO RAI DEPOSITS, EASTERN THAILAND
By	Miss Supparat Promwongnan
Field of Study	Geology
Thesis Advisor	Associate Professor Dr. Chakkaphan Sutthirat
Thesis Co Advisor	Assistant Professor Dr. SAKONVAN CHAWCHAI

Accepted by the Faculty of Science, Chulalongkorn University in Partial Fulfillment of the Requirement for the Master of Science

..... Dean of the Faculty of Science
(Professor Dr. POLKIT SANGVANICH)

THESIS COMMITTEE

..... Chairman
(Professor Dr. MONTRI CHOOWONG)

..... Thesis Advisor
(Associate Professor Dr. Chakkaphan Sutthirat)

..... Thesis Co-Advisor
(Assistant Professor Dr. SAKONVAN CHAWCHAI)

..... Examiner
(Assistant Professor Dr. PIYAPHONG CHENRAI)

..... External Examiner
(Dr. Bhuwadol Wanthanachaisaeng)

ศุภรัตน์ พรหมวงศ์นันท : มลทินแร่ในพลอยทับทิมและแซปไฟร์จากแหล่งบ่อเวฬุและบ่อไร่ ภาคตะวันออกของประเทศไทย. (
MINERAL INCLUSIONS IN RUBY AND SAPPHIRE FROM BO WELU AND BO RAI DEPOSITS, EASTERN THAILAND) อ.ที่ปรึกษาหลัก : รศ. ดร.จักรพันธ์ สุทธิรัตน์, อ.ที่ปรึกษาร่วม : ผศ. ดร.สกลวรรณ ชาวไชย

แหล่งสะสมตัวของพลอยคอรันดัมกระจายอยู่ทั่วโลกตามลักษณะธรณีวิทยาของแหล่งกำเนิดที่อาจแตกต่างกันไป โดยมลทินแร่ในพลอยเหล่านี้สามารถบ่งชี้แหล่งกำเนิดที่ต่างกันได้ จากการศึกษาลักษณะทางกายภาพ คุณสมบัติทางแสง และมลทินแร่ ของพลอยคอรันดัมจากแหล่งบ่อเวฬุและบ่อไร่ ภาคตะวันออกของประเทศไทย พบว่ามีลักษณะภายนอกที่แสดงให้เห็นถึงการกร่อนที่ผิวโดยหินหนืดบะซอลต์ร้อนที่พาพลอยเหล่านี้ขึ้นมาบนผิวโลก มีคุณสมบัติการดูดกลืนแสงที่สัมพันธ์กับปริมาณธาตุร่องรอย ซึ่งเป็นลักษณะเฉพาะของพลอยในพื้นที่นี้

พลอยทับทิม จากบ่อไร่ จังหวัดตราด และ บ่อเวฬุ จังหวัดจันทบุรี ได้ถูกคัดเลือกเพื่อทำการศึกษาในครั้งนี้ พบมลทินแร่หลายชนิด มลทินแร่ที่พบได้ในพลอยทับทิมทั้งสองพื้นที่ ได้แก่ ไดออพไซด์อลูมิเนียมสูง (ฟาไซต์ไพรอกซีน) การ์เนตชนิดไพโรป แพลจิโอเคลสเฟลสปาร์ ซิลิมาไนต์ สปิเนล และซัลไฟด์ ส่วน มลทินแร่อะนาเทสพบเฉพาะในพลอยทับทิมจากบ่อไร่ และมลทินแร่แซปฟิรีน ควอรตซ์ เนฟิลีน และแอนไฮไดรต์ จะพบเฉพาะพลอยทับทิมจากบ่อเวฬุเท่านั้น ส่วนมลทินแร่ในพลอยแซปไฟร์สีน้ำเงินถึงสีน้ำเงินแกมเขียว จากบ่อเวฬุ จังหวัดจันทบุรี ประกอบด้วยมลทิน เพทาย อัลคาไลเฟลด์สปาร์ ซัลไฟด์ โมนาไซต์ และโคลัมไบต์

จากหลักฐานมลทินแร่ข้างต้นบ่งชี้ว่า พลอยทับทิม ทั้งจากจากบ่อไร่ จังหวัดตราด และบ่อเวฬุ จังหวัดจันทบุรี น่าจะมีสภาพแวดล้อมการเกิดคล้ายกันคือตกผลึกในสภาพแวดล้อมที่สัมพันธ์กับหินแปรชนิดเมฟิก ในบริเวณเปลือกโลกตอนล่างถึงเมนเทิลตอนบน ส่วนพลอยแซปไฟร์สีน้ำเงินถึงสีน้ำเงินแกมเขียว จากบ่อเวฬุ จังหวัดจันทบุรี น่าจะมีสภาพแวดล้อมการเกิดมาจากหินหนืดที่มีวิวัฒนาการซับซ้อนภายใต้เปลือกโลกที่ตื้นกว่า แม้ว่าพลอยทับทิมจะเกิดในชั้นที่ลึกกว่า (เมนเทิลตอนบน) ของพลอยแซปไฟร์ (เปลือกโลก/เมนเทิลตอนบน) แต่จากหลักฐานมลทินแร่ที่คล้ายกันบ้าง อาจเป็นผลมาจากพื้นที่กำเนิดร่วมกันในบางบริเวณของพลอยทับทิมและพลอยแซปไฟร์เหล่านี้

สาขาวิชา ธรณีวิทยา ลายมือชื่อนิสิต .....
ปีการศึกษา 2561 ลายมือชื่อ อ.ที่ปรึกษาหลัก .....
ลายมือชื่อ อ.ที่ปรึกษาร่วม .....

5972137423 : MAJOR GEOLOGY

KEYWORD: Basalt, Corundum, Siam, Thailand

Supparat Promwongnan :

MINERAL INCLUSIONS IN RUBY AND SAPPHIRE FROM BO WELU AND BO RAI DEPOSITS, EASTERN THAILAND. Advisor: Assoc. Prof. Dr. Chakkaphan Sutthirat Co-advisor: Asst. Prof. Dr. SAKONVAN CHAWCHAI

Corundum deposits located in several places around the world which appear to have different genesis models. The origins of corundum can be distinguished by mineral inclusions. In this study, most of the rough gem corundum from Bo Rai deposit, Trat Province, and Bo Welu deposit, Chanthaburi Province, in Eastern Thailand show etched or dissolved surfaces that were resulted from dissolution by hot basaltic magma during transportation to the surface. Moreover, these gem corundums also show absorption spectral characteristics related to trace elements which typical for corundum from this area. Corundums from Bo Rai deposit in Trat Province, and from Bo Welu deposit in Chanthaburi Province were collected for this study. Various mineral inclusions in ruby were discovered, particularly high Al diopside (fassaite pyroxene), pyropic garnet, plagioclase feldspar, sillimanite, spinel, and sulphide are also observed in Bo Welu ruby similar to Bo Rai ruby. However, anatase inclusion is only identified in Bo Rai. On the other hand, sapphirine, quartz, nepheline, and anhydrite are only identified as inclusions in Bo Welu ruby. Mineral inclusions in sapphire from Bo Welu deposit are zircon, alkali feldspar, sulphide, monazite, columbite. Based on chemical composition of mineral inclusion, rubies from both Bo Rai and Bo Welu deposits may have originally formed within a similar environment, mafic granulites rocks, probably within lower crust to upper mantle. Blue and bluish green sapphires from Welu deposit may have crystallized from a highly evolved, alkali-rich and silica-poor magma at a shallower level in the lithosphere. Although, the formation of ruby located at deeper levels (upper mantle) than the sapphire (crust/upper mantle), some similar mineral inclusions in both ruby and sapphire may indicate co-crystallization between ruby and sapphire in some places.

Field of Study: Geology Student's Signature .....

Academic Year: 2018 Advisor's Signature .....

Co-advisor's Signature .....

ACKNOWLEDGEMENTS

First and foremost, I would like to express my deep gratitude to my supervisor and co-advisor, Associate Professor Dr. Chakkaphan Sutthirat and Assistant Professor Dr. Sakonvan Chawchai, respectively, for valuable suggestion and meticulous work during this thesis research. Besides my thesis advisors, I would like to thank all of the thesis committee, Professor Dr. Montri Choowong, Assistant Professor Dr. Piyaphong Chenrai, and Dr. Bhuwadol Wanthanachaisaeng; without their insightful comments, this thesis would not be accomplished.

The author also appreciates all staff members of the Department of Geology. Faculty of Science, Chulalongkorn University for providing knowledge and support throughout the experiments. My special thank must deliver to the Training Center and the Gem Testing Laboratory (GIT-GTL) of the Gem and Jewelry Institute of Thailand (GIT) for permission to use Facetron faceting machine, basic equipment, and advanced instruments. Especially, Miss Sopit Poompeang had assisted for Electron Probe Micro-Analysis (EPMA) during the research project.

Without their kind support, this thesis work would not be possible. Thanks are also extended to several people who had assisted during the study, for instance, Dr. Alongkot Fanka for sample preparation and EMPA data analysis, Dr. Visut Pisutha-Anond, Wilawan Atichat, Thanong Leelawattanasuk, and Thitintharee Leelawatanasuk (Gem and Jewelry Institute of Thailand) for knowledge, discussion, and problem solving.

Last but not least, I must express very profound gratitude to my parents, and sisters for unfailing support and continuous warm encouragement throughout researching and thesis writing. Finally, other persons, who cannot be entirely listed, are also thanked. This accomplishment would not have been possible without their support and encouragement.

Supparat Promwongnan

TABLE OF CONTENTS

LIST OF TABLES

Page

LIST OF FIGURES

Page

CHAPTER 1

INTRODUCTION

1.1 General Statement

Gem corundum deposits in Thailand are associated with late Cenozoic alkaline basaltic rocks within the extensional tectonic environments. Most of the corundum sources are generally found as alluvial deposits. The previous studies were initially focused on basaltic rocks, xenoliths and xenocrysts embedded in corundum-related basalts (e.g., Vichit et al., 1978; Yaemniyom and Pongsapich, 1982; Coenraads et al., 1995; Chualaowanich et al., 2008). These studies would give information of the host basalts, their xenoliths and xenocrysts which may/ may not directly relate to the origin of corundum.

Some particular mineral inclusions are direct evidence of assemblages during and after the formation of corundum. Pisutha-Arnond et al. (1999); Pisutha-Arnond et al. (2007) also investigated an alluvial assemblage in Kanchanaburi sapphire deposit that suggested sapphire formation related to contact metamorphic processes at the deep crust or upper mantle.

Analytical data of the dissolved and etched surface of these sapphires were reported by Coenraads (1992); Coenraads et al. (1995); Krzemnicki et al. (1996) and Sutherland et al. (1998b). These evidences indicate that basaltic sapphires were picked up from the deep-crustal source before carrying onto the surface by high-temperature basaltic magma. Some of them were eroded from the host basalt and transported far away to alluvial deposits then their dissolved scars may become dim.

Mineral inclusions of basaltic sapphire were also applied for reconstruction of the genetic linkage between corundum formation and geochemistry of carrier basalt. Previous researchers investigated the mineral inclusions in corundum using the optical microscope and Raman spectroscope (e.g., Dao and Delaigue, 2000; Singbamroong and Thanasuthipitak, 2004; Palanza et al., 2008). Moreover, mineral chemistry also indicates chemical potential of crystallization and physical conditions leading to interpretation of geological processes that relate to the corundum formation. The chemical compositions of mineral inclusions have been studied, using Electron Probe Micro Analyzer (EPMA) (e.g., Gübelin, 1971; Intasopa et al., 1999; Bunnag, 2004; Khamloet et al., 2014; Fanka and Sutthirat, 2018), SEM-EDX technique (e.g., Krzemnicki et al., 1996; Saminpanya and Sutherland, 2011).

Mineral chemistry of syngenetic zircon has also been investigated using iron microprobe (SHRIMP) (e.g., Coenraads, 1992; Sutherland et al., 2002) and ICP-MS technique to determine age of zircon inclusions (e.g., Sutherland et al., 2002; Khamloet et al., 2014).

Although many analytical techniques have been used to interpret genesis models of basaltic-type corundum of the Southeast Asian basaltic province, especially the Chanthaburi-Trat deposit. A few analyses of mineral inclusions have been published from this area. Chemical data of fluid/melt inclusions, in particular, have never been published because these very tiny inclusions are rather difficult to prepare and analyze. Challenge of this study is to decipher the origin of corundum from Chanthaburi-Trat gem field using mineral chemistry of inclusions in corundum. In addition, this study may test the hypothesis, sapphire from the Western zone might have been crystallized from a partially melted Al-rich protolith at mantle or lower crust. On the other hand, rubies from the study areas (Central and Eastern zones) might be crystallized in metamorphosed mafic rocks in the upper mantle.

1.2 Objective

The main objective of this research project is to investigate the mineral chemistry of various types of inclusions in gem corundum samples from Bo Rai and Bo Welu gem fields. These samples include rubies from Bo Rai, rubies and sapphires from Bo Welu. Apart from mineral inclusions, these host rubies and sapphires were also investigated for physical properties. These results provide more evidences of initial formation and genetic model of ruby and sapphire in Chanthaburi-Trat alkali basaltic deposit.

1.3 Scope of Study

Gemological properties of corundum samples were analyzed; these included physical properties, optical characteristics and internal features. Moreover, trace element fingerprint of the gem corundum and mineral chemistry of their inclusions were analyzed for further discussion. The gem corundum samples under this study include rubies from Bo Rai area, Trat, Thailand, rubies and sapphires from Bo Welu area, Chanthaburi, Thailand. The results of this study may be used to differentiate these stones from other sources in Thailand as well as from basaltic deposits elsewhere. Moreover, genesis model of basaltic ruby and sapphire in Thailand can be improved.

1.4 Methodology

Literature reviews: First of all, previous works related to this study were carried out, initially, to receive background information and lead to experimental design.

Sample collections: Corundum collections under this study include: 1) ruby samples from Bo Rai gem deposit, Trat Province (Figure 1.1); 2) ruby and sapphire samples from Bo Welu gem deposit, Chanthaburi Province (Figure 1.2); both gem deposits are located in the Eastern Thailand. These samples were observed and searched particularly for mineral inclusions under a binocular microscope. The samples that contain mineral inclusions were then selected; subsequently, they were polished until mineral inclusions were exposed onto the host's surface. Facetron faceting machine, based at the Training Center of the Gem and Jewelry Institute of Thailand (Public Organization) (Figure 1.3), was used for a few polishing steps. The samples were initially polished on a grit 1200 diamond coated polishing disc until mineral inclusions appeared on the samples' surface before they were repeatedly ground on copper lap with 1 μm diamond powder until the mineral inclusions were completely exposed. The selected samples were finally polished on a frieze with 1/4 μm diamond spray to improve quality of polished surface for further analyses. These polished samples were mounted by epoxy resin prior to carbon coating for Electron Probe Micro-Analysis at Department of Geology, Faculty of Science, Chulalongkorn University.

Figure 1.1 Ruby collection from Bo Rai deposit, Trat Province, Eastern Thailand.

Figure 1.2 Ruby and sapphire collection from Bo Welu deposit, Chanthaburi Province, Eastern Thailand

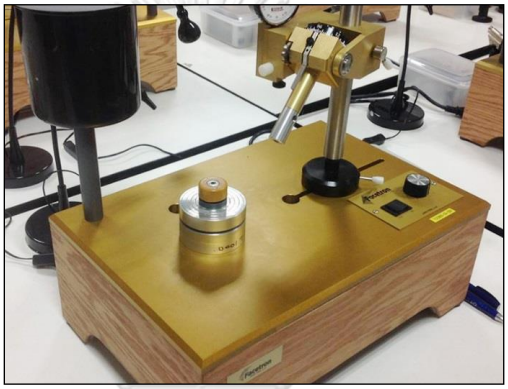

Figure 1.3 Facetron faceting machine based at Training Center of the Gem and Jewelry Institute of Thailand (Public Organization).

Analytical Techniques: Basic gemological properties, such as size, color, and refractive indices (RI) were measured using standard gemological equipment. Fluorescence effects were observed using gemological ultraviolet lamps, long-wave (365 nm) and short-wave (254 nm). External and internal features were observed under a gemological microscope. Photomicrographs were taken using a gem microscope attached with Canon EOS 7D camera. All of these facilities were supported by Gem Testing Laboratory of the Gem and Jewelry Institute of Thailand (Public Organization) (GIT-GTL).

Spectroscopic characteristics were analyzed using Thermo-Nicolet 6700 Fourier-Transform Infrared (FTIR) Spectrometer (Figure 1.4) and PerkinElmer UV-Vis-NIR spectrometer, model Lambda 950 (Figure 1.5) based at GIT-GTL.

IR spectroscopy of corundum with only the transmission spectra were used in this study. Transmission bands were collected in the mid-IR range (4000–400 cm^{-1}) with a resolution of 4.0 cm^{-1} and 128 scans for observation of Al-O stretching or lattice vibrations. UV-Vis-NIR absorption spectra were taken from the range of 250–

800 nm with sampling interval of 3.0 nm and scan speed of 441 nm per minute. This method gives information related to electron transitions in electronic field as well as electron transitions between trace impurities in corundum (e.g., Diep, 2015; Tippawan et al., 2016; Mogmued et al., 2017).

Figure 1.4 Thermo-Nicolet 6700 Fourier-Transform Infrared (FTIR) Spectrometer based at the Gem and Jewelry Institute of Thailand (Public Organization).

Figure 1.5 PerkinElmer Lambda 950 spectrophotometer based at the Gem and Jewelry Institute of Thailand (Public Organization).

A Renishaw inVia Raman spectroscope (Figure 1.6) with the Nd: YAG laser (532 nm) excitation was used in this study for preliminary identification of mineral inclusions. The obtained Raman spectra were advantageous for selection of mineral inclusion for further EPMA analyses.

Figure 1.6 Laser Raman spectroscope (Model 1000, Ranishaw) based at the Gem and Jewelry Institute of Thailand (Public Organization).

Chemical analysis of host corundum was carried out initially by an Energy-dispersive X-ray Fluorescence (ED-XRF) spectroscope, Eagle III system, based at the GIT (Figure 1.7). ED-XRF is a very powerful technique for the semi-qualitative analyses of trace element (e.g., Cr, Fe, Ti, V, Ga) in corundum samples. These analyses can be used to indicate sources of corundum in many world-leading gem testing laboratories (e.g., Hänni, 1994; Sutherland et al., 1998b; Joseph, 2000).

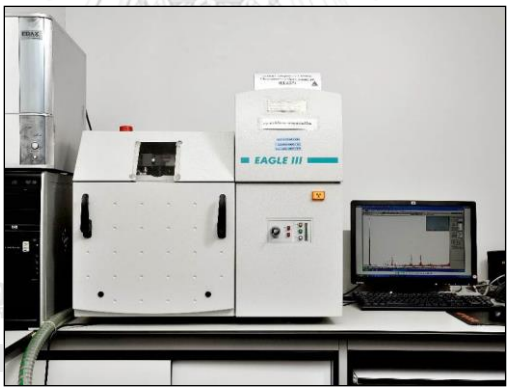

Figure 1.7 Eagle III system, Energy-dispersive X-ray Fluorescence (ED-XRF) spectroscope, based at the Gem and Jewelry Institute of Thailand (Public Organization).

Exposed mineral inclusions and their host corundum samples were analyzed for major and minor compositions using an Electron Probe Micro-Analyzer (EPMA) (Model JXA-8100) at the Geology Department, Faculty of Science, Chulalongkorn University (Figure 1.8). Operating condition for analyses of host corundum and mineral inclusions were set at an accelerating voltage of 15.0 kV, about 25.0 nA sample current, with focused beam (smaller than 1 μm). Measuring times were set at 30 seconds and 10 seconds for peak counts and background counts, respectively, for each element using suitable analytical crystals. For special analyses of zircon and

monazite inclusions, an accelerating voltage of 20.0 kV was set for more accurate results. Appropriate standard materials, including pure elements, pure oxides and natural minerals were used for calibration using the same analytical conditions as reported above; for instance, the selected standards comprise synthetic corundum for Al, wollastonite for Si and Ca, periclase for Mg, fayalite for Fe, potassium titanium phosphate for K, Ti and P, jadeite for Na, barite for Ba, manganosite for Mn, eskolaite for Cr, Gadolinium Ga garnet for Ga, lead vanadium germanium oxide for V, barite for Ba, cerium phosphate for Ce, cobalt oxide for Co, copper, for Cu, dysprosium phosphate for Dy, erbium phosphate for Er, gadolinium phosphate for Gd, holmium phosphate for Ho, indium for In, lanthanum hexaboride for La, lutetium phosphate for Lu, molybdenum for Mo, nickel oxide for Ni, lead vanadium germanium oxide for Pb, praseodymium phosphate for Pr, internal standard for Pt, Ta and As, samarium phosphate for Sm, tin for Sn, yttrium phosphate for Y, thorium for Th, uranium for U, zinc oxide for Zn, strontium barium niobate for Nb, hafnium for Hf, and zirconium for Zr. Consequently, accuracy approaching $\pm$1% (relative) is obtainable and detection limits 100-300 ppm can be attained (Lavrent'ev et al., 2015). The analytical results were then taken automatic ZAF correction before reported in form of percent oxides. Fe^{2+} and Fe^{3+} ratios of some particular minerals, e.g., garnet, pyroxene, were recalculated using equation of Droop (1987).

Figure 1.8 Electron Probe Micro-Analyzer (EPMA), Model JXA-8100, based at Department of Geology, Faculty of Sciences, Chulalongkorn University

Data Management: Finally, data compilation, interpretation and thesis writing were carried out focusing on particular aspects such as chemical fingerprint and distinguish mineral inclusions of these stones. Discussion on genesis model, particularly based on mineral inclusions, will be carried out.

All procedures of this study can be summarized in the following flow chart (Figure 1.9).

Figure 1.9 Schematic diagram showing the methodology and framework of this study.

CHAPTER 2

LITERATURE REVIEWS

2.1 The Chanthaburi-Trat deposits

Ruby and sapphire are abundant at Chanthaburi-Trat (C-T) alkali basaltic gem fields which are located in Southeastern Thailand. Chanthaburi Province is situated along the Eastern shore line, and bordered by Trat to the Southeast, Rayong to the West and Sa Kaeo, Chonburi, and Chachoengsao to the North. Trat Province is bordered by Chanthaburi to the West, Cambodia to the East, and the Gulf of Thailand to the South. Distribution of the corundum deposits within late Cenozoic alkaline basaltic terrane has been found in between 102°00' to 103°00' West longitude and 12°00' to 13°00' North latitude which can be divided into four (Pattamalai, 2015) geographic areas (Figure 2.1). In the Western Chanthaburi Province, Khao Wua hill (89 meters above mean sea level) and Khao Phloi Waen hill (135 meters above mean sea level) are recently the main gem mining areas located in Tha Mai District (Figure 2.1) which have generally produced star and green sapphires more common than blue and yellow sapphires. On the other hand, color-change sapphire occurs rarely and ruby is absent entirely in this area. The corundum-related basalt is composed of high alkali, low silica and high titanium contents, identified as basanitoid or nephelinite basalts (Barr and MacDonald, 1978; Vichit et al., 1978; Barr and Macdonald, 1981; Vichit, 1992). Sapphire deposits in this area can be grouped as residual deposits (e.g., Khao Wua and Khao Phloi Waen), alluvial deposits (e.g., Ban Hua-u, Khlong Phan Salut and Khlong Wat Sa Kheo) and mangrove-covered deposits (e.g., Ban Nong Khayong to Ban Wat Khlang) (Saraphanchotwitthaya et al., 2003; Pattamalai, 2015). Khao Wua basalt, located in the same range of Khao Phloi Waen, is generally fine-grained black to dark grey rock containing megacrysts of clinopyroxene and spinel. This basalt was determined by $^{40}Ar/^{39}Ar$ dating method as 3.1 $\pm$ 0.19 Ma (Sutthirat et al., 1994); besides, K/Ar age was reported early as 0.44 $\pm$ 0.11 Ma (Barr and Macdonald, 1981). Associated minerals found in this sapphire deposit are garnet, zircon, black spinel, black to green pyroxene, magnetite, ilmenite, and phlogopite.

The Central deposits are located between Khlung District in Chanthaburi Province and Khao Saming District in Trat Province. The main gem fields in Chanthaburi were mined in Bo Welu (Bo Waen) which other areas was spread around Ban Sai Khao, Ban Tok Si, Ban Sisiat, Ban Tok Phrom, Ban Bo Khlang, Ban Nong Pla Lai, Ban Chak Lao, Huai Saphan Hin, Ban Saeng Daeng and Ban Saeng Som. Gem mining in Trat was operated at Ban I Rem (sapphire only), Ban Na Wong, Ban Na Ta Mi (ruby

only), Nong Ban Noi and Khong Phaya (Pattamalai, 2015) (Figure 2.1). This deposit zone comprises various shades of blue-green sapphires, including black star sapphires, and rubies. Residual deposits exposed in Khiritarn Dam to Ban Saphan Hin, Ban Bo Wen to Ban Din Daeng and Wat Muang Kao Saen Tum. The Cenozoic basalts in this gem field have been classified as basanitoid (Vichit et al., 1978; Sutthirat et al., 1994) and basanite (Chulaowanich et al., 2008). Associated minerals in this gem field are zircon, ilmenite, black to green pyroxene, black spinel and magnetite with trace of garnet (Vichit, 1992).

The Eastern deposits, produced mainly rubies (sapphires<1%), have been separated into two subareas (Pattamalai, 2015). The first area is Pong Nam Ron District, Chanthaburi Province (Figure 2.1). In this area, rubies were found in colluvium, alluvium, and residual basaltic soil. Associated minerals are garnet, magnetite, ilmenite, spinel, zircon, and pyroxene. The second area is in Nong Bon and Bo Rai areas of Bo Rai District, Trat Province, close to the vicinity of Cambodian, Khao Banthat Mountain Range, and located approximately 4 km from the Thai-Cambodia border (Figure 2.1). In Bo Rai area, rubies are found in colluvium, alluvium, and residual basaltic soil. Their corundum-related basalts are basanite yielded K/Ar age of 1.13 $\pm$ 0.17 Ma (Barr and Macdonald, 1981) and $^{40}Ar/^{39}Ar$ age of 1.33 $\pm$ 0.09 Ma and 1.60 $\pm$ 0.05 Ma (Chulaowanich et al., 2008). In Nong Bon, rubies were discovered in residual basaltic soil and alluvial gravel along stream channels. The Nong Bon basalt located in Bo Rai District is dark grey to black, fine-grained porphyritic rock with phenocrysts of olivine and augite, and megacrysts of clinopyroxene, garnet, spinel, ilmenite, and magnetite embedded in clinopyroxene and glass groundmass. This basalt was classified as nephelinite (Barr and MacDonald, 1978, 1981) and olivine nephelinite (Sirinawin, 1981). The ages of basalt determined by K/Ar and $^{40}Ar/^{39}Ar$ dating methods are 1.31 $\pm$ 0.17 Ma (Barr and Macdonald, 1981) and 2.38 $\pm$ 0.16 Ma (Sutthirat et al., 1994), respectively. Associated minerals found in this zone are garnet, magnetite, ilmenite, and pyroxene (Vichit et al., 1978; Vichit, 1992).

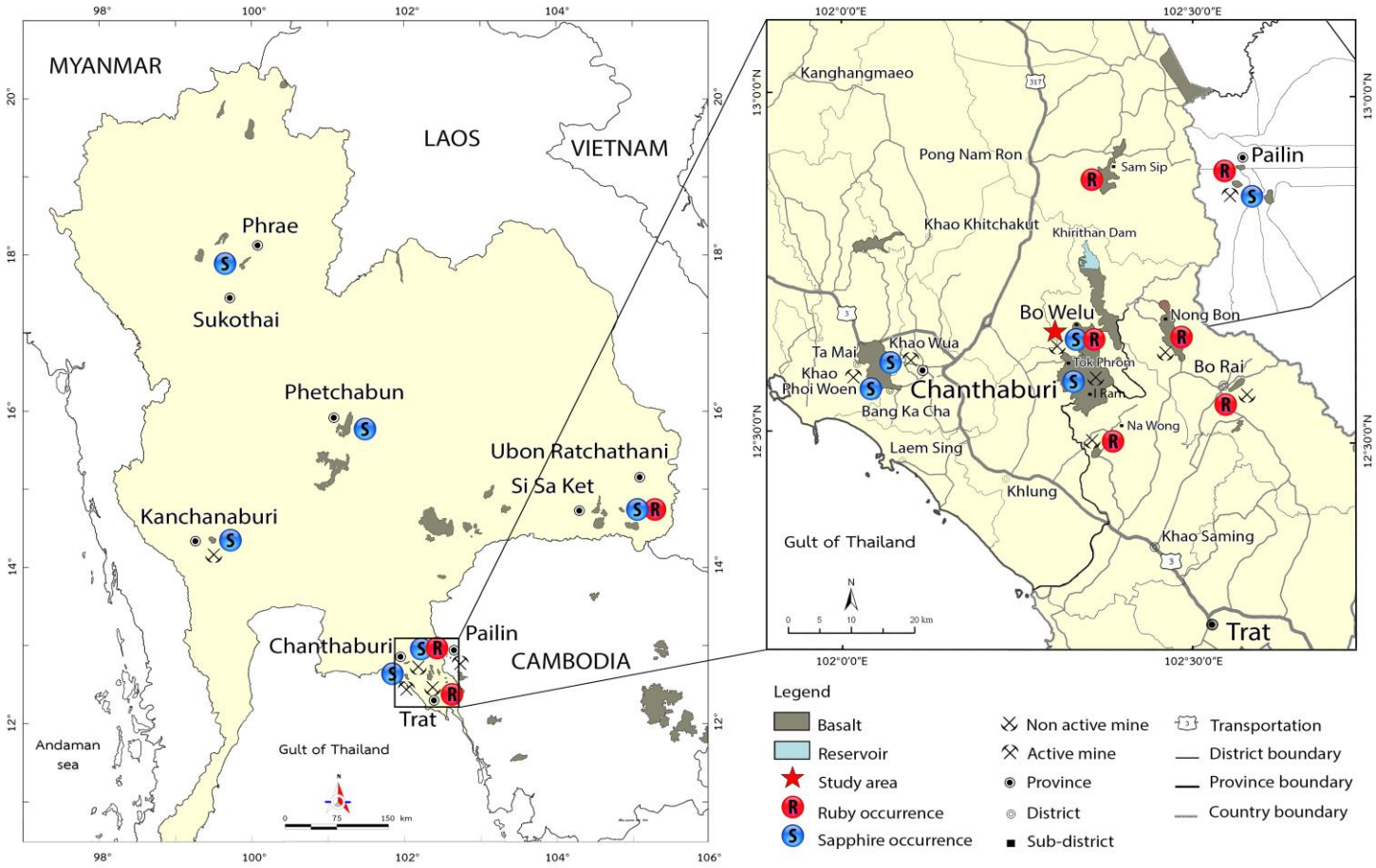

Figure 2.1 Index map of Thailand showing distribution of basalt and corundum (ruby and sapphire) occurrences (left). Ruby and sapphire deposits and associated basalts in Chanthaburi-Trat and Pailin gem field, Eastern Thailand (right) (modified after Hughes (1997); Sutthirat et al. (2001); Barr and Cooper (2013); Pattamalai (2015)).

2.2 Inclusions in Corundum

Inclusions are foreign materials found inside gemstone. They can be varied in phase, size, orientation, formation and other characteristics. Inclusions in gemstone may cause color, phenomena (e.g., asterism, chatoyancy, aventurescence) in the host gems. More detailed chemical analyses of inclusions should provide a clue for determination of formation conditions such as pressure, temperature, and depth. Inclusions in gemstone can form as single-phase inclusions (e.g., solid, liquid and gas) or two-phase inclusions (e.g., liquid-gas, liquid-solid, solid-gas) and even three-phase inclusions. Solid Inclusions can be classified, based on their ages with respect to that of the host crystal, suggested by Gübelin (1973) and Gübelin and Koivula (1986), below.

Protogenetic inclusion is pre-existing inclusions which have formed before the host crystal. These are precisely solid phase. For example, actinolite and biotite in emerald (see Figure 2.2 left), epidote in quartz, pyrrhotite in diamond, molybdenite in quartz and emerald, spinel, quartz in ruby (Figure 2.2 right).

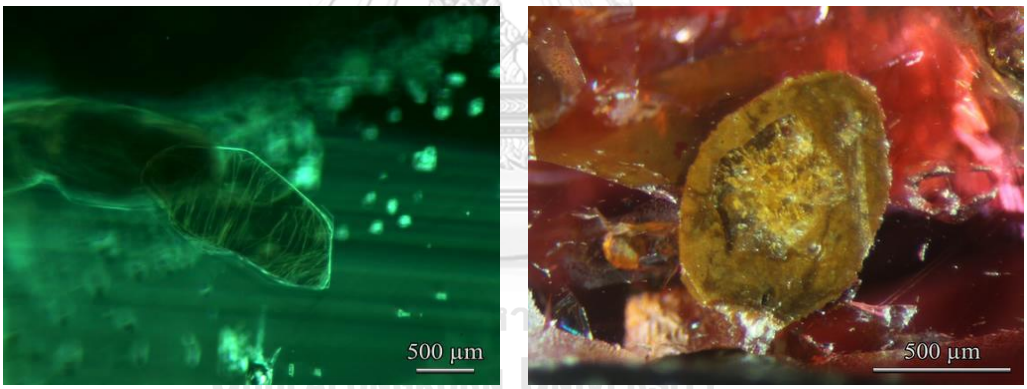

Figure 2.2 Protogenetic inclusions of biotite crystal in natural emerald from Ethiopia (left) and quartz crystal surrounded by iron stain in ruby sample 9TWL095 (right).

Syngenetic inclusion is contemporary inclusions which have formed at the same mineralization process, time and P-T-X conditions, of the host crystal. Generally, syngenetic inclusions have well-formed crystal shapes in comparison to the protogenetic inclusions. They usually present preferably irregular and partially dissolved shapes. For examples, cavities or negative crystals formed within the host crystal was caused by rapidly crystal growing. In addition, primary twinning and growth zoning (Figure 2.3 left) are also formed during the crystal growth. Mineral inclusions have been reported as syngenetic inclusions, for instance: albite, columbite, muscovite, quartz, spessartite and tourmaline in aquamarine; tourmaline in andalusite; garnet and pyroxene in diamond; calcite and dolomite in ruby,

emerald, and spinel; rutile in andalusite, garnet, quartz and corundum (Gübelin and Koivula, 1986) (Figure 2.3 right).

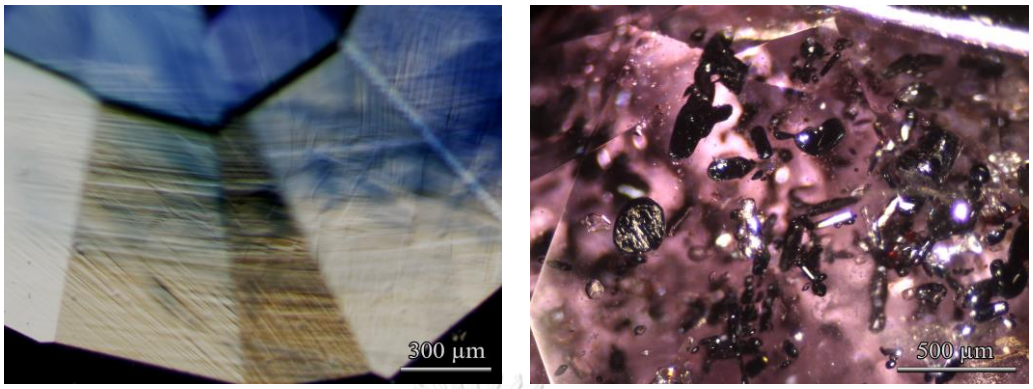

Figure 2.3 Syngenetic internal features of growth zoning in blue sapphire from Madagascar (left) and rutile crystals in ruby from Madagascar (right).

Epigenetic inclusion is secondary inclusions crystallized after cooling of the host which induced the foreign substances (impurities) seeped into cleavages forming such inclusions. For examples, iron stain-filled fracture in Mozambique ruby (Figure 2.4 left), secondary cavities or fingerprint formed by healing process (Figure 2.4 right) and polysynthetic twinning are clearly classified in this category.

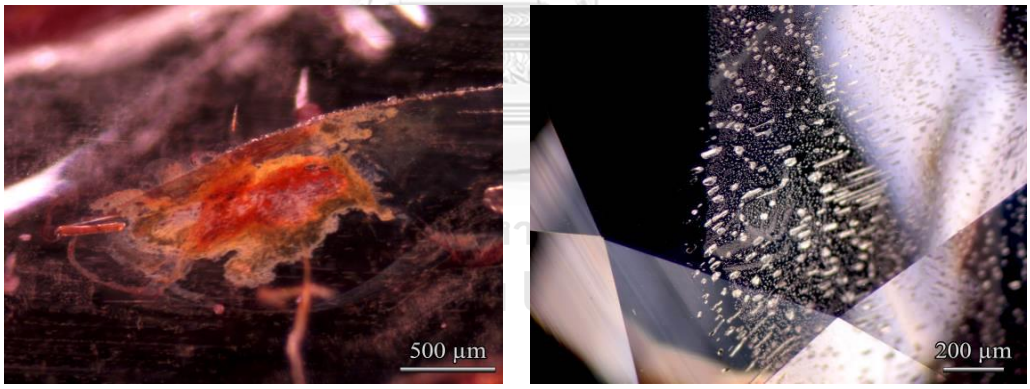

Figure 2.4 Epigenetic features of iron stain-filled fracture in Mozambique ruby (left) and secondary fluid inclusions (fingerprints) in sapphire from Sri Lanka (right).

Mineral inclusions formed very closely to the formation of host rocks have also been reported. Gübelin (1940, 1971) published the typical inclusions of Thai ruby, such as subhexagonal to rounded opaque metallic grains of pyrrhotite, yellowish hexagonal platelet of apatite and reddish brown almandite garnets.

Coenraads et al. (1995) reported inclusions in sapphire from Khao Wua. They were classified as alkali feldspar, columbite, gahnospinel, hercynite, hornblende, ilmenite, niobium-rutile, mica, plagioclase, pyrrhotite, pyrrhotite-pentlandite

intergrowth crystal, thorite, uranium pyrochlore, zircon, iron-rich melt inclusions and two- or three-phase fluid inclusions.

Guo et al. (1996) separated mineral inclusions in alkali basalt-related corundum into two environmental suites: the alkali felsic suite contains feldspar, zircon, uraninite, ilmenorutile and Fe-Cu sulphides); the carbonatic suite includes titaniferous columbite, uranpyrochlore and fersmite.

Mineral inclusions in corundum from basaltic gem field were also proposed as metamorphic origin (such as Mg-rich spinel, sapphirine, high alumina diopside (fassaite) and garnet) and magmatic origin (e.g., feldspar, zircon, Fe-Ti oxides, Nb-Ta oxides, U-Th oxides, rare-earth phosphates) (Sutherland et al., 1998b). Analcime, apatite, calcite, garnet, olivine, clinopyroxene, plagioclase, spinel, biotite, rutile, pyrite and pyrrhotite were mentioned as mineral inclusions in placer ruby from Thailand (Sutherland et al., 1998a).

Intasopa et al. (1999) reported mineral inclusions in corundum from the Chanthaburi-Trat basaltic terrains; they contain spinel, gahnite, hercynite, pleonaste, biotite, mica, diopside, ferro-columbite, zircon, monazite, garnet, rutile, boehmite, feldspar, bismuth, thorite, clinochlore. In addition, these corundums also present fluid inclusions containing CO_2 gas, liquid CO_2, impure CO_2 gas and silicate melt.

Sutthirat et al. (2001); Saminpanya and Sutherland (2011) reported high Ca without Ti (high almandine and grossular components) garnet inclusions in the ruby samples from Bo Rai; these inclusions may have different crystallization condition from garnet xenocrysts in basalt within the same area. Sutthirat et al. (2001) also reported the presence of sapphirine and clinopyroxene in this area. Saminpanya and Sutherland (2011) separated inclusions in Thai corundum into sapphire suite including alkali feldspar (sanidine), nepheline, zircon, hercynite-spinel, and ruby suite containing garnet, high alumina diopside (fassaite) and sapphirine.

Khamloet et al. (2014) categorized mineral inclusions in Bo Phloi sapphire from Kanchanaburi Province, Western Thailand into two main groups: felsic alkaline group (e.g., zircon, nepheline, alkali feldspar, manganiferous ilmenite, monazite, calcite); contact-metamorphic group (e.g., sapphirine, staurolite, silica-rich enstatite, almandine–pyrope garnet, hercynitic spinel, biotite–phlogopite mica).

Summary of mineral inclusion found in corundum from Thailand is present in Table 2.1 and those from other basaltic fields are summarized in Table 2.2 Mineral inclusions and their origins are described in each particular group below.

Silicates group

Zircon is the main mineral in metamorphic and igneous rocks of intermediate to the Si-saturated composition. Their trace compositions such as U, Th, Hf, and REE may indicate crystallization process and age of the protolith. Chemical characteristics of zircon inclusions (e.g., high Hf, Y, and rare earth element) were found in sapphire from basaltic terrains; they suggested host sapphire crystallized from alkaline and highly evolved source material under conditions unrelated to the host basaltic magma (e.g., Coenraads et al., 1990; Coenraads et al., 1995; Guo et al., 1996; Sutherland et al., 2002; Khamloet et al., 2014).

Garnet inclusion can occur in kimberlite (igneous rock) and eclogite (metamorphic rock) (Deer et al., 1997). Cr-poor pyrope is particularly related to eclogite xenoliths (MacGetchin and Silver, 1970). Garnet inclusions can indicate occurrences (pyrope – a liquid magmatic, almandine – a metamorphic, spessartine – a pegmatitic, grossular–a contact-metamorphic) (Gübelin and Koivula, 1986). Lacking of Ca component in garnet inclusion indicates a deep-seated source (mantle or lower crust) (Khamloet et al., 2014). Sutthirat et al. (2001) also reported the presence of pyropic garnet, in ruby from Chanthaburi-Trat gem field.

Staurolite typically occurs in medium-grade regionally metamorphosed pelitic schists with high alumina content under high-temperature condition (Deer et al., 2013).

Pyroxene are inosilicate minerals occurred as a stable phase in many different types of igneous rock, which are related to regional and contact metamorphism (Deer et al., 2013). It is a key constituent of mafic igneous rocks. Fassaite (high alumina diopside) usually occurs in metamorphosed limestones and dolomites, eclogitic, kimberlite, meteorites (Deer et al., 1997) and granulitic xenoliths in alkali basalts (Sutherland et al., 2003).

Feldspar is a group of the main rock-forming tectosilicate minerals ($KAlSi_3O_8$ – $NaAlSi_3O_8$ – $CaAl_2Si_2O_8$). Alkali feldspar is an essential constituent of alkali and acid igneous rocks (Deer et al., 1997). Anorthoclase and sanidine can intergrowth with sapphire in xenoliths in alkali basalt that suggest crystallization from intermediate magmas in the lower crust-upper mantle (Upton et al., 1983; Aspen et al., 1990; Coenraads et al., 1990). The alkali feldspar (low Ca, Na-rich and low to moderate K contents) suggests further that corundum megacrysts were evolved in felsic source rock.

Nepheline is the most common feldspathoid mineral that occurs in alkaline rocks (Deer et al., 2013). Nepheline was found with sapphire in syenitic gneiss, syenitic rock, nepheline-aegerine intrusive rock, and nepheline-bearing gneisses (Meyer, 1968; Waltham, 1999; Ashwal et al., 2007).

Sapphirine is a rare mineral characterized by silicate with magnesium and aluminium. It occurs typically in contact-metamorphic rocks and alumina-rich silica-poor high-grade metamorphic rocks belonging to the granulite and hornblende-granulite facies (Deer et al., 2013). Sapphirine inclusions were reported from Siamese ruby from Bo Rai, Trat (Koivula and Fryer, 1987), and Bo Na Wong (Sutthirat et al., 2001; Saminpanya and Sutherland, 2011). Sapphirine coexisting with spinel inclusions in Australian fancy colored corundums were also reported (Sutherland et al., 1998b). Sapphirine inclusions were reported in sapphire from Bo Phloi, Kanchanaburi, Thailand (Khamloet et al., 2014) which suggested high-grade regional or contact metamorphism environment of sapphire crystallization.

Oxides group

Spinel is generally associated with corundum sources. Co-rich hercynite spinel inclusion was reported in placer sapphire from Bo Phloi, from Northwest of the Chanthaburi-Trat area that suggests lower crust environment which may have involved magma mixing process between a silica-deficient carbonatite melt and alkali-rich felsic melt (Guo et al., 1994; Guo et al., 1996). Cr-poor spinel inclusions ($\leq$0.01 wt% of Cr_2O_3) in sapphire and slightly high Cr-pleonaste spinel (1.05–8.51 wt% of Cr_2O_3) intergrowth with ruby and sapphirine inclusion in ruby from Barrington, Australia indicated that corundum crystallization undertook high temperature environment at 780–940 ºC (Sutherland and Coenraads, 1996; Sutherland et al., 1998b).

Ilmenite generally occurs in igneous and metamorphic rocks formed as massive veins or layers. Ilmenite may form as detrital mineral in sedimentary deposits (Deer et al., 2013). Ilmenite was reported as a rare mineral inclusion in sapphire from Bo Phloi, Kanchanaburi, Thailand (Khamloet et al., 2014).

Anatase, rutile and brookite are polymorph of titanium-oxide which generally form in metamorphic and igneous rocks as well as detrital in sedimentary rock (Deer et al., 2013). Anatase commonly occurs with pointed dipyramids which relate to cool hydrous solutions at temperature 500-600 °C, if it is higher than this temperature range it would transform to rutile. Anatase inclusion can indicate the crystallization temperature of the host mineral (Gübelin and Koivula, 1986).

Phosphates group

Monazite occurs as an accessory mineral in granites. It is an important source of thorium and rare earth elements (REE) such as cerium, lanthanum, neodymium and radioactive element thorium (Deer et al., 2013). Monazite is an important evidence for the basaltic corundum origin (Guo et al., 1996). Monazite crystal usually forms as tabular crystals or horizontal prisms (Gübelin and Koivula, 1986). Monazite inclusions in sapphire were reported from basaltic terrains such as SW Rwanda, Thailand, and Lao PDR (Krzemnicki et al., 1996; Intasopa et al., 1999; Singbamroong, 2004; Khamloet et al., 2014). These support the sapphire crystallization from a highly evolved melt (Krzemnicki et al., 1996; Intasopa et al., 1998; Singbamroong and Thanasuthipitak, 2004).

Apatite is a common accessory mineral in igneous, metamorphic and sedimentary rocks (Deer et al., 2013). It always crystallized to thick tabular or columnar dipyramids hexagonal forms. Apatite can occur as a protogenetic and a syngenetic guest inclusion (Gübelin and Koivula, 1986).

Nb-Ta oxides group

Uranium-rich pyrochlores (uranpyrochlore) inclusions in corundum indicate carbonatite and related alkaline rocks (Guo et al., 1996).

Columbite generally occurs in various granitic rocks and their pegmatitic equivalents (Guo et al., 1996). Columbite is a combination of niobite and tantalite which generally occur in various granitic rocks. Columbite usually occur as thin, tabular, prismatic to an acicular crystal with brown, reddish-brown or black color (Gübelin and Koivula, 1986).

Carbonate group

Calcite commonly occurs in marble-hosted deposit or relates with limestone or metamorphic rocks and also some igneous rocks. Calcite inclusions that may indicate crystallization of nepheline syenites origin (Deer et al., 2013).

Sulphides group

Pyrrhotite is commonly associated with basic plutonic rocks. Carmichael et al. (1974) reported pyrrhotite inclusions appears to be the dominant primitive sulfide in basalt rocks. Gübelin (1971) observed the inclusion formed as subhexagonal to rounded opaque metallic grains of sulphide in Thai rubies; it was identified as chalcopyrite ($CuFeS_2$) by its trace of iron, copper, and sulphur. This indicates of

interactions in contact zones between country rocks and basaltic magma involved in original process of Thai ruby.

Melt inclusion

Glass inclusions can also be found in minerals formed rapidly in magmatic deposits (Gübelin and Koivula, 1986). Melt inclusions are usually composed of solid phases and vapor bubbles. Na- and Ca-rich glassy melt inclusions in Yogo sapphire was reported by Palke et al. (2016) that suggest a magmatic origin.

Table 2.1 Summary of mineral inclusions in Thai corundum (Intasopa et al., 1999; Sutthirat et al., 2001; Saminpanya and Sutherland, 2011; Khamloet et al., 2014)

Mineral group	Mineral inclusions	Chantaburi-Trat - Tok Phrom	Chantaburi-Trat - Bang Kacha	Chantaburi-Trat - Khao Wua	Chantaburi-Trat - Khao Ploy Wan	Chantaburi-Trat - Bo Rai	Chantaburi-Trat - Bo Na Wong	Chantaburi-Trat - Nong Bon	Chantaburi-Trat - Bo Welu	Chantaburi-Trat – Bo I Rem	Chantaburi-Trat – Bo Na Wong	Kanchanaburi - Bo Phloi	Phrae - Den Chai	Ubon-Ratchathani	Sisaket	Chaiangrai	Phetchabun	Sukhothai
Silicates	Zircon	✓	✓	✓	✓	-	-	-	-	-	-	✓	-	-	-	-	-	-
	Garnet	-	-	-	-	✓	-	-	-	-	-	✓	-	-	-	-	-	-
	Sillimanite	-	-	-	-	-	-	-	-	-	-	✓	-	-	-	-	-	-
	Staurolite	-	-	-	-	-	-	-	-	-	-	✓	-	-	-	-	-	-
	Diopside	✓	-	-	-	-	-	-	-	-	-	-	-	-	-	-	-	-
	Fassaite	-	-	-	-	✓	-	✓	-	-	-	-	-	-	-	-	-	-
	Si-rich enstatite	-	-	-	-	-	-	-	-	-	-	✓	-	-	-	-	-	-
	Muscovite	✓	-	-	-	-	-	-	-	-	-	-	-	-	-	-	-	-
	Biotite	-	-	-	-	✓	-	-	-	-	-	✓	-	-	-	-	-	-

Table 2.1 Summary of mineral inclusions in Thai corundums (Intasopa et al., 1999; Sutthirat et al., 2001; Saminpanya and Sutherland, 2011; Khamloet et al., 2014) (continued)

Mineral group	Mineral inclusions	Chantaburi-Trat - Tok Phrom	Chantaburi-Trat - Bang Kacha	Chantaburi-Trat - Khao Wua	Chantaburi-Trat - Khao Ploy Wan	Chantaburi-Trat - Bo Rai	Chantaburi-Trat - Bo Na Wong	Chantaburi-Trat - Nong Bon	Chantaburi-Trat - Bo Welu	Chantaburi-Trat – Bo I Rem	Chantaburi-Trat – Bo Na Wong	Kanchanaburi - Bo Phloi	Phrae - Den Chai	Ubon-Ratchathani	Sisaket	Chaiangrai	Phetchabun	Sukhothai
	Stilpnomelane	-	-	-	-	-	-	-	-	-	-	✓	-	-	-	-	-	-
	K-feldspar	-	-	-	-	-	-	-	-	-	-	✓	✓	-	-	-	-	-
	Plagioclase	-	-	✓	-	-	-	-	-	-	-	-	-	-	-	-	-	-
	Orthoclase	-	-	-	-	-	-	-	-	-	-	✓	-	-	-	-	-	-
	Microcline	✓	-	-	-	-	-	-	-	-	-	-	-	-	-	-	-	-
	Oligoclase	-	-	-	-	-	-	-	-	-	-	✓	-	-	-	-	-	-
	Sanidine	-	-	-	-	-	-	-	-	-	-	-	✓	-	-	-	-	-
	Nepheline	-	-	-	-	-	-	-	-	-	-	✓	-	-	-	-	-	-

Table 2.1 Summary of mineral inclusions in Thai corundums (Intasopa et al., 1999; Sutthirat et al., 2001; Saminpanya and Sutherland, 2011; Khamloet et al., 2014) (continued)

Mineral group	Mineral inclusions	Chantaburi-Trat - Tok Phrom	Chantaburi-Trat - Bang Kacha	Chantaburi-Trat - Khao Wua	Chantaburi-Trat - Khao Ploy Wan	Chantaburi-Trat - Bo Rai	Chantaburi-Trat - Bo Na Wong	Chantaburi-Trat - Nong Bon	Chantaburi-Trat - Bo Welu	Chantaburi-Trat – Bo I Rem	Chantaburi-Trat – Bo Na Wong	Kanchanaburi - Bo Phloi	Phrae - Den Chai	Ubon-Ratchathani	Sisaket	Chaiangrai	Phetchabun	Sukhothai
	Sapphirine	-	-	-	-	-	✓	-	-	-	-	✓	-	-	-	-	-	-
	Thorite	✓	-	-	-	-	-	-	-	-	-	✓	-	-	-	-	-	-
	Mica	✓	-	-	-	-	-	-	-	-	-	-	-	-	-	-	-	-
	Biotite	-	-	-	-	✓	-	-	-	-	-	✓	-	-	-	-	-	-
Oxides	Spinel	-	✓	-	-	*	-	-	-	-	-	✓	-	-	-	-	-	-
	Hercynite	-	-	-	-	✓	-	-	-	-	-	✓	-	-	-	-	-	-
	Gahnite	✓	-	-	-	-	-	-	-	-	-	-	-	-	-	-	-	-
	Pleonaste	-	-	-	-	-	-	-	-	-	-	✓	-	-	-	-	-	-
	Magnetite	-	-	-	-	-	-	-	-	-	-	✓	✓	-	-	-	-	-

Table 2.1 Summary of mineral inclusions in Thai corundums (Intasopa et al., 1999; Sutthirat et al., 2001; Saminpanya and Sutherland, 2011; Khamloet et al., 2014) (continued)

Mineral group	Mineral inclusions	Chantaburi-Trat - Tok Phrom	Chantaburi-Trat - Bang Kacha	Chantaburi-Trat - Khao Wua	Chantaburi-Trat - Khao Ploy Wan	Chantaburi-Trat - Bo Rai	Chantaburi-Trat - Bo Na Wong	Chantaburi-Trat - Nong Bon	Chantaburi-Trat - Bo Welu	Chantaburi-Trat – Bo I Rem	Chantaburi-Trat – Bo Na Wong	Kanchanaburi - Bo Phloi	Phrae - Den Chai	Ubon-Ratchathani	Sisaket	Chaiangrai	Phetchabun	Sukhothai
	Heamatite	-	-	-	-	-	-	-	-	-	-	✓	-	-	-	-	-	-
	Ilmenite	-	✓	-	-	-	-	-	-	-	-	✓	-	-	-	-	-	-
	Rutile	✓	-	-	✓	-	-	-	-	-	-	✓	-	-	-	-	-	-
	Chromite	-	-	-	-	-	-	-	-	-	-	-	✓	-	-	-	-	-
-	Baddeleyite	-	-	-	-	-	-	-	-	-	-	✓	-	-	-	-	-	-
Phosphates	Monazite	✓	-	-	-	-	-	-	-	-	-	✓	-	-	-	-	-	-
	Apatite	✓	-	-	-	-	-	-	-	-	-	-	-	-	-	-	-	-
Chlorite	Clinochlore	-	-	-	-	✓	-	-	-	-	-	-	-	-	-	-	-	-
Niobium	Pyrochlore	-	-	-	-	-	-	-	-	-	-	✓	-	-	-	-	-	-

Table 2.1 Summary of mineral inclusions in Thai corundums (Intasopa et al., 1999; Sutthirat et al., 2001; Saminpanya and Sutherland, 2011; Khamloet et al., 2014) (continued)

Mineral group	Mineral inclusions	Chantaburi-Trat - Tok Phrom	Chantaburi-Trat - Bang Kacha	Chantaburi-Trat - Khao Wua	Chantaburi-Trat - Khao Ploy Wan	Chantaburi-Trat - Bo Rai	Chantaburi-Trat - Bo Na Wong	Chantaburi-Trat - Nong Bon	Chantaburi-Trat - Bo Welu	Chantaburi-Trat – Bo I Rem	Chantaburi-Trat – Bo Na Wong	Kanchanaburi - Bo Phloi	Phrae - Den Chai	Ubon-Ratchathani	Sisaket	Chaiangrai	Phetchabun	Sukhothai
	Columbite	✓	-	-	-	-	-	-	-	-	-	✓	-	-	-	-	-	-
	Fergusonite	-	-	-	-	-	-	-	-	-	-	✓	-	-	-	-	-	-
Al hydroxides	Boehmite	✓	✓	-	-	-	-	-	-	-	-	✓	-	-	-	-	-	-
CO_3	Calcite	-	-	-	-	-	-	-	-	-	-	✓	-	-	-	-	-	-
Cl	NiCl2	-	-	-	-	-	-	-	-	-	-	✓	-	-	-	-	-	-
Sulphides	Galena	-	-	-	-	-	-	-	-	-	-	✓	-	-	-	-	-	-
	Pyrrhotite	-	-	-	-	✓	-	-	-	-	-	-	-	-	-	-	-	-
Native	Gold	-	-	-	-	-	-	-	-	-	-	✓	-	-	-	-	-	-
Other	Bismuth	✓	-	✓	-	✓	-	-	-	-	-	-	-	-	-	-	-	-

Table 2.2 Summary of mineral inclusions in basaltic corundums from other places (Guo et al., 1992; Smith et al., 1995; Intasopa et al., 1999; Intasopa et al., 2002; Sutherland et al., 2002; Singbamroong, 2004; Singbamroong and Thanasuthipitak, 2004; McGee, 2005; Sutthirat et al., 2005).

Mineral group	Mineral inclusion	Cambodia - Pailin	Cambodia - Klong Ta Wan	Cambodia - Bo Thong Su	Cambodia -Bo Ya Da	Cambodia -Bo Hai	Lao- Ban Huai Sai	Vietnam – Gia Nghia	Vietnam – Phan Thiet, Di Linh	Australia - Inverell	Australia – Tasmania	Kenya - Simba	Kenya - Baringo	Madagascar – Diego	China – Changle (Shandong)	Rwanda
Silicates	Zircon	-	-	✓	-	-	✓	✓	✓	✓	✓	-	-	-	✓	✓
	Garnet	-	-	-	✓	-	-	-	-	-	-	-	✓	-	-	-
	Sillimanite	-	-	-	-	-	-	-	-	-	-	-	-	-	-	-
	Staurolite	-	-	-	-	-	-	-	-	-	-	-	-	-	-	-
	Diopside	-	-	-	-	-	-	-	-	-	-	-	-	-	-	-
	Pyroxene	-	-	-	✓	-	-	-	-	-	-	✓	-	-	-	✓
	Augite	-	✓	-	-	-	-	-	-	-	-	-	-	-	-	-
	Diopside	✓	-	-	✓	-	-	-	-	-	-	-	-	-	-	-
	Fassaite	✓	-	-	✓	-	-	-	-	-	-	-	-	-	-	-

Table 2.2 Summary of mineral inclusions in basaltic corundums from other places (Guo et al., 1992; Smith et al., 1995; Intasopa et al., 1999; Intasopa et al., 2002; Sutherland et al., 2002; Singbamroong, 2004; Singbamroong and Thanasuthipitak, 2004; McGee, 2005; Sutthirat et al., 2005) (continued).

Mineral group	Mineral inclusion	Cambodia - Pailin	Cambodia - Klong Ta Wan	Cambodia - Bo Thong Su	Cambodia -Bo Ya Da	Cambodia -Bo Hai	Lao- Ban Huai Sai	Vietnam – Gia Nghia	Vietnam – Phan Thiet, Di Linh	Australia - Inverell	Australia – Tasmania	Kenya - Simba	Kenya - Baringo	Madagascar – Diego	China – Changle (Shandong)	Rwanda
	Si-rich enstatite	-	-	-	-	-	-	-	-	-	-	-	-	-	-	-
	Muscovite	-	-	-	-	-	-	-	-	-	-	-	-	-	-	-
	Biotite	-	-	-	-	-	-	-	-	-	-	-	-	-	-	-
	Stilpnomelane	-	-	-	-	-	-	-	-	-	-	-	-	-	-	-
	Feldspar	-	✓	✓	✓	-	✓	✓	✓	✓	✓	-	✓	-	✓	-
	Orthoclase	-	-	-	-	-	-	-	-	-	-	-	-	-	-	-
	Microcline	-	-	-	-	-	-	-	-	-	-	-	-	-	-	-
	Oligoclase	-	-	-	-	-	-	-	-	-	-	-	-	-	-	-
	Sanidine	-	-	-	-	-	-	-	-	-	-	-	-	-	-	-

Table 2.2 Summary of mineral inclusions in basaltic corundums from other places (Guo et al., 1992; Smith et al., 1995; Intasopa et al., 1999; Intasopa et al., 2002; Sutherland et al., 2002; Singbamroong, 2004; Singbamroong and Thanasuthipitak, 2004; McGee, 2005; Sutthirat et al., 2005) (continued).

Mineral group	Mineral inclusion	Cambodia - Pailin	Cambodia - Klong Ta Wan	Cambodia - Bo Thong Su	Cambodia -Bo Ya Da	Cambodia -Bo Hai	Lao- Ban Huai Sai	Vietnam – Gia Nghia	Vietnam – Phan Thiet, Di Linh	Australia - Inverell	Australia – Tasmania	Kenya - Simba	Kenya - Baringo	Madagascar – Diego	China – Changle (Shandong)	Rwanda
	Nepheline	-	-	-	-	-	-	-	-	-	-	-	-	-	-	-
	Sapphirine	-	-	-	✓	-	-	-	-	-	-	-	-	-	-	-
	Olivine	-	-	-	-	-	-	-	-	-	✓	-	-	-	-	-
	Amphibole	-	-	-	-	-	-	-	-	-	-	-	-	-	-	✓
Oxides	Spinel	✓	-	-	-	-	-	-	✓	-	✓	✓	-	-	✓	✓
	Hercynite	-	-	-	-	-	✓	-	-	-	-	-	-	-	-	-
	Gahnite	✓	-	-	-	-	-	-	-	-	-	-	-	-	-	-
	Pleonaste	-	-	✓	-	-	-	-	-	-	-	-	-	-	-	-
	Magnetite	-	-	-	-	-	✓	-	-	-	-	-	-	-	-	-

Table 2.2 Summary of mineral inclusions in basaltic corundums from other places (Guo et al., 1992; Smith et al., 1995; Intasopa et al., 1999; Intasopa et al., 2002; Sutherland et al., 2002; Singbamroong, 2004; Singbamroong and Thanasuthipitak, 2004; McGee, 2005; Sutthirat et al., 2005) (continued).

Mineral group	Mineral inclusion	Cambodia - Pailin	Cambodia - Klong Ta Wan	Cambodia - Bo Thong Su	Cambodia -Bo Ya Da	Cambodia -Bo Hai	Lao- Ban Huai Sai	Vietnam – Gia Nghia	Vietnam – Phan Thiet, Di Linh	Australia - Inverell	Australia – Tasmania	Kenya - Simba	Kenya - Baringo	Madagascar – Diego	China – Changle (Shandong)	Rwanda
	Hematite	-	-	-	-	-	-	-	-	-	-	-	-	-	-	✓
	Ilmenite	-	-	-	-	-	-	-	✓	-	-	-	-	-	✓	✓
	Rutile	✓	✓	-	-	-	-	-	-	-	-	-	✓	-	-	✓
	Anatase	-	-	-	-	-	-	-	-	-	-	-	-	-	-	-
	Chromite	-	-	-	-	-	-	-	-	-	-	-	-	-	-	-
-	Baddeleyite	-	-	-	-	-	✓	-	-	-	-	-	-	-	-	-
Phosphates	Monazite	-	-	-	-	-	✓	-	-	-	-	-	-	-	-	-
	Apatite	-	-	-	-	-	-	-	-	-	-	-	-	-	✓	-
	Cheralite	-	-	-	-	-	✓	-	-	-	-	-	-	-	-	✓

Table 2.2 Summary of mineral inclusions in basaltic corundums from other places (Guo et al., 1992; Smith et al., 1995; Intasopa et al., 1999; Intasopa et al., 2002; Sutherland et al., 2002; Singbamroong, 2004; Singbamroong and Thanasuthipitak, 2004; McGee, 2005; Sutthirat et al., 2005) (continued).

Mineral group	Mineral inclusion	Cambodia - Pailin	Cambodia - Klong Ta Wan	Cambodia - Bo Thong Su	Cambodia -Bo Ya Da	Cambodia -Bo Hai	Lao- Ban Huai Sai	Vietnam – Gia Nghia	Vietnam – Phan Thiet, Di Linh	Australia - Inverell	Australia – Tasmania	Kenya - Simba	Kenya - Baringo	Madagascar – Diego	China – Changle (Shandong)	Rwanda
Chlorite	Clinochlore	✓	-	-	-	-	-	-	-	-	-	-	-	-	-	-
	Chlorite	✓	-	-	-	-	✓	-	-	-	-	-	-	-	-	✓
Niobium	Pyrochlore	-	-	-	-	-	-	-	✓	-	-	-	-	-	-	-
	Columbite	✓	-	✓	-	-	-	-	✓	-	-	-	-	-	✓	-
	Fergusonite	-	-	-	-	-	-	-	-	-	-	-	-	-	-	-
	Nb-Ta-rich	-	-	-	-	-	-	-	-	-	✓	-	-	-	-	-
Al hydroxides	Boehmite	-	-	-	-	-	-	-	-	-	-	-	-	-	-	-
CO_3	Calcite	-	-	-	-	-	-	-	-	-	-	-	-	-	-	-
Cl	$NiCl_2$	-	-	-	-	-	-	-	-	-	-	-	-	-	-	-

Table 2.2 Summary of mineral inclusions in basaltic corundums from other places (Guo et al., 1992; Smith et al., 1995; Intasopa et al., 1999; Intasopa et al., 2002; Sutherland et al., 2002; Singbamroong, 2004; Singbamroong and Thanasuthipitak, 2004; McGee, 2005; Sutthirat et al., 2005) (continued).

Mineral group	Mineral inclusion	Cambodia - Pailin	Cambodia - Klong Ta Wan	Cambodia - Bo Thong Su	Cambodia -Bo Ya Da	Cambodia -Bo Hai	Lao- Ban Huai Sai	Vietnam – Gia Nghia	Vietnam – Phan Thiet, Di Linh	Australia - Inverell	Australia – Tasmania	Kenya - Simba	Kenya - Baringo	Madagascar – Diego	China – Changle (Shandong)	Rwanda
Sulphides	Galena	-	-	-	-	-	-	-	-	-	-	-	-	-	-	-
	Pyrrhotite	-	-	-	-	-	-	-	✓	-	-	-	-	-	-	-
	Molybdenite	-	-	-	-	-	-	-	-	-	✓	-	-	-	-	-
Clay mineral	Kaolinite	-	-	-	-	-	-	-	-	✓	-	✓	-	-	-	-
Native Elements	Gold	-	-	-	-	-	-	-	-	-	-	-	-	-	-	-

2.3 Genetic models of basaltic corundum

Corundum formations associated with basaltic terrain have been proposed in several models. Corundum was crystallized at lower crustal or upper mantle depths prior to upwarding rapidly to the surface during the subsequent alkali-rich magmatic eruption. Some genetic models are reported below.

2.3.1. Plutonic crystallization

1) Corundum crystallization may take place in an undersaturated and fractionated felsic melt which related to intraplate magmas at high pressure in upper mantle and lower crustal depth (Irving, 1986).

2) Corundum may be produced by low to moderate degrees of partial melting of amphibolitised mantle at metasomatized lithosphere by contact metamorphism (Sutherland and Coenraads, 1996; Sutherland et al., 1998a; Sutherland et al., 1998b).

3) Coenraads et al. (1990) and Oakes et al. (1996) also proposed that corundum crystallization may occur in evolved basaltic magmas which were generated by low degrees of partial mantle melting near the boundary between lower crust-upper mantle.

4) Aspen et al. (1990) reported mineral inclusions such as anorthoclase, Fe-rich biotite, clinopyroxene, magnetite, zircon, and apatite which introduce plutonic crystallization of corundum from syenitic melts in crustal to upper mantle. This is similar to the model of Upton et al. (1999) who proposed that loss of alkalis and carbonatitic fractions may lead to aluminous enrichment.

2.3.2. Magma mixing at mid-crustal levels

Guo et al. (1996) studies mineral inclusions in basaltic corundum and subsequently suggested that mixing of carbonatitic and felsic melts (Si-rich) magmas at mid-crustal depth (15-25 km) under relatively low temperatures around 400-600°C should produce corundum in the such hybrid zone.

2.3.3 Metamorphic recrystallization

Metamorphic recrystallization of Al-rich and Si-poor rocks may also cause corundum crystallization. This process would be formed by thermal contacting processes of ocean-floor subduction below the continental crust (Levinson and Cook, 1994; Sutherland and Coenraads, 1996).

Sutthirat et al. (2001) used thermodynamic calculation to indicate the crystallization environment of clinopyroxene + corundum from Chanthaburi-Trat gem field. Their results indicated temperature range of 800 - 1150 ℃ and pressure range of 10 - 25 kbar suggesting Thai ruby presumably formed from high-grade metamorphosed mafic rocks.

Sutthirat et al. (2018) recently reported ruby-bearing xenoliths, mafic granulites (Pl–Cpx–Sp ± Grt ± Cor) from Bo Rai deposit which is the direct evidence of initial ruby formation in Bo Rai. As the result, they suggested mafic granulites xenoliths are the original source of these rubies.

CHAPTER 3

BO RAI RUBY

3.1 General characteristics

Eighty eight samples of Bo Rai ruby were collected for this study. These rough single-crystal ruby samples range from 0.03 and 0.86 cts. Most samples are tabular habits with slightly rounded or tumbled grains which are typical for corundum from alluvial or eluvial deposits. Some grains present evidence of weathering like etched or dissolved features which are typically observed in corundum from basaltic terrain (Figure 3.1). Selected samples were polished with at least one window for analyzing mineral inclusion. Diaphaneity of these polished samples ranges from semi-transparent to transparent (Figure 3.2).

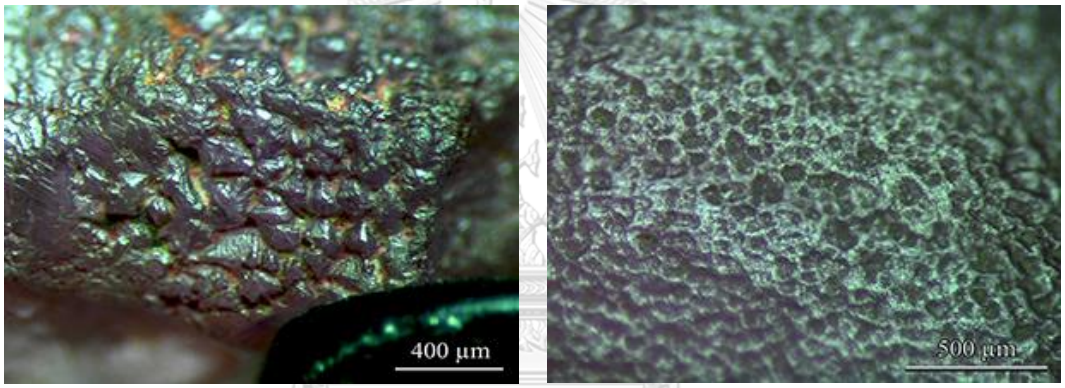

Figure 3.1 Photomicrographs showing etched or dissolved surfaces of samples from Bo Rai deposit; this feature is typically observed in corundum roughs from basaltic terrains.

GIA gem set color masters were used for color grading; Bo Rai ruby samples range from medium to slightly purplish red (2.27%), red-purple (78.41%), reddish purple (17.05%) and purple (2.27%). The samples with purple hue seem to be bigger than the others (Figure 3.2). However, most of samples are red-purple (Figure 3.3). Their refractive indices (RI) range from 1.760 to 1.771 with birefringence of 0.008 to 0.010. These samples show inert to moderate red fluorescence under long-wave ultraviolet (LWUV) lamp and inert under short-wave ultraviolet (SWUV) lamp. These general characteristics (i.e., color, fluorescence, weight, and refractive indices) are collected in Appendix A.

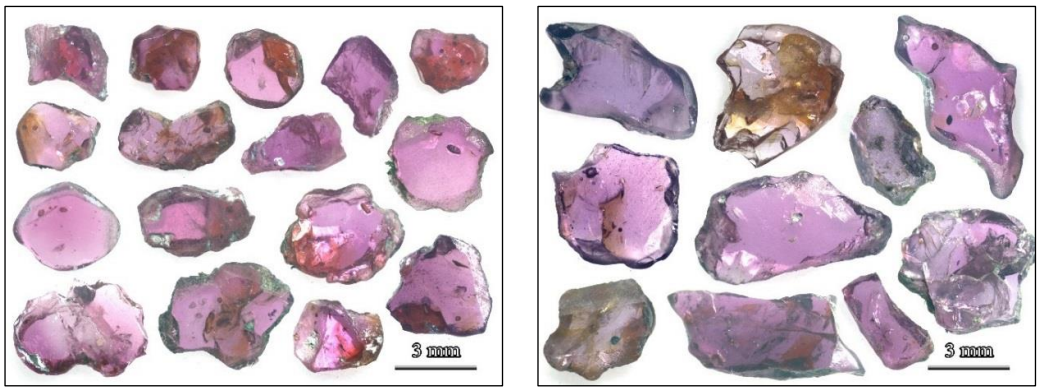

Figure 3.2 Representative polished Bo Rai samples show semi-transparence to transparence with colors ranging between medium to slightly purplish red to red-purple (left) and reddish purple to purple (right).

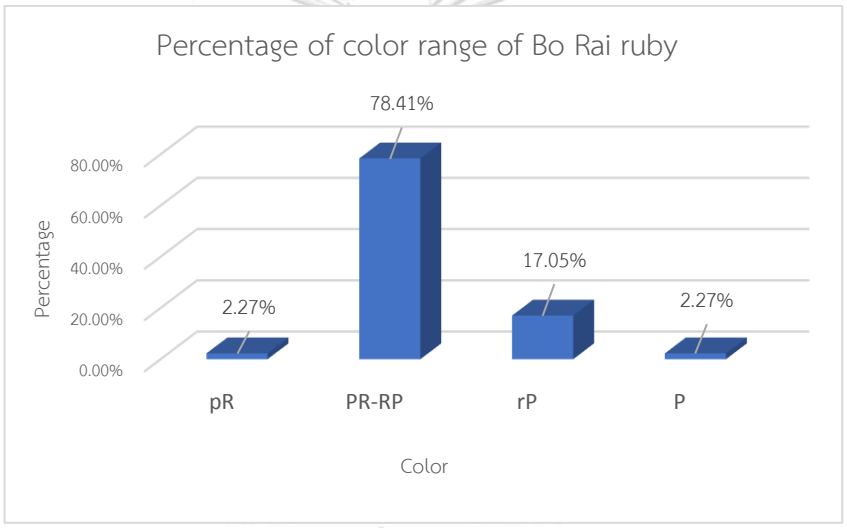

Figure 3.3 Colors of Bo Rai samples show 2.27% purplish red, 78.41% red-purple, 17.05% reddish purple and 2.27% purple samples.

3.2 Spectroscopic Features

A series of the absorption band in the mid-infrared range (4000–400 cm^{-1}) of representative samples are reported in Appendix C. Most of Bo Rai ruby samples revealed similar peaks at approximately 2363 and 2342 cm^{-1} due to CO_2 (Figure 3.4, blue spectrum); 2924 and 2852 cm^{-1} due to C-H stretching. In addition, a shoulder at about 3170 cm^{-1} and sharp peaks at 3697, 3669, 3652, 3620 cm^{-1} due to kaolinite - $Al_2Si_2O_5(OH)_4$ phase (Figure 3.4, red spectrum) as suggested by Beran and Rossman (2006) and Schwarz et al. (2008). Kaolinite phase is usually present in unheated corundums from various places such as basaltic sapphire from Vietnam as reported by Smith et al. (1995). The presence of kaolinite-related IR spectrum in the study samples suggest that rubies are not undergone heat treatment process.

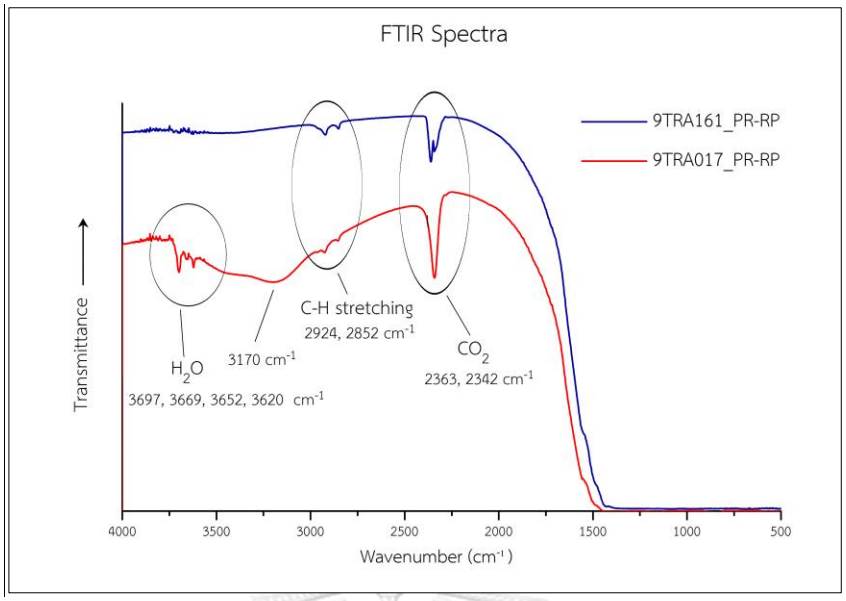

Figure 3.4 Representative Mid-IR spectra of Bo Rai ruby reveal peaks at approximately 2363 and 2342 cm^{-1} due to CO_2; 2924 and 2852 cm^{-1} due to C-H stretching (blue spectrum of red-purple (PR-RP) sample 9TRA161 and red spectrum of red-purple (PR-RP) sample 9TRA090). In addition, a shoulder at about 3170 cm^{-1} and sharp peaks at 3697, 3669, 3652, 3620 cm^{-1} due to kaolinite mineral phase are also present (red spectrum of sample 9TRA090).

Most of sample have windows properly parallel to c-axis, their UV-Vis-NIR spectra clearly represent ordinary rays of samples. The absorption peaks, related to high iron content, are observed around 330 nm in most purplish red to red-purple samples (Figure 3.5, blue spectrum) and over-absorption in this position occurred in reddish purple and purple samples (Figure 3.5, red spectrum). However, most purplish red and red-purple samples show chromium-dominated absorptions at around 410, 560 and 694 nm causing red color (Figure 3.5, blue spectrum). On the other hand, most reddish purple to purple ruby samples show clearly iron-related absorptions at 387 and 450 nm more intense than chromium-related absorption particularly observed at 410 nm (Figure 3.5, red spectrum); consequently, blue hue influences their body color. More representative UV-Vis-NIR spectra of Bo Rai ruby samples are collected in Appendix D.

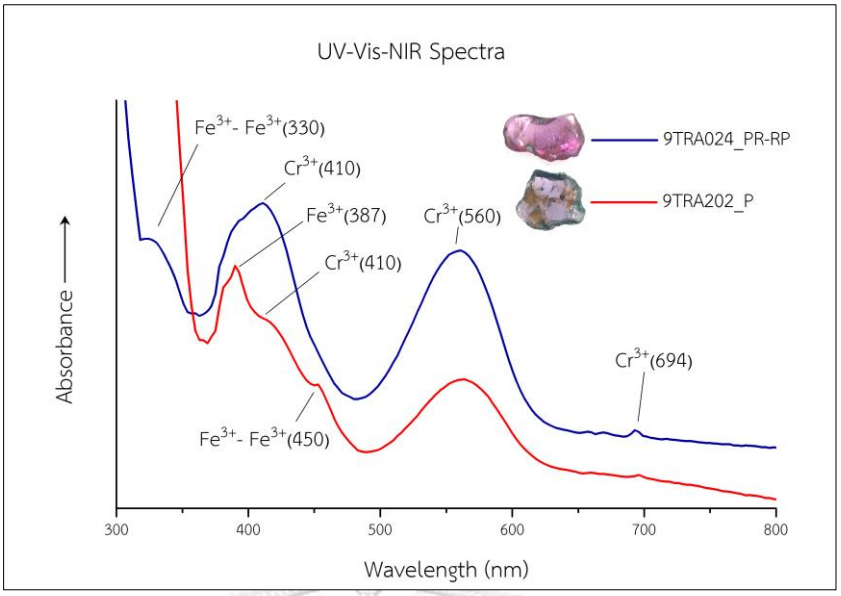

Figure 3.5 Representative UV-Vis-NIR absorption spectra (ordinary rays) of Bo Rai ruby: blue spectrum of red-purple ruby sample 9TRA024 reveals Fe^{3+} related at around 330 nm and chromium-dominated absorptions at around 410, 560 and 694 nm causing red color. Red spectrum of purple ruby sample 9TRA202 reveals obvious Fe^{3+} related with over-absorption around 330 nm including peaks at 387 and 450 nm which intense than Cr^{3+} related absorptions around 410 nm.

3.3 Chemical analyses

3.3.1 EDXRF analyses

Semi-quantitative chemical analyses of major composition (Al) and trace element contents (i.e., Fe, Ti, Cr, Ga, and V) of 74 Bo Rai ruby samples are collected in Appendix F. These analyses vary with in narrow ranges of individual elements which are quite similar in all color varieties. The Fe- and Ti-concentrations are reported at 0.35-1.26 wt% Fe_2O_3 and 0.01-0.67 wt% TiO_2, respectively. The Ga contents of some samples are not detected. The highest Ga content is 0.03 wt% Ga_2O_3. The Cr contents fall within 0.06-0.92 wt% Cr_2O_3. About twenty percent of samples are not yield V contents below the detection limit which the highest V content is recorded at 0.04 wt% V_2O_5. The Representative semi-quantitative EDXRF analyses of Bo Rai ruby samples show in Table 3.1.

Most samples show Fe_2O_3/TiO_2, and Cr_2O_3/Ga_2O_3 ratios below 100, TiO_2/Ga_2O_3 ratios below 25, and Fe_2O_3/Cr_2O_3 ratios below 8. Most Cr_2O_3/Ga_2O_3 ratio above 3 that indicates metamorphic origin similar to ruby from West Pailin as suggested by Sutherland et al. (1998b). However, it should be notified that most of reddish purple

and purple ruby samples apparently contain Cr_2O_3/Ga_2O_3 ratios lower than purplish red and red-purple samples (Figure 3.6 left). On the other hand, most of reddish purple and purple ruby samples apparently contain Fe_2O_3/Cr_2O_3 ratios higher than purplish red and red-purple samples (Figure 3.6 right).

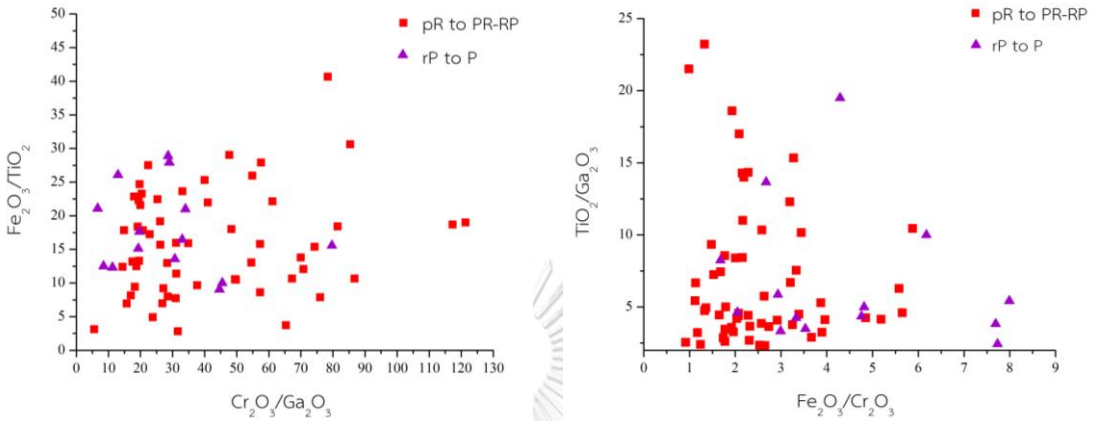

Figure 3.6 Chemical plots of Bo Rai ruby samples showing: (left) Fe_2O_3/TiO_2 mostly below 50 and Cr_2O_3/Ga_2O_3 above 3; (right) TiO_2/Ga_2O_3 ratios below 25, and Fe_2O_3/Cr_2O_3 ratios below 8.

Table 3.1 Representative semi-quantitative EDXRF analyses of Bo Rai ruby.

Element Oxides (wt.%)	purplish red to red-purple samples						reddish purple to purple samples						
	9TRA075	9TRA045	9TRA208	9TRA212	9TRA124	9TRA078	9TRA219	9TRA217	9TRA137	9TRA156	9TRA228	9TRA029	9TRA155
V_2O_5	0.01	ND	0.01	0.01	0.01	ND	0.01	ND	0.04	0.01	0.01	ND	0.01
TiO_2	0.44	0.17	0.04	0.06	0.08	0.67	0.04	0.05	0.07	0.08	0.02	0.02	0.08
Al_2O_3	98.16	98.49	99.13	99.09	98.75	97.83	99.07	98.91	98.54	98.95	99.29	99.44	98.83
Cr_2O_3	0.50	0.48	0.27	0.26	0.35	0.45	0.24	0.26	0.31	0.18	0.08	0.06	0.12
Ga_2O_3	ND	0.02	0.01	0.01	0.02	ND	ND	0.01	0.02	ND	0.01	0.01	0.01
Fe_2O_3	0.89	0.84	0.55	0.57	0.79	1.05	0.64	0.77	1.03	0.78	0.60	0.46	0.95
Total	100.00	100.00	100.00	100.00	100.00	100.00	100.00	100.00	100.00	100.00	100.00	100.00	100.00

ND = not detected

3.3.2 EPMA Analyses

Major, minor and trace elements i.e., Al, Fe, Ti, Cr, Ga, V, Si, Mg, and Mn, of representative 38 ruby samples were analyzed by Electron Probe Micro-Analyzer (EPMA). All analyses are collected in Appendix G and some representatives are shown in Table 3.2. Trace element analyses (i.e., Si, Ti, V, Ga, Mg, and Mn) in some samples are below detection limits of analytical method. The highest contents of Si, Ti, V, Ga, Mg, and Mn are recorded at 0.71 wt% SiO_2, 0.08 wt% TiO_2, 0.03 wt% V_2O_5, 0.10 wt% Ga_2O_3, 0.06 wt% MgO, and 0.08 wt% MnO, respectively. The Fe-concentrations fall within 0.22-0.69 wt% Fe_2O_3. The Cr contents range within 0.07-0.55 wt% Cr_2O_3. Most ruby samples show Fe_2O_3/TiO_2, Cr_2O_3/Ga_2O_3, ratios below 100 whereas TiO_2/Ga_2O_3 and Fe_2O_3/Cr_2O_3 ratios range below 10. In addition, Ga_2O_3/MgO below 3 and Fe_2O_3/MgO below 100 may suggest metamorphic origin (Peucat et al., 2007; Uher et al., 2012). The EMPA analyses cannot indicate the main cause of blue hue in the body color because the beam spots are very small whereas most samples contain color zones.

Table 3.2 Representative EPMA analyses of Bo Rai ruby

Element Oxides (wt.%)	purplish red to red-purple samples						reddish purple to purple samples					
	9TRA016	9TRA016	9TRA017	9TRA017	9TRA023	9TRA023	9TRA029	9TRA029	9TRA036	9TRA036	9TRA156	9TRA156
SiO_2	0.09	ND	0.03	0.03	0.05	0.09	0.02	ND	0.05	0.05	0.05	0.09
TiO_2	0.02	0.02	0.05	0.06	ND	0.01	98.16	98.09	ND	0.04	0.02	0.02
Al_2O_3	98.92	98.92	99.00	98.83	99.49	98.01	0.15	0.09	99.45	99.11	98.12	98.94
Cr_2O_3	0.08	0.24	0.24	0.31	0.15	0.20	ND	ND	0.08	0.10	0.35	0.08
Ga_2O_3	0.01	0.01	ND	0.02	0.03	ND	ND	ND	0.01	0.03	0.05	0.01
V_2O_3	ND	ND	ND	ND	0.01	ND	0.01	ND	ND	0.01	ND	ND
FeO total	0.39	0.36	0.64	0.69	0.33	0.37	0.43	0.47	0.44	0.45	0.30	0.39
MnO	ND	0.04	ND	0.03	ND	ND	0.01	ND	ND	0.04	ND	ND
MgO	0.02	0.02	0.01	0.01	0.03	0.02	ND	ND	0.01	0.01	0.02	0.02
Total	99.53	99.61	99.97	99.98	100.09	98.70	98.83	98.75	100.04	99.84	98.91	99.55
Fe_2O_3/TiO_2	19.50	18.00	12.80	11.50	-	37.00	-	-	-	11.25	15.00	19.50
Cr_2O_3/Ga_2O_3	8.00	24.00	-	15.50	5.00	-	-	-	8.00	3.33	7.00	8.00
TiO_2/Ga_2O_3	2.00	2.00	-	3.00	ND	-	-	-	ND	1.33	0.40	2.00
Fe_2O_3/Cr_2O_3	4.88	1.50	2.67	2.23	2.20	1.85	2.87	5.22	5.50	4.50	0.86	4.88
3 (O)												
Si	0.002	0.000	0.001	0.001	0.001	0.002	0.000	0.000	0.001	0.001	0.001	0.002
Ti	0.000	0.000	0.001	0.001	0.000	0.000	0.000	0.000	0.000	0.001	0.000	0.000
Al	1.992	1.992	1.989	1.987	1.993	1.991	1.993	1.994	1.993	1.992	1.990	1.992
Cr	0.001	0.003	0.003	0.004	0.002	0.003	0.002	0.001	0.001	0.001	0.005	0.001
Ga	0.000	0.000	0.000	0.000	0.000	0.000	0.000	0.000	0.000	0.000	0.001	0.000
V	0.000	0.000	0.000	0.000	0.000	0.000	0.000	0.000	0.000	0.000	0.000	0.000
Fe^{3+}	0.004	0.005	0.008	0.009	0.005	0.004	0.006	0.007	0.006	0.006	0.004	0.004
Fe^{2+}	0.001	0.000	0.001	0.001	0.000	0.001	0.000	0.000	0.001	0.001	0.001	0.001
Mn	0.000	0.001	0.000	0.000	0.000	0.000	0.000	0.000	0.000	0.001	0.000	0.000
Mg	0.001	0.001	0.000	0.000	0.001	0.001	0.000	0.000	0.000	0.000	0.001	0.001
Total*	2.001	2.002	2.003	2.003	2.002	2.001	2.002	2.002	2.002	2.002	2.001	2.001

ND = not detected

3.4 Internal Feature

Microscopic evidences of all samples show no indications of heating. Epigenetic inclusions such as iron oxides are quite commonly observed in most fractures (Figure 3.7a). A few samples show parallel twinning planes (Figure 3.7b) and needle-like inclusions (Figure 3.7c-d). Healed fractures (fingerprints) are visible under dark-field illumination (Figure 3.7e). Their typical characteristics are crystals with equatorial thin films which can be seen using surface-reflected light (Figure 3.7f), including two-phase (S-G) inclusions which can be captured using a combination of fiber-optic and bright-field illumination (Figure 3.7g-j).

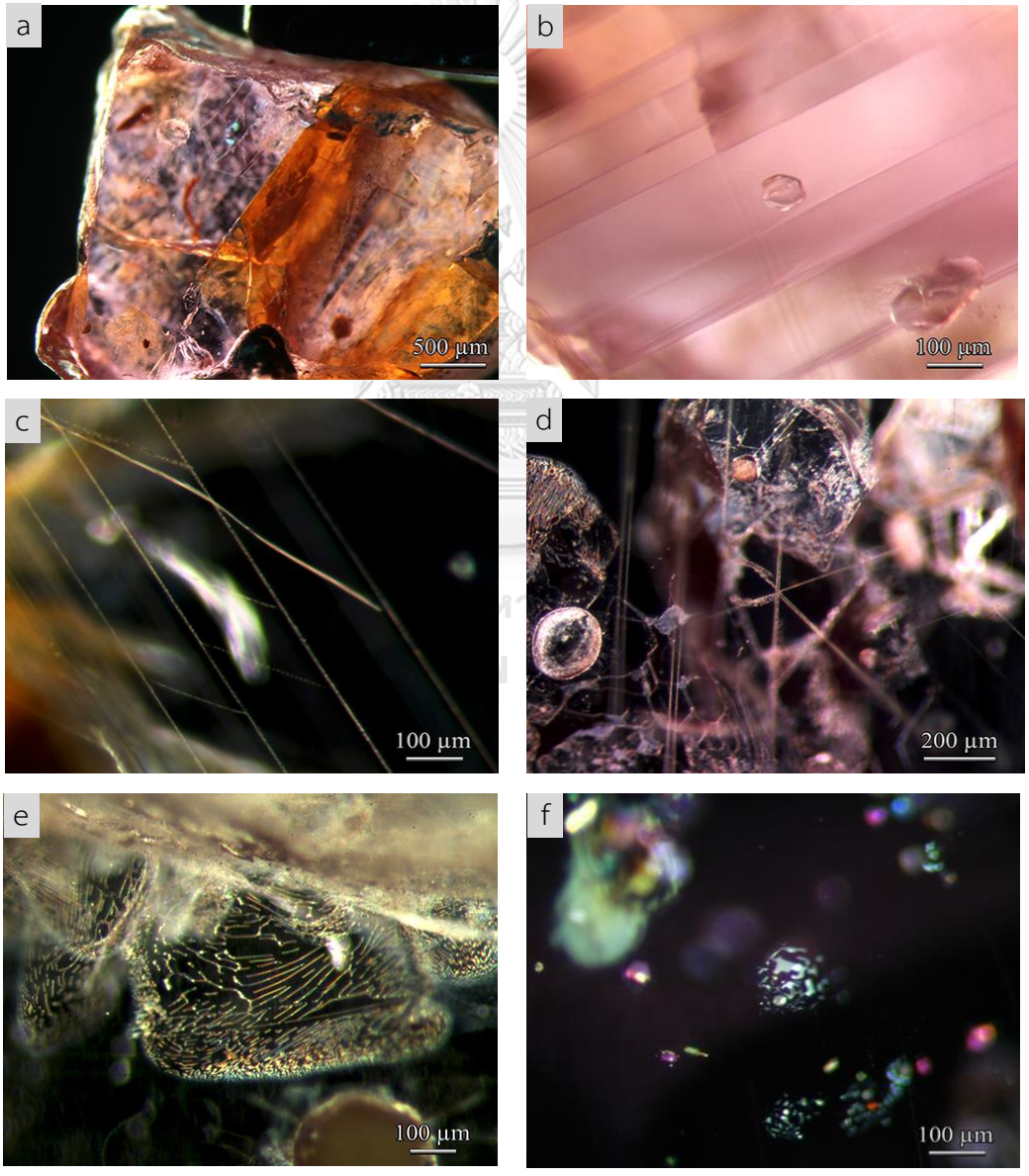

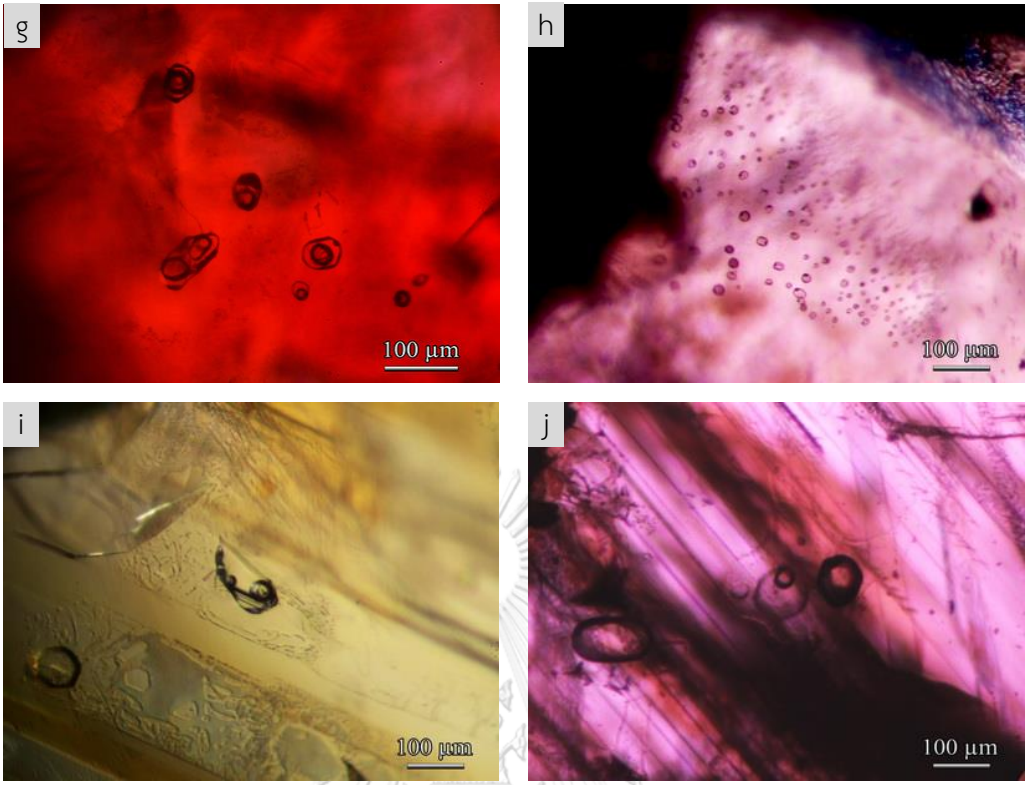

Figure 3.7 Microscopic observation using oblique fiber-optic illumination showing: a) iron oxides in fractures (sample 9TRA023); b) parallel twinning planes (sample 9TRA095); c) parallel tubes (sample 9TRA202); d) intersection of other tubules (sample 9TRA151); e) healed fractures (fingerprints) clearly observed under dark-field and fiber-optic illumination (sample 9TRA118); f) crystal inclusions with equatorial thin films (sample 9TRA232); group of two-phase inclusions in samples 9TRA026 (g), 9TRA026 (h), 9TRA169 (i), 9TRA017 (j) using combination of fiber-optic light and bright-field illumination.

3.5 Mineral Inclusions

Rubies from Bo Rai area, Trat were polished until the mineral inclusions were exposed onto the surface prior to identification using Raman spectroscope which all Raman spectroscopic data are shown in Appendix E and summarized in Table 3.3. Photomicrographs of mineral inclusions are collected in Appendix B. Representative mineral inclusions were analyzed by Electron Probe Micro-Analyzer (EPMA) for mineral chemical investigation. Their analytical data are reported in Appendix H.

Table 3.3 Summary of mineral inclusions in the Bo Rai ruby, initially identified by Raman and/or additionally analyzed by EPMA.

Mineral group	Mineral inclusions	Frequency	Purplish red	Red-purple	Reddish purple	Purple
Silicates	Garnet	**	-	✓	✓	-
	Sillimanite	*	-	✓	-	-
	Pyroxene	***	✓	✓	✓	✓
	Plagioclase	*	-	✓	✓	-
Oxides	Spinel	*	-	✓	-	-
	Anatase[1]	*	-	✓	-	-
Sulphide	Pyrrhotite	**	-	✓	✓	✓

*** often found in this study
** moderately found in this study
* rarely found in this study
[1] Identified by Raman only

Garnet

Garnet inclusions observed in red-purple and reddish purple samples are generally subhedral shapes which are either colorless or pale purplish red (Figure 3.8a-b). The garnet inclusion in ruby sample 9TRA053 is noticeably oriented along trigonal crystal structure of the host (Figure 3.8c). In ruby sample 9TRA029, ellipsoidal garnet crystal is adhered with rounded opaque metallic (pyrrhotite?) (Figure 3.8d) which is similar to those reported previously by (Gübelin, 1940, 1971). More photographs of garnet inclusions are collected in Appendix B. The representative Raman spectrum is shown in Figure 3.9; more spectra are reported in Appendix E.

Most EPMA analyses of garnet inclusions are reported in Appendix H and some representatives are summarized in Table 3.4. Most garnet inclusions in Bo Rai ruby contain very low chromium contents but they show high $Mg/(Mg+Fe^{2+})$ ratios varying from 0.71 to 0.91. Their compositions are clearly pyropic garnet ($py_{55-67}alm_{7-22}grs_{21-24}$) which is similar to garnet inclusion in Bo Rai ruby, previously reported by Sutthirat et al. (2001) and Saminpanya and Sutherland (2011). Only garnet inclusion associated with round black crystals (probably pyrrhotite) in reddish purple sample 9TRA029 found (Figure 3.8d) yields higher Fe and slightly lower Mg than the other garnet inclusions mostly found in red-purple samples.

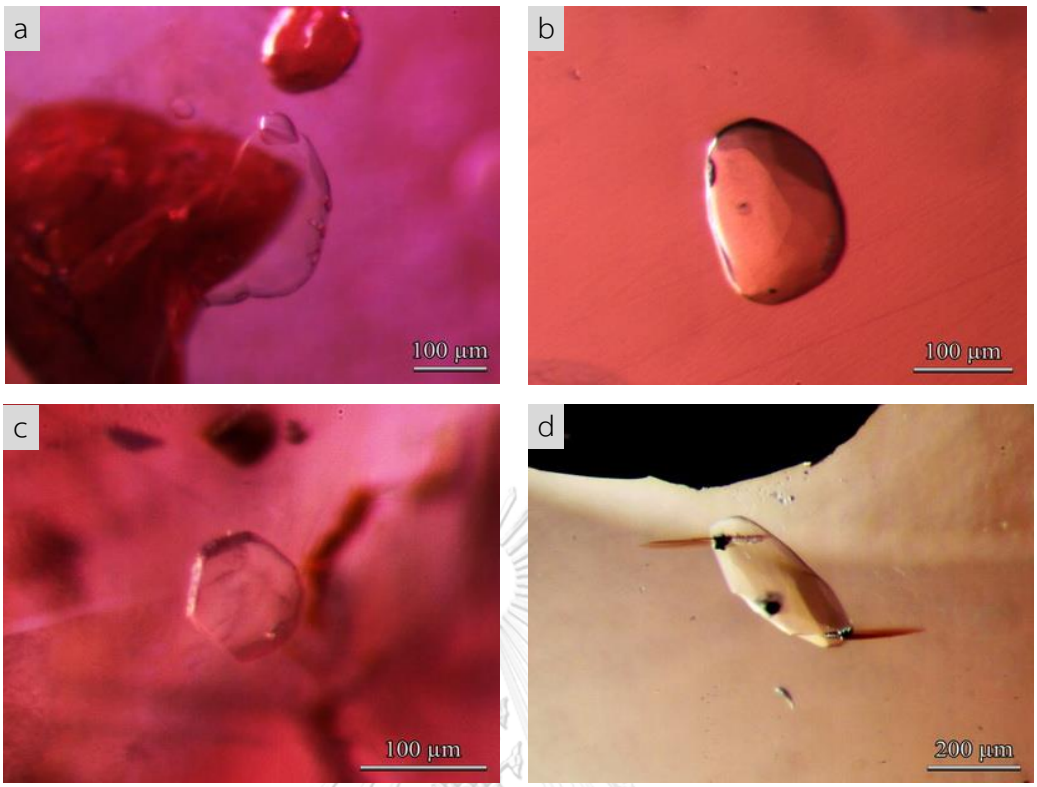

Figure 3.8 Garnet inclusions viewed in dark field condition; most garnet inclusions observed in Bo rai ruby are irregular shape (a) in sample 9TRA049, (b) in sample 9TRA215); c) garnet inclusion in sample 9TRA053 noticeably oriented along the host trigonal structure; d) ellipsoidal garnet crystal adhered with rounded opaque metallic in sample 9TRA029.

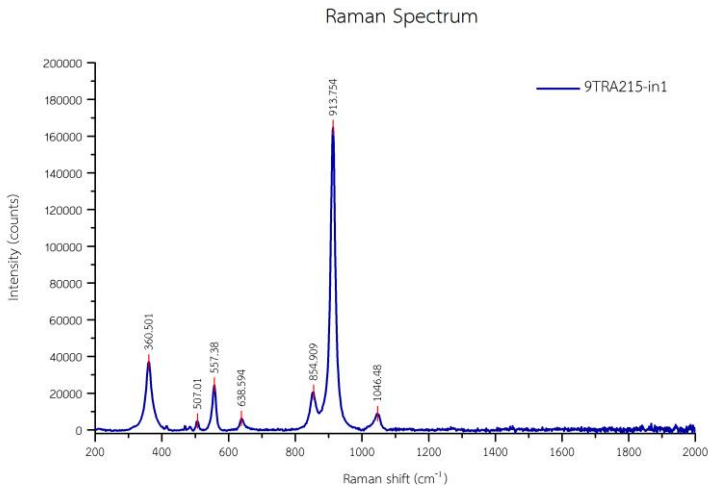

Figure 3.9 Representative Raman spectrum of garnet inclusion observed in Bo Rai ruby sample 9TRA215.

Table 3.4 Representative EPMA analyses of garnet inclusions found with Bo Rai ruby samples.

Mineral phase analysis (wt%)	PR-RP						rP
	9TRA049-in1	9TRA053-in1	9TRA053-in2	9TRA206-in3	9TRA215-in1	9TRA218-in1	9TRA029-in1
SiO_2	41.77	42.56	41.94	41.88	42.07	41.43	41.45
TiO_2	0.02	0.01	0.03	0.01	0.05	0.02	0.05
Al_2O_3	23.01	23.30	23.32	22.65	23.39	24.12	23.09
Cr_2O_3	0.18	0.06	0.10	0.05	0.09	0.10	0.02
FeO total	6.55	7.09	7.05	7.21	9.27	6.29	11.29
MnO	0.20	0.22	0.16	0.20	0.19	0.12	0.23
MgO	18.33	17.97	18.27	17.21	15.69	18.71	15.65
CaO	8.78	8.48	8.35	9.43	9.33	9.90	8.58
K_2O	ND	ND	ND	ND	ND	ND	0.01
Na_2O	0.02	0.02	0.02	ND	ND	ND	ND
Total	98.85	99.70	99.73	99.73	100.07	99.73	100.36
12 (O)							
Si	3.004	3.033	3.005	3.030	3.023	2.933	2.997
Ti	0.001	0.001	0.002	0.001	0.003	0.001	0.003
Al	1.950	1.957	1.969	1.932	1.981	2.012	1.967
Cr	0.010	0.004	0.006	0.003	0.005	0.006	0.001
Fe^{3+}	0.048	0.000	0.023	0.005	0.000	0.169	0.051
Fe^{2+}	0.346	0.422	0.399	0.432	0.557	0.203	0.631
Mn	0.012	0.013	0.010	0.012	0.012	0.007	0.014
Mg	1.965	1.908	1.951	1.856	1.681	1.974	1.687
Ca	0.677	0.647	0.641	0.731	0.718	0.751	0.665
K	0.000	0.000	0.000	0.000	0.000	0.000	0.001
Na	0.003	0.002	0.003	0.000	0.000	0.000	0.000
Total*	8.016	7.987	8.008	8.002	7.981	8.057	8.017
ΣR^{2+}	3.000	2.991	3.001	3.031	2.968	2.935	2.997
ΣR^{3+}	2.009	1.961	2.000	1.940	1.989	2.188	2.022
$Mg/(Mg+Fe^{2+})$	0.850	0.819	0.830	0.811	0.751	0.907	0.728
Alm% (Fe^{2+})	11.53	14.11	13.30	14.25	18.77	6.92	21.05
Pyr% (Mg)	65.50	63.81	65.01	61.23	56.64	67.26	56.29
Gro% (Ca)	21.90	21.58	21.03	24.01	24.09	23.53	21.59
Sps% (Mn)	0.40	0.43	0.33	0.40	0.40	0.24	0.47
Uv%	0.11	0.04	0.06	0.04	0.06	0.07	0.01
And%	0.54	0.00	0.25	0.06	0.00	1.98	0.56
Ca-Ti Gt	0.01	0.01	0.02	0.01	0.04	0.01	0.03

$\Sigma R^{2+} = Fe^{2+}+Mn+Mg+Ca$, $\Sigma R^{3+} = Fe^{3+}+Ti+Al+Cr$

ND = not detected

Sillimanite

A few remarkable inclusions of single sillimanite crystal and intergrowth sillimanite-spinel inclusion are observed in red-purple ruby (sample 9TRA169) and purplish red ruby (sample 9TRA024), respectively. These are significant indicator of high temperature of crystallization. The single sillimanite inclusion forms nearly dipyramidal shapes surrounded by liquid inclusion; it also contains rounded orange material inside (Figure 3.10 left). Backscattered-Electron (BSE) Image with high magnification is clearly present its shape (Figure 3.10 right). The intergrowth sillimanite-spinel inclusion shows subhedral sillimanite adhered with euhedral spinel (Figure 3.11 left) which clearly differentiated using Backscattered-Electron (BSE) Imaging (Figure 3.11 right). The representative Raman spectra of sillimanite and spinel inclusion are present in Figure 3.12. Although, Raman spectra of sillimanite are unclearly determinable, its crystal shape and chemical composition can be used to support. Moreover, this is the first report of sillimanite and spinel inclusions discovered in Bo Rai ruby.

EPMA analyses of sillimanite and spinel inclusions are present in Table 3.5. EPMA analyses of sillimanite and their recalculated atomic proportions are close to perfect formula (Al_2SiO_5). Regarding to spinel inclusion in sample 9TWL024, its composition falls within spinel-spinel range, based on classification diagram (Haggerty, 1991) (see Figure 3.13). Pleonastic spinel inclusion was previously reported in ruby from West Pailin Cambodia; the spinel inclusion found in this study is composed of higher Mg content (purer spinel composition).

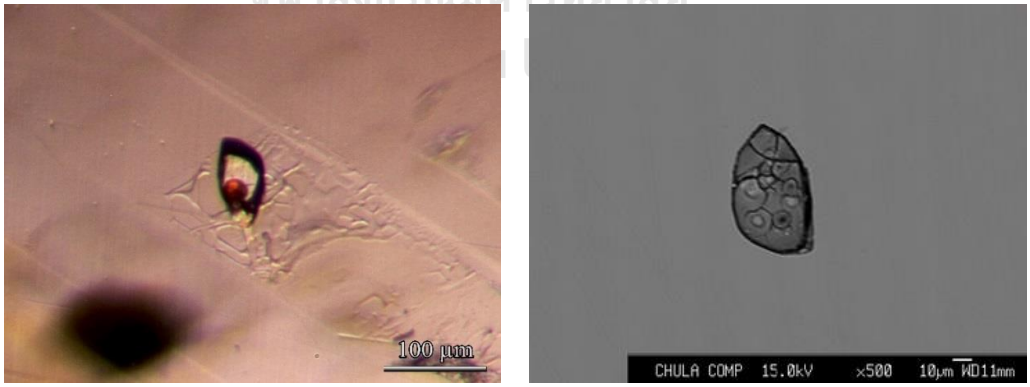

Figure 3.10 Sillimanite inclusion in Bo Rai ruby (sample 9TRA169) observed under bright field conditions (left); similar dipyramidal gain surrounded by liquid inclusion and contain rounded orange material inside; Backscattered-Electron (BSE) Image with high magnification (right) clearly present shape of the same sillimanite inclusion.

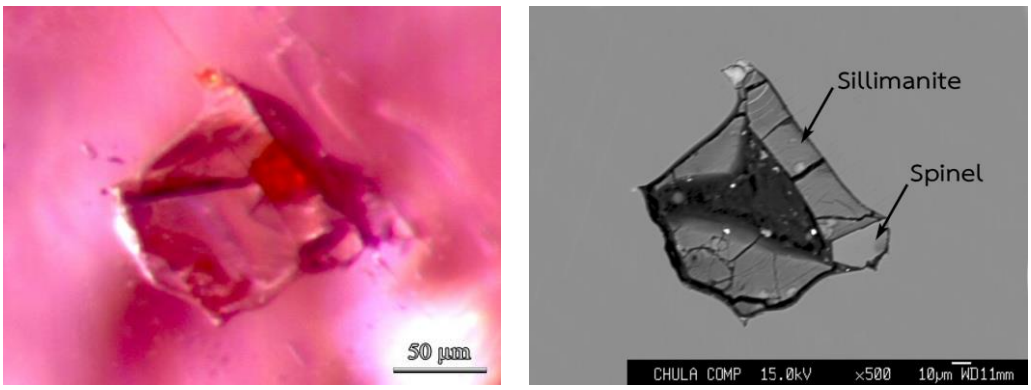

Figure 3.11 Intergrowth sillimanite-spinel inclusion found in Bo Rai ruby sample 9TRA024 observed under dark field illumination (left) showing subhedral prismatic sillimanite adhered with euhedral spinel; they are clearly differentiated using Backscattered-Electron (BSE) Imaging (right).

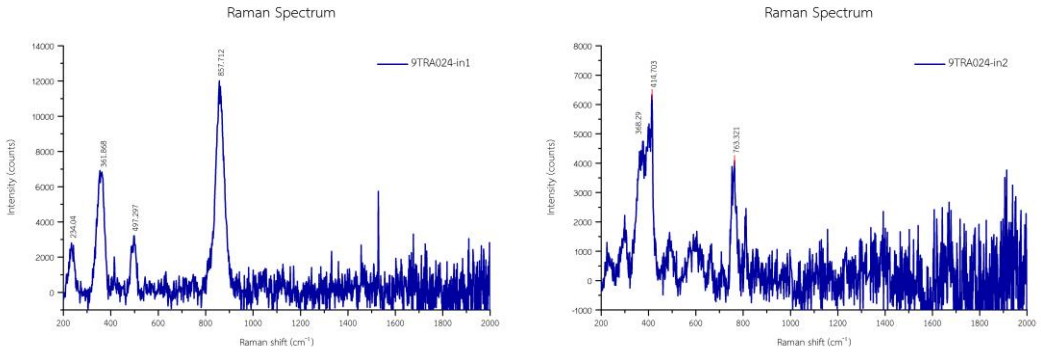

Figure 3.12 Representative Raman spectra of sillimanite (left) and spinel (right) inclusion observed in the Bo Rai ruby (sample 9TRA024).

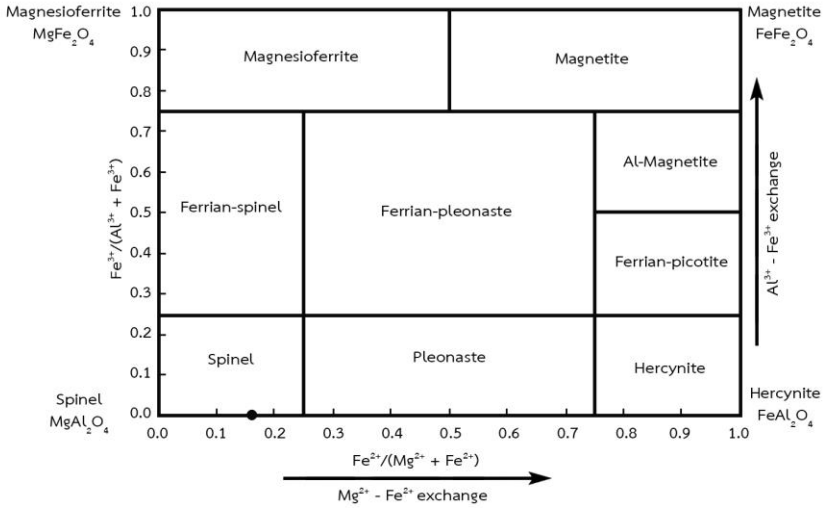

Figure 3.13 Compositional plot of spinel inclusion found in Bo Rai ruby (sample 9TWL024) falling within spinel-spinel range (Haggerty, 1991).

Table 3.5 EPMA analyses of sillimanite and spinel inclusions in red-purple Bo Rai ruby.

Mineral phase analysis (wt%)	Sillimanite		Spinel
	9TRA169-in1	9TRA024-in1	9TRA024-in2
SiO_2	36.60	36.49	0.09
TiO_2	ND	ND	ND
Al_2O_3	62.42	62.24	67.59
Cr_2O_3	0.02	0.21	1.41
FeO total	0.39	0.73	8.12
MnO	ND	0.01	0.03
MgO	0.07	0.12	22.59
CaO	0.27	0.16	ND
K_2O	0.18	0.08	0.01
Na_2O	0.03	0.03	0.01
Total	99.98	100.07	99.85
Formula	20 (O)		4 (O)
Si	3.969	3.960	0.002
Ti	0.000	0.000	0.000
Al	7.977	7.960	1.969
Cr	0.002	0.018	0.028
Fe^{3+}	0.035	0.066	0.000
Fe^{2+}	0.000	0.000	0.168
Mn	0.000	0.001	0.001
Mg	0.011	0.019	0.832
Ca	0.031	0.019	0.000
K	0.025	0.011	0.000
Na	0.006	0.006	0.000
Total*	12.057	12.060	3.000

ND = not detected

Pyroxene

The most common mineral inclusion observed in all color varieties of Bo Rai ruby samples is pyroxene which usually forms subhedral crystals in different shapes and colors. The most common pyroxene inclusion is colorless rounded crystal with twinning lamellae (Figure 3.14a). Although, a few pyroxene inclusions are brownish (Figure 3.14b) and some grains show columnar or thick stalk-like (Figure 3.14c). Moreover, some melted pyroxene inclusions are also observed with ellipsoidal shape (Figure 3.14d). More photographs of pyroxene inclusions are shown in Appendix B. A representative Raman spectrum is shown in Figure 3.15; more spectra are reported in Appendix E.

Chemical compositions of representative pyroxene inclusions were analyzed using EPMA and reported in Appendix H; the whole range of oxide compositions and their recalculated atomic proportion, based on six oxygen atoms, are summarized in Table 3.6. These pyroxenes are clearly characterized by Al-rich (0.58-0.70 Al) diopside, closely to tschermaks clinopyroxene (fassaite), which they have percentages of Ca: Mg: Fe ranging narrowly 51.91-56.61: 38.60-46.31: 0.27-7.83, respectively. These compositions are similar to pyroxenes associated with alluvial ruby from Bo Rai and corundum-bearing pyroxene xenocryst found in alkali basalt from Nong Bon (Sutthirat et al., 2001) and pyroxene in ruby-bearing xenolith found in alkali basalt from Bo Rai area, recently reported by Sutthirat et al. (2018). The chemical compositions of representative pyroxene inclusions from this study were plotted in the quadrilateral diagram (Morimoto et al., 1988) (see Figure 3.16). They are unclearly different in compositions of pyroxene inclusions found in different ruby varieties.

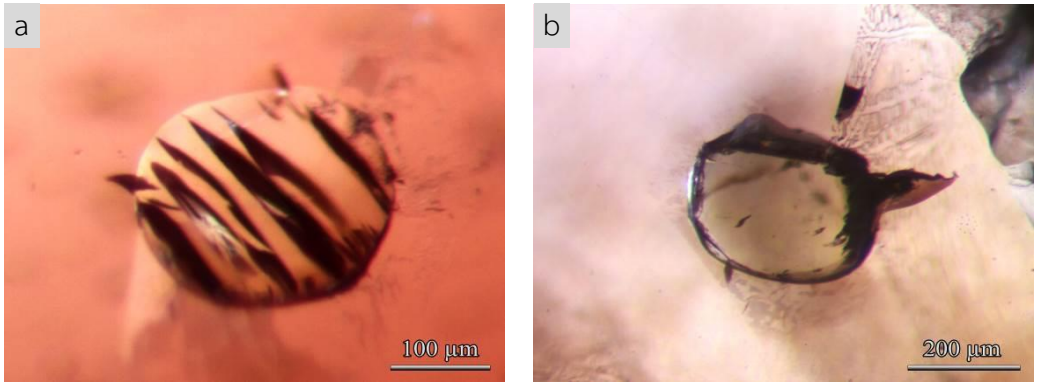

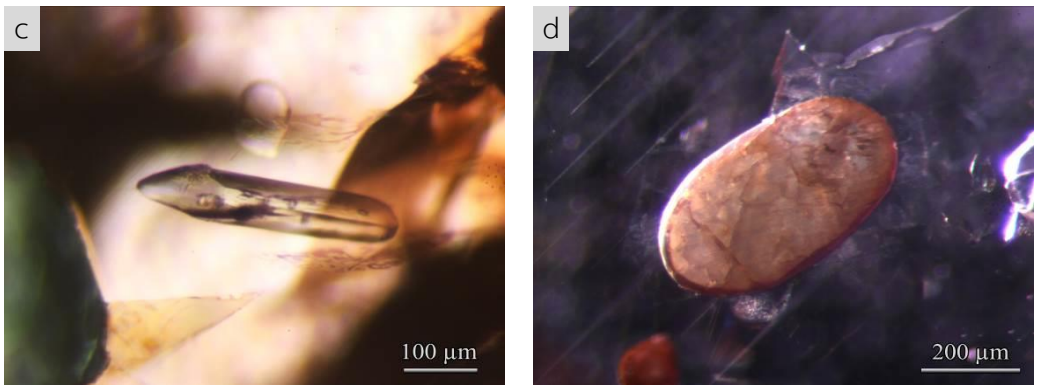

Figure 3.14 Combination of a fiber-optic light and/or bright-field illumination under gemological microscope applied for observation of pyroxene inclusions showing: a) colorless anhedral crystal (sample 9TRA212); b) brown crystal (sample 9TRA156); c) columnar or thick stalk-like crystal (sample 9TRA086); d) melted ellipsoidal pyroxene (sample 9TRA051).

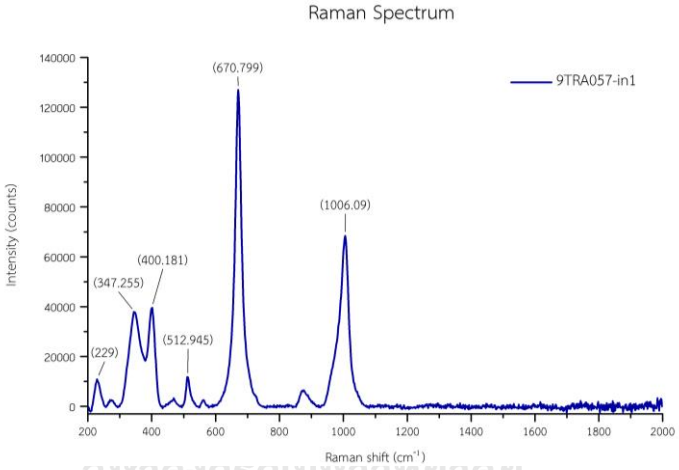

Figure 3.15 A representative Raman spectrum of pyroxene inclusion observed in the Bo Rai ruby sample 9TRA057.

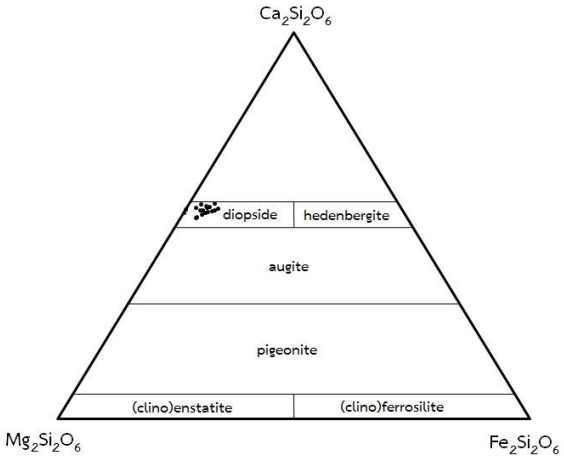

Figure 3.16 Compositional plots s of high-Al diopside inclusions found in Bo Rai ruby (diagram after Morimoto et al. (1988))

Table 3.6 Representative chemical compositions of pyroxene inclusions found in Bo Rai ruby.

Mineral phase analysis (wt%)	PR-RP																rP	P
	9TRA 016-in1	9TRA 023-in1	9TRA 038-in1	9TRA 039-in1	9TRA 051-in2	9TRA 052-in1	9TRA 057-in1	9TRA 061-in2	9TRA 113-in1	9TRA 118-in1	9TRA 118-in2	9TRA 124-in1	9TRA 126-in1	9TRA 126-in2	9TRA 126-in3	9TRA 218-in2	9TRA 036-in1	9TRA 156-in1
SiO_2	46.51	47.10	46.21	47.13	47.30	47.46	46.58	46.76	46.80	47.6	46.85	46.16	47.05	47.48	48.14	47.08	46.55	47.56
TiO_2	0.14	0.04	0.12	0.35	0.22	0.34	0.05	0.12	0.06	0.02	0.03	0.08	0.07	0.06	0.06	0.11	0.11	0.60
Al_2O_3	14.68	14.69	16.29	14.88	13.94	13.41	15.22	14.83	14.78	14.9	14.50	15.81	16.71	14.31	14.10	14.63	13.88	14.15
Cr_2O_3	0.14	0.08	0.04	0.15	0.06	0.05	0.07	0.24	0.06	0.08	0.04	0.13	0.09	0.05	0.07	0.08	0.04	0.07
FeO total	2.25	2.25	2.61	2.26	3.31	3.32	2.68	2.48	3.03	2.94	3.39	2.79	2.06	2.23	2.18	2.28	2.67	3.51
MnO	ND	0.04	0.03	0.04	0.04	0.04	0.04	0.05	0.06	ND	0.08	0.02	ND	ND	0.06	0.05	0.01	0.05
MgO	11.93	11.65	11.61	12.08	11.41	11.69	12.35	11.42	11.94	11.8	11.97	11.10	12.95	12.91	12.53	11.87	13.32	11.01
CaO	22.09	21.76	20.87	21.55	21.63	21.67	20.38	21.58	21.00	20.8	20.98	22.24	20.97	21.19	21.50	21.97	21.34	21.47
K_2O	0.01	0.01	0.03	0.02	0.01	0.01	ND	ND	0.02	0.01	0.01	0.02	0.01	0.01	ND	0.01	0.01	ND
Na_2O	1.02	1.20	1.11	1.16	1.06	1.14	1.61	1.03	1.29	1.46	1.44	0.87	0.98	1.05	1.08	0.97	0.97	1.41
Total	98.76	98.81	98.91	99.60	98.96	99.14	98.99	98.52	99.03	99.7	99.29	99.21	100.9	99.29	99.71	99.05	98.89	99.81
6 (O)																		
Si	1.705	1.722	1.686	1.709	1.734	1.739	1.701	1.716	1.712	1.72	1.713	1.687	1.677	1.724	1.740	1.718	1.706	1.731
Ti	0.004	0.001	0.003	0.010	0.006	0.009	0.001	0.003	0.002	0.00	0.001	0.002	0.002	0.002	0.002	0.003	0.003	0.016
Al	0.634	0.633	0.701	0.636	0.602	0.579	0.655	0.642	0.637	0.63	0.625	0.681	0.702	0.612	0.601	0.629	0.599	0.607
Cr	0.004	0.002	0.001	0.004	0.002	0.001	0.002	0.007	0.002	0.00	0.001	0.004	0.003	0.001	0.002	0.002	0.001	0.002
Fe^{3+}	0.025	0.005	0.000	0.006	0.000	0.007	0.078	0.000	0.040	0.01	0.071	0.000	0.008	0.014	0.000	0.000	0.077	0.000
Fe^{2+}	0.044	0.063	0.080	0.062	0.101	0.095	0.004	0.076	0.053	0.07	0.032	0.085	0.054	0.054	0.066	0.070	0.005	0.107
Mn	0.000	0.001	0.001	0.001	0.001	0.001	0.001	0.002	0.002	0.00	0.002	0.001	0.000	0.000	0.002	0.002	0.000	0.002
Mg	0.652	0.635	0.632	0.653	0.624	0.638	0.672	0.625	0.651	0.63	0.653	0.605	0.688	0.699	0.675	0.646	0.727	0.597
Ca	0.868	0.853	0.816	0.837	0.850	0.851	0.797	0.849	0.823	0.80	0.822	0.871	0.801	0.824	0.833	0.859	0.838	0.837
K	0.000	0.001	0.001	0.001	0.000	0.000	0.000	0.000	0.001	0.00	0.000	0.001	0.000	0.000	0.000	0.000	0.001	0.000
Na	0.073	0.085	0.078	0.082	0.075	0.081	0.114	0.073	0.091	0.10	0.102	0.062	0.068	0.074	0.076	0.069	0.069	0.099
Total*	4.008	4.002	3.999	4.002	3.996	4.002	4.026	3.993	4.013	4.00	4.024	3.999	4.003	4.005	3.995	3.998	4.026	3.998
% Ca	55.50	55.00	53.40	53.93	53.97	53.72	54.11	54.77	53.90	53.1	54.55	55.80	51.91	52.25	52.92	54.54	53.38	54.32
% Mg	41.69	40.94	41.36	42.07	39.62	40.28	45.62	40.32	42.63	42.0	43.33	38.76	44.59	44.32	42.88	41.02	46.31	38.74
% Fe	2.81	4.06	5.24	3.99	6.41	6.00	0.27	4.90	3.47	4.80	2.12	5.45	3.50	3.42	4.19	4.44	0.32	6.94
Total**	100.0	100.0	100.0	100.0	100.0	100.0	100.0	100.0	100.0	100.	100.0	100.0	100.0	100.0	100.0	100.0	100.0	100.0

ND = not detected

Feldspar

Most feldspar inclusions occur in red-purple and reddish purple samples. These feldspar crystals usually form rounded grains (Figure 3.14 left); however, some crystals are present as ellipsoidal shape (Figure 3.17 right). More photographs of feldspar inclusions are given in Appendix B. The representative Raman spectrum is shown in Figure 3.18. More spectra were collected in Appendix E.

Representative EPMA analyses of feldspar inclusions are present in Table 3.7, and most of analyses are reported in Appendix H. Their compositions are plotted in the ternary feldspar diagram. Their compositions are classified as plagioclase feldspars which only one feldspar inclusion ($Ab_{56}An_{38}Or_6$) in sample 9TRA031 falls clearly in andesine composition. The other feldspar inclusions are Ca-rich plagioclase ($Ab_{11\text{-}23}An_{77\text{-}89}Or_{0.1\text{-}0.8}$) mostly falling in bytownite range close to anorthite (Figure 3.19).

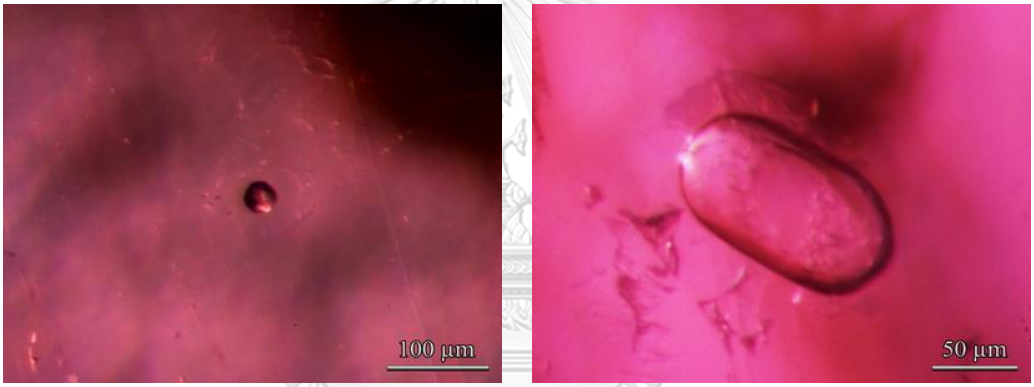

Figure 3.17 Feldspar inclusions in Bo Rai ruby viewed under bright field conditions: a) feldspar inclusion is nearly *rounded shape (sample 9TRA031); b) an ellipsoidal feldspar inclusion (sample 9TRA017).*

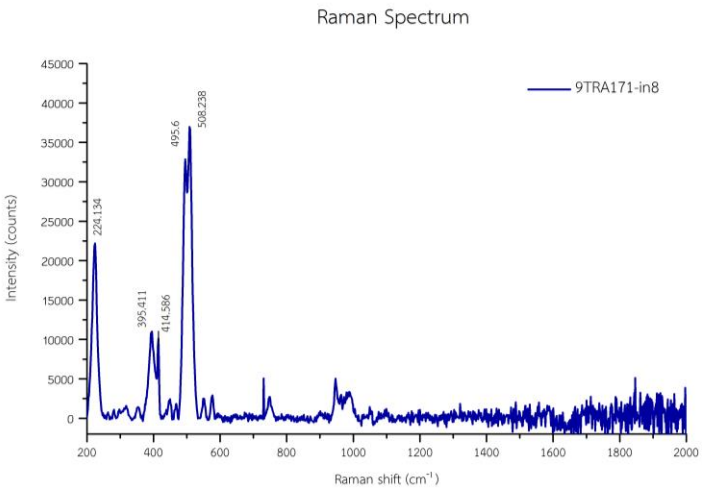

Figure 3.18 A representative Raman spectrum of feldspar inclusion observed in the Bo Rai ruby sample 9TRA171.

Table 3.7 Representative EPMA analyses of feldspar inclusions in Bo Rai ruby samples.

Mineral phase analysis (wt%)	PR-RP		rP	
	9TRA017-in1	9TRA031-in1	9TRA171-in8	9TRA219-in2
SiO_2	47.20	58.17	45.34	46.31
TiO_2	ND	0.08	0.01	ND
Al_2O_3	33.36	24.72	33.87	34.47
CaO	17.52	7.52	18.13	17.02
FeO	0.13	0.46	0.42	0.22
MnO	ND	0.02	0.03	ND
MgO	0.01	0.64	ND	0.07
K_2O	0.02	1.05	0.02	0.03
Na_2O	1.68	6.02	1.48	1.14
Total	99.92	98.68	99.30	99.26
8 (O)				
Si	2.171	2.643	2.111	2.139
Ti	0.000	0.003	0.000	0.000
Al	1.808	1.324	1.858	1.876
Ca	0.863	0.366	0.905	0.842
Fe	0.005	0.017	0.016	0.008
Mn	0.000	0.001	0.001	0.000
Mg	0.001	0.043	0.000	0.005
K	0.001	0.061	0.001	0.002
Na	0.149	0.530	0.134	0.102
Total*	4.998	4.988	5.026	4.974
Atomic%				
Ca	85.15	38.27	87.02	89.02
Na	14.73	55.40	12.87	10.79
K	0.12	6.34	0.11	0.19
Total**	100.00	100.00	100.00	100.00

ND = not detected

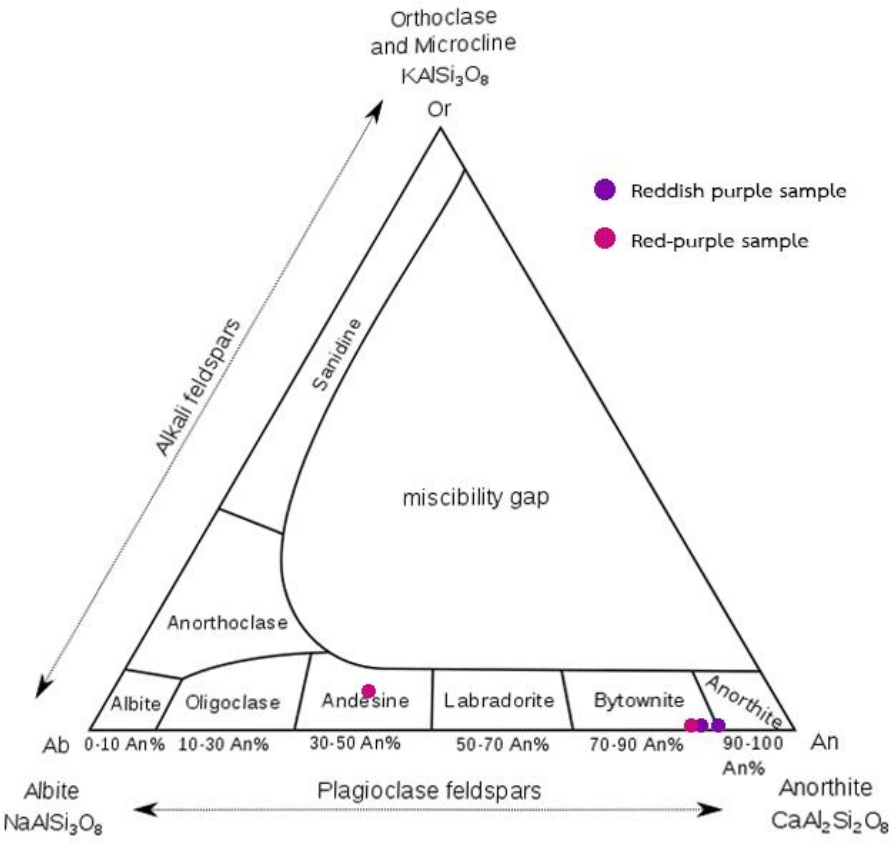

Figure 3.19 Ternary plotting of feldspar composition plots of inclusions in rubies from Bo Rai gem field. Most feldspar inclusions in ruby samples fall within plagioclase ranges.

Anatase

A very small irregular shape of nearly opaque inclusion is observed in the red-purple ruby from Bo Rai (Figure 3.20 left). Its polished surface presents yellow metallic luster (Figure 3.20 right) under reflected light. Raman spectrum is perfectly matched with anatase spectrum from database (Figure 3.21). However, it is very tiny crystal and unable to be analyzed by EPMA.

Anatase belongs to TiO_2 polymorphs; the other forms are rutile and brookite Although anatase indicates low temperature (500-600 °C) equilibration (Gübelin and Koivula, 1986); however, this is the first report of anatase inclusion with Raman identification in Bo Rai ruby. It may indicate that dissolution and subsequent phase transformation of TiO_2 component have been taken place from the host ruby under solid-stage (subsolidus) during the cooling process.

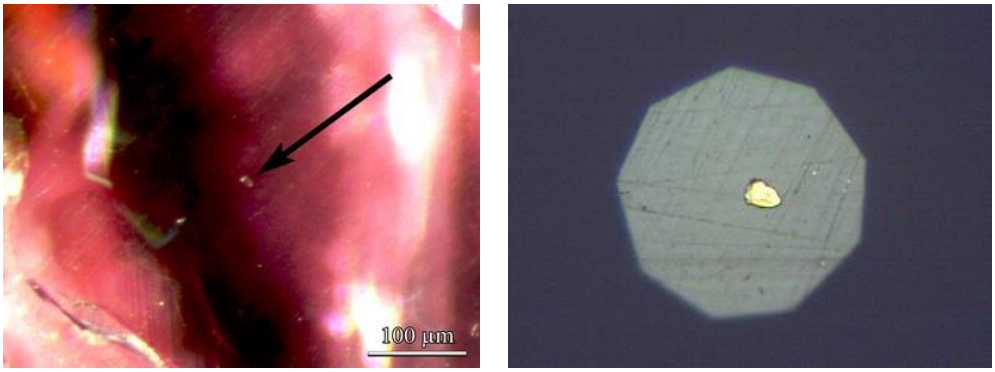

Figure 3.20 Photograph with high magnification under dark field conditions showing nearly opaque anatase inclusion with irregular shape (left); reflected light photograph reveal yellow metallic luster on the polished surface of anatase inclusion (right).

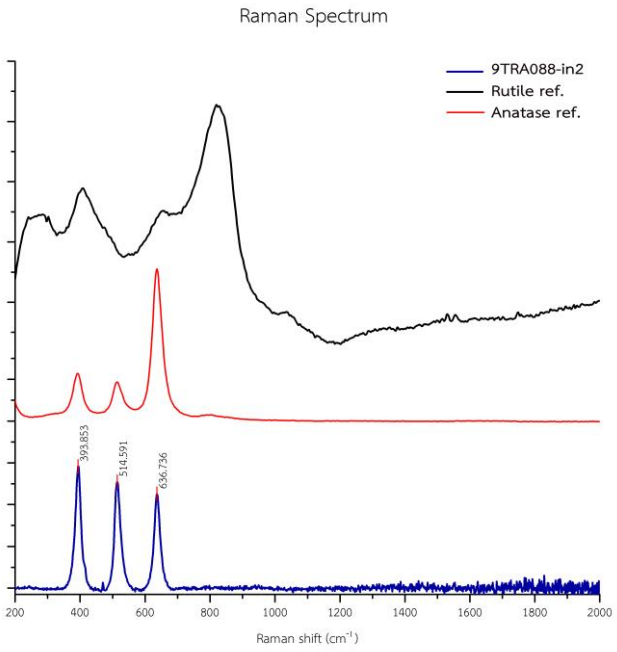

Figure 3.21 Raman *spectrum* of anatase inclusion in the Bo Rai ruby (sample 9TRA088) compared to Raman spectra of rutile and anatase from RRUFF database.

Sulphide

Many black opaque inclusions in Bo Rai ruby samples are identified as sulphides which were recognized in red-purple, reddish purple and purple samples. Most of them are rounded grains surrounded by tension disc (Figure 3.22a) or by fingerprint (Figure 3.22b). The biggest sulphide inclusion is about 150 x 130 µm (Figure 3.22c). A few inclusions show subhedral shape surrounded by healed fracture (Figure 3.22d). More photographs of sulphide inclusions are collected in Appendix B. A number of inclusions were prepared by several steps of polishing until they expose o

the hosts' surface. These polished sulphide inclusions usually show metallic, yellow, opaque, and rounded grains which are mostly identified as pyrrhotite by Raman spectroscopic analysis. The representative Raman spectrum are shown in Figure 3.23. More Raman spectra are reported in Appendix E.

EPMA analyses of these sulphide inclusions show various contents of the main iron and sulphur compositions (see Table 3.8). However, only the sulphide inclusion in ruby sample 9TRA231 yields analyses relevant to pyrrhotite (FeS). On the other hand, other sulphide analyses contains nickel and copper as the major and minor elements. Analysis of sulphide inclusion in ruby sample 9TRA055 yields 22.6% Ni which it is close to pentlandite $(Fe, Ni)_9S_8$. Ruby samples 9TRA214, 9TRA176, and 9TRA160 contain sulphide inclusions which give similar compositions of 51.7-64.4% Cu but only the sample 9TRA160 is close the digenite formula (Cu_9S_5). The variation of these sulphides may reflect locally syngenetic environments.

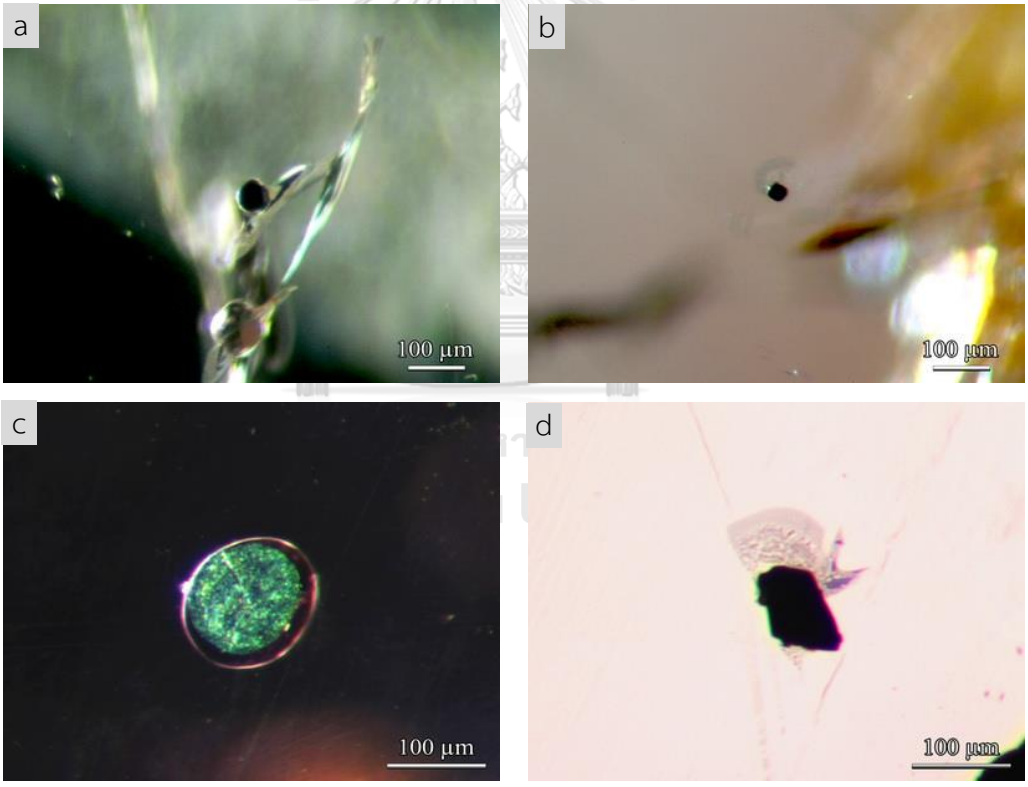

Figure 3.22 Photographs of sulphide inclusions taken under a fiber-optic illuminator: a) rounded sulphide inclusion surrounded by tension disc (sample 9TRA202); b) another rounded sulphide inclusion surrounded by fingerprint (sample 9TRA202); c) the biggest sulphide inclusion with size of about 150 x 130 µm (sample 9TRA231); d) in bright field view showing, subhedral opaque sulphide surrounded by healed fracture (sample 9TRA160).

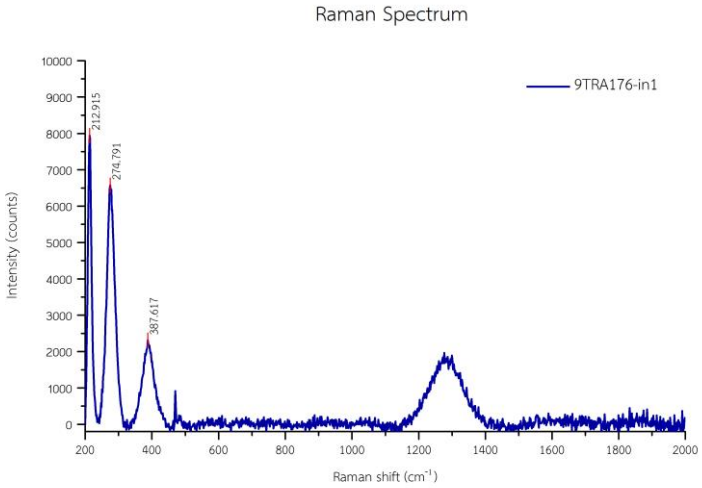

Figure 3.23 A representative Raman spectrum of sulphide inclusion (sample 9TRA176) fitting well with pyrrhotite spectrum from database.

Table 3.8 Representative EPMA analyses of sulphide inclusions in Bo Rai ruby samples.

Mineral phase analysis (wt%)	PR-RP					rP	P
	9TRA214-in1	9TRA160-in1	9TRA176-in1	9TRA208-in1	9TRA055-in1	9TRA231-in1	9TRA202-in1
Tl	0.29	ND	0.04	0.21	0.37	0.18	0.30
Al	0.09	0.04	0.06	0.05	0.04	0.11	0.03
In	0.01	ND	ND	0.05	ND	ND	ND
Ba	0.28	0.35	0.27	0.22	ND	ND	0.11
Fe	9.39	9.19	9.21	21.61	34.68	42.42	31.21
S	18.71	19.35	14.93	22.12	27.72	25.34	26.49
As	ND	NA	ND	ND	NA	NA	ND
Pb	ND	ND	ND	ND	ND	ND	ND
Cu	62.17	64.39	51.69	42.88	0.03	1.05	18.32
Ni	0.06	0.06	4.59	0.14	22.63	4.58	11.67
Mo	0.23	0.39	0.43	0.44	0.42	0.44	0.45
Pt	ND	ND	ND	ND	0.02	0.14	0.04
Sn	ND	NA	ND	ND	NA	NA	ND
Zn	ND	NA	ND	ND	NA	NA	ND
Co	ND	NA	ND	ND	NA	NA	ND
Total*	91.24	93.78	81.22	87.71	85.90	74.25	88.63
Formula							
Tl	0.008	0.000	0.001	0.003	0.017	0.001	0.003
Al	0.020	0.012	0.014	0.004	0.013	0.005	0.002
In	0.001	0.000	0.000	0.001	0.000	0.000	0.000
Ba	0.012	0.021	0.012	0.004	0.000	0.000	0.001
Fe	1.000	1.364	1.000	1.000	5.747	1.000	1.000
S	3.472	5.000	2.824	1.782	8.000	1.040	1.478
As	0.000	0.000	0.000	0.000	0.000	0.000	0.000
Pb	0.000	0.000	0.000	0.000	0.000	0.000	0.000
Cu	5.821	8.395	4.933	1.744	0.004	0.022	0.516
Ni	0.006	0.008	0.474	0.006	3.568	0.103	0.356
Mo	0.014	0.033	0.027	0.012	0.040	0.006	0.008
Pt	0.000	0.000	0.000	0.000	0.001	0.001	0.000
Sn	0.000	0.000	0.000	0.000	0.002	0.000	0.000
Zn	0.000	0.000	0.000	0.000	0.000	0.000	0.000
Co	0.000	0.000	0.000	0.000	0.000	0.000	0.000
Total**	10.354	14.833	9.285	4.556	17.390	2.178	3.365

NA = not analyzed, ND = not detected

Silicate melts

Apart from mineral inclusions, two-phase inclusions containing silicate melt (solid) and CO_2 (?) phases are also observed in red-purple samples (see Figure 3.24). These inclusions cannot be identified by Raman spectroscopic technique because specific Raman peaks are disappeared (Figure 3.25). Both silicate melt inclusions were analyzed by EPMA technique; consequently, they yield major compositions of SiO_2, Al_2O_3, and CaO, with some minor contents of FeO, MgO, Na_2O, and K_2O (Table 3.9).

Figure 3.24 Photographs viewed under fiber-optic illumination showing rounded two-phase inclusions containing a gas bubble and silicate melt in samples 9TRA073 (left) and 9TRA195 (right).

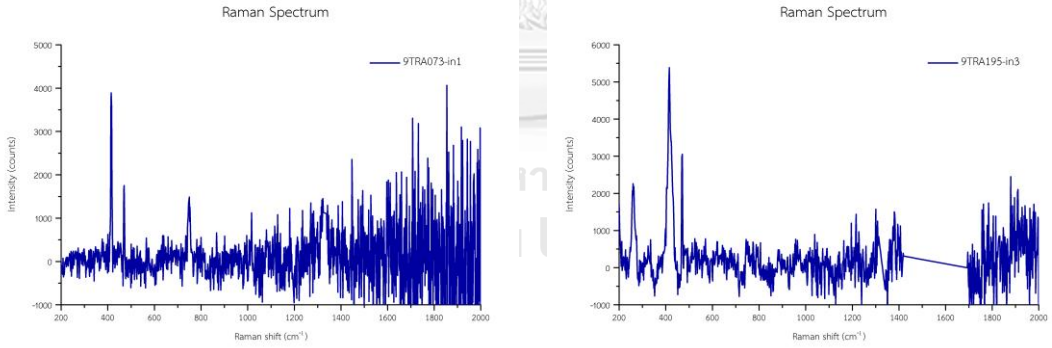

Figure 3.25 The Raman spectra without any specific peak yielded from silicate melt inclusions in the Bo Rai ruby samples 9TRA073 (left) and 9TRA195 (right).

Table 3.9 Chemical compositions (analyzed by EPMA) of melt phase in two-phase inclusions found in red-purple Bo Rai ruby samples.

Mineral phase analysis (wt%)	9TRA073-in1	9TRA195-in3
SiO_2	56.51	48.54
TiO_2	0.10	0.07
Al_2O_3	26.44	31.86
Cr_2O_3	0.03	0.01
CaO	9.65	11.09
FeO	2.00	1.55
MnO	0.02	0.03
MgO	3.19	2.96
K_2O	0.44	1.26
Na_2O	0.75	1.37
Total	99.13	98.74

CHAPTER 4

BO WELU RUBY AND SAPPHIRE

4.1 General characteristics

Rough samples of fifty-eight rubies and forty-one sapphires were collected from Bo Welu gem field, Chanthaburi Province. Most ruby samples are slightly rounded tabular similar to Bo Rai ruby samples. Bo Welu sapphires are mostly characterized by hexagonal crystal habit with basal parting. However, some of them may have been tumbled naturally, yielding disappearance of crystal face. Moreover, surfaces of these rough rubies and sapphires appear to have undertaken corrosion from magma (Figures 4.1a-b and e-h) which this characteristic is generally observed in corundum from basaltic terrains. Some of ruby rough crystals also show triangular growth marks on the surface (Figures 4.1c and d).

Bo Welu corundum samples were polished with at least one window for analyses of mineral inclusion. Ruby samples range widely between 0.07 and 0.72 cts in weight. They are relatively bigger than ruby samples from Bo Rai. Diaphaneity of these polished samples are usually semi-transparent to transparent.

GIA gem set color masters were used for color grading of this sample collection. In general, Bo Welu ruby samples range from medium to slightly purplish red, red-purple, reddish purple and purple (Figure 4.2). Statistically, most of Bo Welu ruby samples are red-purple (44.83%) and reddish purple (44.83%) whereas purplish red and purple samples are rarely found about 3.45% and 6.90%, respectively (Figure 4.3).

For sapphire collection, diaphaneity of the polished samples (0.20 and 6.87 ct) is semi-transparent to transparent and their colors vary widely from blue to yellow and green shades. The polished sapphire samples are, however, predominantly blue to greenish blue or blue-green with medium to dark tones (Figure 4.4) in which 70% of them are greenish blue (Figure 4.5).

Ruby samples usually show weak to weak to moderate red fluorescence under longwave ultraviolet (LWUV) lamp and inert under shortwave ultraviolet (SWUV) lamp. Their refractive indices (RI) range from 1.760 to 1.770 with birefringence of about 0.009 to 0.010. On the other hand, sapphire samples are generally inert under longwave ultraviolet (LWUV) and shortwave ultraviolet (SWUV) lamps. Standard gemological testing yields refractive indices (RI) range of 1.760 to 1.771 with a corresponding birefringence of 0.009 to 0.010. Color, fluorescence, weight, and refractive indices of all samples are summarized in Appendix A.

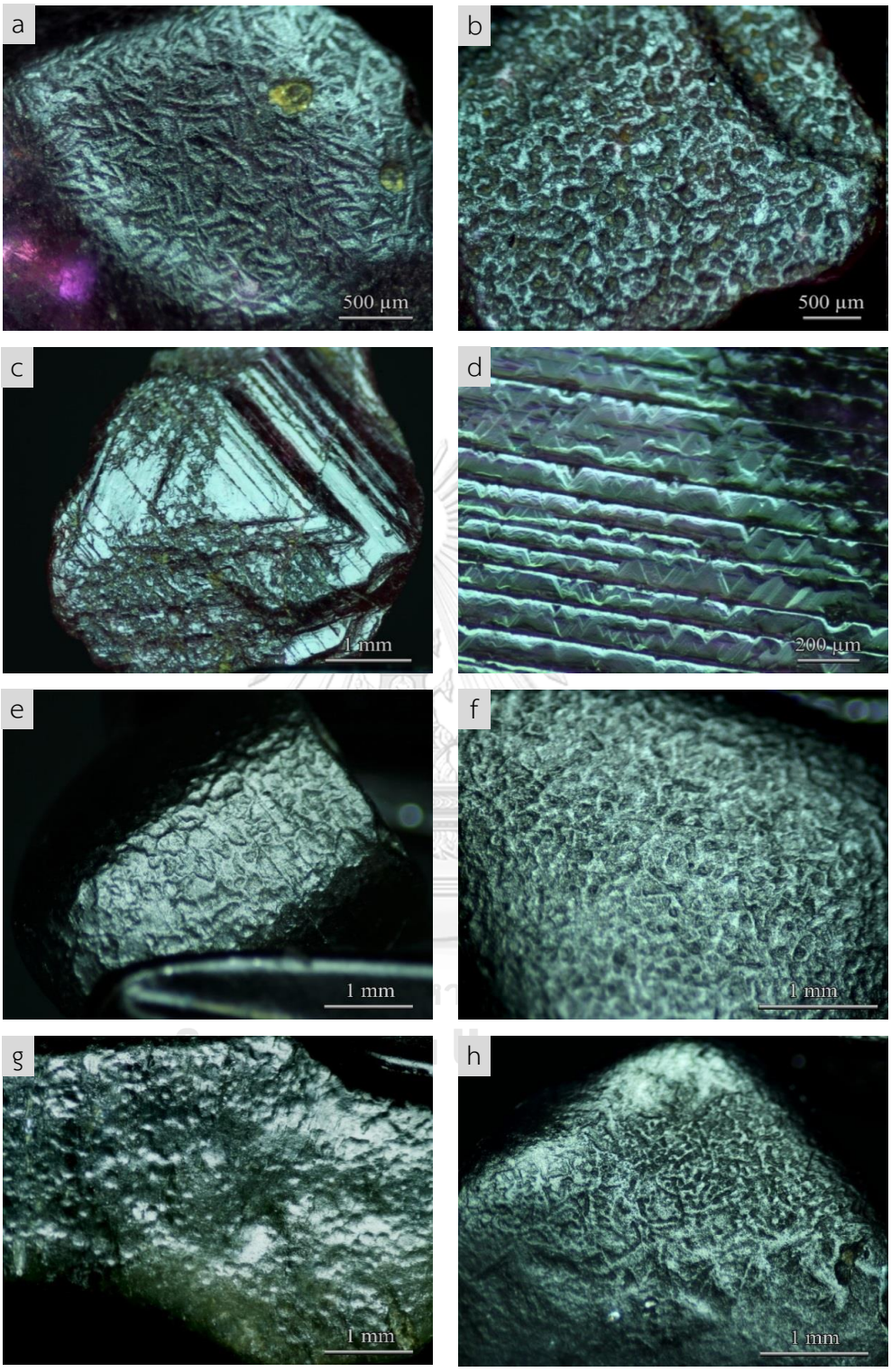

Figure 4.1 Photomicrographs of the surfaces of rough ruby and sapphire samples from Bo Welu gem field taken under reflected light showing: a-b) etched or dissolved features of the ruby surfaces; c-d) triangular growth marks on the surfaces of some ruby samples; e-h) severely etched or dissolved features on the surfaces of some sapphires.

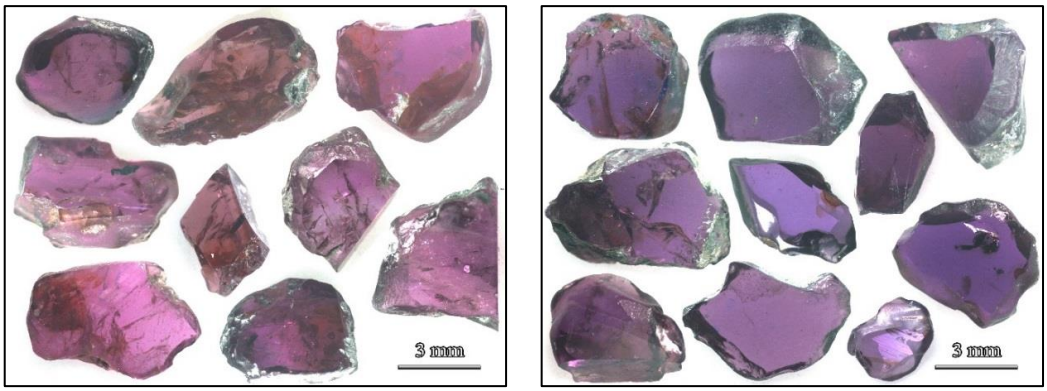

Figure 4.2 Representative polished ruby samples from Bo Welu gem field, showing their colors varied from purplish red to red-purple (left) and reddish purple to purple (right).

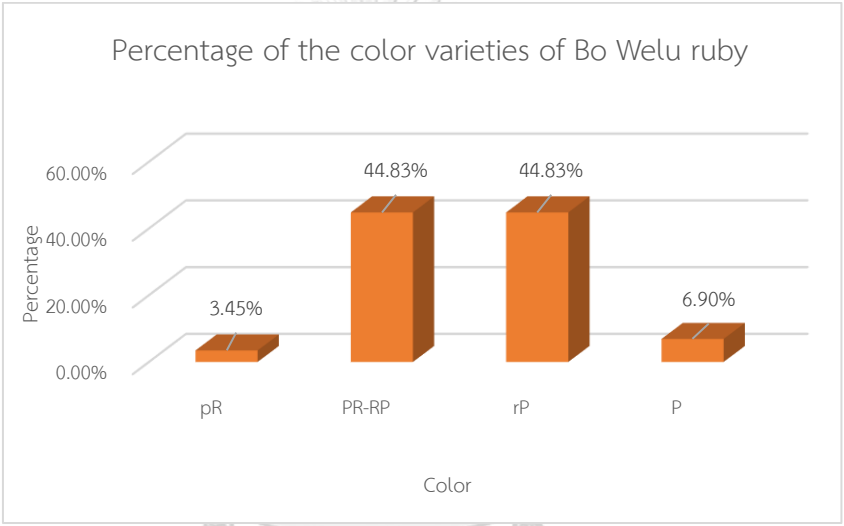

Figure 4.3 Ruby samples collected from Bo Welu gem field contains about 3.45% purplish red, 44.83% red-purple, 44.83% reddish purple and 6.90% purple varieties.

Figure 4.4 Polished sapphires are predominantly blue to greenish blue or blue-green varieties having medium to dark tones.

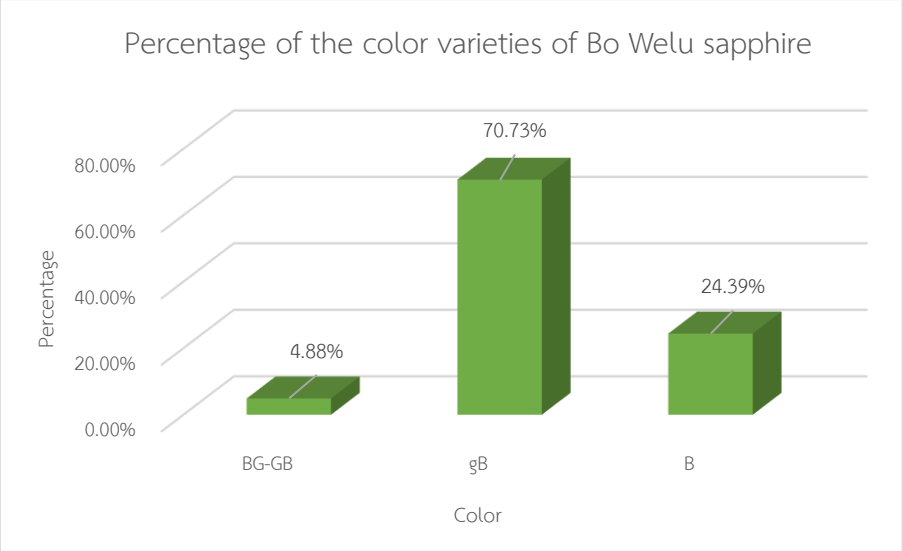

Figure 4.5 Sapphire samples collected from Bo Welu contain about 4.88% blue-green, 70.73% greenish blue, and 24.39% blue varieties.

4.2 Spectroscopic Features

Most mid-infrared absorption spectra of Bo Welu ruby and sapphire reveal similar peaks at approximately 2363 and 2342 cm^{-1} due to CO_2, 2924 and 2852 cm^{-1} due to C-H stretching (Figures 4.6 and 4.7). In addition, a shoulder at about 3170 cm^{-1} and sharp peaks at 3697, 3669, 3652, 3620 cm^{-1} due to kaolinite - $Al_2Si_2O_5(OH)_4$ phase (Figure 4.6, blue spectrum and Figure 4.7, red spectrum) as suggested by Beran and Rossman (2006) and Schwarz et al. (2008). Kaolinite phase is usually present in unheated corundums from various places such as basaltic sapphire from Vietnam as reported by Smith et al. (1995). The kaolinite-related IR spectrum in the ruby samples suggest they are not undergone heat treatment process. Regarding to Bo Welu sapphire, absorption bands peaked at 3309, 3230, 3184 cm^{-1} indicating OH-group (Beran, 1991; Diep, 2015) are additionally observed (Figure 4.7, blue spectrum). More details for series of the absorption bands within the mid-infrared range **(**4000–400 cm^{-1}**)** of representative Bo Welu corundum samples are reported in Appendix C.

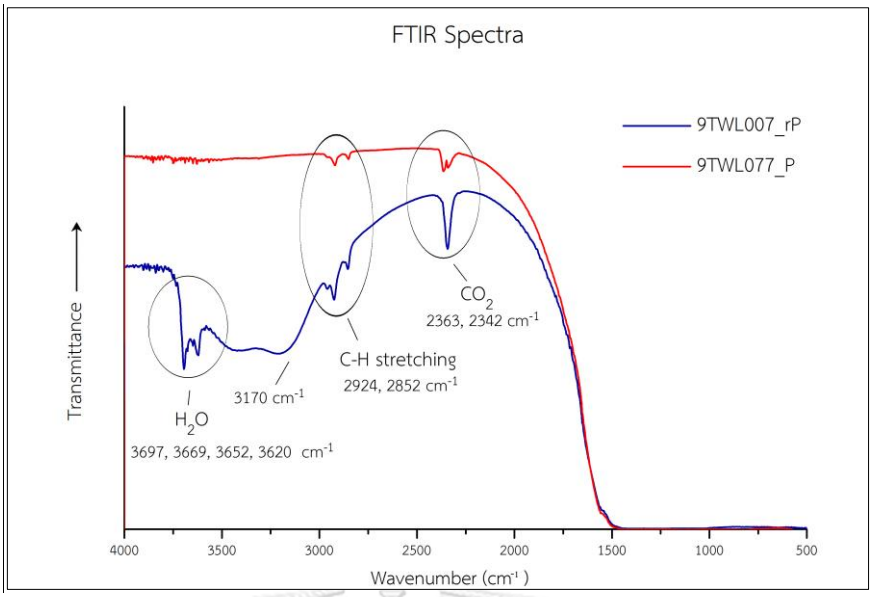

Figure 4.6 Representative Mid-IR spectra of Bo Welu ruby samples revealing absorption peaks at approximately 2363 and 2342 cm^{-1} due to CO_2; 2924 and 2852 cm^{-1} due to C-H stretching (red spectrum of purple (P) sample 9TWL077 and blue spectrum of reddish purple (rP) sample 9TWL007), a shoulder at about 3170 cm^{-1} and sharp peaks at 3697, 3669, 3652, 3620 cm^{-1} due to kaolinite phase (blue spectrum of sample 9TWL007).

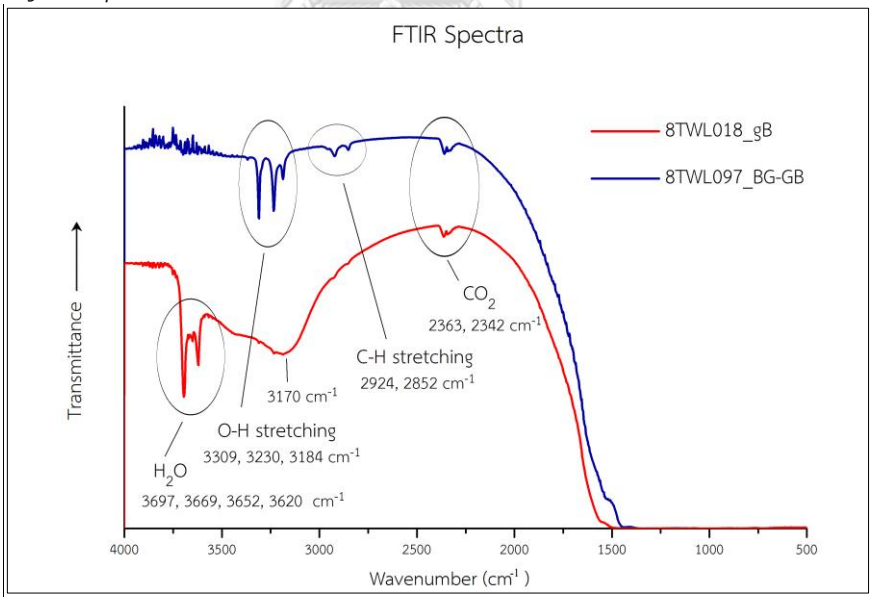

Figure 4.7 Representative Mid-IR spectra of Bo Welu sapphire samples from Bo Welu deposit revealing absorption peaks of CO_2, C-H stretching, and kaolinite similar to ruby samples (see red spectrum of greenish blue (gB) sample 8TWL018). Moreover, sapphire samples always present weak to strong absorption bands peaked at 3309, 3230 and 3184 cm^{-1} indicating OH-group appearances (blue spectra

of blue-green (BG-GB) sample 8TWL097).

Most polished ruby samples are flat tabular in shape which makes it difficult to measure the extraordinary ray (e-ray), hence only ordinary ray (o-ray) was collected in the UV-Vis-NIR range instead. Most absorption peaks, related to high iron content, are recognized around 330 nm in both purplish red and red-purple (see Figure 4.8, blue spectrum) and over-absorption covering this position mostly occurred in reddish purple to purple samples (see Figure 4.8, red spectrum). However, most purplish red and red-purple samples show chromium-dominated absorptions at around 410, 560 and 694 nm causing red color (Figure 4.8, blue spectrum). On the other hand, most reddish purple to purple ruby samples show clearly iron-related absorptions at 387 and 450 nm more intense than chromium-related absorption particularly observed at 410 nm (Figure 4.8, red spectrum); consequently, blue hue influences their body color. More representative UV-Vis-NIR spectra of Bo Welu ruby samples are collected in Appendix D.

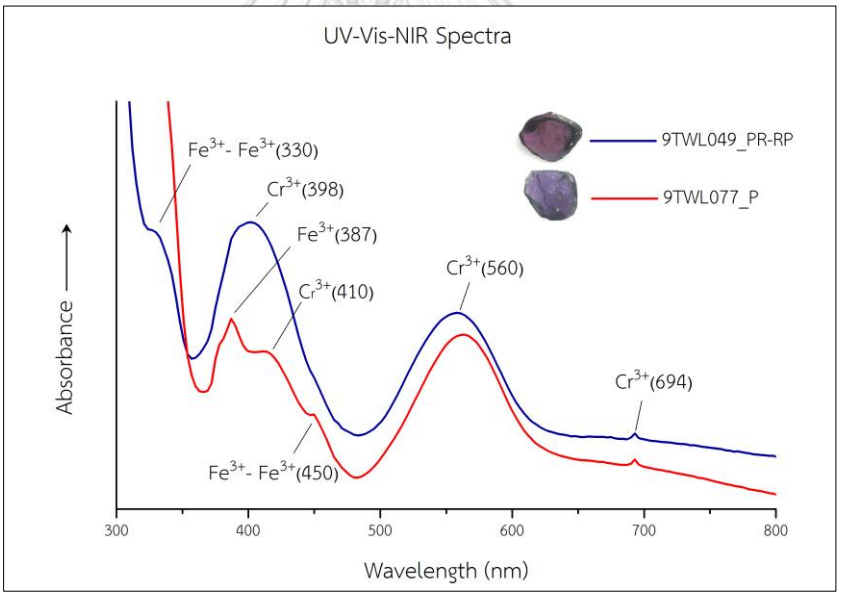

Figure 4.8 Representative UV-Vis-NIR absorption spectra (ordinary rays) of Bo Welu ruby: blue spectrum of red-purple ruby sample 9TWL049 reveals Fe^{3+} related at around 330 nm and chromium-dominated absorptions at around 398, 560 and 694 nm causing red color. Red spectrum of purple ruby sample 9TWL077 reveals obvious Fe^{3+} related with over-absorption around 330 nm including peaks at 387 and 450 nm which intense than Cr^{3+} related absorptions around 410 nm.

All Bo Welu sapphire samples show Fe^{2+}-Fe^{3+} intervalence charge transfer (IVCT) with absorption maxima around 800-900 nm toward the near infrared region which is typical characteristic of blue sapphire from basaltic deposit (Sutherland et

al., 1998b). Blue and greenish blue samples (Figure 4.9, red and blue spectra) are clearly the main cause of blue hue by Fe^{2+}-Ti^{4+} IVCT band around 550 nm as suggested by Schmetzer (1987), Fritsch and Rossman (1987, 1988). On the other hand, blue-green samples usually show Fe^{2+}-Ti^{4+} IVCT band weaker than Fe^{3+} absorption bands in ultraviolet range (peaked at 378 and 387 nm) and in visible region (peaked at 450 nm), causes of yellow hue as suggested by Ferguson and Fielding (1971, 1972) (see Figure 4.9, green spectrum). More representative UV-Vis-NIR spectra of Bo Welu sapphire are reported in Appendix D.

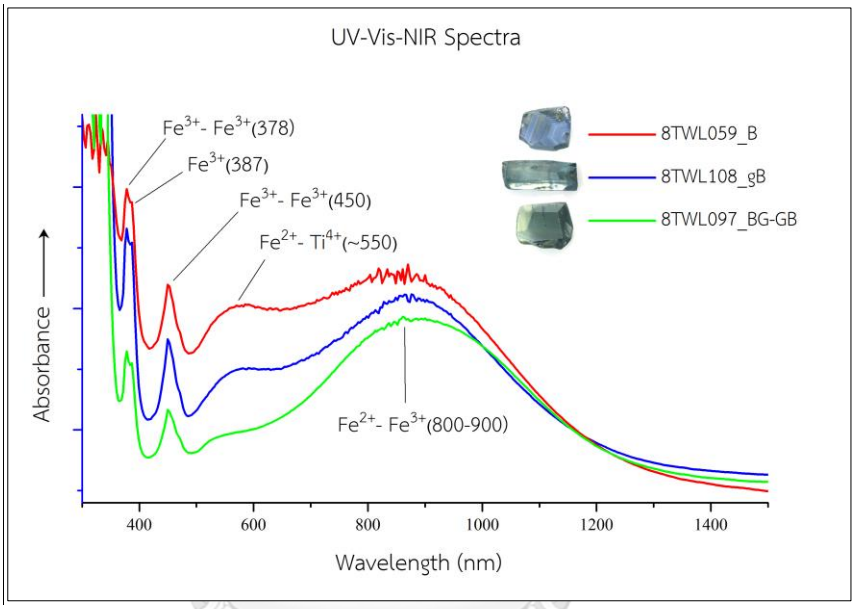

Figure 4.9 Representative UV-Vis-NIR absorption spectra (ordinary rays) of Bo Welu sapphire show Fe^{2+}-Fe^{3+} IVCT absorption around 800-900 nm toward the near infrared region. Blue sapphire sample 8TWL059 (red spectrum) and greenish blue sapphire sample 8TWL108 (blue spectrum) reveal Fe^{2+}-Ti^{4+} IVCT band with peak around 550 nm higher than those blue-green sapphire sample 8TWL097 (green spectrum). Fe^{3+} absorption bands in ultraviolet range (378, 387 nm) and visible region (450 nm) are effect to yellow tone in blue-green sapphire sample.

4.3 Chemical analysis

4.3.1 EDXRF Analyses

Semi-qualitative chemical analysis using Energy Dispersive X-ray Fluorescence (EDXRF) spectrometer was carried on representative ruby and sapphire samples; major composition (Al) and trace element contents (i.e., Fe, Ti, Cr, Ga, and V) are reported in percent oxides and collected in Appendix F. These analyses vary within narrow ranges of individual elements which are quite similar in all color varieties. In

general, ruby samples are chemically characterized within narrow ranges of 0.36-0.89 wt% Fe_2O_3, 0.01- 0.12 wt% TiO_2, 0.06-0.94 wt% Cr_2O_3; moreover, trace amounts of vanadium and gallium are negligible ≤0.01 wt% V_2O_5 and ≤0.02 wt% Ga_2O_3, respectively.

Most samples show Fe_2O_3/TiO_2 and Cr_2O_3/Ga_2O_3 below 100. On the other hand, TiO_2/Ga_2O_3 and Fe_2O_3/Cr_2O_3 ratios are quite low, mostly below 10. Most ruby samples show high Cr and low Ga with Cr_2O_3/Ga_2O_3 ratio above 3 that indicates metamorphic origin similar to ruby from West Pailin as suggested by Sutherland et al. (1998b). However, it should be notified that reddish purple and purple ruby samples apparently contain Cr_2O_3/Ga_2O_3 ratio lower than purplish red and red-purple samples (Figure 4.10 left). On the other hand, all ruby varieties show similarly ratios of TiO_2/Ga_2O_3 (< 10) and Fe_2O_3/Cr_2O_3 (< 7) which cannot be differentiated (Figure 4.10 right).

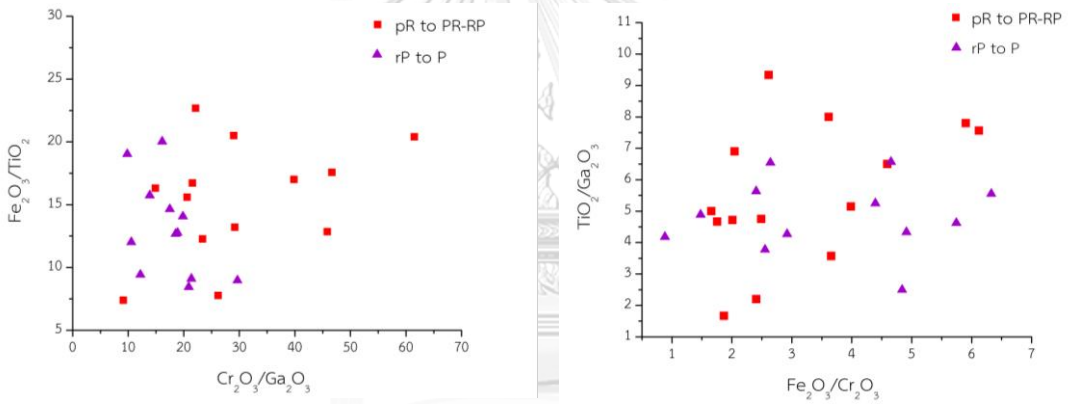

Figure 4.10 Chemical plots of Bo Welu ruby samples showing: (left) Fe_2O_3/TiO_2 mostly below 25 and Cr_2O_3/Ga_2O_3 above 3; (right) TiO_2/Ga_2O_3 below 10 and Fe_2O_3/Cr_2O_3 below 7 ratios which are similarly low.

Semi-qualitative chemical analyses of the representative Bo Welu sapphire samples yield 0.45-1.38 wt% Fe_2O_3, 0.01-0.09 wt% TiO_2, ≤0.01wt% Cr_2O_3, and 0.01-0.05 wt% Ga_2O_3. Most sapphire varieties show low Cr and high Ga with Cr_2O_3/Ga_2O_3 below 1 indicating magmatic origin (Sutherland et al., 1998b) whereas their TiO_2/Ga_2O_3 ratios are similarly below 2 (Figure 4.11 left). On the other hand, higher ratios of Fe_2O_3/TiO_2 and Fe_2O_3/Cr_2O_3 identically present in all sapphire varieties, mostly ranging between 10-100 of Fe_2O_3/TiO_2 ratio and above 50 of Fe_2O_3/Cr_2O_3 ratio (Figure 4.11 right). Therefore, chemical characteristics of blue, greenish blue, and blue-green varieties are unable to be differentiated; this may be caused by multiple color zones in these samples.

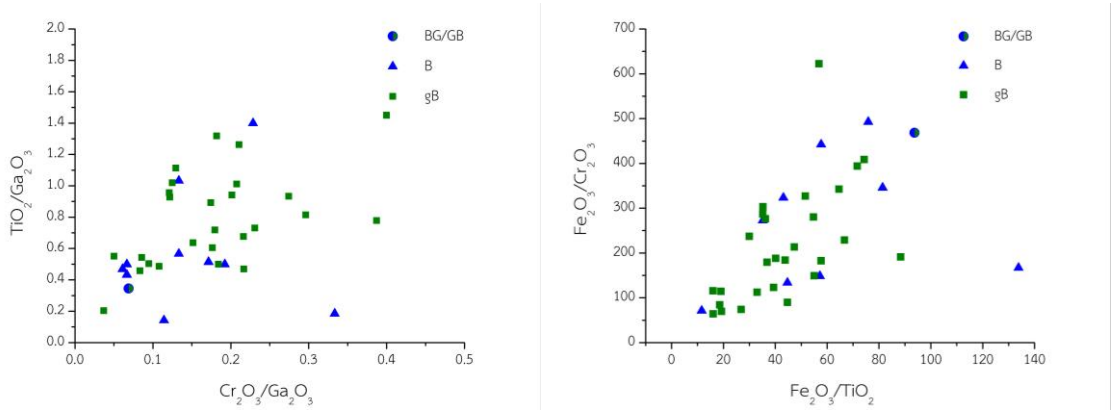

Figure 4.11 Chemical plots of Bo Welu sapphire varieties showing: (left) low ratios of TiO_2/Ga_2O_3 (<2) and Cr_2O_3/Ga_2O_3 (<1); (right) high ratios of Fe_2O_3/TiO_2 (10-100) and Fe_2O_3/Cr_2O_3 (>50).

Table 4.1 Representative semi-quantitative EDXRF analyses Bo Welu ruby.

Element Oxides (wt.%)	purplish red to red-purple samples						reddish purple to purple samples						
	9TWL013	9TWL020	9TWL021	9TWL010	9TWL035	9TWL023	9TWL045	9TWL081	9TWL055	9TWL054	9TWL051	9TWL077	9TWL073
V_2O_5	0.01	ND	0.01	ND	0.01	0.01	0.01	0.01	0.01	ND	0.01	0.01	ND
TiO_2	0.06	*0.03*	0.01	0.03	0.07	0.02	0.04	0.05	0.03	0.04	0.04	0.05	0.05
Al_2O_3	98.93	*99.19*	99.03	99.12	99.11	99.45	99.19	99.15	99.26	99.21	99.08	99.24	99.40
Cr_2O_3	0.27	*0.28*	0.33	0.28	0.26	0.15	0.14	0.14	0.12	0.12	0.13	0.10	0.06
Ga_2O_3	0.01	*0.01*	0.01	0.01	0.01	0.01	0.01	0.01	0.01	0.01	0.01	0.01	ND
Fe_2O_3	0.72	*0.49*	0.61	0.56	0.54	0.36	0.62	0.65	0.57	0.61	0.74	0.60	0.48
Total	100.00	100.00	100.00	100.00	100.00	100.00	100.00	100.00	100.00	100.00	100.00	100.00	100.00

ND = not detected

Table 4.2 Representative semi-quantitative EDXRF analyses Bo Welu sapphire.

Element Oxides (wt.%)	gray samples	blue samples					greenish blue samples				blue-green samples	
	8TWL016	8TWL114	8TWL116	8TWL068	8TWL112	8TWL113	8TWL104	8TWL028	8TWL053	8TWL106	8TWL097	8TWL103
V_2O_5	0.01	ND	ND	ND	ND	ND	ND	0.01	ND	0.01	ND	0.01
TiO_2	0.03	0.05	0.01	0.01	0.01	0.02	0.03	0.02	0.02	0.09	0.01	0.04
Al_2O_3	99.38	99.33	98.81	99.28	99.30	98.57	99.47	98.89	98.76	98.67	99.02	98.68
Cr_2O_3	0.01	0.01	0.01	ND	ND	ND	0.01	0.01	ND	ND	ND	ND
Ga_2O_3	0.02	0.03	0.03	0.03	0.03	0.03	0.04	0.03	0.04	0.04	0.03	0.05
Fe_2O_3	0.56	0.57	1.15	0.67	0.65	1.38	0.45	1.03	1.18	1.19	0.94	1.23
Total	99.97	100.00	100.00	100.00	100.00	100.00	100.00	100.00	100.00	100.00	100.00	100.00

ND = not detected

4.3.2 EPMA Analyses

Electron Probe Micro-Analyzer (EPMA) was used to analyze representative rubies and sapphires from Bo Welu; these data should give more accurate mineral chemistry of these samples. Apart from major Al component and main trace elements (e.g., Fe, Ti, Cr, Ga, V), Si, Mg, and Mn can also be detected. All the details of EPMA analyses are collected in Appendix G and selectively summarized in Tables 4.3 and 4.4.

In general, ruby samples show high contents of iron (0.29-0.78 wt% Fe_2O_3), traces of titanium (0.01- 0.13 wt% TiO_2), and chromium (0.03-1.29 wt% Cr_2O_3). Although, Si, V, Ga, Mg, and Mn concentrations can be detected, many of them are below the detection limits. The highest Si, V, Ga, Mg, and Mn contents are recorded at 0.15 wt% SiO_2, 0.02 wt% V_2O_3, 0.18 wt% Ga_2O_3, 0.07 wt% MgO, and 0.07 wt% MnO, respectively.

Most ruby samples show Fe_2O_3/TiO_2, Cr_2O_3/Ga_2O_3, ratios below 100 whereas TiO_2/Ga_2O_3 and Fe_2O_3/Cr_2O_3 ratios fall below 10 which these ratios are similar to those found in Bo Rai ruby. In addition, Ga_2O_3/MgO below 3 and Fe_2O_3/MgO below 100 may suggest metamorphic origin (Peucat et al., 2007; Uher et al., 2012).

Regarding to sapphire samples, some of trace element analyses, of Si, V, Cr, Ga, Mg, and Mn are below the detection limits. The highest Si, Ti, V, Cr, Ga, Mg, and Mn contents are recorded at 0.08 wt% SiO_2, 0.23 wt% TiO_2, 0.03 wt% V_2O_3, 0.07 wt% Cr_2O_3, 0.26 wt% Ga_2O_3, 0.02 wt% MgO, and 0.05 wt% MnO, respectively. For iron and TI contents (the main trace element) range from 0.51 to 1.92 wt% Fe_2O_3 and 0.01 to 0.09 wt% TiO_2, respectively.

Most sapphire samples show Fe_2O_3/TiO_2 below 100 whereas TiO_2/Ga_2O_3 and Cr_2O_3/Ga_2O_3, ratios are below 1. These characteristics indicate sapphire from basaltic terrains (Sutherland et al., 1998a). In addition, Fe_2O_3/Cr_2O_3 over 20, Ga_2O_3/MgO below 10, and Fe_2O_3/MgO below 100 are also recognized. However, chemical compositions of Bo Welu sapphires are quite similar in all varieties, i.e., blue, greenish blue, and blue-green samples; these may relate to their obvious color zones.

Table 4.3 Representative EPMA analyses of Bo welu ruby.

Element Oxides (wt.%)	purplish red to red-purple samples						reddish purple to purple samples					
	9TWL011	9TWL019	9TWL132	9TWL136	9TWL154	9TWL172	9TWL046	9TWL105	9TWL114	9TWL143	9TWL152	9TWL174
SiO_2	0.10	0.10	0.08	0.05	0.12	0.05	0.11	0.11	0.15	0.15	0.04	0.03
TiO_2	0.02	0.01	0.04	0.03	0.01	0.04	0.04	0.03	0.03	0.04	0.04	0.10
Al_2O_3	97.21	97.50	97.98	99.03	97.74	97.52	97.81	98.55	97.41	97.70	97.46	98.60
Cr_2O_3	1.08	0.23	0.25	0.34	0.76	0.45	0.23	0.08	0.22	0.13	0.14	0.25
Ga_2O_3	0.07	0.01	0.08	0.03	ND	ND	0.18	0.01	0.09	0.12	0.02	0.01
V_2O_3	ND	0.01	ND	ND	0.01	0.02	0.01	ND	ND	0.01	0.02	ND
FeO total	0.51	0.78	0.29	0.45	0.48	0.60	0.52	0.51	0.53	0.70	0.77	0.64
MnO	0.02	0.02	ND	0.01	0.05	ND	0.05	0.03	0.02	0.03	0.02	0.07
MgO	ND	ND	ND	ND	ND	ND	ND	0.03	ND	0.04	ND	ND
Total	99.01	98.66	98.72	99.94	99.17	98.68	98.95	99.35	98.45	98.92	98.51	99.70
Fe_2O_3/TiO_2	25.50	78.00	7.25	15.00	48.00	15.00	13.00	17.00	17.67	17.50	19.25	6.40
Cr_2O_3/Ga_2O_3	15.43	23.00	3.13	11.33	-	-	1.28	8.00	2.44	1.08	7.00	25.00
TiO_2/Ga_2O_3	0.29	1.00	0.50	1.00	-	-	0.22	3.00	0.33	0.33	2.00	10.00
Fe_2O_3/Cr_2O_3	0.47	3.39	1.16	1.32	0.63	1.33	2.26	6.38	2.41	5.38	5.50	2.56
3 (O)	25.50	78.00	7.25	15.00	48.00	15.00	13.00	17.00	17.67	17.50	19.25	6.40
Si	0.002	0.002	0.001	0.001	0.002	0.001	0.002	0.002	0.003	0.003	0.001	0.001
Ti	0.000	0.000	0.001	0.000	0.000	0.001	0.001	0.000	0.000	0.001	0.001	0.001
Al	1.977	1.986	1.990	1.989	1.982	1.986	1.986	1.990	1.987	1.985	1.988	1.987
Cr	0.015	0.003	0.003	0.005	0.010	0.006	0.003	0.001	0.003	0.002	0.002	0.003
Ga	0.001	0.000	0.001	0.000	0.000	0.000	0.002	0.000	0.001	0.001	0.000	0.000
V	0.000	0.000	0.000	0.000	0.000	0.000	0.000	0.000	0.000	0.000	0.000	0.000
Fe^{3+}	0.006	0.010	0.002	0.005	0.005	0.007	0.006	0.006	0.005	0.008	0.010	0.008
Fe^{2+}	0.002	0.002	0.002	0.001	0.001	0.001	0.002	0.001	0.003	0.002	0.001	0.001
Mn	0.000	0.000	0.000	0.000	0.001	0.000	0.001	0.000	0.000	0.000	0.000	0.001
Mg	0.000	0.000	0.000	0.000	0.000	0.000	0.000	0.001	0.000	0.001	0.000	0.000
Total*	2.002	2.003	2.001	2.002	2.002	2.002	2.002	2.002	2.002	2.003	2.003	2.003

ND = not detected

Table 4.4 Representative EPMA analyses of Bo Welu sapphire.

Element Oxides (wt.%)	gray samples	greenish blue samples							blue-green samples			
	8TWL016	8TWL002	8TWL028	8TWL046	8TWL093	8TWL099	8TWL101	8TWL111	8TWL059	8TWL112	8TWL113	8TWL114
SiO_2	0.01	ND	0.01	ND	0.02	0.04	0.03	0.05	0.05	0.05	0.04	0.07
TiO_2	0.03	0.08	0.02	0.01	0.01	0.02	ND	0.02	0.10	0.05	0.02	0.01
Al_2O_3	99.16	99.29	98.03	98.24	98.39	98.70	98.85	98.77	98.92	97.74	98.72	98.42
Cr_2O_3	ND	ND	0.03	ND	0.04	0.02	ND	0.01	ND	ND	0.01	0.02
Ga_2O_3	0.15	ND	0.05	0.26	ND	0.02	0.03	0.09	ND	ND	0.07	ND
V_2O_3	0.01	0.01	0.03	0.01	ND	ND	ND	ND	ND	ND	0.01	ND
FeO total	0.71	1.34	1.04	1.65	1.30	0.55	1.02	1.11	1.05	0.76	1.65	0.65
MnO	ND	ND	0.02	ND	ND	ND	0.03	ND	ND	ND	ND	ND
MgO	ND	ND	ND	ND	ND	ND	ND	ND	0.01	0.02	ND	ND
Total	100.05	100.72	99.23	100.18	99.76	99.35	99.95	100.05	100.12	98.61	100.51	99.17
Fe_2O_3/TiO_2	28.44	16.75	52.00	165.00	130.00	27.50	-	55.50	10.50	15.20	82.50	65.00
Cr_2O_3/Ga_2O_3	0.00	-	0.60	0.00	-	1.00	0.00	0.11	-	-	0.14	-
TiO_2/Ga_2O_3	0.17	-	0.40	0.04	-	1.00	0.00	0.22	-	-	0.29	-
Fe_2O_3/Cr_2O_3 (O)	-	-	34.67	-	32.50	27.50	-	111.00	-	-	165.00	32.50
Si	0.000	0.000	0.000	0.000	0.000	0.001	0.001	0.001	0.001	0.001	0.001	0.001
Ti	0.000	0.001	0.000	0.000	0.000	0.000	0.000	0.000	0.001	0.001	0.000	0.000
Al	1.991	1.986	1.988	1.981	1.986	1.993	1.989	1.987	1.987	1.990	1.982	1.992
Cr	0.000	0.000	0.000	0.000	0.001	0.000	0.000	0.000	0.000	0.000	0.000	0.000
Ga	0.002	0.000	0.001	0.003	0.000	0.000	0.000	0.001	0.000	0.000	0.001	0.000
V	0.000	0.000	0.000	0.000	0.000	0.000	0.000	0.000	0.000	0.000	0.000	0.000
Fe^{3+}	0.010	0.018	0.015	0.023	0.018	0.007	0.014	0.015	0.013	0.010	0.022	0.008
Fe^{2+}	0.000	0.001	0.000	0.000	0.001	0.001	0.000	0.001	0.002	0.001	0.001	0.001
Mn	0.000	0.000	0.000	0.000	0.000	0.000	0.000	0.000	0.000	0.000	0.000	0.000
Mg	0.000	0.000	0.000	0.000	0.000	0.000	0.000	0.000	0.000	0.001	0.000	0.000
Total*	2.003	2.006	2.005	2.008	2.006	2.002	2.005	2.005	2.004	2.003	2.008	2.003

ND = not detected

4.4 Internal Features

Bo Welu ruby: The significant internal features of ruby samples examined by the binocular microscope are healed fractures (fingerprints) (Figure 4.12a), intersection of needle-like inclusions (Figure 4.12b), network of tiny crystals (Figure 4.12c), and unusual anhedral crystal surrounded by tension crack (Figure 4.12d). In addition, crystal inclusions with equatorial thin films are also commonly observed in Bo Welu ruby (Figure 4.12e-f) as well as many two-phase (S-G) inclusions are usually captured using a combination of fiber-optic and darkfield illumination (Figure 4.12g-j).

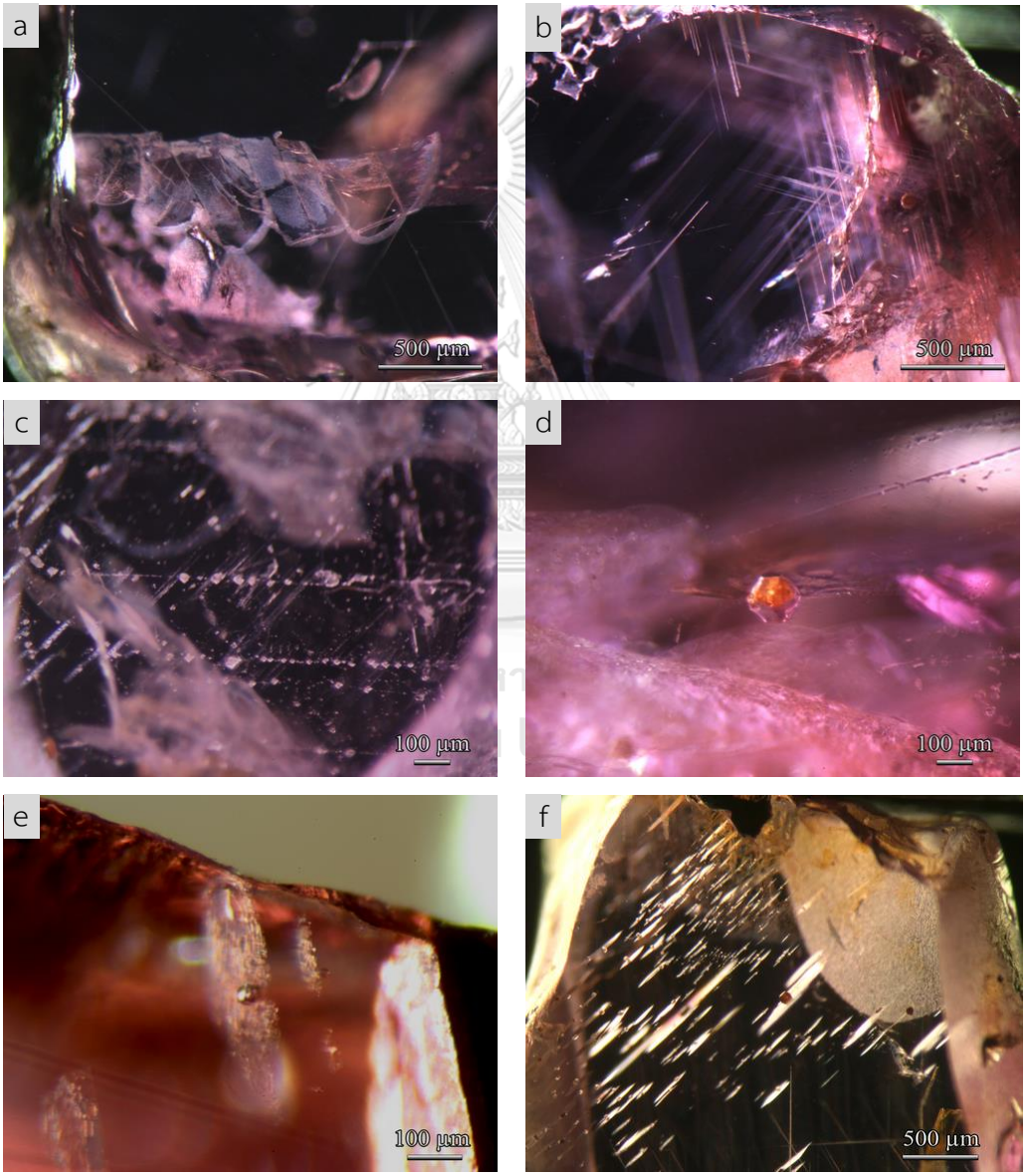

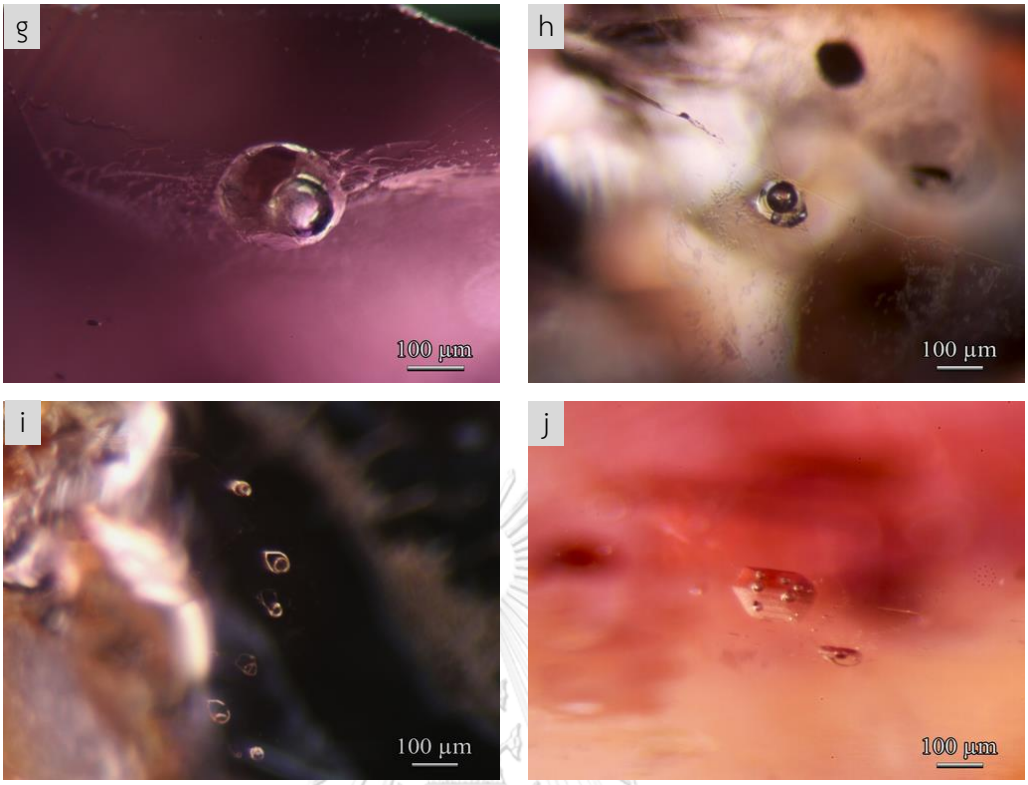

Figure 4.12 Photos of Bo Welu ruby samples viewed using darkfield illumination: a) healed fractures (fingerprints) (sample 9TWL045); b) intersection of needle-like inclusions (sample 9TWL045); c) a network of tiny crystals (sample 9TWL049); d) unusual anhedral crystal surrounded by tension crack (sample 9TWL039); crystal with thin film inclusions in samples 9TWL013 (e) and 9TWL141 (f); two-phase (S-G) inclusions in samples 9TWL054 (g), 9TWL073 (h), and 9TWL093 (i and j).

Bo Welu sapphire: The most common internal features are clearly strong color zoning (Figure 4.13a) and many fine minute particles (Figure 4.13b-d). A few samples also show orange crystal with tail of minute particles (Figure 4.13e). Network of silk and thin-film are visible under darkfield illumination (Figure 4.13f). Moreover, healed fractures (fingerprints, Figure 4.13g) and columbite with coarse crystal and acicular crystal can be captured using a combination of fiber-optic and brightfield illumination (Figure 4.13h).

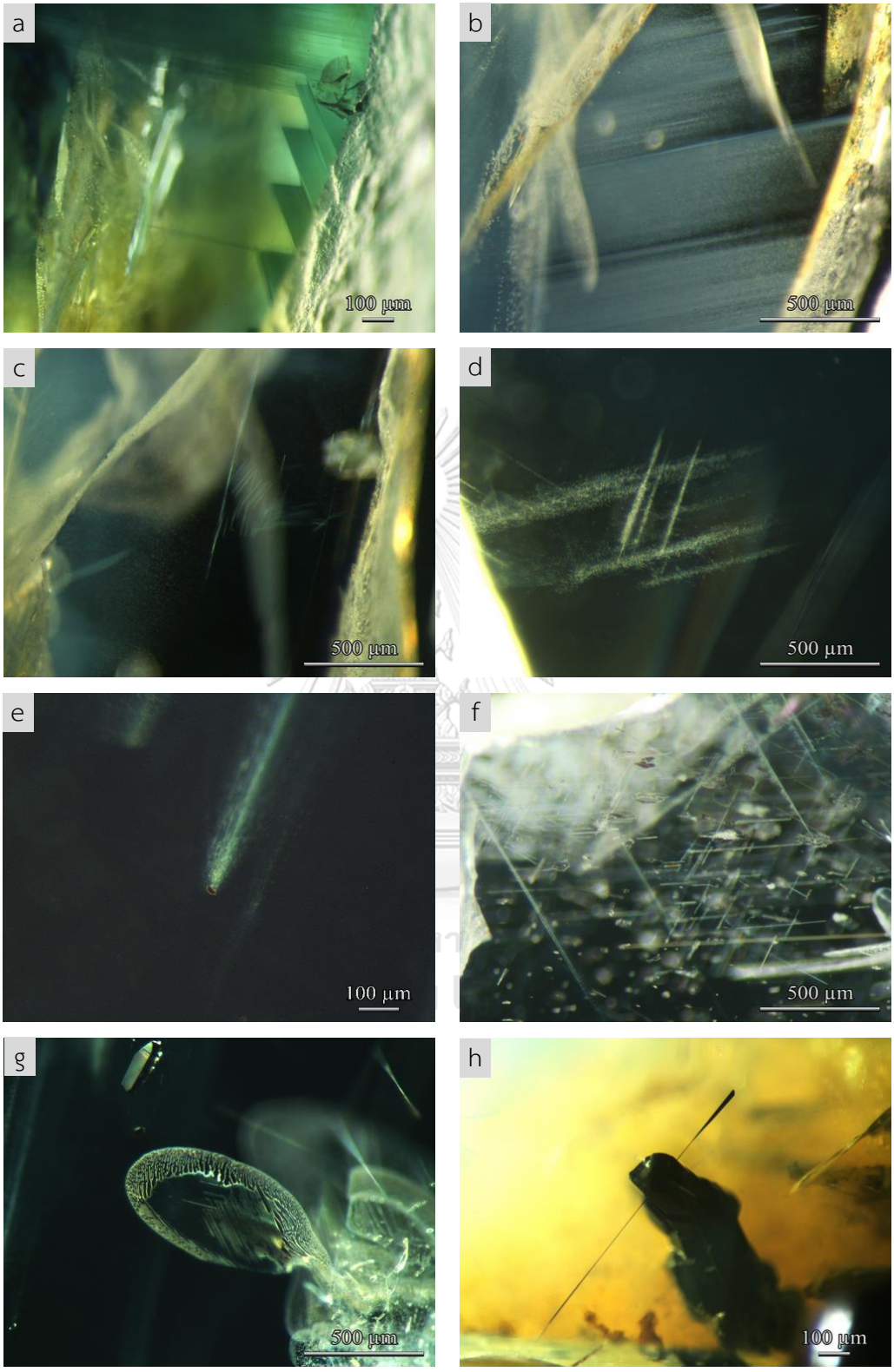

Figure 4.13 Photographs of common internal features found in Bo Welu sapphire: a) strong color zoning (sample 8TWL036); various fine minute particles sample 8TWL067 (b and c), and sample 8TWL096 (d); e) orange crystal with tail of minute

particles (sample 8TWL096); f) network of silk and thin film under dark field illumination (sample 8TWL074). (g) healed fractures (fingerprints) in sample 8TWL096 and (h) columbite crystal (identified by Raman) sample 8TWL114 captured using a combination of fiber-optic and bright field illumination.

4.5 Mineral Inclusion

For analyses of mineral inclusions, both ruby and sapphire samples were polished in several steps until the target mineral inclusions expose onto the surface prior to identification using Raman spectroscope and Electron Probe Micro-Analyzer (EPMA). All Raman spectra are collected in Appendix E and selectively summarized in Tables 4.5 and 4.6. Photomicrographs of these mineral inclusions are also taken and collected in Appendix B. Representative mineral inclusions were subsequently analyzed by EPMA for mineral chemical investigation. Their analytical data are reported in Appendix H and some representative analyses of crucial mineral inclusions are summarized in Tables 4.7 to 4.16. Details of mineral chemistry of these inclusions are reported below.

Table 4.5 Summary of mineral inclusions in Bo Welu ruby, initially identified by Raman and EPMA.

Mineral group	Mineral inclusions	Frequency	Purplish red	Red-purple	Reddish purple	Purple
Silicates	Garnet	**	-	✓	✓	✓
	Sillimanite	*	-	-	✓	-
	Pyroxene	***	✓	✓	✓	-
	Sapphirine	*	--	✓	-	-
	Nepheline	*	-	✓	✓	-
	Quartz	*	-	✓	-	-
	Alkali feldspars	*	-	-	✓	-
	Plagioclase	**	-	✓	✓	-
Oxides	Spinel	**	-	✓	-	-
Sulphates	Anhydrite	*	-	-	✓	-
Sulphide	Pyrrhotite	**	-	✓	✓	✓

*** often found in this study, ** moderately found in this study, * rarely found in this study

Table 4.6 Summary of mineral inclusions in Bo Welu sapphire, initially identified by Raman and EPMA.

Mineral group	Mineral inclusions	Frequency	Blue	Greenish blue	Blue-Green
Silicates	Zircon	**	✓	✓	-
	Alkali feldspar	***	✓	✓	✓
Phosphates	Monazite	**	✓	✓	-
Niobium	Columbite	**	✓	✓	✓
Sulphide	Pyrrhotite	*	-	✓	-

*** often found in this study, ** moderately found in this study, * rarely found in this study

Garnet

Most garnet inclusions are observed in red-purple, reddish purple and purple ruby samples from Bo Welu are subhedral shape which are either colorless or pale purplish red (Figure 4.14a-d). Some garnet inclusions are surrounded by tension cracks (Figure 4.14d). More photographs of garnet inclusions are reported in Appendix B. The representative Raman spectrum is shown in Figure 4.15. More Raman spectra are collected in Appendix E.

Chemical composition of garnet inclusions was analyzed by Electron Probe Micro-Analyzer (EPMA) which results are reported in Appendix H. Most garnet inclusions in Bo Welu ruby samples are chemically characterized by pyrope-rich composition ($py_{56-66}alm_{11-21}grs_{20-24}$) with very low chromium content. Their $Mg/(Mg+Fe^{2+})$ ratios vary from 0.72 to 0.86 (Table 4.7). These garnet inclusion are similar to garnet inclusion in Bo Rai ruby, previously reported by Sutthirat et al. (2001) and Saminpanya and Sutherland (2011).

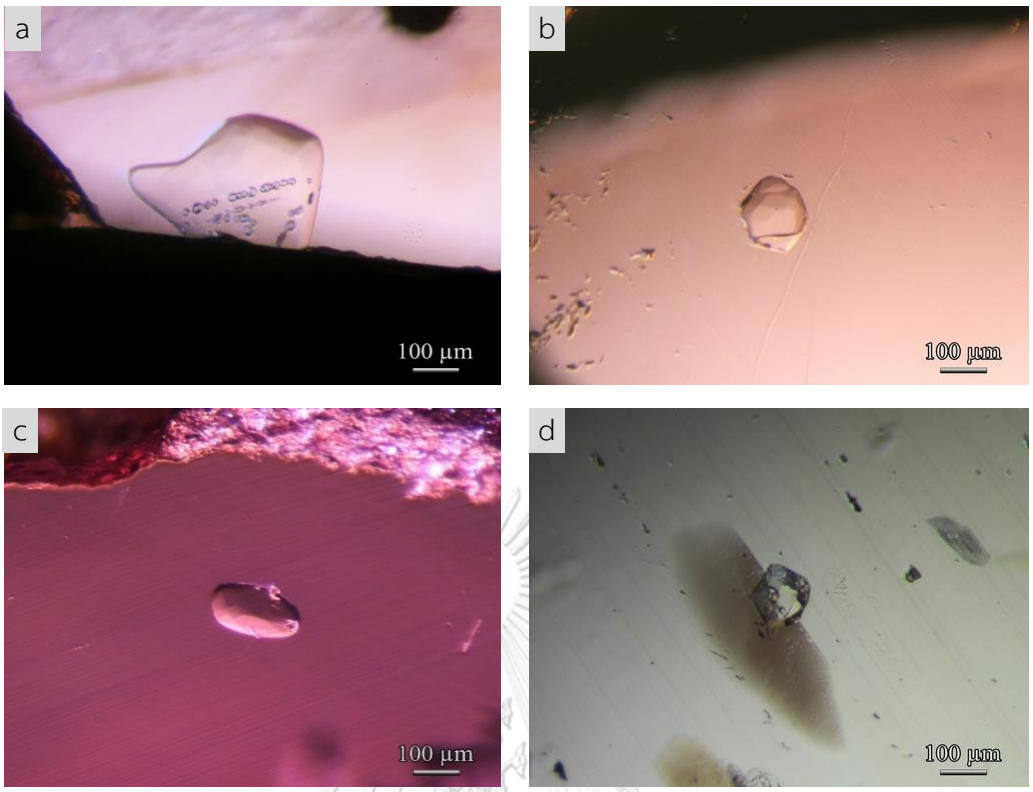

Figure 4.14 Photographs of garnet inclusions taken under a combination of a fiber-optic light and brightfield illumination: irregular-shaped garnet inclusions observed in samples 9TWL059 (a), 9TWL092 (b), and 9TWL089 (c); a garnet inclusion surrounded by tension crack observed in sample 9TWL158 (d).

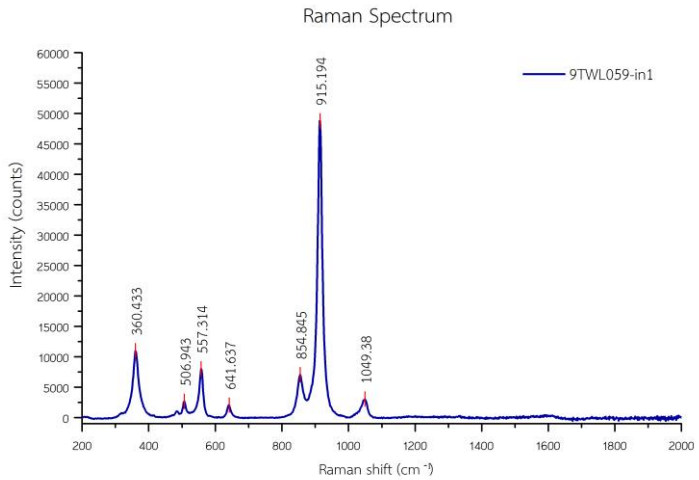

Figure 4.15 The representative Raman spectrum of garnet inclusion in Bo Welu ruby sample 9TWL059.

Table 4.7 Representative EPMA analyses of garnet inclusions in Bo Welu ruby samples.

Mineral phase analysis (wt%)	PR-RP		rP	P	
	9TWL059-in1	9TWL089-in1	9TWL087-in1	9TWL092-in1	9TWL092-in2
SiO_2	42.03	43.16	42.47	42.14	42.57
TiO_2	0.07	0.01	0.04	0.08	0.10
Al_2O_3	23.26	23.62	23.20	22.81	23.17
Cr_2O_3	0.02	0.11	ND	0.10	0.05
FeO	9.71	6.59	8.67	10.28	10.33
MnO	0.20	0.17	0.18	0.25	0.19
MgO	15.82	17.53	16.34	15.49	15.21
CaO	8.85	8.76	8.21	8.29	8.17
K_2O	0.01	ND	ND	ND	0.02
Na_2O	ND	0.01	ND	0.04	0.02
Total	99.98	99.96	99.10	99.47	99.82
12 (O)					
Si	3.026	3.057	3.060	3.053	3.067
Ti	0.004	0.001	0.002	0.004	0.005
Al	1.974	1.972	1.970	1.947	1.967
Cr	0.001	0.006	0.000	0.006	0.003
Fe^{3+}	0.000	0.000	0.000	0.000	0.000
Fe^{2+}	0.584	0.390	0.522	0.623	0.622
Mn	0.012	0.010	0.011	0.015	0.012
Mg	1.698	1.851	1.755	1.673	1.633
Ca	0.683	0.665	0.633	0.643	0.631
K	0.001	0.000	0.000	0.000	0.002
Na	0.000	0.001	0.000	0.005	0.003
Total*	7.983	7.954	7.953	7.969	7.945
ΣR^{2+}	2.977	2.916	2.922	2.954	2.898
ΣR^{3+}	1.979	1.979	1.972	1.957	1.975
Mg/(Mg+Fe^{2+})	0.744	0.826	0.771	0.729	0.724
Alm% (Fe^{2+})	19.64	13.39	17.88	21.08	21.47
Pyr% (Mg)	57.03	63.47	60.06	56.62	56.37
Gro% (Ca)	22.87	22.72	21.66	21.67	21.67
Sps% (Mn)	0.41	0.35	0.38	0.52	0.40
Uv%	0.01	0.07	0.00	0.06	0.03
And%	0.00	0.00	0.00	0.00	0.00

ΣR^{2+}= Fe^{2+}+Mn+Mg+Ca , ΣR^{3+}= Fe^{3+}+Ti+Al+Cr

ND = not detected

Sillimanite

Sillimanite inclusion, observed in reddish purple ruby 9TWL152 (Figure 4.16), is subhedral shape with a hexagonal habit and surrounded by healed fractures. Raman spectra of this sillimanite (Figure 4.17) are unclearly determinable, its chemical composition can be used to support. EPMA analyses of sillimanite are present in Table 4.8. It contains major contents of SiO_2 and Al_2O_3 with traces of FeO and MgO. This is the first report of sillimanite inclusion in Siam ruby. Sillimanite inclusion may suggest high temperature (over 550°C) of crystallization related to Bo Welu ruby.

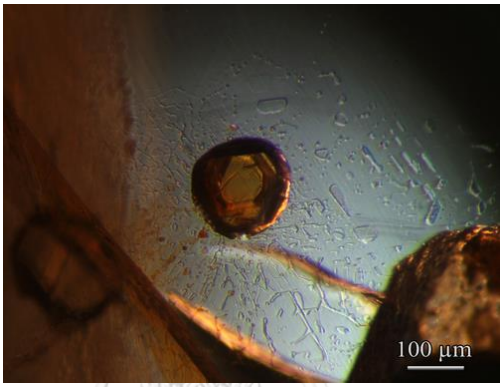

Figure 4.16 Sillimanite inclusion, viewed under dark field illumination, shows anhedral shape with hexagonal habit; it is surrounded by healed fractures (sample 9TWL152).

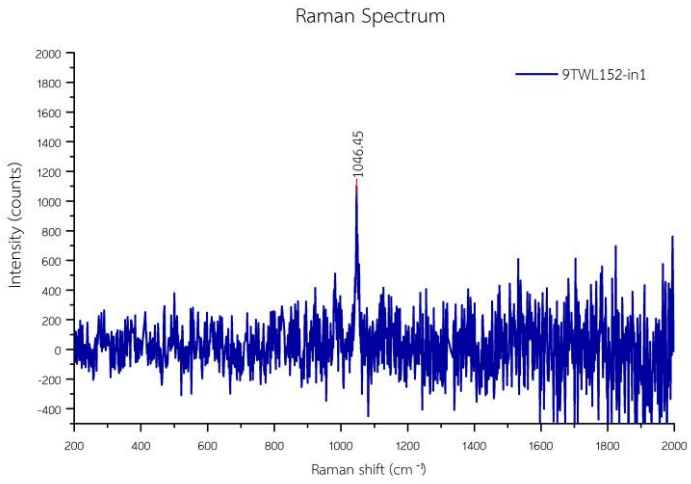

Figure 4.17 Raman spectrum of this sillimanite inclusion in Bo Welu ruby sample 9TWL152.

Table 4.8 Representative EPMA analyses of spinel, sillimanite, quartz, sapphirine, and nepheline inclusions in Bo Welu ruby samples.

Mineral phase analysis (wt%)	Spinel				Quartz	Sapphirine	Sillimanit	Nepheline			Anhydrite	Sulphide
	PR-RP			rP	PR-RP	PR-RP	rP	PR-RP	rP		rP	rP
	9TWL154-in2*	9TWL019-in2*	9TWL085-in2	9TWL180-in2*	9TWL095-in2	9TWL026-in1	9TWL152-in1	9TWL026-in1	9TWL012-in1	9TWL153-in1	9TWL096-in1	9TWL096-in2
SO_3	NA	NA	NA	NA	NA	NA	NA	NA	NA	NA	55.62	53.72
SiO_2	0.10	0.04	0.09	0.06	99.61	13.97	36.38	43.54	47.61	45.99	0.03	0.02
TiO_2	2.51	0.43	0.00	1.09	0.00	0.00	0.01	0.02	0.00	0.07	0.00	0.01
Al_2O_3	63.37	64.71	67.46	64.25	0.05	61.06	61.62	35.61	30.79	34.02	0.03	0.03
Cr_2O_3	1.67	0.25	0.38	0.13	0.00	0.31	0.00	0.00	0.00	0.00	0.00	0.09
FeO total	10.61	13.11	11.81	13.50	0.28	3.32	1.43	0.27	0.22	0.15	0.02	44.97
MnO	0.24	0.09	0.27	0.10	0.00	0.03	0.00	0.00	0.00	0.00	0.06	0.00
MgO	20.59	20.19	19.96	20.56	0.00	19.62	0.50	0.00	0.20	0.05	0.01	0.01
NiO	NA	NA	NA	NA	NA	0.41	NA	NA	NA	NA	NA	NA
ZnO	0.04	0.09	NA	0.04	NA	NA	NA	NA	NA	NA	NA	NA
CaO	0.01	0.00	0.03	0.04	0.01	0.14	0.15	4.29	4.67	3.09	44.23	1.12
K_2O	0.00	0.00	0.00	0.02	0.00	0.02	0.01	3.33	1.32	1.84	0.00	0.02
Na_2O	0.00	0.00	0.00	0.03	0.00	0.00	0.00	12.82	15.10	14.80	0.02	0.00
Total	99.14	98.91	100.00	99.82	99.95	98.87	100.10	99.88	99.91	100.01	100.00	99.99
Formula	4 (O)	4 (O)	4 (O)	4 (O)	2 (O)	20 (O)	20 (O)	4 (O)	4 (O)	4 (O)	4 (O)	-
S	-	-	-	-	-	-	-	-	-	-	0.966	1.008
Si	0.002	0.001	0.002	0.002	0.998	1.655	3.958	1.028	1.116	1.074	0.001	0.000
Ti	0.048	0.008	0.000	0.021	0.000	0.000	0.001	0.000	0.000	0.001	0.000	0.000
Al	1.893	1.948	1.990	1.921	0.001	8.527	7.902	0.991	0.851	0.936	0.001	0.001
Cr	0.033	0.005	0.007	0.003	0.000	0.029	0.000	0.000	0.000	0.000	0.000	0.002
Fe^{3+}	0.000	0.038	0.000	0.044	0.002	0.196	0.130	0.000	0.000	0.000	0.000	0.940
Fe^{2+}	0.225	0.242	0.247	0.242	0.000	0.133	0.000	0.005	0.004	0.003	0.000	
Mn	0.005	0.002	0.006	0.002	0.000	0.003	0.000	0.000	0.000	0.000	0.001	0.000
Mg	0.778	0.769	0.745	0.778	0.000	3.466	0.081	0.000	0.007	0.002	0.000	0.001
Ni	-	-	-	-	-	0.039	-	-	-	-	-	-
Zn	0.001	0.002	-	0.001	-	-	-	-	-	-	-	-
Ca	0.000	0.000	0.001	0.001	0.000	0.017	0.017	0.109	0.117	0.077	1.097	0.030
K	0.000	0.000	0.000	0.001	0.000	0.003	0.002	0.100	0.039	0.055	0.000	0.001
Na	0.000	0.000	0.000	0.001	0.000	0.000	0.000	0.587	0.686	0.670	0.001	0.000
Total*	2.986	3.014	2.999	3.017	1.001	14.069	12.091	2.820	2.821	2.819	2.067	1.982

*spinel composited with feldspar inclusion
NA = not analyzed, ND = not detected

Pyroxene

Pyroxene is the most common mineral inclusions in Bo Welu ruby which is usually observed in purplish red, red-purple, and reddish purple samples. They are mostly colorless and very rounded grain (Figure 4.18a) but sometimes are present as ellipsoidal shape crystal (Figure 4.18b) with twinning lamellae (Figure 4.18c). A few pyroxene inclusions show well developed crystal faces (Figure 4.18d). More photographs of pyroxene inclusions are collected in Appendix B. The representative Raman spectrum is shown in Figure 4.19 whereas more spectra are reported in Appendix E.

Electron Probe Micro-Analyzer (EPMA) analyses of representative pyroxene inclusions are reported in Appendix H and the whole range of composition and recalculated atomic proportions on the basis of six oxygen atoms are representatively summarized in Table 4.9.; these atomic proportions are plotted in pyroxene quadrilateral diagram (Morimoto et al., 1988) (see Figure 4.20). In general, these pyroxene inclusions are composed of Al-rich (0.38-0.71 Al) component with $Mg+Fe^{2+}$ and $Mg/(Mg+Fe^{2+})$ ratios varying from 0.59 to 0.80 and 0.81 to 1.00, respectively.

They are clearly characterized by Al-rich diopside, closely to tschermaks clinopyroxene (fassaite), which they have percentages of Ca: Mg: Fe ranging narrowly 53.34-60.32 : 32.96-42.94 : 0.-7.85, respectively. In comparison with pyroxene inclusions found in Bo Rai ruby, pyroxene inclusions in Bo Welu ruby are slightly higher Ca and lower Mg components than those of Bo Rai ruby.

Diopside inclusions in alluvial ruby were previously reported in Bo Rai ruby (e.g., Sutthirat et al., 2001; Saminpanya and Sutherland, 2011) and Pailin ruby (Sutherland et al., 1998b). However, pyroxenes found in Bo Welu ruby have wider range of composition covering the compositions of pyroxene inclusions in Bo Rai and Pailin rubies.

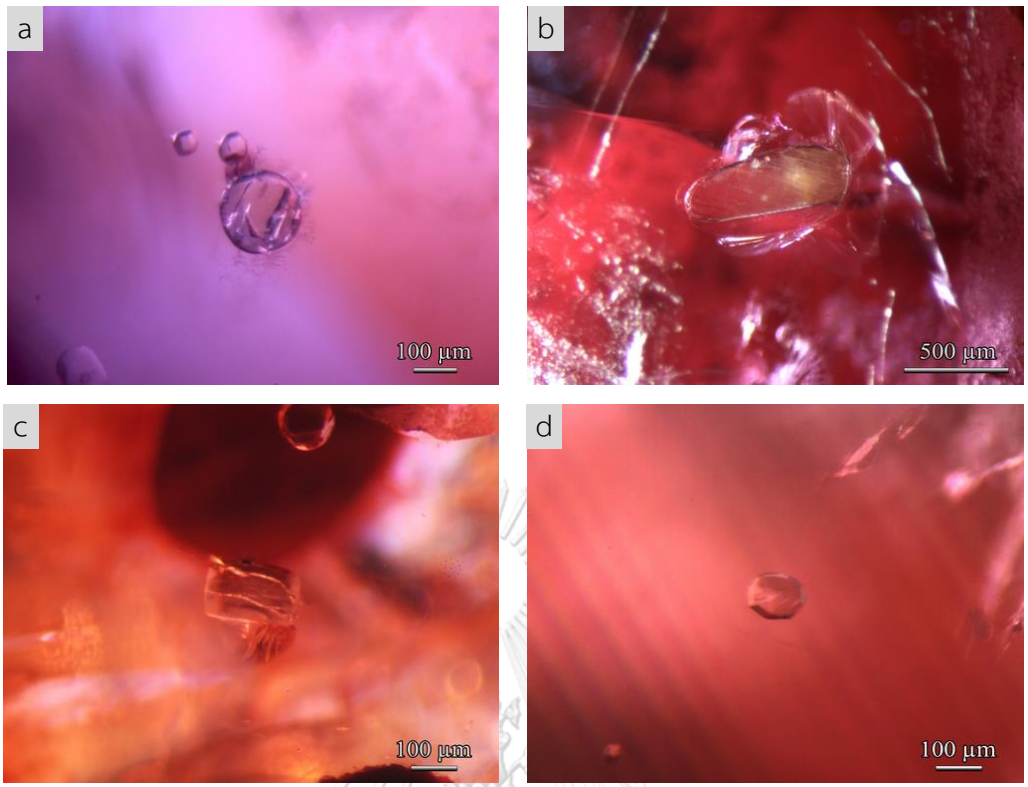

Figure 4.18 Photographs of pyroxene inclusions taken under a combination of a fiber-optic light and/or brightfield illumination: a) pyroxene inclusion with colorless and very rounded shape (sample 9TWL020); b) ellipsoidal pyroxene inclusion (sample 9TWL105); c) pyroxene inclusion with twinning lamellae (sample 9TWL095); d) pyroxene inclusions with well developed crystal faces (sample 9TWL053).

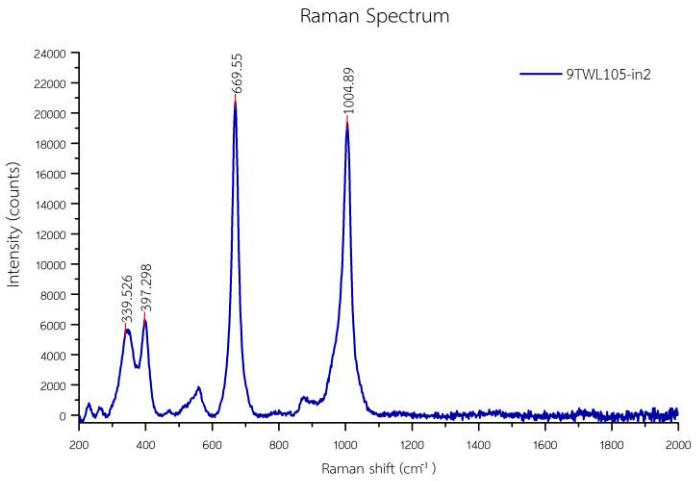

Figure 4.19 The representative Raman spectrum of pyroxene inclusion in Bo Welu ruby sample 9TWL105.

Table 4.9 Representative EPMA analyses of pyroxene inclusions in Bo Welu ruby samples.

Mineral phase analysis (wt%)	pR	PR-RP								rP					
	9TWL 011-in1	9TWL 020-in1	9TWL 020-in2	9TWL 020-in3	9TWL 021-in1	9TWL 023-in1	9TWL 029-in1	9TWL 035-in1	9TWL 053-in2	9TWL 095-in1	9TWL 086-in1	9TWL 086-in2	9TWL 086-in3	9TWL 099-in1	9TWL 105-in1	9TWL 105-in2
SiO_2	46.09	47.85	47.72	46.81	46.55	48.39	44.85	49.28	46.75	45.57	47.43	47.08	47.14	46.33	45.17	44.72
TiO_2	0.61	0.30	0.34	0.32	0.14	0.11	0.24	0.75	0.16	0.25	0.85	0.86	0.70	0.24	0.19	0.22
Al_2O_3	14.32	15.42	15.02	14.85	15.98	14.69	16.50	8.82	15.44	15.38	13.50	13.31	13.27	14.40	16.05	16.15
Cr_2O_3	0.51	0.15	0.20	0.15	0.18	0.13	0.17	0.13	0.04	0.14	0.04	0.01	0.07	0.11	0.06	0.09
FeO total	3.48	3.74	3.59	3.32	2.99	2.39	3.04	3.28	2.93	2.87	3.41	3.37	3.17	3.53	3.18	3.13
MnO	ND	ND	0.05	0.03	0.10	0.08	ND	0.01	ND	0.06	0.01	ND	0.02	0.05	0.07	0.07
MgO	10.78	9.08	9.86	9.10	9.48	10.54	11.41	12.88	10.45	11.34	11.46	11.21	11.11	11.41	11.38	11.44
CaO	22.71	21.77	21.65	23.18	22.11	22.39	22.52	23.99	22.06	22.16	22.09	21.88	21.92	22.33	22.89	23.07
K_2O	ND	0.02	0.01	0.01	ND	ND	0.02	ND	0.01	ND	ND	ND	ND	0.02	ND	ND
Na_2O	1.27	1.65	1.27	1.22	1.13	1.07	1.11	0.76	1.22	1.62	1.19	1.20	1.17	1.49	0.93	0.98
Total	99.76	99.99	99.70	99.00	98.66	99.80	99.85	99.90	99.07	99.39	99.99	98.90	98.57	99.90	99.92	99.88
6 (O)																
Si	1.691	1.738	1.736	1.724	1.711	1.750	1.639	1.805	1.711	1.672	1.726	1.732	1.738	1.695	1.651	1.638
Ti	0.017	0.008	0.009	0.009	0.004	0.003	0.006	0.021	0.004	0.007	0.023	0.024	0.019	0.007	0.005	0.006
Al	0.619	0.660	0.644	0.645	0.692	0.626	0.711	0.381	0.666	0.665	0.579	0.577	0.577	0.621	0.691	0.697
Cr	0.015	0.004	0.006	0.004	0.005	0.004	0.005	0.004	0.001	0.004	0.001	0.000	0.002	0.003	0.002	0.003
Fe^{3+}	0.062	0.000	0.000	0.000	0.000	0.000	0.110	0.027	0.000	0.131	0.006	0.000	0.000	0.116	0.091	0.123
Fe^{2+}	0.045	0.114	0.109	0.102	0.092	0.072	0.000	0.073	0.090	0.000	0.098	0.104	0.098	0.000	0.006	0.000
Mn	0.000	0.000	0.002	0.001	0.003	0.002	0.000	0.000	0.000	0.002	0.000	0.000	0.001	0.002	0.002	0.002
Mg	0.589	0.492	0.535	0.500	0.520	0.568	0.622	0.703	0.570	0.620	0.622	0.614	0.611	0.622	0.620	0.625
Ca	0.893	0.847	0.844	0.915	0.870	0.868	0.882	0.942	0.865	0.871	0.861	0.862	0.866	0.875	0.896	0.905
K	0.000	0.001	0.000	0.001	0.000	0.000	0.001	0.000	0.001	0.000	0.000	0.000	0.000	0.001	0.000	0.000
Na	0.091	0.116	0.090	0.087	0.080	0.075	0.079	0.054	0.087	0.115	0.084	0.086	0.083	0.105	0.066	0.070
Total*	4.021	3.980	3.975	3.987	3.977	3.969	4.037	4.009	3.995	4.044	4.002	3.999	3.995	4.039	4.031	4.041
% Ca	58.48	58.29	56.72	60.32	58.70	57.56	58.64	54.83	56.72	58.42	54.46	54.56	54.98	58.45	58.87	59.15
% Mg	38.57	33.86	35.95	32.96	35.09	37.67	41.36	40.92	37.38	41.58	39.34	38.86	38.79	41.55	40.74	40.85
% Fe	2.95	7.85	7.33	6.72	6.21	4.77	0.00	4.25	5.90	0.00	6.20	6.58	6.22	0.00	0.39	0.00
Total**	100.00	100.00	100.00	100.00	100.00	100.00	100.00	100.00	100.00	100.00	100.00	100.00	100.00	100.00	100.00	100.00

ND = not detected

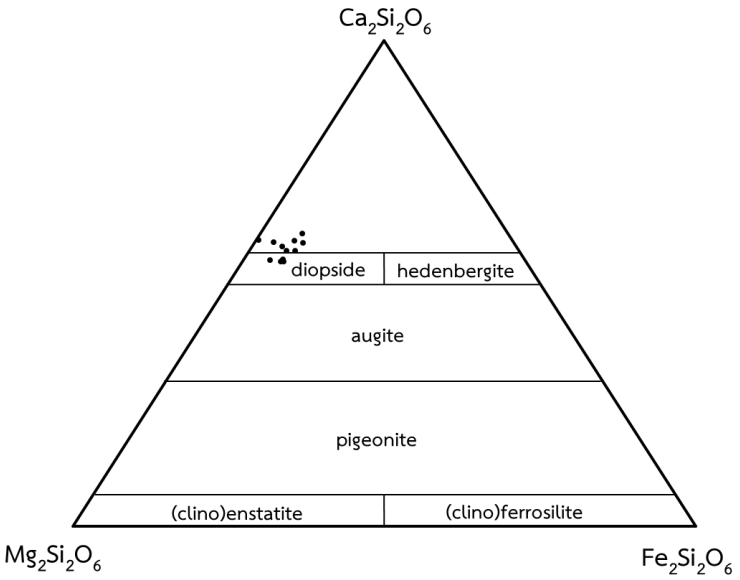

Figure 4.20 Compositional plots of high-Al diopside inclusions found in Bo Welu ruby samples (diagram after Morimoto et al. (1988)).

Sapphirine

Blue-green sapphirine inclusion was found in the red-purple sample 9TWL160 (Figure 4.21); it was initially identified by Raman spectrum (Figure 4.22). Subsequently, its chemical composition (Table 4.8) was analyzed by EPMA. This analysis is recalculated to atomic proportion, based on 20 oxygen atoms, yielding $(Fe_{0.1}Mg_{3.5}Al_{4.4})(Fe_{0.2}Al_{4.}1Si1_{.7})O_{20}$ which is close to ideal formula, $(Mg,Al)_8(Al,Si)_6O_{20}$, with a slight substitution of iron in both divalent and trivalent sites. Sapphirine inclusion has been reported previously in ruby from Bo Rai deposit, Trat by Koivula and Fryer (1987). In this study, the sapphirine inclusion is chemically similar to those of sapphirine inclusions in alluvial corundum from Bo Na Wong deposit, Chanthaburi Province, about 50 km North of the Bo Welu deposit which was previously reported by and Sutthirat et al. (2001) and Saminpanya and Sutherland (2011). Moreover, the similar chemical compositions of sapphirine inclusions were also reported from Pailin deposit (Sutherland et al. (1998b).

Sapphirine typically occurs in high-grade metamorphic rocks belonging to granulite and hornblende-granulite facies within Al-rich and Si-poor provenance. Sapphirine co-existing with spinel have been reported in pink sapphire and ruby from basaltic terrain in Australia by Sutherland and Coenraads (1996) and Sutherland et al. (1998a). They suggested a crystallization temperature for the aggregates and reactions with magma at over 1000°C. The presence of sapphirine may indicate Bo welu ruby was crystallized at high temperature condition of regional or contact metamorphism

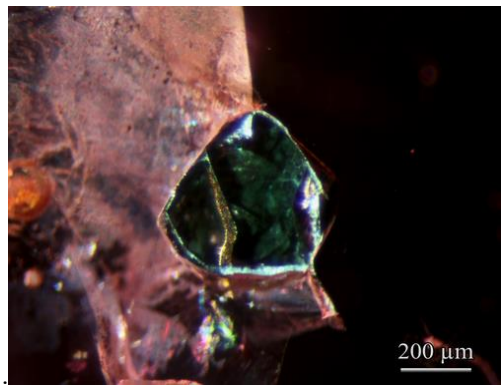

Figure 4.21 Blue-green sapphirine inclusion viewed under dark field illumination in Bo Welu ruby sample 9TWL160.

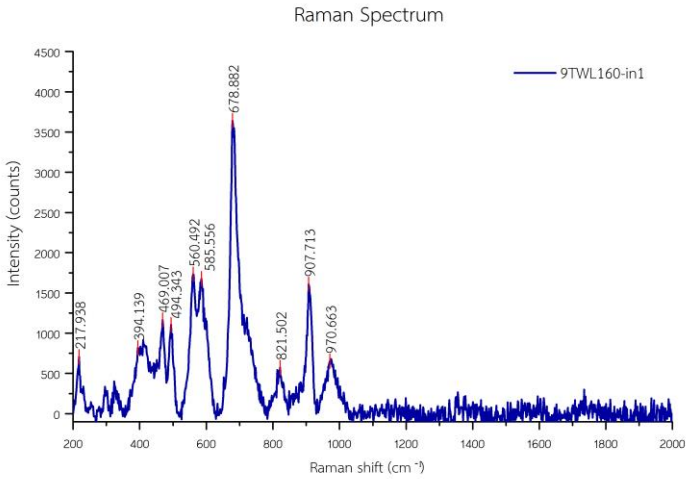

Figure 4.22 The representative Raman spectrum of sapphirine inclusion in Bo Welu ruby sample 9TWL160.

Nepheline

The exceptional nepheline inclusions are recognized in red-purple and reddish purple ruby samples; these nephelines are rounded crystal (Figure 4.23). More photographs of nepheline inclusions are present in Appendix B. A representative Raman spectrum is shown in Figure 4.24; more spectra are reported in Appendix E. Chemical compositions of these inclusions analyzed by EPMA are also shown in Table 4.8. They contain major contents of SiO_2 and Al_2O_3 with traces of CaO, K_2O, Na_2O, and FeO. Many researchers reported nepheline inclusions in sapphire from Bo Phloi in Kanchanaburi, Den Chai in Phrae of Thailand and Hua Sai of Lao PDR (Khamloet, 2011; Saminpanya and Sutherland, 2011; Khamloet et al., 2014). However, this is the first report of nepheline inclusion in Siam ruby.

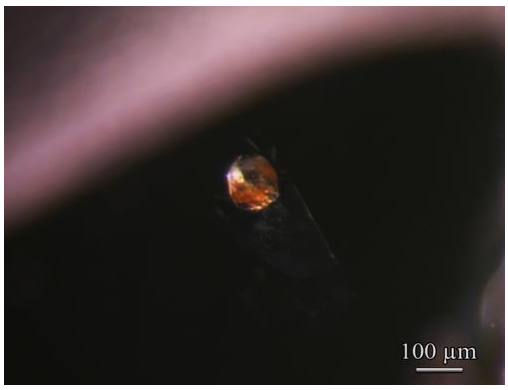

Figure 4.23 Magnified view of nepheline inclusion observed in Bo Welu ruby sample 9TWL153.

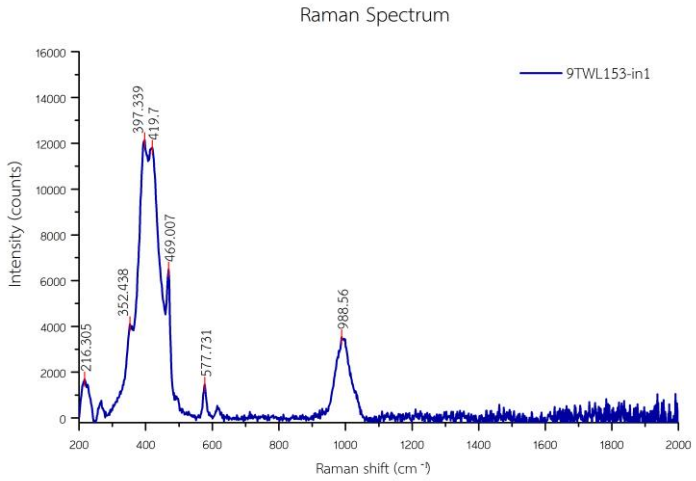

Figure 4.24 The representative Raman spectrum of nepheline inclusion in Bo Welu ruby sample 9TWL153.

Quartz

An exogenous inclusion such as quartz is found in red-purple ruby sample 9TWL095; this quartz inclusion is surrounded by iron stain rim (Figure 4.25). It was initially analyzed by Raman spectroscope before chemical composition was analyzed by Electron Probe Micro-Analyzer (EPMA) as shown in Table 4.8. Its composition is almost pure silica (99.6% SiO_2) with trace of iron. Raman spectrum is shown in Figure 4.26.

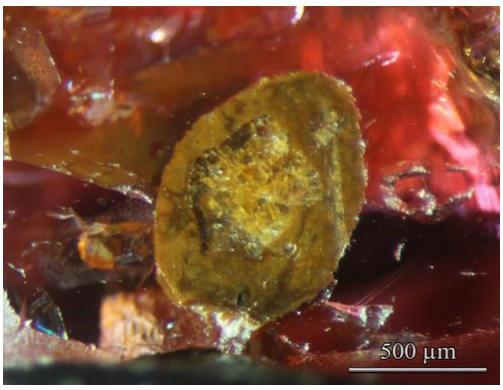

Figure 4.25 Quartz inclusion in ruby sample 9TWL095 surrounded by iron stain edge viewed under reflected light

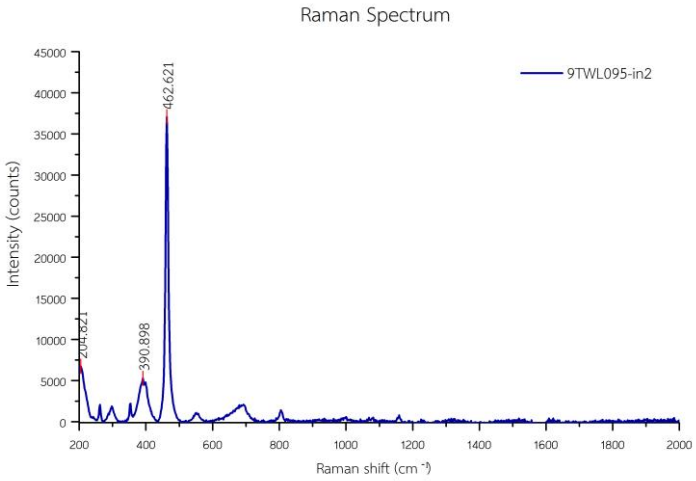

Figure 4.26 The representative Raman spectrum of quartz inclusion in Bo Welu ruby sample 9TWL095.

Feldspar

A single crystal of feldspar inclusions in the red-purple and reddish purple ruby samples are typically almost rounded form (Figure 4.27a) and some crystals are irregular shape (Figure 4.27b). It should be notified that feldspar-spinel composite inclusions are observed in sample 9TWL180 (Figure 4.27c), 9TWL154 (Figure 4.27e), and 9TWL019 (Figure 4.27g) which they are clearly distinguished using Backscattered-Electron (BSE) Image (Figure 4.27d, f, h). Raman spectra of feldspar and combined spinel inclusions are shown in Figure 4.28. More photographs of feldspar inclusions are present in Appendix B whereas all Raman spectra of feldspar inclusions are reported in Appendix E.

Representative Electron Probe Micro-Analyses (EPMA) of feldspar inclusions in ruby samples are present in Table 4.10, and more data are reported in Appendix H.

These feldspar compositions are plotted in the ternary feldspar diagram. They fall within plagioclase ranges varying from bytownite ($Ab_{19-20}An_{79-80}Or_{0.1-0.7}$) to labradorite ($Ab_{38-48}An_{51-62}Or_{0.-1}$), and andesine ($Ab_{53-69}An_{31-46}Or_{0.2-8}$). Feldspar combined with spinel inclusions are also plotted (triangular sign) on the labradorite field (Figure 4.29). Moreover, an unusual rounded alkali feldspar with anorthoclase composition ($Ab_{73}An_{8}Or_{19}$) is recognized in reddish purple sample 9TWL012; its Raman spectrum is similar to other feldspar inclusions but slightly shift to the right Although Gübelin (1971) reported feldspar inclusion in Siam ruby, feldspar-spinel composite inclusion in Siam ruby is firstly reported from this study.

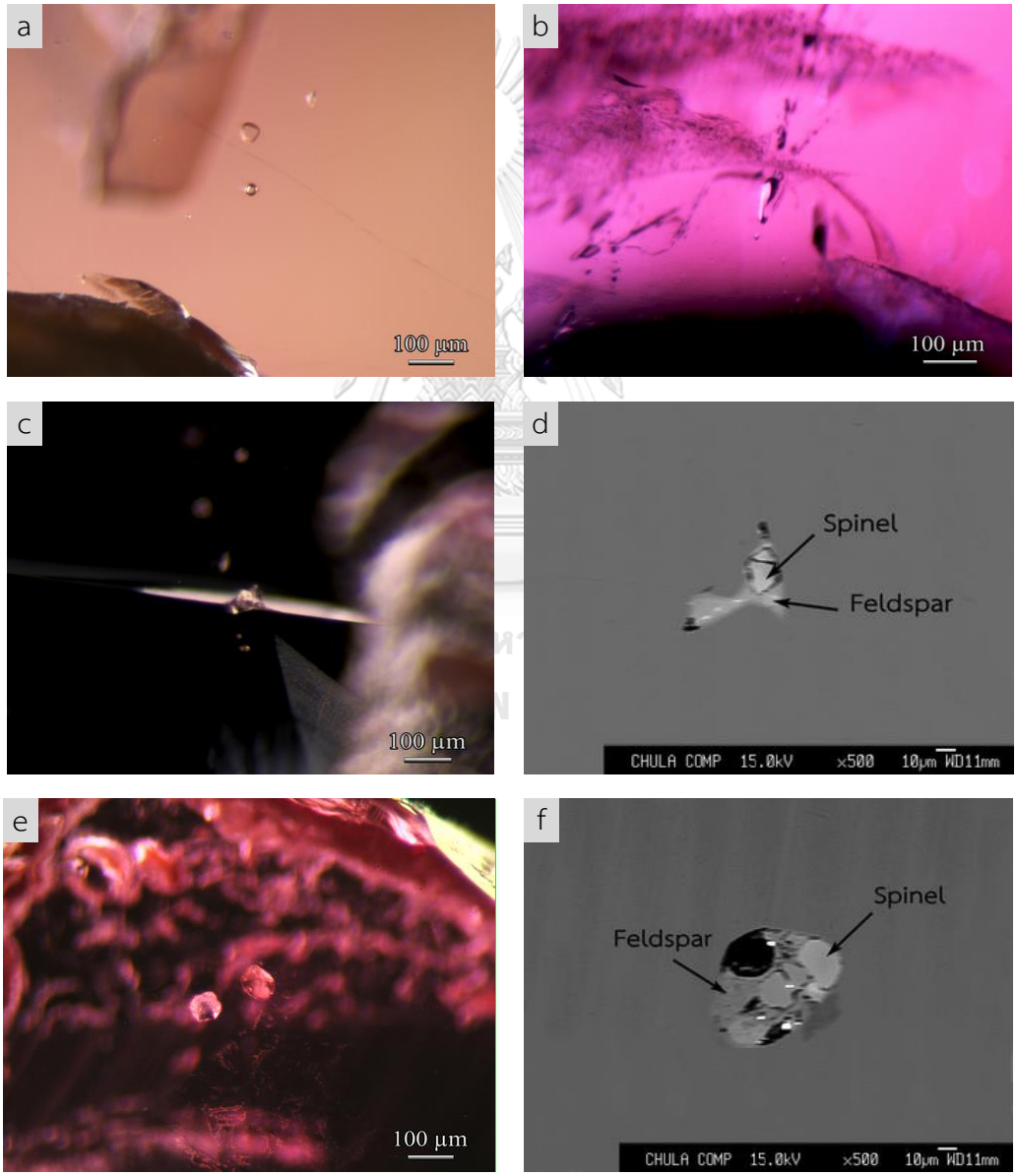

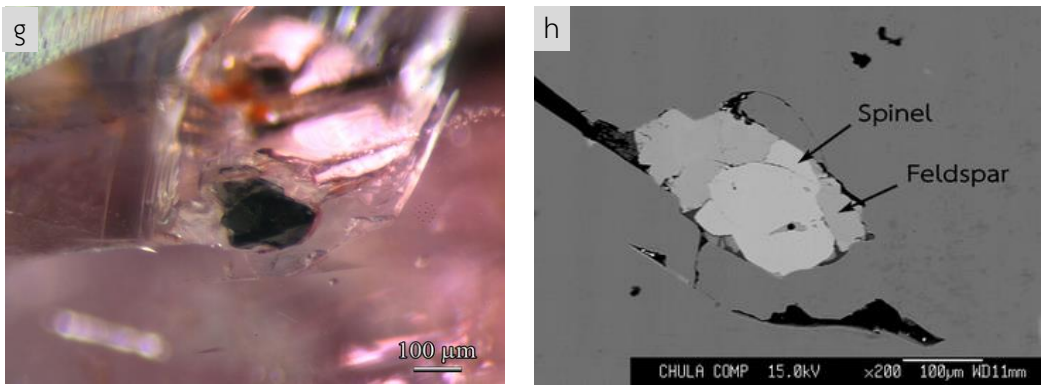

Figure 4.27 Photographs of single feldspar and feldspar-spinel composite inclusions, in Bo Welu ruby, taken under a combination of a fiber-optic light and bright field illumination; a) feldspar inclusions with almost rounded shape (sample 9TWL022); b) irregular-shaped feldspar inclusion (sample 9TWL010); high magnification revealing colorless feldspar combined with spinel inclusions surrounded by fracture in sample 9TWL180 (c), and in sample 9TWL154 (e); feldspar intergrowth with black spinel inclusions observed in samples 9TWL019 (g); Backscattered-Electron (BSE) Images revealing clearly feldspar inclusions intergrowth with spinel inclusions (d, f, and h).

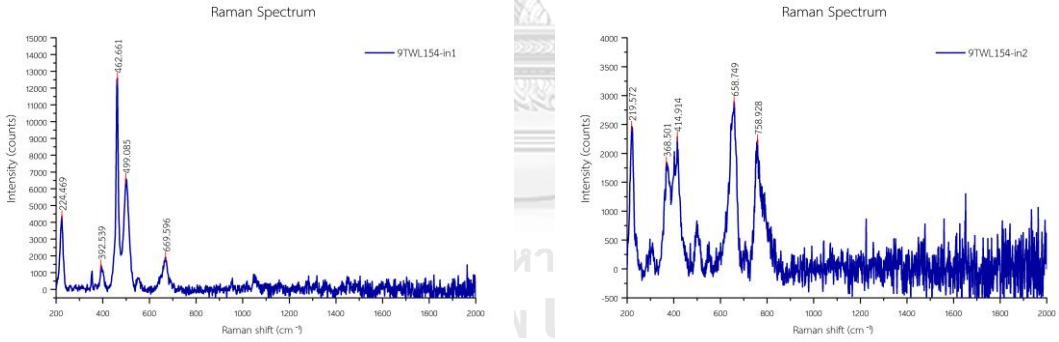

Figure 4.28 Representative Raman spectra of feldspar inclusion (left) and spinel (right) inclusions in Bo Welu ruby sample 9TWL154.

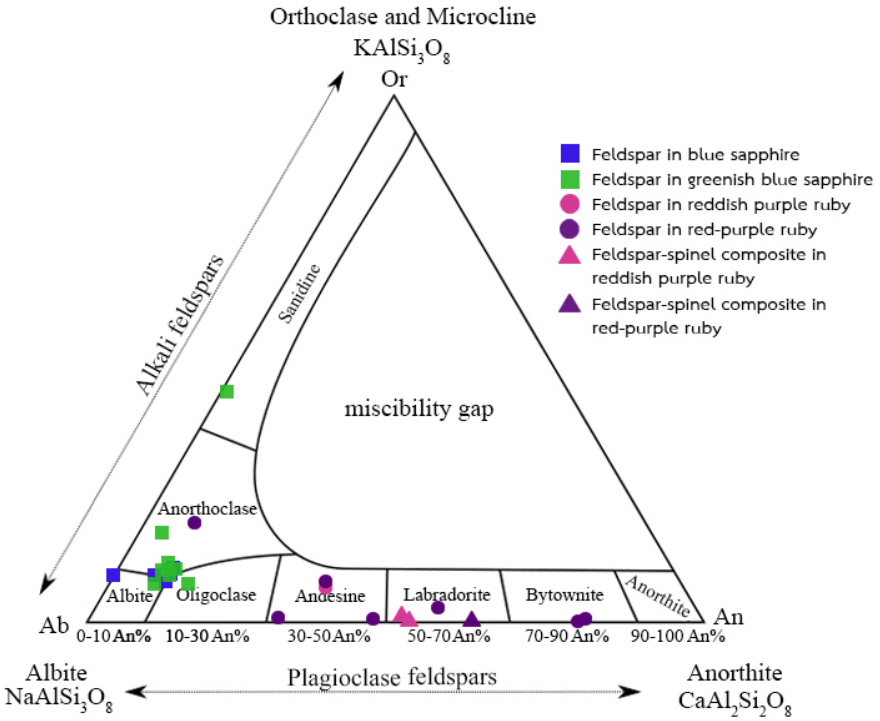

Figure 4.29 Ternary plotting of feldspar inclusions in various rubies and sapphires from Bo Welu gem field. Most feldspar inclusions in ruby samples fall within plagioclase feldspar (including feldspar-spinel composite inclusion symbolized as triangular sign). An unusual anorthoclase composition recorded from inclusion in sample 9TWL012 of reddish purple ruby. On the other hand, most feldspar inclusions in sapphire samples are characterized by alkali feldspar. Only one sanidine inclusion is recorded in a greenish blue sapphire (sample 8TWL093).

Table 4.10 Representative EPMA analyses of feldspar inclusions in Bo Welu ruby samples.

Mineral phase analysis (wt%)	PR-RP			rP							
	9TWL053-in1	9TWL154-in1*	9TWL019-in1*	9TWL007-in1	9TWL122-in3	9TWL122-in4	9TWL012-in2	9TWL055-in1	9TWL176-in1	9TWL178-in1	9TWL180-in1*
SiO_2	58.21	55.99	54.15	53.31	49.18	48.61	64.91	58.02	61.34	60.45	52.02
TiO_2	0.09	0.03	ND	0.04	ND	ND	0.03	0.04	0.07	0.02	ND
Al_2O_3	26.30	26.97	29.16	28.84	31.71	32.46	21.54	26.36	23.67	24.72	30.72
FeO	0.01	0.25	0.24	0.13	0.12	0.07	0.12	0.09	0.46	0.23	0.39
MnO	ND	ND	0.04	ND	0.02	0.03	0.01	0.04	ND	0.01	0.09
MgO	0.27	0.03	ND	ND	0.02	0.03	ND	0.05	0.20	ND	0.02
CaO	7.38	11.04	10.60	12.08	16.45	16.51	1.48	7.30	6.29	8.83	12.03
K_2O	1.22	0.02	0.17	0.47	0.01	0.12	3.08	1.35	0.07	0.04	ND
Na_2O	6.69	5.51	5.60	4.97	2.31	2.14	7.71	6.66	7.76	5.64	4.00
Total	100.17	99.84	99.96	99.84	99.82	99.97	98.88	99.91	99.86	99.94	99.27
8 (O)											
Si	2.607	2.527	2.448	2.424	2.254	2.228	2.899	2.606	2.732	2.690	2.369
Ti	0.003	0.001	0.000	0.001	0.000	0.000	0.001	0.001	0.002	0.001	0.000
Al	1.388	1.435	1.553	1.545	1.713	1.753	1.134	1.396	1.243	1.296	1.648
Fe	0.000	0.010	0.009	0.005	0.005	0.003	0.004	0.004	0.017	0.009	0.015
Mn	0.000	0.000	0.001	0.000	0.001	0.001	0.000	0.002	0.000	0.000	0.003
Mg	0.018	0.002	0.000	0.000	0.001	0.002	0.000	0.003	0.013	0.000	0.002
Ca	0.354	0.534	0.513	0.588	0.808	0.811	0.071	0.352	0.300	0.421	0.587
K	0.070	0.001	0.010	0.027	0.001	0.007	0.175	0.077	0.004	0.002	0.000
Na	0.580	0.482	0.490	0.438	0.205	0.190	0.668	0.580	0.670	0.486	0.353
Total*	5.02	4.992	5.024	5.028	4.988	4.995	4.952	5.021	4.981	4.905	4.977
Atomic%											
Ca	35.25	52.46	50.64	55.84	79.67	80.47	7.74	34.86	30.82	46.30	62.41
K	6.96	0.12	0.97	2.58	0.07	0.67	19.18	7.66	0.41	0.22	0.01
Na	57.79	47.42	48.40	41.58	20.26	18.85	73.08	57.49	68.77	53.48	37.58
Total**	100.00	100.00	100.00	100.00	100.00	100.00	100.00	100.00	100.00	100.00	100.00

* Feldspar combined with spinel inclusion
ND = not detected

Feldspar inclusions are commonly observed in all color varieties of Bo Welu sapphire. They usually form subhedral crystals (Figure 4.30a-c) to euhedral crystals (Figure 4.30d-f). Some crystals are also associated with heal fracture or tension crack (Figure 4.30g-h). More photographs of feldspar inclusions are collected in Appendix B. A representative Raman spectrum is shown in Figure 4.31 and more spectra are reported in Appendix E.

The representative Electron Probe Micro-Analyses of feldspar inclusions are present in Table 4.11, and more analytical data are collected in Appendix H. Plots of feldspar compositions in the ternary atomic Ca-Na-K diagram indicate that these inclusions are Na rich alkali feldspar (albite) (Ab_{80}-91$An0_{.1-13}Or_{7-17}$) (Figure 4.29). Only one analysis in greenish blue sample (sample 8TWL093) yields high Na contents ($Ab_{56}An_{0.7}Or_{44}$) in sanidine range which it forms subhedral crystal surrounded by tension crack (Figure 4.32). Raman spectrum of this sanidine inclusion are showed in Figure 4.33.

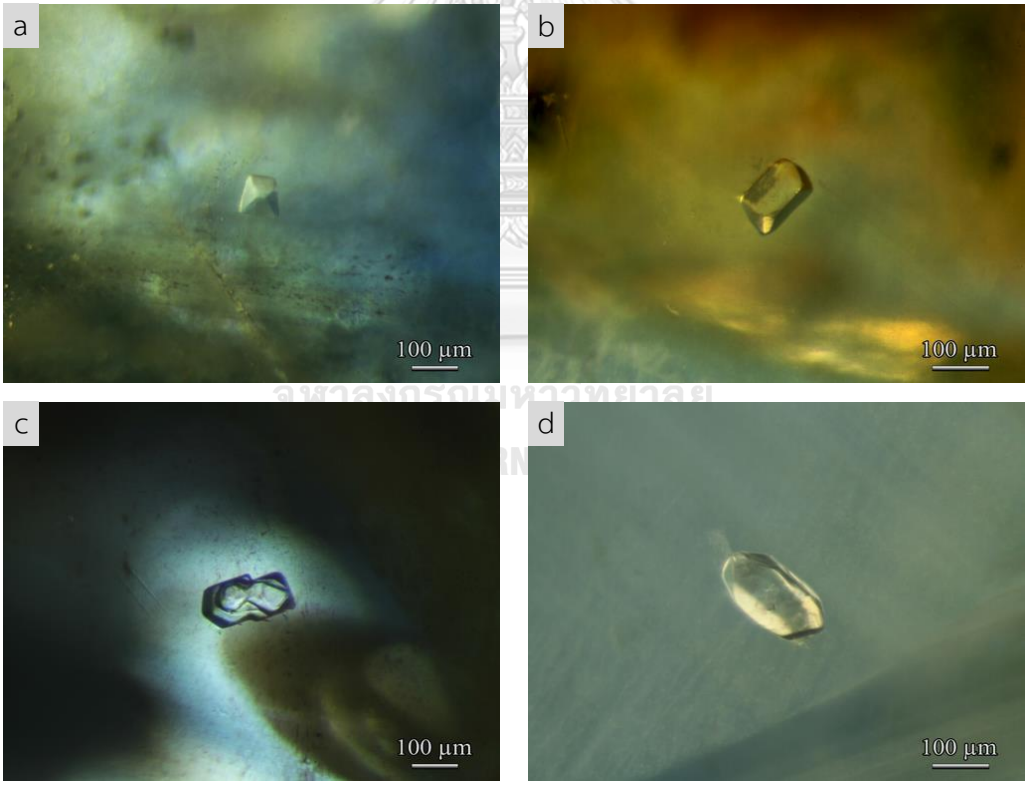

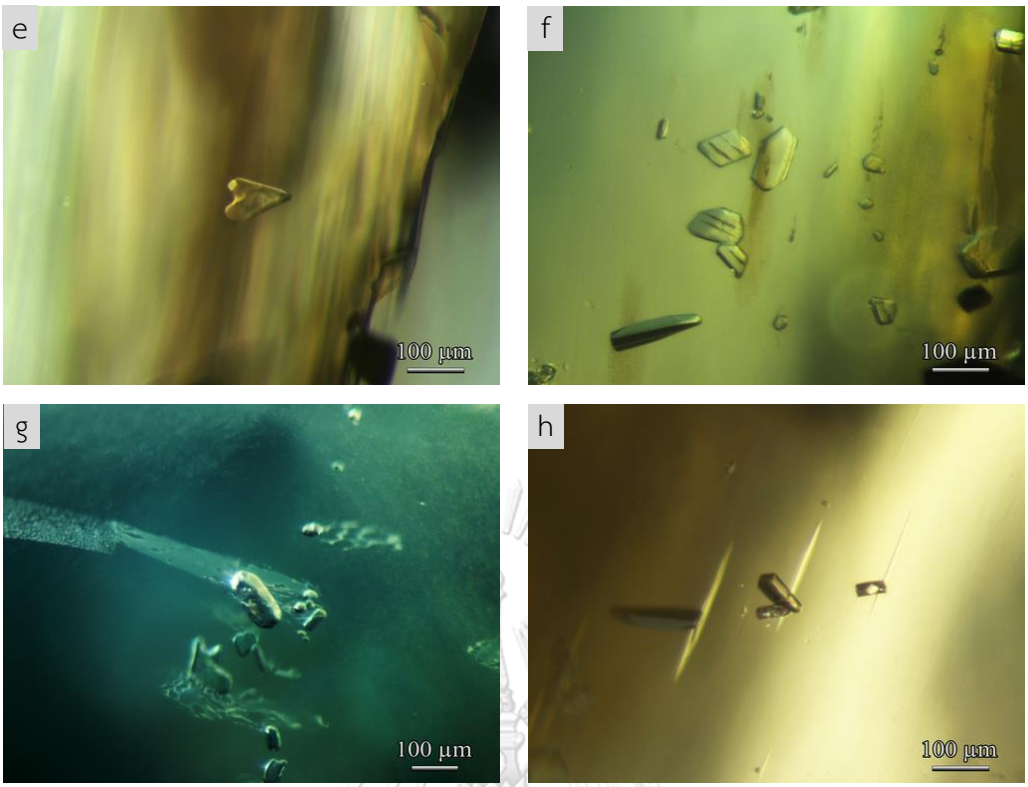

Figure 4.30 Photographs viewed using a combination of fiber-optic and bright field illumination: subhedral feldspar inclusions observed in sapphire sample 8TWL031 (a), 8TWL099 (b), and 8TWL116 (c); euhedral feldspar inclusions in sample 8TWL099 (d), 8TWL099 (e), and 8TWL114 (f); some feldspar crystals situated in heal fracture or tension cracks in sample 8TWL002 (g) and 8TWL114 (h).

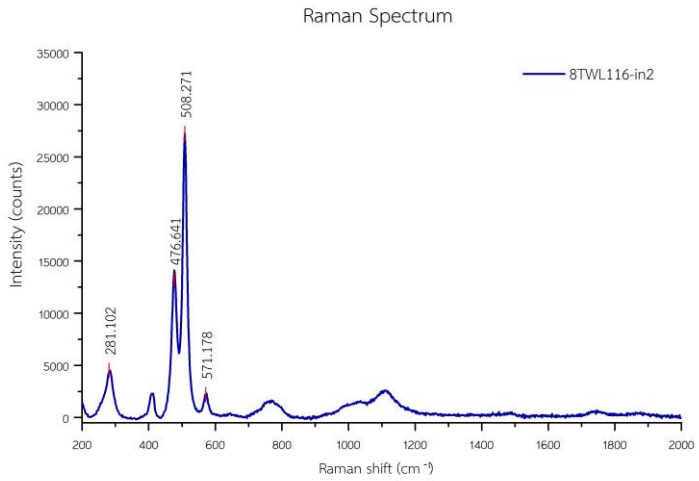

Figure 4.31 Representative Raman spectrum of feldspar inclusion observed in Bo Welu sapphire sample 8TWL116.

Figure 4.32 Na-rich sanidine inclusion in Bo Welu sapphire sample 8TWL093 showing subhedral shape surrounded by tension crack.

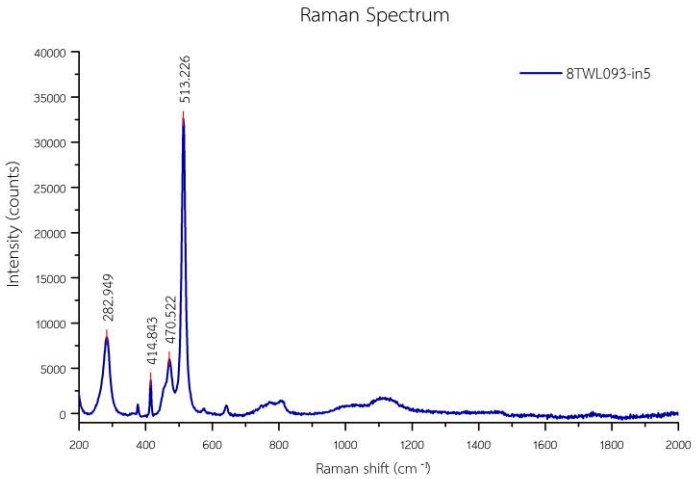

Figure 4.33 Representative Raman spectrum of sanidine inclusion observed in Bo Welu sapphire sample 8TWL093.

Table 4.11 Representative EPMA analyses of feldspar inclusions in Bo Welu sapphire.

Mineral phase analysis (wt%)	B					gB						
	8TWL067-in1	8TWL102-in1	8TWL102-in2	8TWL116-in1	8TWL114-in25	8TWL002-in1	8TWL018-in2	8TWL018-in3	8TWL026-in4	8TWL026-in5	8TWL031-in1	8TWL083-in2
SiO_2	66.59	65.56	66.50	66.88	66.47	66.70	66.65	66.97	65.55	65.39	66.36	66.19
TiO_2	ND	0.03	ND	0.04	0.01	ND	ND	0.02	ND	ND	0.06	ND
Al_2O_3	20.61	21.36	21.57	20.11	20.92	21.32	20.57	21.40	21.41	21.15	21.87	20.85
FeO	0.07	0.10	0.03	0.05	0.59	0.07	0.10	0.65	0.11	0.13	0.09	0.08
MnO	ND	ND	0.02	ND	0.04	0.01	ND	0.04	0.01	0.06	ND	ND
MgO	ND	ND	0.01	ND	0.02	0.01	ND	ND	ND	ND	0.01	ND
CaO	1.46	1.80	1.85	1.83	0.02	1.58	1.50	0.73	1.60	1.75	1.78	2.50
K_2O	1.46	1.48	1.67	1.27	1.40	1.58	1.18	2.69	1.67	1.55	1.42	1.07
Na_2O	9.70	8.76	8.82	9.14	9.45	8.92	9.62	8.47	8.74	8.66	9.05	8.54
Total	99.89	99.09	100.47	99.32	98.92	100.19	99.62	100.97	99.09	98.69	100.64	99.23
8 (O)												
Si	2.934	2.908	2.910	2.954	2.944	2.922	2.939	2.925	2.908	2.911	2.898	2.926
Ti	0.000	0.001	0.000	0.001	0.000	0.000	0.000	0.001	0.000	0.000	0.002	0.000
Al	1.070	1.116	1.112	1.047	1.092	1.101	1.069	1.102	1.119	1.110	1.126	1.086
Fe	0.069	0.086	0.087	0.086	0.001	0.074	0.071	0.034	0.076	0.083	0.083	0.118
Mn	0.003	0.004	0.001	0.002	0.022	0.003	0.004	0.024	0.004	0.005	0.003	0.003
Mg	0.000	0.000	0.001	0.000	0.001	0.000	0.000	0.001	0.000	0.002	0.000	0.000
Ca	0.000	0.000	0.001	0.000	0.001	0.000	0.000	0.000	0.000	0.000	0.001	0.000
K	0.082	0.084	0.093	0.071	0.079	0.089	0.066	0.150	0.094	0.088	0.079	0.060
Na	0.829	0.753	0.748	0.783	0.811	0.758	0.822	0.718	0.752	0.747	0.766	0.732
Total*	4.987	4.952	4.953	4.944	4.951	4.947	4.971	4.955	4.953	4.946	4.958	4.925
Atomic%												
Ca	7.02	9.28	9.35	9.18	0.10	8.06	7.39	3.79	8.26	9.08	8.97	13.01
K	8.38	9.09	10.03	7.59	8.89	9.62	6.91	16.62	10.22	9.58	8.52	6.62
Na	84.61	81.63	80.62	83.23	91.01	82.32	85.70	79.60	81.52	81.34	82.51	80.37
Total**	100.00	100.00	100.00	100.00	100.00	100.00	100.00	100.00	100.00	100.00	100.00	100.00

ND = not detected

Table 4.11 Representative EPMA analyses of feldspar inclusions in Bo Welu sapphire. (continued)

Mineral phase analysis (wt%)	gB								BG-GB			
	8TWL093-in4	8TWL093-in5	8TWL099-in1	8TWL099-in2	8TWL099-in3	8TWL105-in1	8TWL117-in2	8TWL119-in1	8TWL097-in2	8TWL097-in3	8TWL097-in4	8TWL097-in5
SiO_2	66.82	69.26	66.00	65.59	66.00	66.92	66.92	66.34	67.24	66.23	64.88	67.21
TiO_2	ND	0.06	0.02	0.03	0.02	ND	0.02	0.01	ND	ND	0.01	ND
Al_2O_3	20.99	16.47	20.91	22.14	22.65	21.30	20.61	21.57	19.70	20.88	22.62	19.55
FeO	0.09	0.31	0.01	0.05	0.04	0.11	0.09	0.05	0.09	0.12	0.23	0.07
MnO	ND	ND	ND	ND	0.01	ND	ND	0.03	0.01	ND	0.01	ND
MgO	ND	ND	0.01	ND	ND	ND	ND	ND	ND	ND	ND	0.01
CaO	1.80	0.14	0.38	1.83	1.73	1.71	1.37	1.07	2.13	1.90	1.82	1.88
K_2O	1.40	7.43	1.74	1.43	1.48	1.67	1.30	1.14	1.20	1.30	1.46	1.37
Na_2O	9.11	6.25	9.68	8.88	8.84	8.89	9.25	9.34	9.74	8.80	9.35	9.81
Total	100.21	99.92	98.75	99.95	100.77	100.60	99.56	99.55	100.11	99.23	100.38	99.90
8 (O)												
Si	2.928	3.095	2.934	2.884	2.876	2.921	2.945	2.919	2.958	2.929	2.853	2.961
Ti	0.000	0.002	0.001	0.001	0.001	0.000	0.001	0.000	0.000	0.000	0.000	0.000
Al	1.084	0.868	1.095	1.148	1.163	1.096	1.069	1.119	1.021	1.088	1.172	1.015
Fe	0.003	0.011	0.000	0.002	0.001	0.004	0.003	0.002	0.003	0.004	0.009	0.003
Mn	0.000	0.000	0.000	0.000	0.001	0.000	0.000	0.001	0.000	0.000	0.000	0.000
Mg	0.000	0.000	0.001	0.000	0.000	0.000	0.000	0.000	0.000	0.000	0.000	0.001
Ca	0.084	0.007	0.018	0.086	0.081	0.080	0.064	0.050	0.100	0.090	0.086	0.089
K	0.078	0.424	0.099	0.080	0.082	0.093	0.073	0.064	0.067	0.073	0.082	0.077
Na	0.774	0.542	0.834	0.757	0.747	0.752	0.789	0.796	0.831	0.755	0.797	0.838
Total*	4.951	4.949	4.982	4.958	4.952	4.946	4.944	4.951	4.980	4.939	4.999	4.984
Atomic%												
Ca	9.01	0.69	1.88	9.32	8.89	8.65	6.94	5.52	10.04	9.80	8.87	8.84
K	8.35	43.58	10.40	8.70	9.03	10.06	7.90	7.05	6.73	7.96	8.51	7.68
Na	82.64	55.72	87.72	81.98	82.08	81.29	85.16	87.43	83.24	82.23	82.62	83.48
Total**	100.00	100.00	100.00	100.00	100.00	100.00	100.00	100.00	100.00	100.00	100.00	100.00

ND = not detected

Spinel

Apart from feldspar-spinel composite inclusions are observed, single spinel inclusion is also observed as rounded crystals in red-purple sample (sample 9TWL085) (Figure 4.34). The Raman spectrum of such single spinel is shown in Figure 4.35. Chemical compositions of all spinel inclusions analyzed by Electron Probe Micro-Analyzer (EPMA) are present in Table 4.8. They contain high Al (63.4-67.5 wt% Al_2O_3) and Mg (20.0-20.6 wt% MgO) contents with subordinate Fe amount (10.6-13.5 wt% FeO). These compositions are plotted in the classification diagram of spinel group (Haggerty, 1991) (Figure 4.36). The single spinel inclusion is present as black spot and other spinel composite inclusions are symbolized as red spots. Pleonaste spinel inclusion was reported in ruby from West Pailin by Sutherland et al. (1998b); consequently, its Mg content is clearly lower than spinel inclusion in Thai ruby

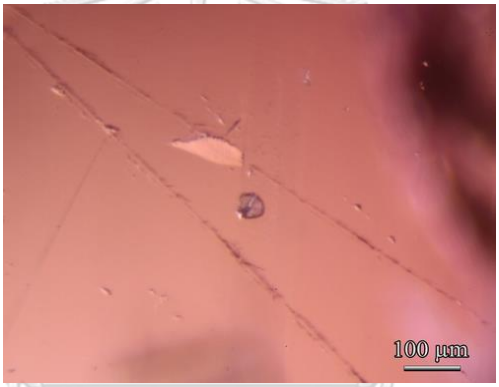

Figure 4.34 Microscopic observation using brightfield illumination showing clearly rounded spinel inclusion in sample 9TWL085.

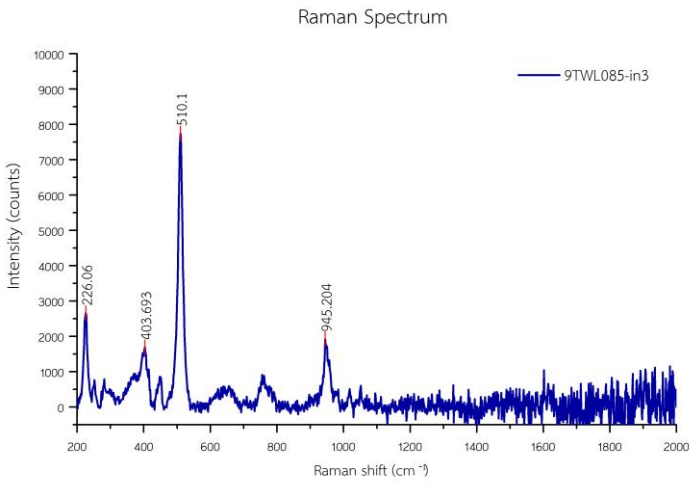

Figure 4.35 Representative Raman spectrum of spinel inclusion observed in Bo Welu sapphire sample 9TWL085.

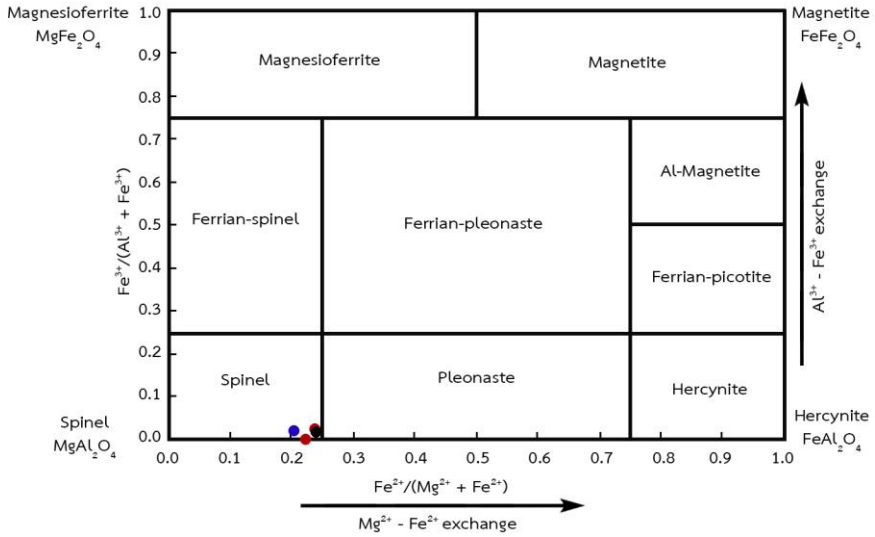

Figure 4.36 Compositional plots of single spinel inclusion (blue spot) and feldspar with colorless spinel composite inclusion (red spots) and black spinel (black spots) in Bo Welu rubies, classification diagram of spinel group minerals (Haggerty, 1991).

Anhydrite

Anhydrite inclusion forms a subhedral crystal containing sulphide inside which this unexpected assemblage is found in a reddish purple ruby (sample 9TWL096), see Figure 4.37, left). Backscattered-Electron (BSE) Imaging (Figure 4.37, right) clearly reveal different compositions of the assemblage. Raman spectrum of the anhydrite and sulphide inclusion are present in Figure 4.38. Chemical compositions of both anhydrite and sulphide in this assemblage were analyzed by Electron Probe Micro-Analyzer (EPMA) and present in Table 4.8. The sulphide ($Fe_{0.94}S$) is purely pyrrhotite composition. In addition, anhydrite inclusion in Siam ruby is firstly reported.

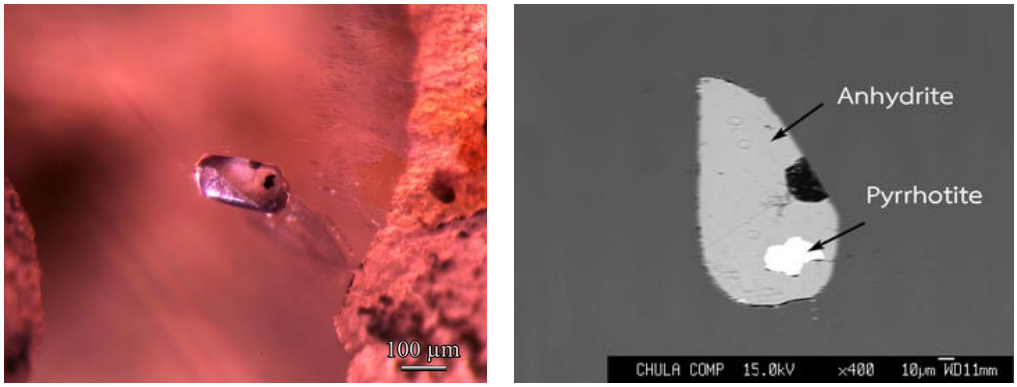

Figure 4.37 Intergrowth anhydrite-sulphide inclusion found in Bo Welu ruby sample 9TWL096: photograph viewed under dark field illumination (left) showing euhedral anhydrite with subhedral black sulphide inside; their Backscattered-Electron (BSE) Image showing clearly different compositions (right).

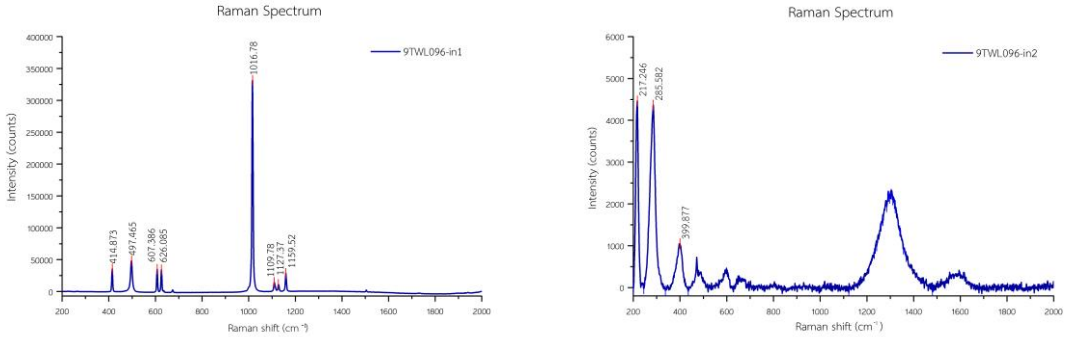

Figure 4.38 Raman spectrum of anhydrite (left) and sulphide (right) inclusions in Bo Welu ruby (sample 9TWL096).

Sulphide

A number of black single crystal of sulphide inclusions have also been identified as mineral inclusion in red-purple, reddish purple and purple ruby samples. They are mostly rounded shape surrounded by tension disc (Figure 4.39a) or fingerprint (Figure 4.39b-c). A few of sulphide inclusions show subhedral shape surrounded by healed fracture (Figure 4.39d). More photographs of sulphide inclusions are present in Appendix B. Exposed crystals were identified as sulphide by Raman spectrum analysis (Figure 4.40). Chemical compositions of these sulphides were analyzed by Electron Probe Micro-Analyzer (EPMA) which their results are summarized in Table 4.12. More Raman spectra and EPMA analyses are reported in Appendices E and H, respectively. All sulphide inclusions are unclearly matched with the ideal formula of pyrrhotite (FeS); they contain nickel and copper as addition components. Their compositions fall within $Cu_{0\text{-}41}Ni_{0\text{-}8.7}Fe_{25.4\text{-}57.2}S_{22.7\text{-}27.7}$ range. Subhexagonal to rounded opaque metallic sulphide inclusion with chalcopyrite ($CuFeS_2$) composition in Thai ruby was ever reported by Gübelin (1971).

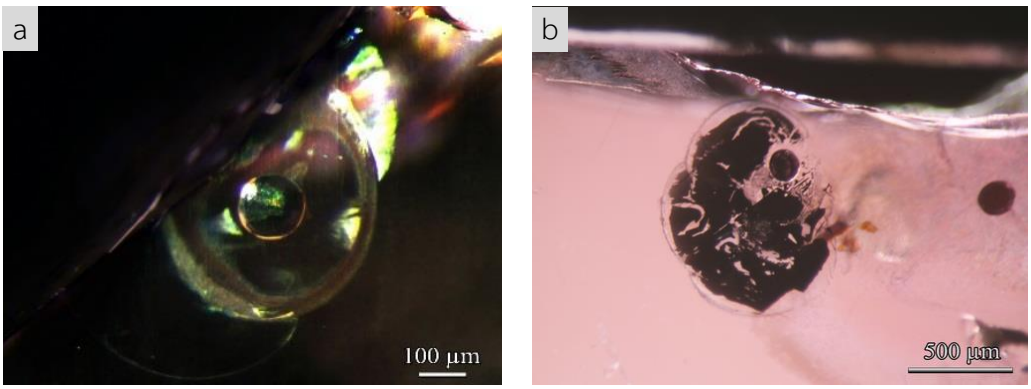

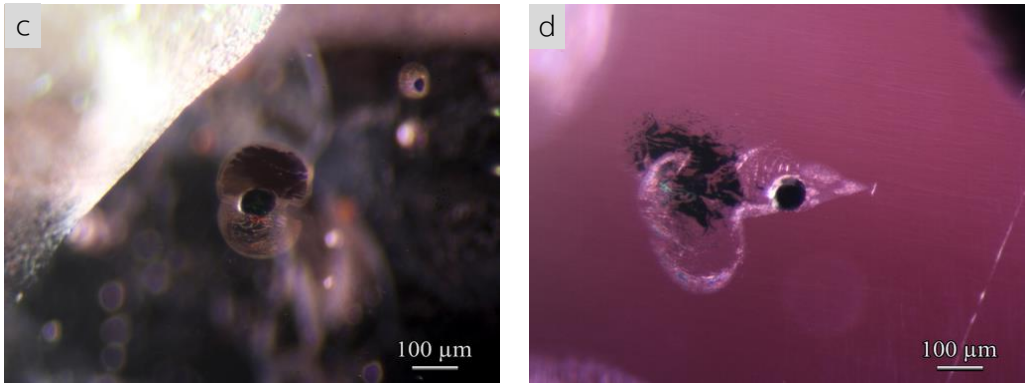

Figure 4.39 Photographs viewed under fiber-optic illuminator: a) rounded sulphide inclusions surrounded by tension disc (sample 9TWL143); b-c) rounded sulphide inclusions surrounded healed fracture (sample 9TWL114, 9TWL100); d) subhedral sulphide inclusion surrounded by healed fracture (sample 9TWL046).

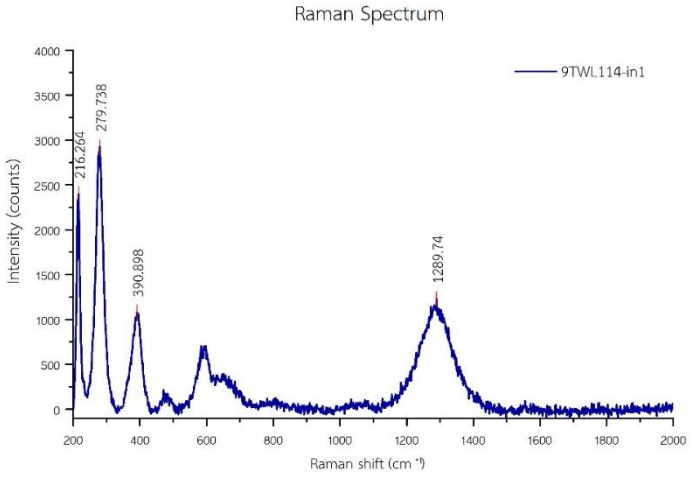

Figure 4.40 Representative Raman spectrum of sulphide inclusion observed in Bo Welu ruby (sample 9TWL114).

Sulphide inclusion is rarely observed in studied sapphire, some small black opaque crystals set in the core areas of light blue-green trapiche sapphire, sample 8TWL046 (Figure 4.41) are recognized as sulphide by Raman spectroscopy (Figure 4.42) and subsequently analyzed by Electron Probe Micro-Analyzer (EPMA). EPMA results are present in Table 4.12 which its composition ($FeS_{1.1}$) is closely to pyrrhotite formula similar to New England sulphide analysed by Sutherland et al. (1998a). On the other hand, these compositions are different from sulphide inclusion in sapphire from New South Wales in Australia that contains trace compositions of Cu and Zn (Guo et al. (1996). However, it must be notified that this is the first discovery of sulphide inclusion in Thai sapphire.

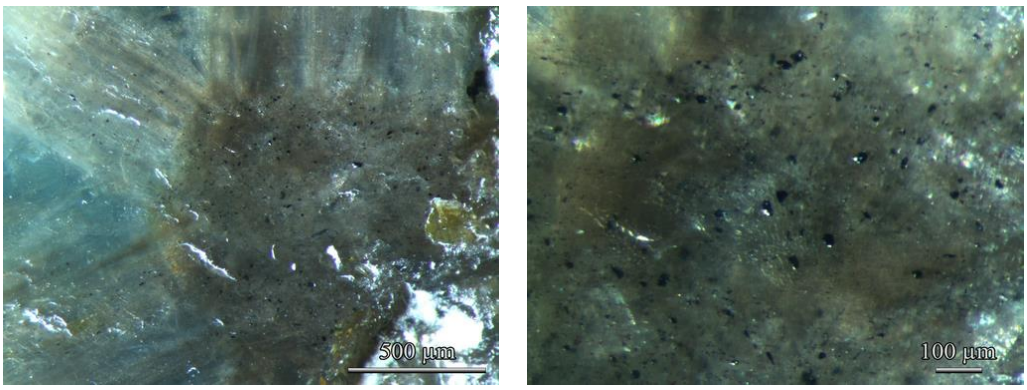

Figure 4.41 A light blue-green Bo Welu sapphire (sample 8TWL046) with chatoyancy effect containing a number of small irregular black opaque sulphide inclusions.

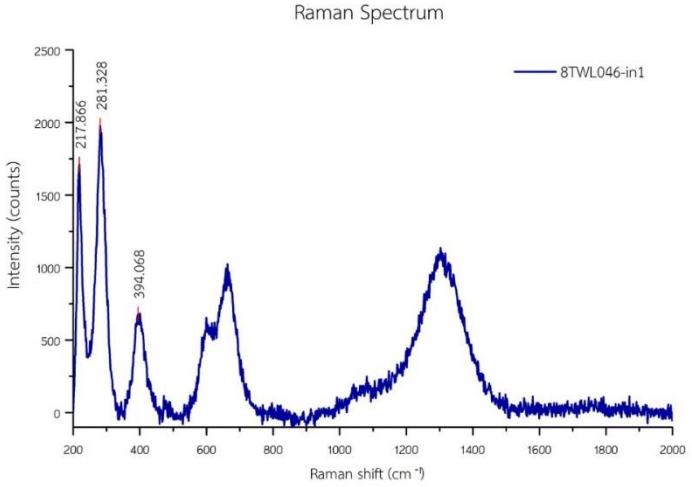

Figure 4.42 Representative Raman spectrum of sulphide inclusion observed in Bo Welu sapphire (sample 8TWL046).

Table 4.12 Representative EPMA analyses of sulphide inclusions in Bo Welu ruby and sapphire.

Mineral phase analysis (wt%)	Ruby				Sapphire
	PR-RP	rP		P	gB
	9TWL100-in1	9TWL114-in1	9TWL143-in1	9TWL046-in1	8TWL046-in1
Tl	0.18	0.17	0.21	0.23	ND
Al	0.04	0.01	0.03	0.01	3.84
In	ND	0.01	0.01	ND	0.01
Ba	0.13	0.09	0.12	0.02	NA
Fe	25.39	57.19	33.80	50.65	58.26
S	22.73	27.66	23.78	27.56	37.22
As	ND	ND	ND	ND	ND
Pb	ND	ND	ND	ND	0.25
Cu	40.98	ND	29.89	0.04	0.03
Ni	0.18	4.14	ND	8.74	ND
Mo	0.48	0.47	0.45	0.61	ND
Pt	ND	0.09	0.01	ND	0.01
Sn	0.01	ND	ND	0.02	ND
Zn	ND	0.04	ND	ND	NA
Co	ND	ND	ND	ND	ND
Total*	90.12	89.85	88.30	87.88	99.63
Formula					
Tl	0.002	0.001	0.002	0.001	0.00
Al	0.004	0.000	0.002	0.001	0.14
In	0.000	0.000	0.000	0.000	0.00
Ba	0.002	0.001	0.001	0.000	0.00
Fe	1.000	1.000	1.000	1.000	1.00
S	1.559	0.842	1.225	0.948	1.11
As	0.000	0.000	0.000	0.000	0.00
Pb	0.000	0.000	0.000	0.000	0.00
Cu	1.418	0.000	0.777	0.001	0.00
Ni	0.007	0.069	0.000	0.164	0.00
Mo	0.011	0.005	0.008	0.007	0.00
Pt	0.000	0.000	0.000	0.000	0.00
Sn	0.000	0.000	0.000	0.000	0.00
Zn	0.000	0.001	0.000	0.000	0.00
Co	0.000	0.000	0.000	0.000	0.00
Total**	4.003	1.919	3.016	2.122	2.25

NA = not analyzed, ND = not detected

Silicate melts

Rounded two-phase inclusions containing gas bubble and silicate melt are also observed in red-purple, reddish purple, and purple ruby samples (Figure 4.43, left). This type of inclusion was found more often in Bo Welu ruby than Bo Rai ruby. They sometimes show subhedral shape (Figure 4.43, right). More photographs of these inclusions are collected in Appendix B. Unfortunately, their Raman spectra do not match GIT-GTL reference (Figure 4.44, left). Raman spectrum of CO_2 inclusion in sample 9TWL132 shows peaks at 1284 and 1388 cm^{-1} (Figure 4.44, right) (Dao and Delaigue, 2000). The chemical compositions of these inclusions were analyzed by Electron Probe Micro-Analyzer (EPMA) which their analyses are present in Table 4.13. They contain major contents of SiO_2 and Al_2O_3 with minor components of CaO, FeO, and MgO. More chemical compositions are reported in Appendix H.

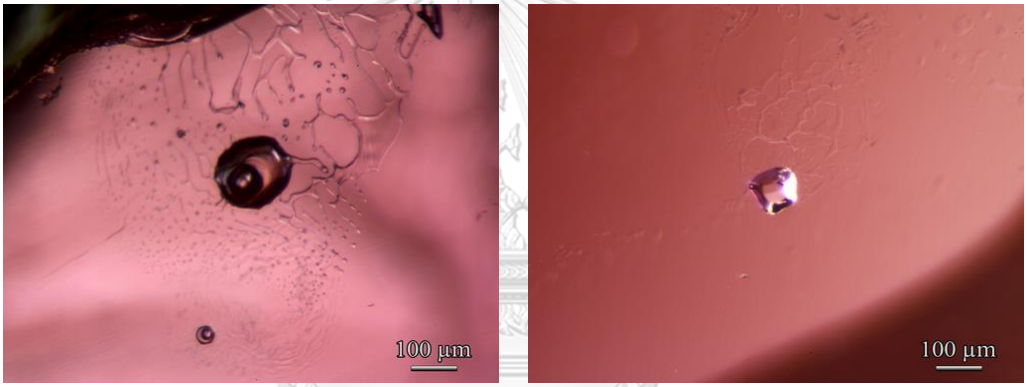

Figure 4.43 Two-phase inclusions containing gas bubble and silica melt, in Bo Welu ruby. These photographs were captured using a combination of bright field and fiber-optic illumination. Most samples are rounded shape (left, sample 9TWL077) some subhedral shape (right, sample 9TWL131).

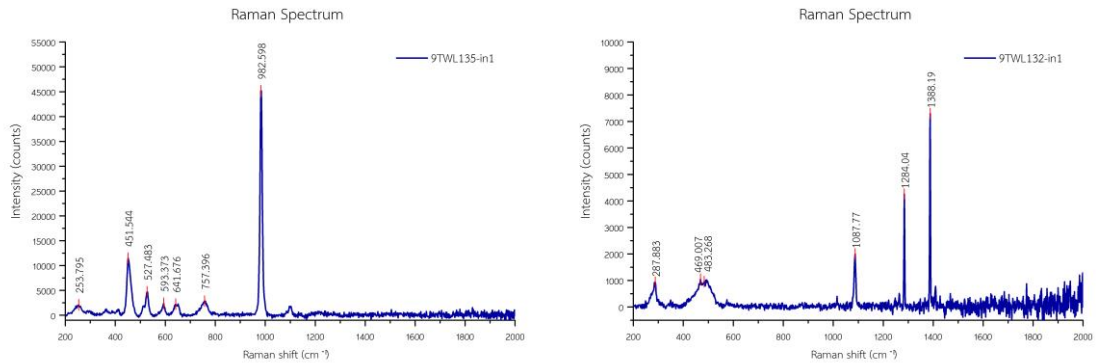

Figure 4.44 Representative Raman spectrum of silicate melt inclusions in Bo Welu ruby sample 9TWL135 (left); Raman spectrum of CO_2 inclusion in sample 9TWL132 (right).

Table 4.13 Representative EPMA analyses of two-phase inclusions in Bo Welu ruby samples.

Mineral phase analysis (wt%)	PR-RP			rP		P
	9TWL067-in1	9TWL132-in1	9TWL135-in1	9TWL131-in1	9TWL174-in2	9TWL077-in1
SO_3	NA	ND	6.50	0.25	NA	0.03
SiO_2	43.56	60.26	45.06	61.74	55.66	46.13
TiO_2	0.54	0.03	0.02	0.23	0.83	0.79
Al_2O_3	30.43	24.70	26.46	25.52	27.96	34.96
Cr_2O_3	0.01	ND	0.09	ND	ND	0.01
Ga_2O_3	NA	0.11	ND	0.06	0.05	0.04
V_2O_3	NA	0.01	0.01	0.01	ND	0.01
CaO	20.59	3.45	18.07	5.73	5.73	5.94
FeO	1.70	0.86	0.11	1.59	2.49	2.04
MnO	ND	0.04	ND	ND	0.08	0.01
MgO	2.10	1.41	0.21	1.65	2.05	3.38
K_2O	0.01	5.44	0.02	0.12	0.41	0.03
Na_2O	1.14	3.41	3.21	2.68	4.20	5.59
Total	100.08	99.72	99.76	99.57	99.45	98.95

NA = not analyzed, ND = not detected

Zircon

Zircon inclusions occur commonly as prismatic grain (Figure 4.45a-b) or cube crystal with stress fissures (Figure 4.45c). Cluster of zircons surrounded by stress fissures are also observed (Figure 4.45d). More photographs of zircon inclusions are present in Appendix B. A representative Raman spectrum is shown in Figure 4.46 and more spectra are collected in Appendix E.

Representative EPMA analyses of Bo Welu zircon inclusions are present in Table 4.14. They have narrow compositional range of about 2-3 wt% HfO_2, ≤0.7 wt% UO_2, mostly <0.1 wt% ThO_2, <0.5 wt% Y_2O_3, ≤0.3 wt% REE. They show uniform chemical compositions as plotted in the Si-Zr-Hf ternary diagram (Figure 4.47).

Zircon inclusions in Thai sapphire from other deposits as previously reported from Bo Phloi, Kanchanaburi (Saminpanya and Sutherland, 2011; Khamloet et al., 2014), Kao Wua, Chanthaburi (Sutherland et al., 1998a) and Den Chai, Phare (Khamloet, 2011). Moreover, Zircon inclusion from Ban Huai Sai sapphire, Lao PDR was reported by Sutherland et al. (2002).

The Bo Welu zircon shows values overlaping with those of zircon inclusion from Bo Phloi sapphire (Khamloet et al., 2014) but they contain slightly higher HfO_2 content than those of Kao Wua and Den Chai and slightly lower than Ban Huai Sai sapphire. The fairly similar Hf content may indicate similar provenance of these host sapphire. In addition, the zircon incluisons in Bo Welu sappphire contain higher HfO_2 content than those alluvial zircon which were reported by Sutthirat (2001) indicating different origin of both zircons. Hf content in zircon inclusion can reflect degree of differentiation of parental melt (Wark and Miller, 1993). The high abundances of Hf content in zircon inclusion may indicate initial formation of host sapphire was related to highly evolved material.

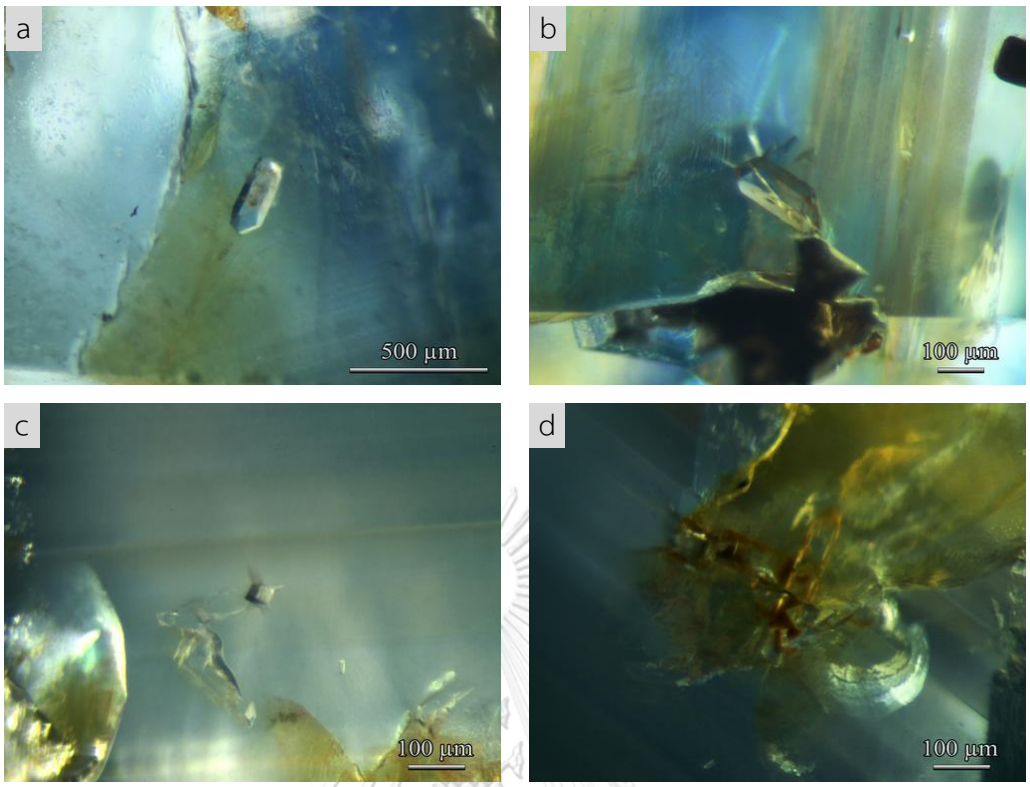

Figure 4.45 Prismatic zircon inclusions in sapphire samples 8TWL035 (a) and 8TWL040 (b); c) cubic-like zircon without pyramid face (sample 8TWL059); d) cluster of zircon crystals with fractures (sample 8TWL059).

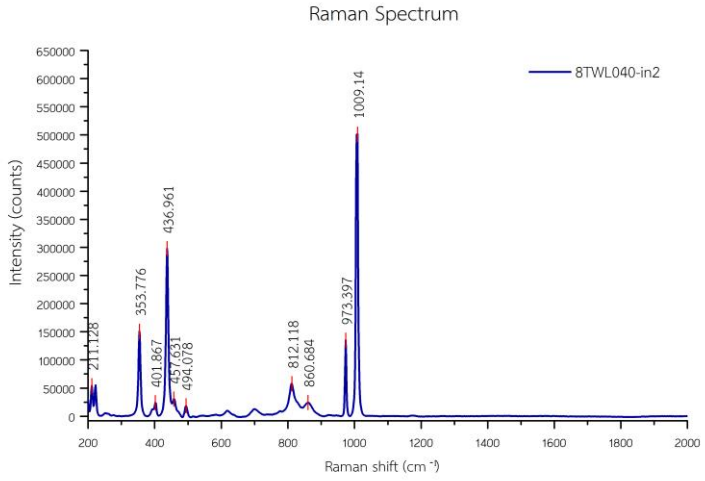

Figure 4.46 Representative Raman spectrum of zircon inclusion observed in Bo Welu sapphire (sample 8TWL040).

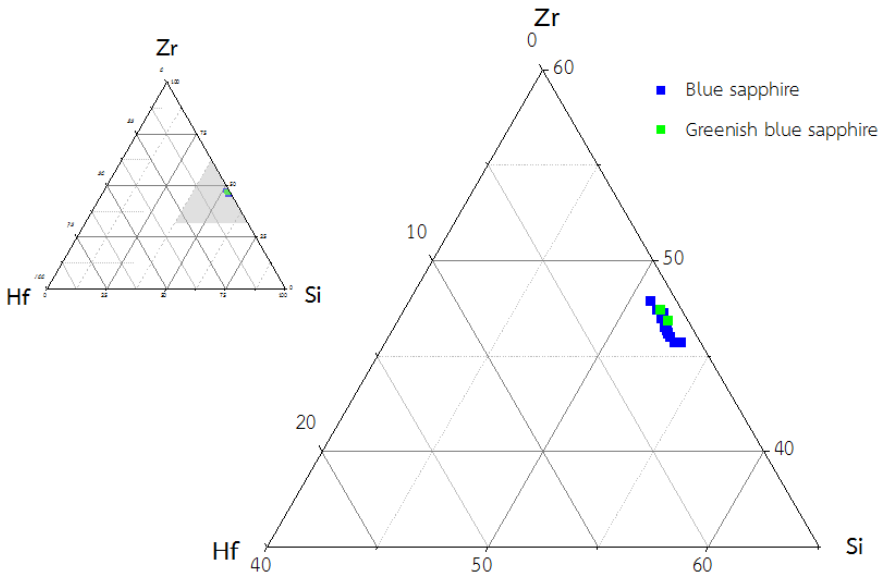

Figure 4.47 Ternary Si-Zr-Hf plots of zircon inclusions in Bo Welu sapphire.

Table 4.14 Representative EPMA analyses of zircon inclusions in Bo Welu sapphire.

Mineral phase analysis (wt%)	B											gB	
	8TWL 040-in2	8TWL 059-in1	8TWL 059-in2	8TWL 059-in3	8TWL 059-in4	8TWL 059-in5	8TWL 059-in6	8TWL 059-in7	8TWL 059-in8	8TWL 059-in10	8TWL 059-in12	8TWL 035-in1	8TWL 101-in1
P_2O_5	ND	ND	0.48	0.49	0.41	0.09	0.57	0.44	ND	0.20	0.40	0.12	ND
HfO_2	2.09	2.72	2.62	2.64	2.77	2.63	2.80	2.80	2.53	2.06	2.58	2.12	2.23
SiO_2	34.78	34.26	33.63	32.95	33.51	32.99	33.86	33.32	33.17	32.88	32.09	33.56	33.15
ThO_2	0.07	0.06	1.21	0.59	0.37	0.08	0.47	0.62	ND	0.01	0.50	1.19	0.01
UO_2	0.24	0.30	1.13	0.76	0.62	0.53	0.75	0.91	0.23	0.28	0.66	0.70	0.07
ZrO_2	61.13	62.18	59.39	60.24	59.95	61.32	60.66	60.17	62.81	61.55	61.96	61.81	62.54
Al_2O_3	0.07	ND	0.01	0.11	0.02	ND	ND	ND	ND	0.02	ND	0.02	0.09
Dy_2O_3	ND	ND	0.09	0.08	0.07	ND	0.12	0.14	0.02	0.01	0.09	0.06	ND
Er_2O_3	0.04	ND	0.15	0.20	0.18	0.03	0.18	0.08	0.02	0.01	0.01	0.11	ND
Lu_2O_3	0.10	ND	ND	0.10	0.15	0.06	0.06	0.27	0.07	0.11	0.08	0.18	ND
Nd_2O_3	0.02	ND	ND	0.02	0.06	0.07	ND	ND	ND	0.03	ND	ND	0.01
Pr_2O_3	ND	ND	ND	0.09	ND	1.17	0.97	0.29	ND	0.91	0.46	ND	0.26
Y_2O_3	0.17	0.05	0.85	0.80	0.74	0.11	0.81	0.74	0.04	0.16	0.82	0.37	0.06
FeO	0.08	0.05	0.07	0.09	0.08	0.06	0.08	0.10	0.04	0.05	0.07	0.02	0.11
PbO	ND	ND	0.79	ND	ND	ND	0.04	ND	ND	ND	ND	0.15	ND
Total	98.79	99.62	100.42	99.16	98.93	99.14	101.37	99.88	98.93	98.28	99.72	100.41	98.53
4 (O)													
P	0.000	0.000	0.013	0.013	0.011	0.002	0.015	0.011	0.000	0.005	0.011	0.003	0.000
Hf	0.018	0.024	0.023	0.023	0.024	0.023	0.024	0.025	0.022	0.018	0.023	0.019	0.020
Si	1.062	1.046	1.035	1.021	1.036	1.026	1.027	1.027	1.026	1.024	0.997	1.030	1.027
Th	0.000	0.000	0.008	0.004	0.003	0.001	0.003	0.004	0.000	0.000	0.004	0.008	0.000
U	0.002	0.002	0.008	0.005	0.004	0.004	0.005	0.006	0.002	0.002	0.005	0.005	0.000
Zr	0.910	0.926	0.891	0.910	0.903	0.930	0.897	0.904	0.948	0.935	0.939	0.925	0.945
Al	0.003	0.000	0.000	0.004	0.001	0.000	0.000	0.000	0.000	0.001	0.000	0.001	0.003
Dy	0.000	0.000	0.001	0.001	0.001	0.000	0.001	0.001	0.000	0.000	0.001	0.001	0.000
Er	0.000	0.000	0.001	0.002	0.002	0.000	0.002	0.001	0.000	0.000	0.000	0.001	0.000
Lu	0.001	0.000	0.000	0.001	0.001	0.001	0.001	0.002	0.001	0.001	0.001	0.002	0.000
Nd	0.000	0.000	0.000	0.000	0.001	0.001	0.000	0.000	0.000	0.000	0.000	0.000	0.000
Pr	0.000	0.000	0.000	0.001	0.000	0.013	0.011	0.003	0.000	0.010	0.005	0.000	0.003
Y	0.003	0.001	0.014	0.013	0.012	0.002	0.013	0.012	0.001	0.003	0.014	0.006	0.001
Fe	0.002	0.001	0.002	0.002	0.002	0.002	0.002	0.003	0.001	0.001	0.002	0.001	0.003
Pb	0.000	0.000	0.007	0.000	0.000	0.000	0.000	0.000	0.000	0.000	0.000	0.001	0.000
Total**	2.001	2.000	2.003	2.000	2.001	2.005	2.001	1.999	2.001	2.000	2.002	2.003	2.002
Atomic%													
Hf	0.92	1.19	1.18	1.20	1.24	1.18	1.25	1.26	1.12	0.93	1.17	0.94	0.99
Si	53.36	52.42	53.10	52.24	52.74	51.84	52.71	52.51	51.41	51.79	50.90	52.19	51.57
Zr	45.73	46.39	45.72	46.57	46.01	46.98	46.04	46.23	47.47	47.28	47.93	46.87	47.44
Total**	100.00	100.00	100.00	100.00	100.00	100.00	100.00	100.00	100.00	100.00	100.00	100.00	100.00

ND = not detected

Monazite

Monazite inclusions (ideal formula: (Ce, La) PO_4) in Bo Welu sapphire samples are typically colorless to very light yellow which they form nearly horizontal prisms (Figure 4.48a-b). An unusual monazite crystal contains albite feldspar inclusion inside (Figure 4.48c) which is clearly seen in Backscattered-Electron (BSE) Image. It shows strong brightness monazite compared to inside feldspar (Figure 4.48d). Electron Probe Micro-Analyzer (EPMA) was used to analyze this feldspar inclusions (sample 8TWL114-in25); its result is present in Table 4.11. A representative Raman spectrum of monazite inclusion is shown in Figure 4.49. More photographs and Raman spectra of monazite inclusions are collected in Appendices B and E, respectively.

Representative EPMA analyses of monazite inclusions are present in Table 4.15, and more data are reported in Appendix H. Monazite inclusions in Bo Welu sapphire generally vary in composition widely 35-46 wt% ThO_2, 15-24 wt% Ce_2O_3 and 16-22 wt% P_2O_5. Monazite inclusions in sapphire were previously identified by Laser Raman spectroscope and reported from basaltic sapphire such as in SW Rwanda (Krzemnicki et al., 1996), in Tok Phrom, Chanthaburi and Bo Phloi, Kanchanaburi (Intasopa et al., 1998), and Lao PDR (Singbamroong and Thanasuthipitak, 2004). Monazite inclusions in Bo Welu sapphire have higher phosphorus and lower lanthanum than monazite in Bo Phloi which was reported by Khamloet et al. (2014). Moreover, monasite inclusion also support that the host sapphire should have crystallized from a highly evolved melt.

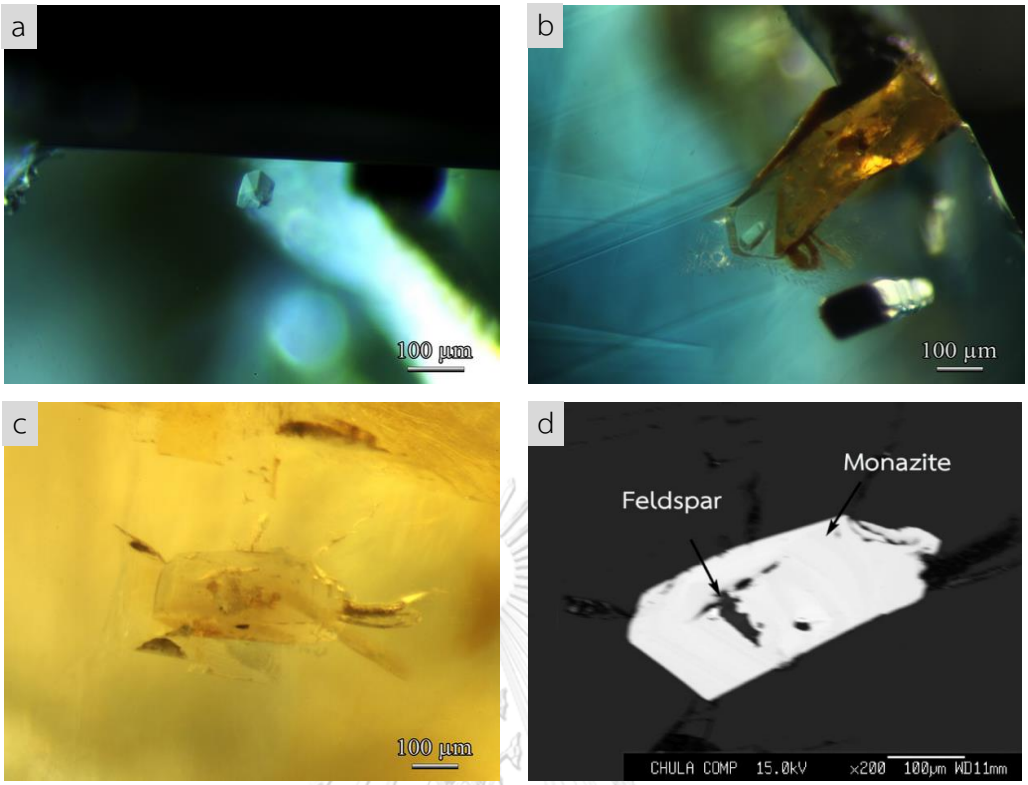

Figure 4.48 Monazite inclusions in Bo Welu sapphire samples 8TWL104 (a) and 8TWL053 (b) are typically colorless subhedral crystals. Monazite crystal in sample 8TWL114 (c) contains albite felspar inclusion inside which is clearly distinguished by Backscattered-Electron (BSE) Imaging (d).

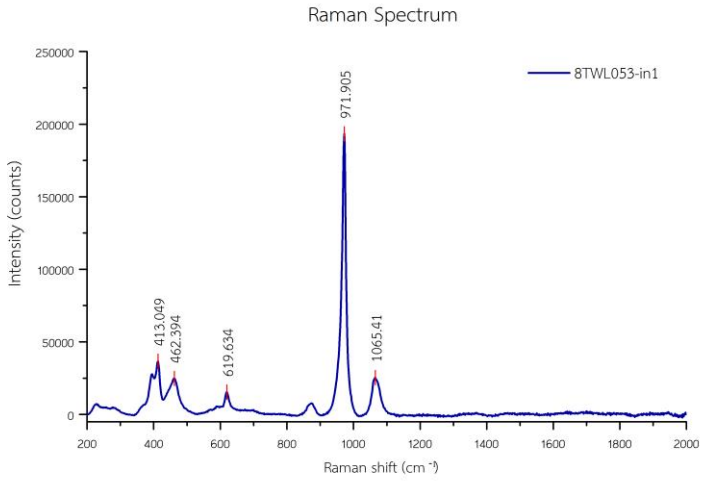

Figure 4.49 Representative Raman spectrum of monazite inclusion observed in Bo Welu sapphire (sample 8TWL053).

Table 4.15 Representative EPMA analyses of monazite inclusions in Bo Welu sapphire.

Mineral phase analysis (wt%)	B		ɡB						
	8TWL068-in2	8TWL114-in24*	8TWL036-in3	8TWL036-in4	8TWL036-in5	8TWL036-in7	8TWL082-in7	8TWL104-in3	8TWL119-in2
P_2O_5	17.69	18.14	16.13	15.81	21.09	21.62	18.72	16.49	16.36
Ta_2O_5	NA	0.41	NA	NA	0.20	0.51	0.15	NA	NA
HfO_2	NA	0.28	NA	NA	ND	0.13	ND	NA	NA
SiO_2	4.28	4.80	4.86	3.71	4.53	4.59	5.31	4.77	3.05
ThO_2	39.59	38.14	44.42	46.46	36.30	35.15	45.12	37.82	46.08
UO_2	0.94	0.05	1.06	0.95	ND	ND	ND	0.86	1.08
ZrO_2	NA	ND	NA	NA	0.12	0.02	ND	NA	NA
Al_2O_3	0.04	ND	0.08	0.07	ND	ND	ND	0.04	0.07
Ce_2O_3	21.31	24.30	21.24	19.28	23.26	24.32	15.38	21.26	17.42
Dy_2O_3	0.52	0.07	0.65	0.60	0.14	0.06	0.22	0.72	0.59
Gd_2O_3	1.18	0.71	1.02	1.14	0.84	0.57	0.92	1.70	1.75
La_2O_3	1.23	ND	0.69	1.04	ND	ND	ND	1.68	1.63
Nd_2O_3	5.40	6.41	3.81	5.33	7.81	6.94	7.33	6.42	5.70
Pr_2O_3	4.10	4.80	4.56	3.04	3.63	4.50	2.80	3.37	3.71
Sm_2O_3	1.16	0.12	0.89	0.80	0.09	0.24	0.20	1.24	1.03
Y_2O_3	0.21	0.48	0.24	0.08	0.22	0.22	0.99	0.76	0.44
FeO	0.05	ND	0.08	0.09	ND	0.20	0.07	0.02	0.04
CaO	0.75	1.70	0.30	0.24	1.14	0.24	2.19	1.64	1.29
Total	98.45	100.39	100.03	98.64	99.36	99.28	99.38	98.79	100.24
4 (O)									
P	0.709	0.699	0.657	0.669	0.782	0.795	0.715	0.662	0.680
Ta	-	0.005	-	-	0.002	0.006	0.002	-	-
Hf	-	0.004	-	-	0.000	0.002	0.000	-	-
Si	0.203	0.219	0.234	0.186	0.198	0.199	0.240	0.226	0.150
Th	0.426	0.395	0.486	0.529	0.362	0.347	0.463	0.408	0.515
U	0.010	0.000	0.011	0.011	0.000	0.000	0.000	0.009	0.012
Zr	-	0.000	-	-	0.003	0.000	0.000	-	-
Al	0.002	0.000	0.005	0.004	0.000	0.000	0.000	0.002	0.004
Ce	0.369	0.405	0.374	0.353	0.373	0.387	0.254	0.369	0.313
Dy	0.008	0.001	0.010	0.010	0.002	0.001	0.003	0.011	0.009
Gd	0.018	0.011	0.016	0.019	0.012	0.008	0.014	0.027	0.028
La	0.021	0.000	0.012	0.019	0.000	0.000	0.000	0.029	0.029
Nd	0.091	0.104	0.065	0.095	0.122	0.108	0.118	0.109	0.100
Pr	0.071	0.080	0.080	0.055	0.058	0.071	0.046	0.058	0.066
Sm	0.019	0.002	0.015	0.014	0.001	0.004	0.003	0.020	0.017
Y	0.005	0.012	0.006	0.002	0.005	0.005	0.024	0.019	0.011
Fe	0.002	0.000	0.003	0.004	0.000	0.007	0.003	0.001	0.002
Ca	0.038	0.083	0.015	0.013	0.054	0.011	0.106	0.083	0.068
Total**	1.992	2.019	1.989	1.983	1.973	1.952	1.990	2.033	2.004

* Monazite combined with feldspar inclusion (NA = not analyzed, ND = not detected)

Columbite

Black opaque inclusion most common in Bo Welu sapphire. Some of them form irregular shape (Figure 4.50a), orthorhombic crystal (Figure 4.50b), and flat shape (Figure 4.50c) which they are characterized by columbite (ideally $Fe^{2+}Nb_2O_6$). Some high relief crystals are associate with tension cracks (Figure 4.50d). A few columbite inclusions are dark orange color (Figure 4.50e) and adhered with minute particle (Figure 4.50f). More photographs of columbite inclusions are collected in Appendix B. A representative Raman spectrum is shown in Figure 4.51 and more spectra are reported in Appendix E.

The representative EPMA analyses of columbite inclusions are present in Table 4.16. These columbite inclusions have narrow range of composition, e.g., 72.4-78.1 wt% Nb_2O_5, 0.1-1.1 wt% Ta_2O_5, 0.3-3.1 wt% TiO_2, 0-1.0 wt% MgO, 1.2-14.2 wt% FeO. More data are collected in Appendix H. Their compositions are plotted on the $FeTa_2O_6$ -$FeNb_2O_6$ - $MnNb_2O_6$ - $MnTa_2O_6$ quadrilateral diagram (Cerny and Ercit, 1985) for columbite-tantalite classification. These columbite inclusions fall distinctively in Ferro columbite (Figure 4.52). Columbite inclusions in Tok Phrom sapphire in Chanthaburi, and Pailin sapphire in Cambodia were also reported by (Intasopa et al., 1998); however, they were identified by the Raman technique. Khamloet (2011) reported fairly similar chemical composition of columbite inclusions in Pailin sapphire with slightly higher Ta content than those in Bo Welu sapphire.

However, columbite chemistry of Bo Welu and Pailin sapphires have Ti, Ta and Fe oxides less than columbite in basaltic sapphire from New England, Wenchang and Lava Plains in Australia, previously reported by (Guo et al., 1996; Sutherland et al., 1998a).

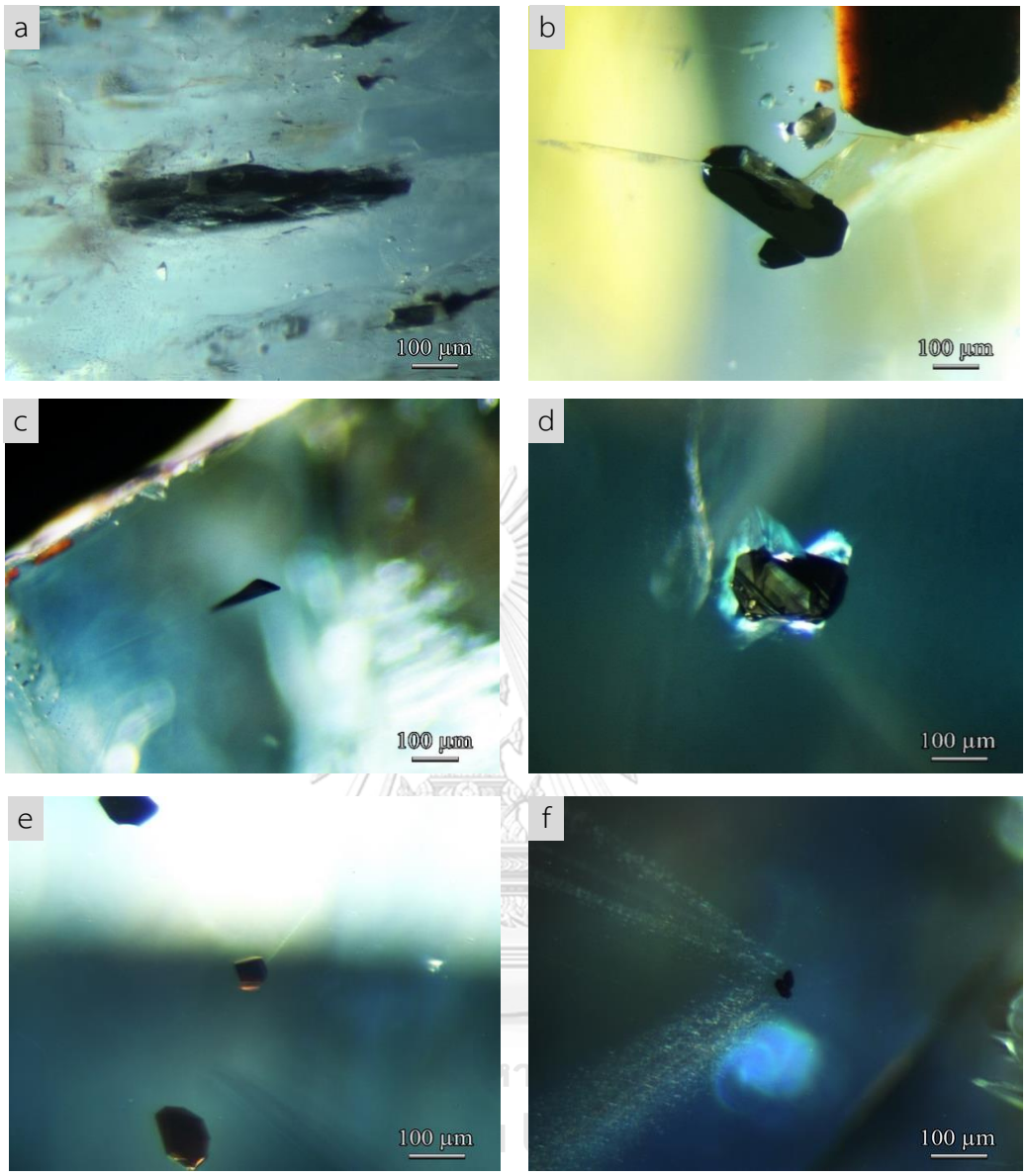

Figure 4.50 Microscopic observation of columbite inclusions in Bo Welu sapphire, using oblique fiber-optic illumination showing: a) irregular columbite (sample 8TWL001); b) subhedral grain (sample 8TWL026); c) flat shape (sample 8TWL106; d) columbite associated with tension crack (sample 8TWL108); e) dark orange columbite (sample 8TWL108); f) columbite crystal composited with minute particle (sample 8TWL101).

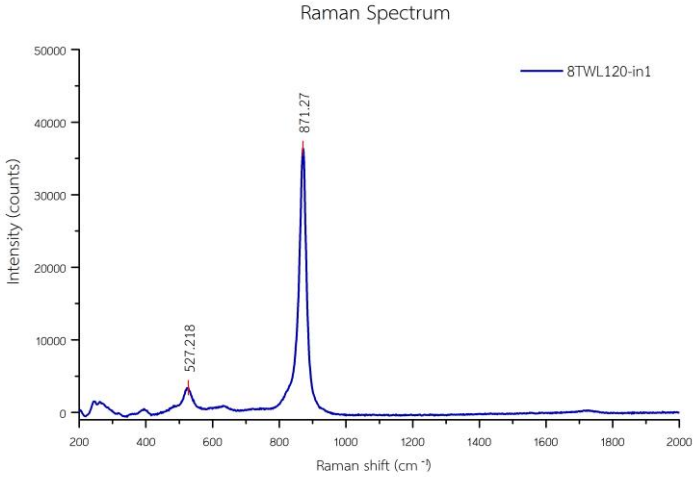

Figure 4.51 A representative Raman spectrum of columbite inclusion observed in Bo Welu sapphire 8TWL120.

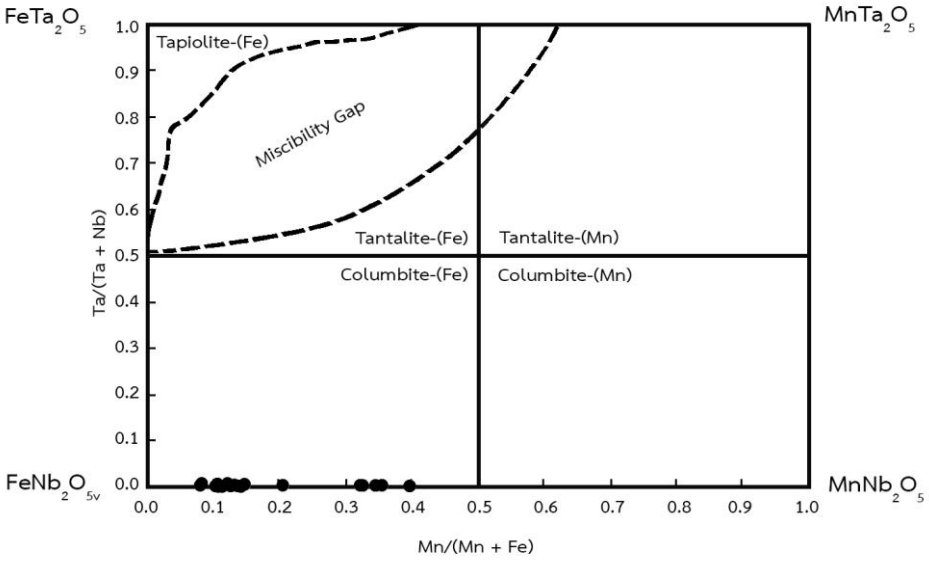

Figure 4.52 Compositional plots of ferrocolumbite inclusions found in Bo Welu sapphire base on quadrilateral diagram which proposed by Cerny and Ercit (1985).

Table 4.16 Representative EPMA analyses of columbite inclusions in Bo Welu sapphire.

Mineral phase	gB	gB	gB	gB	gB	gB	gB	BG-GB	
analysis (wt%)	8TWL001-in1	8TWL001-in2	8TWL001-in3	8TWL120-in1	8TWL022-in1	8TWL106-in1	8TWL036-in2	8TWL097-in7	8TWL097-in8
Nb_2O_5	74.32	75.23	76.53	75.36	72.63	75.01	74.39	74.57	72.44
Ta_2O_5	0.46	0.54	0.57	0.42	0.54	0.30	0.31	0.16	0.21
ThO_2	ND	0.21	ND	0.03	ND	ND	0.87	0.11	0.30
TiO_2	1.11	1.31	0.93	0.85	1.54	1.13	0.37	0.40	0.40
UO_2	0.02	0.05	0.05	ND	ND	0.01	3.45	2.10	2.59
ZrO_2	0.57	0.54	0.28	0.04	0.94	0.62	0.57	0.83	0.81
Al_2O_3	0.08	0.08	0.03	ND	0.13	0.15	0.15	0.14	0.14
Ce_2O_3	ND	0.10	0.08	ND	ND	0.13	1.27	1.85	1.59
Nd_2O_3	0.02	ND	0.03	0.01	ND	0.07	1.46	1.93	1.80
Sm_2O_3	ND	ND	ND	0.01	0.02	ND	0.76	0.77	0.70
Y_2O_3	ND	ND	ND	ND	ND	ND	3.19	3.46	3.33
FeO	12.52	12.84	11.99	12.60	14.26	11.37	10.37	10.45	10.38
MnO	5.95	6.01	6.51	6.53	3.61	7.37	1.48	1.24	1.31
MgO	0.73	0.62	0.49	0.41	1.00	0.36	0.09	0.16	0.12
CaO	0.05	0.13	0.10	0.08	0.05	0.10	0.47	0.81	0.70
Na_2O	ND	ND	ND	ND	ND	ND	ND	ND	ND
Total	95.84	97.65	97.59	96.33	94.72	96.63	99.18	98.97	96.80
6 (O)									
Nb	1.950	1.942	1.976	1.974	1.923	1.955	1.967	1.961	1.955
Ta	0.007	0.008	0.009	0.007	0.009	0.005	0.005	0.003	0.003
Th	0.000	0.003	0.000	0.000	0.000	0.000	0.012	0.001	0.004
Ti	0.049	0.056	0.040	0.037	0.068	0.049	0.016	0.018	0.018
U	0.000	0.001	0.001	0.000	0.000	0.000	0.045	0.027	0.034
Zr	0.016	0.015	0.008	0.001	0.027	0.017	0.016	0.023	0.023
Al	0.005	0.005	0.002	0.000	0.009	0.010	0.010	0.010	0.010
Ce	0.000	0.002	0.002	0.000	0.000	0.003	0.027	0.039	0.035
Nd	0.000	0.000	0.001	0.000	0.000	0.001	0.030	0.040	0.038
Sm	0.000	0.000	0.000	0.000	0.000	0.000	0.015	0.015	0.014
Y	0.000	0.000	0.000	0.000	0.000	0.000	0.099	0.107	0.106
Fe	0.608	0.613	0.573	0.610	0.698	0.548	0.507	0.508	0.518
Mn	0.293	0.291	0.315	0.321	0.179	0.360	0.073	0.061	0.066
Mg	0.063	0.053	0.042	0.035	0.087	0.031	0.008	0.014	0.011
Ca	0.003	0.008	0.006	0.005	0.003	0.006	0.030	0.051	0.045
Na	0.000	0.000	0.000	0.000	0.000	0.000	0.000	0.000	0.000
Total*	2.996	2.996	2.973	2.991	3.003	2.986	2.861	2.879	2.881

ND = not detected

Table 4.16 Representative EPMA analyses of columbite inclusions in Bo Welu sapphire. (continued)

Mineral phase analysis (wt%)	B				gB				
	8TWL064-in1	8TWL108-in3	8TWL096-in2	8TWL120-in2	8TWL036-in1	8TWL028-in2	8TWL108-in1	8TWL108-in2	8TWL100-in1
Nb_2O_5	74.37	74.95	76.74	73.48	75.86	78.10	76.99	77.66	76.40
Ta_2O_5	0.25	0.51	0.34	0.31	0.88	1.10	1.03	0.58	0.79
ThO_2	0.85	0.71	0.16	0.04	1.02	0.54	0.59	0.44	0.57
TiO_2	0.43	0.47	0.30	0.35	3.10	2.92	2.56	2.34	2.86
UO_2	3.50	0.81	0.82	3.58	0.62	0.73	0.57	0.70	0.48
ZrO_2	0.78	1.10	1.33	0.93	ND	0.10	0.08	ND	0.11
Al_2O_3	0.29	0.22	0.12	0.13	0.69	0.58	0.75	0.70	0.53
Ce_2O_3	1.36	0.66	0.89	0.73	0.97	0.72	0.80	0.82	0.79
Nd_2O_3	1.42	0.98	1.28	1.25	0.28	0.25	0.12	0.13	0.23
Sm_2O_3	0.72	0.60	0.60	0.61	0.03	0.01	0.05	ND	ND
Y_2O_3	2.76	3.96	3.60	3.77	ND	ND	ND	ND	ND
FeO	9.79	9.71	9.95	10.23	1.25	1.22	1.25	1.24	1.40
MnO	1.58	1.45	1.56	1.15	0.15	0.11	0.18	0.11	0.23
MgO	0.08	0.18	0.20	0.15	ND	ND	ND	0.01	ND
CaO	0.42	0.67	0.42	0.52	5.20	5.46	5.37	5.21	5.19
Na_2O	ND	ND	ND	ND	7.07	7.50	6.99	7.15	ND
Total	98.61	96.97	98.30	97.23	97.12	99.32	97.34	97.09	89.59
6 (O)									
Nb	1.973	1.981	2.000	1.969	1.919	1.928	1.938	1.957	2.068
Ta	0.004	0.008	0.005	0.005	0.013	0.016	0.016	0.009	0.013
Th	0.011	0.009	0.002	0.001	0.013	0.007	0.007	0.006	0.008
Ti	0.019	0.021	0.013	0.016	0.130	0.120	0.107	0.098	0.129
U	0.046	0.010	0.010	0.047	0.008	0.009	0.007	0.009	0.006
Zr	0.022	0.031	0.037	0.027	0.000	0.003	0.002	0.000	0.003
Al	0.020	0.015	0.008	0.009	0.045	0.037	0.049	0.046	0.038
Ce	0.029	0.014	0.019	0.016	0.020	0.014	0.016	0.017	0.017
Nd	0.030	0.021	0.026	0.026	0.005	0.005	0.002	0.003	0.005
Sm	0.015	0.012	0.012	0.012	0.001	0.000	0.001	0.000	0.000
Y	0.086	0.123	0.110	0.119	0.000	0.000	0.000	0.000	0.000
Fe	0.481	0.475	0.480	0.507	0.059	0.056	0.058	0.058	0.070
Mn	0.079	0.072	0.076	0.058	0.007	0.005	0.008	0.005	0.012
Mg	0.007	0.016	0.017	0.013	0.000	0.000	0.000	0.001	0.000
Ca	0.026	0.042	0.026	0.033	0.312	0.320	0.321	0.311	0.333
Na	0.000	0.000	0.000	0.000	0.767	0.794	0.754	0.772	0.000
Total*	2.847	2.851	2.842	2.858	3.298	3.314	3.288	3.291	2.702

ND = not detected

CHAPTER 5

DISCUSSION, CONCLUSION, AND RECOMMENDATION

5.1 Gemological Characteristics

Siam ruby has been very well known in the world gem markets for decades. These rubies were mined crucially in the main gem fields of Bo Rai and Bo Welu, the study areas. However, gem mining in these areas are no longer operated in these areas. Due to their rarity, Siam ruby is highly demanded in the gem market and leading to high value appraisal. Their chemical fingerprinting and specific inclusion characteristics are significant because they can be used for origin determination. Therefore, initial part of this project is designed to collect such information for further interpretation.

Bo Rai Ruby: Varieties of Bo Rai ruby samples range from medium-slightly purplish red, to red-purple, reddish purple and purple. Most rough stones usually are present as platy water-worn crystals with etched or dissolved surface; these are typical features of corundum roughs from basaltic deposits (Coenraads, 1992; Coenraads et al., 1995; Krzemnicki et al., 1996; Sutherland et al., 1998b). Their refractive indices (RI) range from 1.760 to 1.771 with birefringence of 0.008 to 0.010. They show inert to moderate red fluorescence under long-wave ultraviolet (LWUV) lamp and inert under short-wave ultraviolet (SWUV) lamp.

Absorption bands within the mid-IR range of these natural (untreated) rubies indicate CO_2 and some spectroscopic features of hydrous minerals, kaolinite in particular. The presence of kaolinite-related IR spectrum in the study samples suggest that rubies are not undergone heat treatment process

UV-Vis-NIR spectra of the Bo Rai ruby show combination between iron-related and chromium-related absorptions. Most purplish red and red-purple samples show chromium-dominated absorption causing red color. On the other hand, most reddish purple to purple ruby samples show clearly iron-related absorption more intense than chromium-related absorption; consequently, blue hue influences their body color. These absorptions are compatible with their trace chemical compositions which usually show Fe_2O_3/Cr_2O_3 ratio >3.

Trace elements of Bo Rai rubies, analyzed by EDXRF and EPMA, indicate higher iron component and lower contents of chromium, silica, gallium, titanium, manganese, magnesium, and vanadium. (see Tables 3.1 and 3.2 in Chapter III).

Regarding to EDXRF analyses, these Bo Rai rubies are relatively rich in Cr and poor in Ga with Cr_2O_3/Ga_2O_3 and Fe_2O_3/TiO_2 ratios are below 100. Moreover, TiO_2/Ga_2O_3 ratio is mostly below 25, and Fe_2O_3/Cr_2O_3 ratio is below 8. Most Cr_2O_3/Ga_2O_3 ratios are above 3 indicating metamorphic origin which is similar to ruby from West Pailin as suggested by Sutherland et al. (1998b). Therefore, initial formation of these rubies should have related to metamorphism prior to transportation to the earth surface via basaltic volcanism as suggested by Sutherland et al. (1998a)

Typical internal features of Bo Rai ruby are crystals with equatorial thin films, two-phase inclusion and high alumina diopside (fassaite) inclusion. Moreover, other mineral inclusions are garnet, pyrrhotite, plagioclase feldspar and silicate melt. It must be notified that mineral inclusions of sillimanite, spinel, and anatase are firstly reported from this study.

Bo Welu Ruby: Color varieties of Bo Welu ruby samples are rather being more purplish red than Bo Rai ruby (see Figure 5.1). Most rough rubies from Bo Welu gem field are rounded tabular habits. Some grains are etched or show dissolved features similar to those found in Bo Rai ruby. Their refractive indices (RI) range from 1.760 to 1.770 with birefringence of 0.009 to 0.010. Bo Welu ruby samples show weak to moderate red fluorescence under longwave ultraviolet (LWUV) lamp and inert under shortwave ultraviolet (SWUV) lamp also similar to Bo Rai ruby.

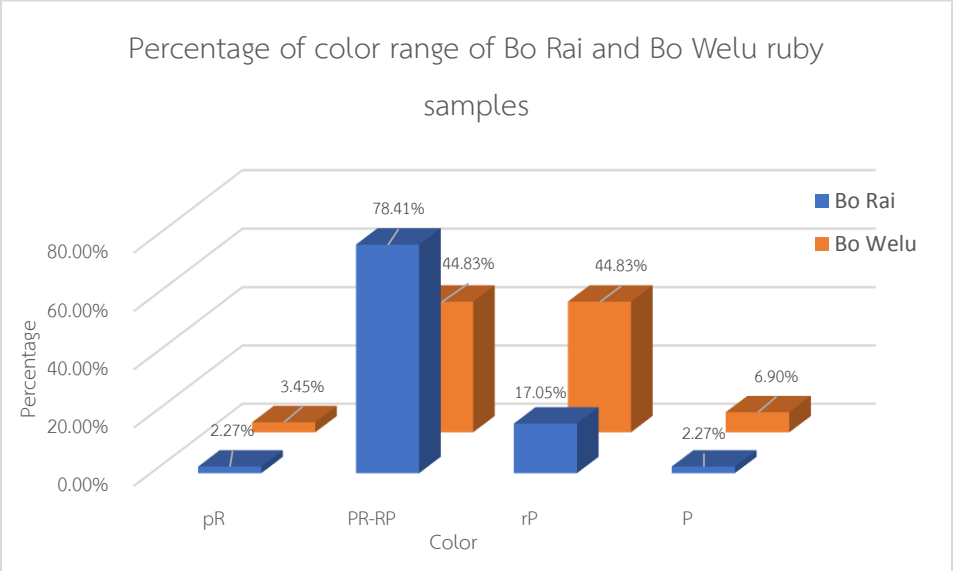

Figure 5.1 Color varieties of ruby samples from Bo Rai and Bo Welu showing statistical difference from purplish red to red-purple, reddish purple and purple colors.

Absorption bands of Bo Welu ruby within the mid-IR range also show CO_2 and the OH-group absorption bands related to kaolinite mineral, similar to those found in Bo Rai ruby. Most UV-Vis-NIR spectra of Bo Welu ruby represent a combination of high Fe-related and Cr-related absorption bands. The purplish red and red-purple samples show chromium-dominated absorptions. On the other hand, the reddish purple to purple ruby samples show clearly iron-related absorption more intense than chromium-related absorption; consequently, blue hue influences their body color similar to Bo Rai ruby.

Chemical fingerprinting of Bo Welu rubies, based on analyses of EDXRF and EPMA, appears to indicate a higher iron content with lower contents of chromium, silica, gallium, titanium, manganese, magnesium, and vanadium (see Tables 4.1 and 4.3 in Chapter IV). Regarding to EDXRF analyses, these Bo Welu rubies are relatively rich in Cr and poor in Ga with Cr_2O_3/Ga_2O_3 and Fe_2O_3/TiO_2 ratios below 100. Moreover, $TiO_2/Ga2O_3$ ratios and Fe_2O_3/Cr_2O_3 ratios are mostly below 10. Most Cr_2O_3/Ga_2O_3 ratios are above 3 indicating metamorphic origin which is similar to ruby from West Pailin as suggested by Sutherland et al. (1998b). Moreover, ratios of TiO_2/Ga_2O_3, Cr_2O_3/Ga_2O_3, and Fe_2O_3/TiO_2, are also similar in rubies from both deposits (Figure 5.2, left). However, Bo Welu ruby appears to have V, Cr, and Fe contents lower than those of Bo Rai ruby (Figure 5.2, right).

When comparing the chemical compositions of rubies from Bo Rai and Bo Welu gem fields with those from basalt-related ruby elsewhere from significant deposits such as Cambodia (Pailin, Kao Tawow and Bo Yakha) and Kenya (Simba and Baringo), data provided by the Gem Testing Laboratory of the Gem and Jewelry Institute of Thailand or GIT-GTL), it is found that Ratios of TiO_2/Ga_2O_3 of rubies from Bo Rai, Bo Welu, and Cambodia are slightly higher than the Kenya (see Figure 5.3, left). On the other hand, these deposits (Bo Rai, Bo Welu, and Cambodia) have Fe, V, and Cr contents similar to the Simba, but higher Fe content than the Baringo, Kenya (Figure 5.3 right).

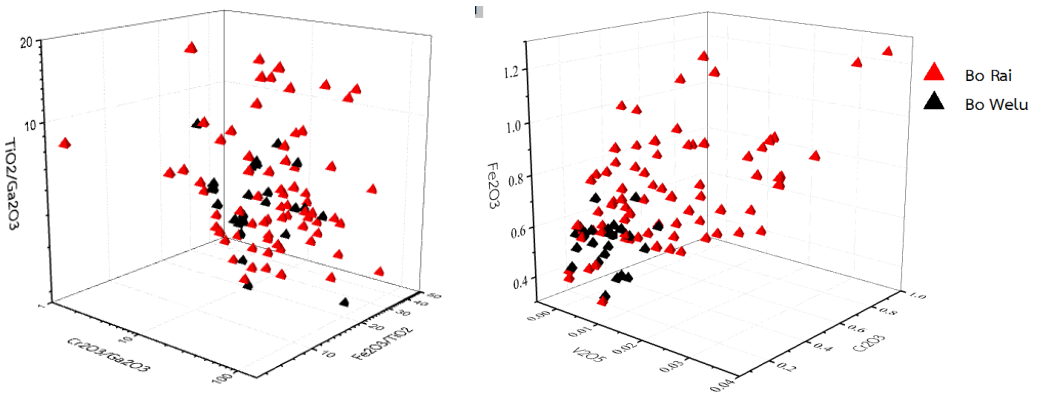

Figure 5.2 3D plotting chemical compositions, analyzed by EDXRF, of Bo Rai and Bo Welu rubies.

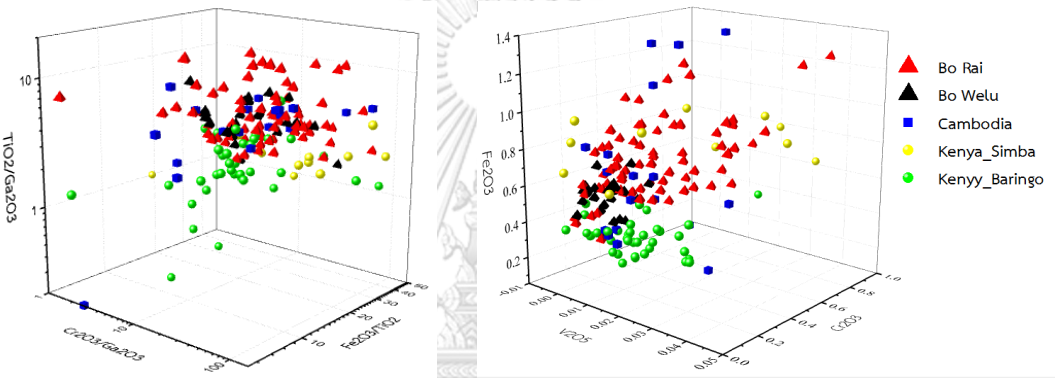

Figure 5.3 3D plotting of chemical compositions, analyzed by EDXRF, of Bo Rai, Bo Welu, Cambodia and Kenya rubies (data from GIT-GTL).

In general, internal features observed in rubies from both Bo Welu and Bo Rai gem fields are quite similar. However, two-phase inclusions are observed in Bo Welu ruby more often than Bo Rai ruby. The most significant mineral inclusion is high alumina diopside (fassaite) which contains magnesium slightly lower than fassaite pyroxene inclusions in Bo Rai ruby. Moreover, mineral inclusions of pyrope garnet, plagioclase feldspar, sillimanite, spinel and pyrrhotite are also observed in Bo Welu ruby similar to Bo Rai ruby. However, anatase inclusion are only identified in Bo Rai. On the other hand, sapphirine, quartz, nepheline and anhydrite inclusions are only identified in Bo Welu ruby. It must be notified that mineral inclusions of sillimanite, spinel, nepheline and anhydrite are firstly reported from this study.

Bo Welu sapphire: Varieties of samples range from medium-dark blue to greenish blue, and blue-green colors. Rough sapphires usually occur as hexagonal crystals. Some of these rough stones appear to be water-worn without crystal faces. Some grains show etched or dissolved surface-features similar to rubies from Bo Rai and Bo Welu. The stones are generally inert under both longwave ultraviolet (LWUV)

and shortwave ultraviolet (SWUV) lamps. Standard gemological testing yields refractive indices (RI) range of 1.760 to 1.771 with corresponding birefringence of 0.009 to 0.010.

Absorption bands within the mid-IR range of Bo Welu sapphire show peaks at 3309, 3230, 3184 cm^{-1} which are caused by OH-group (Beran, 1991; Diep, 2015) and kaolinite phase. Absorption caused by kaolinite is observed similarly to Bo Rai ruby and Bo Welu ruby. All Bo Welu sapphire samples show Fe^{2+}-Fe^{3+} IVCT with absorption maxima around 800-900 nm, the typical characteristic of blue sapphire from basaltic deposit (Sutherland et al., 1998b). Colors of blue and greenish blue sapphires from Bo Welu are mainly caused by Fe^{2+}-Ti^{4+} IVCT band around 550 nm as suggested by Schmetzer (1987) and Fritsch and Rossman (1987, 1988). On the other hand, blue-green samples usually show Fe^{2+}-Ti^{4+} IVCT band weaker than Fe^{3+} absorption band in which the later absorption band leads to yellow tone as suggested by Ferguson and Fielding (1971, 1972).

Regarding to chemical fingerprinting, Bo Welu sapphires were also analyzed by EDXRF and EPMA; these analyses yield higher iron content with lower contents of gallium, titanium, silica, chromium, manganese, vanadium, and magnesium (see Tables 4.2 and 4.4 in Chapter IV). EDXRF analyses of Bo Welu sapphires are relatively poor in Cr and high in Ga with Cr_2O_3/Ga_2O_3 below 1 indicating magmatic origin (Sutherland et al., 1998b). In comparison with sapphires from other gem fields in Thailand (i.e., Bo Ploi, Phrae, Tokphrom, Khao Ploi Wuen, and Khao Wua), Bo Welu sapphire has Fe_2O_3/TiO_2 ratio higher than sapphire from Phrae and Bo Ploi, and Fe_2O_3/Ga_2O_3 ratio lower than sapphire from Khao Ploi Wuen and Khao Wua (Figure 5.4 left). In addition, they have higher Ga and lower V contents than sapphire from other places (Figure 5.4 right).

Comparing to basalt-related sapphire around the world (i.e., Australia, Madagascar (Diego), Nigeria, Cambodia (Pailin, Botongsu), and Lao PDR (Hua Sai), Bo Welu sapphires have Fe_2O_3/TiO_2 ratio higher than basaltic sapphire from Nigeria, Cambodia, and Lao PDR (Figure 5.5 left). In additions, they appear to have lower V content than basaltic sapphire from other places (Figure 5.5 right).

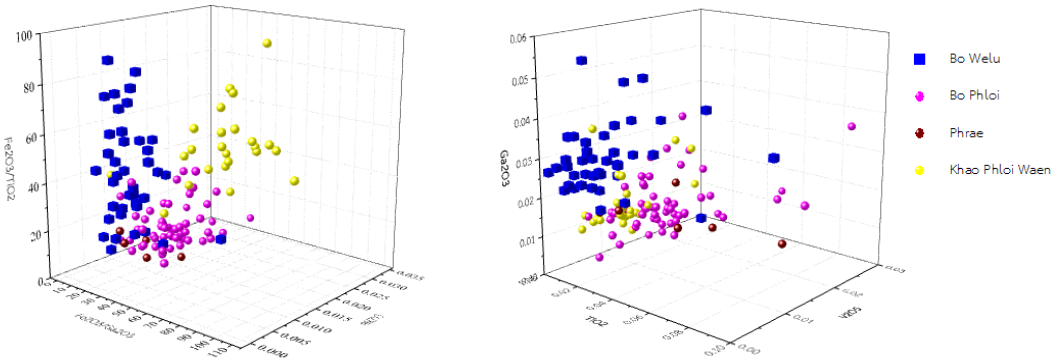

Figure 5.4 3D plotting of EDXRF analyses of Bo Welu sapphires compared to sapphires from other gem fields in Thailand (from GIT-GTL database).

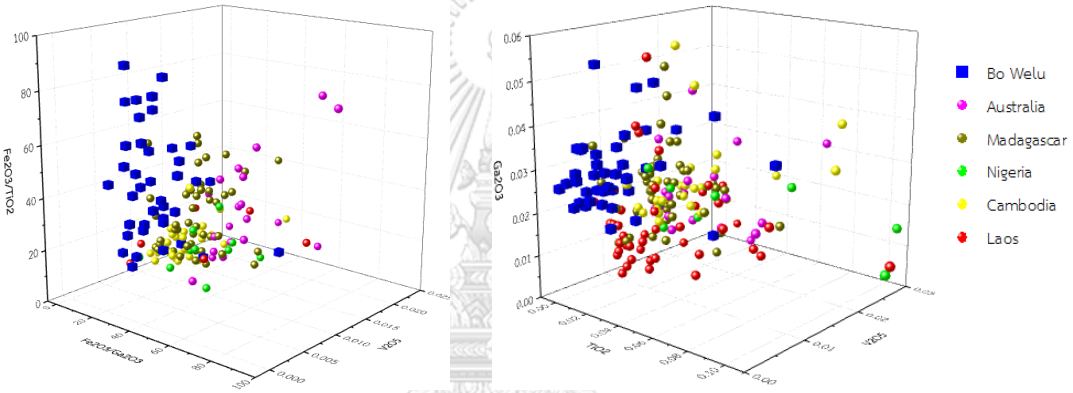

Figure 5.5 3D plotting of EDXRF analyses of Bo Welu sapphires compared to other basaltic sapphires from significant gem fields around the world (from GIT-GTL database).

Most common mineral inclusions found in Bo Welu sapphire are Na-rich alkali feldspar (albite). Only one sanidine, which indicate sapphire may have originally crystallized from high temperature, was found. Moreover, monazite, columbite, and zircon inclusions are also identified in the samples from this area similar to other basaltic gem fields. Indeed, this is the first report of rare inclusions of sulphide inclusion in Thai sapphire (see Table 5.1).

Table 5.1 Summary of mineral inclusions discovered in Bo Rai and Bo Welu corundum comparing to those reported from surrounding basaltic gem fields.

		Ruby						Sapphire							
Mineral group	Mineral inclusions	Cambodia - Pailin	Trat - Bo Rai	Trat - Bo Na Wong	Trat - Nong Bon	Chanthaburi - Tok Phrom	Chanthaburi-Trat - Bo Welu	Chanthaburi-Trat - Bo Welu	Chanthaburi - Tok Phrom	Chanthaburi - Bang Kacha	Chanthaburi- Khao Wua	Chanthaburi - Khao Ploy Wan	Kanchanaburi - Bo Phloi	Phrae - Den Chai	Cambodia - Pailin
Silicates	Zircon	-	-	-	-	-	-	✓*	-	-	✓6	-	✓3,4	✓9	-
	Garnet	-	✓2,3,*	-	-	-	✓*	-	-	-	-	-	✓4	✓9	✓9
	Sillimanite	-	✓*	-	-	-	✓*	-	-	-	-	-	-	-	-
	Staurolite	-	-	-	-	-	-		-	-	-	-	✓4	-	-
	Diopside	✓7	✓2,3,*	-	-	-	✓*	-	-	-	-	-	-	-	-
	Enstatite	-	-	-	-	-	-	-	-	-	-	-	✓4	✓9	✓9
	Sapphirine	✓7	✓5	✓2,3	-	-	✓*	-	-	-	-	-	✓4	-	-
	Nepheline	-	-	-	-	-	✓*	-	-	-	-	-	✓3,4	✓9	-

*This study using Raman and EPMA; [1]Guo et al. (1994) using EPMA and PMP; [2]Sutthirat et al. (2001) using EPMA; [3]Saminpanya and Sutherland (2011) using SEM-EDS, [4]Khamloet et al. (2014) using Raman and EPMA; [5]Koivula and Fryer (1987) using XRD; [6]Sutherland et al. (1998a) using EPMA; [7]Sutherland et al. (1998b) using EPMA; [8]Gübelin (1971) using EPMA; [9]Khamloet (2011) using EPMA

Table 5.1 Summary of mineral inclusions discovered in Bo Rai and Bo Welu corundum comparing to those reported from surrounding basaltic gem fields (continued).

		Ruby						Sapphire							
Mineral group	Mineral inclusions	Cambodia - Pailin	Trat - Bo Rai	Trat - Bo Na Wong	Trat - Nong Bon	Chanthaburi - Tok Phrom	Chanthaburi-Trat - Bo Welu	Chanthaburi-Trat - Bo Welu	Chanthaburi - Tok Phrom	Chanthaburi - Bang Kacha	Chanthaburi- Khao Wua	Chanthaburi - Khao Ploy Wan	Kanchanaburi - Bo Phloi	Phrae - Den Chai	Cambodia - Pailin
Silicates	Quartz	-	-	-	-	-	✓*	-	-	-	-	-	-	-	-
	Alkali feldspars	-	-	-	-	-	✓*	✓*	-	-	-	-	✓3,4	✓3,9	✓9
	Plagioclase	-	✓8,*	-	-	-	✓*	-	-	-	-	-	-	-	-
Oxides	Spinel	✓7	✓*	-	-	-	✓*	-	-	-	-	-	✓1,3	✓9	✓7
	Ilmenite	-	-	-	-	-	-	-	-	-	-	-	✓4	-	-
	Anatase	-	✓*	-	-	-	-	-	-	-	-	-	-	-	-
	Columbite	-	-	-	-	-	-	✓*	-	-	-	-	-	-	✓9
	Pyrochlore	-	-	-	-	-	-	-	-	-	-	-	-	-	✓9

*This study using Raman and EPMA; [1]Guo et al. (1994) using EPMA and PMP; [2]Sutthirat et al. (2001) using EPMA; [3]Saminpanya and Sutherland (2011) using SEM-EDS, [4]Khamloet et al. (2014) using Raman and EPMA; [5]Koivula and Fryer (1987) using XRD; [6]Sutherland et al. (1998a) using EPMA; [7]Sutherland et al. (1998b) using EPMA; [8]Gübelin (1971) using EPMA; [9]Khamloet (2011) using EPMA

Table 5.1 Summary of mineral inclusions discovered Bo Rai and Bo Welu corundum comparing to those reported from surrounding basaltic gem fields (continued).

		Ruby						Sapphire							
Mineral group	Mineral inclusions	Cambodia - Pailin	Trat - Bo Rai	Trat - Bo Na Wong	Trat - Nong Bon	Chanthaburi - Tok Phrom	Chanthaburi-Trat - Bo Welu	Chanthaburi-Trat - Bo Welu	Chanthaburi - Tok Phrom	Chanthaburi - Bang Kacha	Chanthaburi- Khao Wua	Chanthaburi - Khao Ploy Wan	Kanchanaburi - Bo Phloi	Phrae - Den Chai	Cambodia - Pailin
Phosphates	Monazite	-	-	-	-	-	-	✓*	-	-	-	-	✓[4]	-	-
Carbonate	Calcite	-	-	-	-	-	-	-	-	-	-	-	✓[4]	-	-
Sulphide	Pyrrhotite	-	✓[8,*]	-	-	-	✓*	✓*	-	-	-	-	-	-	-
Sulphates	Anhydrite	-	-	-	-	-	✓*	-	-	-	-	-	-	-	-

*This study using Raman and EPMA; [1]Guo et al. (1994) using EPMA and PMP; [2]Sutthirat et al. (2001) using EPMA; [3]Saminpanya and Sutherland (2011) using SEM-EDS, [4]Khamloet et al. (2014) using Raman and EPMA; [5]Koivula and Fryer (1987) using XRD; [6]Sutherland et al. (1998a) using EPMA; [7]Sutherland et al. (1998b) using EPMA; [8]Gübelin (1971) using EPMA; [9]Khamloet (2011) using EPMA

5.2 Initial Formation of Bo Rai Ruby

Gübelin (1971) initially described and published a typical inclusion suite of Thai rubies, such as sub-hexagonal to rounded opaque metallic grains of pyrrhotite, yellowish hexagonal platelets of apatite, reddish brown almandite garnets and plagioclase feldspar. Subsequently, mineral inclusions in corundum from basaltic gem fields have been investigated, particularly on the basis of Raman spectroscopic identification and mineral chemical analysis. Consequently, Sutherland et al. (1998b), distinguished two suites of mineral inclusions in basaltic-type gem corundum; they included 1) metamorphic origin (e.g., as Mg-rich spinel, sapphirine, fassaite, garnet) and 2) magmatic origin (e.g., feldspar, zircon, Fe-Ti oxides, Nb-Ta oxides, U-Th oxides, rare-earth phosphates). Moreover, Intasopa et al. (1999) reported mineral inclusions in corundum from the Chanthaburi-Trat basaltic terrains; they were identified as spinel, gahnite, hercynite, pleonaste, biotite, mica, diopside, ferro-columbite, zircon, monazite, garnet, rutile, boehmite, feldspar, bismuth, thorite, and clinochlore. In addition, those corundum samples also carried fluid inclusions containing CO_2 gas, liquid CO_2, impure CO_2 gas and silicate melt. Eventually, they suggested the crystallization model related to peraluminous alkaline felsic magma which may have partially melted from metasomatized lithospheric rocks in corporation with crustal contamination at the depth shallower than 80 km.

Sutthirat et al. (2001) used thermodynamic calculation to indicate the crystallization environment of clinopyroxene + corundum assemblages from alluvial Chanthaburi-Trat gem fields. The results indicated temperature range of 800-1150 °C and pressure range of 10 - 25 kbar for equilibration of Thai ruby formation, presumably from high-grade metamorphosed mafic rocks.

Saminpanya and Sutherland (2011) separated inclusions in Thai corundum into sapphire suite (e.g., alkali feldspar (sanidine), nepheline, zircon, hercynite-spinel), and ruby suite (e.g., garnet, fassaite, sapphirine). They suggested that Thai rubies could have crystallized in high-pressure metamorphic rock of ultramafic/mafic composition. On the other hand, Thai sapphires could have crystallized in high-grade metamorphic (gneissic) rock or from magmas of highly alkaline composition, located at shallower levels in the lithosphere than those hosting the Thai rubies.

Sutthirat et al. (2018) recently reported ruby-bearing xenoliths from Bo Rai deposit which was the direct evidence of initial ruby formation in Bo Rai. As the result, they suggested mafic granulite xenoliths were the original source of these rubies.

In this study, the most common mineral inclusions observed in the Bo Rai ruby are high alumina diopside (fassaite). These compositions are similar to pyroxenes in ruby-bearing xenocryst which found in alkali basalt from Nong Bon (Sutthirat et al., 2001) and pyroxene in ruby-bearing xenolith found in alkali basalt from Bo Rai area, recently reported by Sutthirat et al. (2018). Therefore, it is clearly that alluvial rubies in Bo Rai gem field should have originated significantly in mafic granulites as previously reported.

Garnet inclusions in alluvial Bo Rai ruby are classified as Cr-poor pyropic garnet which is similar to garnet inclusion in Bo Rai ruby, garnet xenocryst from Nong Bon and garnet in pyriclasite xenolith from Bo Welu which were previously reported by Sutthirat et al. (2001). These pyropic garnet inclusions in Bo Rai ruby should have crystallized within the mafic/ultramafic composition rocks at pressures of >18 kbar. Moreover, these garnet inclusions are also similar to those in ruby-bearing xenoliths, mafic granulites (Pl–Cpx–Sp ± Grt ± Cor) reported by Sutthirat et al. (2018); mafic granulites are clearly original source of alluvial ruby in Bo Rai gem field. These Cr-poor pyropic garnets may be related to eclogite as suggested by MacGetchin and Silver (1970) and Deer et al. (1997); however, their occurrences can be associated with liquid magma as suggested by (Gübelin and Koivula, 1986). The pyropic garnet inclusions in Bo Rai ruby are distinctively located in Group A eclogite which are similar to garnet inclusion in Bo Rai ruby (previously reported by Saminpanya and Sutherland (2011) suggesting garnet crystallization within mafic/ultramafic composition.

The composition of plagioclase feldspar and spinel inclusions are similar to those of mafic granulites (Pl–Cpx–Sp ± Grt ± Cor bearing) xenoliths reported by Sutthirat et al. (2018) suggesting mafic granulites as the original source of these rubies.

Anatase, as identified by Raman technique, is the first report of inclusion in Thai ruby. It is actually low temperature (500-600 °C) TiO_2 phase (a TiO_2 polymorph of rutile and brookite; (Gübelin and Koivula, 1986) that should indicate dissolution and perhaps transformation of TiO_2 from the host ruby under solid-stage (subsolidus) during the cooling process.

More importantly, sillimanite inclusion is firstly discovered in Bo Rai ruby under this study. It clearly suggests high temperature (over 550°C) of crystallization. Moreover, two-phase inclusions containing silicate melt (solid) and CO_2 (?) phases are also observed in Bo Rai ruby samples. This inclusion links quite well with the origin of

the Bo Rai ruby that appears to have high temperature reaching partial melting prior to rapid cooling. Sillimanite and two-phase inclusions occur with primary fingerprint are significant evidence indicating that the host ruby should have formed during a partial melting process at high temperature.

Exogenous mineral inclusions, particularly sulphide was as found in Bo Rai ruby samples these may be the result of subduction process taking these shallow crustal materials downward and mixing with mafic mantle source.

Based on the evidences reported above, Bo Rai ruby and its main mineral inclusions seem to have originated as mafic granulites which may have high temperature environments reaching to partial melt during the ancient subduction event.

5.3 Initial Formations of Bo Welu Ruby and Sapphire

Compositions of pyroxene inclusion in Bo Welu ruby are similar to pyroxene inclusion in Bo Rai ruby in this study; although, they have slightly higher Ca with lower Mg components. They are also close to pyroxenes' composition of inclusion in ruby and ruby-bearing xenolith investigated by Sutthirat et al. (2001) and Sutthirat et al. (2018) which indicate mafic granulites.

Most garnet inclusions in Bo Welu ruby are chemically characterized by pyrope-rich composition which is quite similar to those observed from inclusion in Bo Rai ruby. Therefore, these pyropic garnet inclusions in Bo Welu ruby indicate that host ruby may have crystallized within the mafic/ultramafic composition rocks similar to the formation of Bo Rai ruby.

Most of feldspar inclusions in Bo Welu ruby are plagioclase. Only an unusual alkali feldspar with anorthoclase composition is observed in this study.

Compositions of pyroxene, garnet, plagioclase, and spinel inclusions support mafic granulites related to original source of ruby as reported by Sutthirat et al. (2018) and Promprated et al. (2003). Sillimanite's chemical composition in Bo Welu ruby is similar to sillimanite inclusion in Bo Rai ruby with slightly higher Fe content. A number of two-phase inclusions containing gas bubble and silicate melt are also observed in Bo welu ruby. The chemical compositions of these inclusions similar to those found in Bo Rai ruby; this type of inclusion is found more often in Bo Welu ruby. Anorthoclase, sillimanite and silicate melt occurred as primary inclusions

indicate that crystallization of the host ruby may have high temperature reaching partial melt of the initial rock formation.

Sapphirine typically occurs in high-grade metamorphic rocks belonging to granulite and hornblende-granulite facies within Al-rich and Si-poor provenance (Deer et al., 2013). Blue-green sapphirine inclusion in Bo Welu ruby has chemical composition similar to those of sapphirine inclusions in alluvial ruby from Bo Na Wong deposit, Chanthaburi Province, previously reported by (Sutthirat et al., 2001). It may suggest crystallization of sapphirine and host ruby at 800-1150 °C and pressure range between 1 and 2.5 GPa.

Nepheline is the most common feldspathoid mineral and occurs in alkaline rocks (Deer et al., 2013). Nepheline was found with a sapphire in syenitic gneiss, syenitic rock, nepheline- aegirine intrusive rock, and nepheline-bearing gneisses (Meyer, 1968; Waltham, 1999; Ashwal et al., 2007). This is the first report of nepheline inclusions in Bo Welu ruby; these nephelines and their host ruby indicate that some rubies may have formed in a silica-poor (undersaturated) and alkali-rich (Na and K) environment.

Exogenous mineral such as anhydrite, sulphide, and quartz inclusions are observed in Bo Welu ruby might be related to submarine volcanism before a subduction process had taken these shallow crustal materials downward and mixed with mafic materials in the mantle region.

Based on the main mineral inclusions, the initial formation of Bo Welu ruby appear to have originated in mafic granulites with extremely high temperature environment reaching partial melt.

Regarding to formation of sapphire related to basaltic terranes, some researchers have proposed genetic models based on inclusions observed in alluvial gem sapphires, mainly from SE Asia and Australia. For examples, Guo et al. (1996) reported mineral inclusions in corundum samples associated with alkali basalts in Australia, China, Thailand, USA, Kenya and they separated these inclusions into two suites, including 1) alkali felsic suite (e.g., feldspar, zircon, uraninite, ilmenorutile, Fe-Cu sulphides) and 2) carbonatitic suite (e.g., titaniferous columbite, uranpyrochlore, fersmite). Consequently, they proposed a model of corundum genesis that appears to have involved hybridization between granitic and carbonatite magmas at mid crustal level. Subsequently, Sutherland et al. (1998a) reported different melt origins for blue, green, and yellow (BGY) sapphires from Australia, Thailand, Cambodia, and Lao PDR which was reconstructed on the basis of mineral inclusions observed in

these sapphires. They separated mineral inclusions in sapphire from basalt fields in Australia and Asia as metamorphic origin (based on inclusions such as Mg-rich spinel, sapphirine, high alumina diopside (fassaite), and garnet) and magmatic origin (using inclusion identified as feldspar, zircon, Fe-Ti oxides, Nb-Ta oxides, U-Th oxides, and rare-earth phosphates). Finally, they suggest that these sapphires may crystallize directly from volatile-rich saturated felsic melts prior to generating and fractionating extensively under the mantle/lower crust conditions. Temperature estimated from magnetite exsolution, feldspar compositions and homogenization of fluid inclusion yield at 685±900 °C. Pisutha-Arnond et al. (1999) and Pisutha-Arnond et al. (2007) also investigated alluvial assemblages in Kanchanaburi sapphire deposit, Western Thailand; they suggested the sapphire formation may be related to contact metamorphic processes at the deep crust or upper mantle. Recently, Khamloet et al. (2014) reported mineral inclusions in Bo Phloi sapphire from the same deposit of Kanchanaburi and suggest bimodal genetic model based on mineral inclusions. They strongly support syenitic-melt crystallization represented by particular inclusions such as zircon, nepheline, alkali feldspar, manganiferous ilmenite, monazite, and calcite in corporation with consequent contact-metamorphism as indicated by some inclusions, e.g., sapphirine, staurolite, silica-rich enstatite, almandine–pyrope garnet, hercynitic spinel, biotite–phlogopite mica.

For this study, a wide variety of inclusions related to alkaline felsic magma, such as alkali feldspar, monazite, columbite, and zircon are discovered in Bo Welu sapphire. The alkali feldspar inclusions are mostly classified as albite, anorthoclase, and oligoclase, with an unusual Na-rich alkali feldspar (sanidine)**.** In general, sanidine is a high temperature phase usually crystallized directly from felsic melt. Saminpanya and Sutherland (2011) suggested that sanidine inclusion in Denchai sapphire may have crystallized at minimum temperature of about 1000 °C. In addition, Khamloet et al. (2014) also suggest that sapphire from Bo Phloi gem field in the Western Thailand may have crystallized from a high-alkali felsic melt in the lower crust. Moreover, monazite inclusions in Bo Welu sapphire also indicate highly evolved melt (Krzemnicki et al., 1996; Intasopa et al., 1998; Singbamroong and Thanasuthipitak, 2004; Khamloet et al., 2014).

Chemical characteristics of zircon inclusion (e.g., high contents of Hf and Y with some rare earth elements presented) have been found in sapphire from basaltic terrains elsewhere which may suggest that the host sapphire crystallized from alkaline and highly evolved source material under conditions unrelated to the

associated basaltic magma (e.g., Coenraads et al., 1990; Coenraads et al., 1995; Guo et al., 1996; Sutherland et al., 2002; Khamloet et al., 2014).

In addition, exogenous mineral such as sulphide inclusions are also discovered in Bo Welu sapphire, particularly in light blue-green sapphire with chatoyancy effect. Although the Al_2O_3 content was detected in some sulphide inclusions which is probably due to contamination from the sapphire host, their analyses are close to pyrrhotite formula without nickel and copper contents. They differ from a previous report from New South Wales sulphide, analyzed by Guo et al. (1996), which iron sulphide inclusion contain Cu and Zn as trace elements. However, these sulfur compositions indicate initial source of material may relate to subduction and hybridization within deep crust. Columbite generally occurs in various granitic rocks (Guo et al., 1996). Columbite inclusion is often found in Bo Welu sapphire. The high Nb content in columbite indicated Nb-rich environment. Sutherland et al. (1998a) suggested that columbite inclusion usually crystalizes from silicate melt. The Ti and Ta contents of columbite inclusions in Bo Welu sapphire are less than those of columbite inclusions previously reported from sapphire in New South Wales by Guo et al. (1996) who proposed that the columbite indicated a source composition related to carbonatitic formation. However, columbite could possibly relate to either silicate melt or carbonate condition or both environments.

In conclusion, based on the occurrences of these mineral inclusions, the Bo Welu sapphires appear to have crystallized from a highly evolved, alkali-rich, silica-poor melt such as syenitic magma.

5.4 Conclusions and Recommendations

1.) Bo Rai and Bo Welu rubies contain some significant inclusions, particularly high alumina diopside (fassaite), garnet, and sapphirine and their trace compositions are Cr-rich and Ga-poor with Cr_2O_3/Ga_2O_3 ratio above 3. This chemical fingerprint indicates metamorphic origin similar to ruby from West Pailin as suggested by Sutherland et al. (1998b). On the other hand, Bo Welu sapphires are relatively poor in Cr and high in Ga with Cr_2O_3/Ga_2O_3 below 1 indicating magmatic origin (Sutherland et al., 1998b). Moreover, many crystals show strong magmatic corrosion and fusion crusts which indicate transportation of basaltic magma.

2.) Various mineral inclusions are discovered similarly in Bo Rai ruby, and Bo Welu ruby. For examples, high alumina diopside (fassaite), pyrope garnet, plagioclase feldspar, sillimanite, spinel and sulphide are also

observed in both Bo Welu ruby and Bo Rai ruby. However, anatase inclusion is identified only in Bo Rai ruby. On the other hand, sapphirine, quartz, nepheline and anhydrite inclusions are discovered only in Bo Welu ruby. Regarding to Bo Welu sapphires, their observable mineral inclusions, such as zircon, alkali feldspar, sulphide, monazite, columbite, are different from those inclusions found in rubies from both Bo Rai and Bo Welu.

3.) Compositions of crucial inclusions such as plagioclase feldspar, pyroxene, spinel and garnet in Bo Rai and Bo Welu rubies are similar to minerals in mafic granulite (Pl–Cpx–Sp ± Grt ± Cor) xenoliths) xenolith embedded in basalts from Bo Rai reported by Sutthirat et al. (2018) and garnet-rich granulite in basalt from Bo Welu, reported by Promprated et al. (2003). These, therefore, suggest the same original source of mafic granulites as the initial ruby formation.

4.) Moreover, this is the first discovery of significant inclusions such as sillimanite, spinel, anatase, nepheline, and anhydrite in Thai ruby.

5.) Sapphire from Bo Welu should have different original formation from the rubies. It appears to have formed by partially melting of Al-rich protolith at shallower levels (upper mantle or lower crust). This model is supported by the occurrence of a felsic alkaline suite of inclusions such as alkaline feldspar, monazite and columbite.

Recommendations for future works

To improve more supporting evidences, further investigation is recommended as following:

1) REE and some trace element analyses of monazite inclusion should be performed using the LA-ICP-MS technique. The information from such study should give a better understanding on their host sapphires.
2) The detailed U-Pb dating on the zircon inclusion found in these sapphires should be carried out for reconstructing relevant tectonic genesis model of the sapphire formation.
3) Multi-equilibriums of the silicate melt inclusions should also be reconstructed to give P-T condition of corundums' crystallization.

REFERENCES

Ashwal, L.D., Armstrong, R.A., Roberts, R.J., Schmitz, M.D., Corfu, F., Hetherington, C.J., Burke, K. and Gerber, M., 2007. Geochronology of zirconmegacrysts from nepheline-bearing gneisses as constraints on tectonic setting: implications for resetting the U-Pb and Lu-Hf isotopic systems. Contributions to Mineralogy and Petrology, 153(389–403).

Aspen, P., Upton, B.G.J. and Dickin, A.P., 1990. Anorthoclase, sanidine and associated megacrysts in Scottish alkali basalts: highpressure syenitic debris from upper mantle sources? European Journal of Mineralogy, 2: 503–517.

Barr, S. and Cooper, M., 2013. Late Cenozoic basalt and gabbro in the subsurface in the Phetchabun Basin, Thailand: Implications for the Southeast Asian Volcanic Province. Journal of Asian Earth Sciences, 76: 169-184.

Barr, S.M. and MacDonald, A.S., 1978. Geochemistry and petrogenesis of Late Cenozoic alkaline basalts of Thailand. The Bulletin of the Geological Society of Malaysia, 10: 25-52.

Barr, S.M. and Macdonald, A.S., 1981. Geochemistry and geochronology of late Cenozoic basalts of Southeast Asia. Geological Society of America Bulletin, 92(Part 2): 1069-1142.

Beran, A., 1991. Trace hydrogen in Verneuil-grown corundum and its colour varieties—an IR spectroscopic study. European Journal of Mineralogy, 3: 971-976.

Beran, A. and Rossman, G.R., 2006. OH in naturally occurring corundum. European Journal of Mineralogy, 18(4): 441-447.

Bunnag, N., 2004. Mineral chemistry of spinel associated with Thai and Myanmar corundum deposits. Doctoral dissertation, Chiang Mai: Graduate School Chiang Mai University, 2004.

Carmichael, I.S., Turner, F.J. and Verhoogen, J., 1974. Igneous petrology. McGraw-Hill Companies, Ca, New York, NY.

Cerny, P. and Ercit, T.S., 1985. Some recent advances in the mineralogy and geochemistry of Nb and Ta in rare-element granitic pegmatites. Bulletin de

Mineralogie, 108: 499-532.

Chualaowanich, T., Sutthirat, C., Pisutha-Arnond, V., Hauzenberger, C. and Charusiri, P., 2008. Genetic Constraints of Siamese Ruby: Evidence from Ruby-bearing Xenoliths and a New $^{40}Ar/^{39}Ar$ Age of the Host Basalt from the Eastern Gem Field, Thailand. Proceedings of the the 2nd International Gem and Jewelry Conference (GIT 2008): 195-198.

Chulaowanich, T., Saisuthichai, D. and Saraphanchotwitthaya, P., 2008. $^{40}Ar/^{39}Ar$ Geochronology of Thai Basalt, Bureau of Mineral Resources, Department of Mineral Resources, Bangkok, Thailand, No.19/2008, pp. 67.

Coenraads, R.R., 1992. Surface features on natural rubies and sapphires derived from volcanic provinces. Journal of Gemmology, 23(3): 151-160.

Coenraads, R.R., Sutherland, F.L. and Kinny, P.D., 1990. The origin of sapphires: U–Pb dating of zircon inclusions sheds new light. Mineralogical Magazine 54: 113-122.

Coenraads, R.R., Vichit, P. and Sutherland, F.L., 1995. An unusual sapphire-zircon-magnetite xenolith from the Chanthaburi Gem Province, Thailand. Mineralogical Magazine, 59(3): 465-479.

Dao, N.Q. and Delaigue, L., 2000. Raman micro-spectrometry and its applications to the identification of inclusions in natural rubies. Analusis, 28(1): 34-38.

Deer, W.A., Howie, R.A. and Zussman, J., 2013. An Introduction to the Rock-forming Minerals, 3nd Edition. Longman, Essex, UK: 696

Deer, W.A., Howie, R.A. and Zussman, J.E., 1997. Rock-forming minerals: single-chain silicates, Volume 2A. Geological Society of London.

Diep, P.T.M., 2015. Internal characteristics, chemical compounds and spectroscopy of sapphire as single crystals. Doctoral dissertation, Fachbereich Chemie, Pharmazie und Geowissenschaften, Johannes Gutenberg-Universität Mainz: 140.

Droop, G., 1987. A general equation for estimating Fe 3+ concentrations in ferromagnesian silicates and oxides from microprobe analyses, using stoichiometric criteria. Mineralogical magazine, 51(361): 431-435.

Fanka, A. and Sutthirat, C., 2018. Petrochemistry, Mineral Chemistry, and Pressure–Temperature Model of Corundum-Bearing Amphibolite from Montepuez, Mozambique. Arabian Journal for Science and Engineering: 1-17.

Ferguson, J. and Fielding, P.E., 1971. The origins of the colours of yellow, green and blue sapphires. Chemical Physics Letters, 10(3): 262-265.

Ferguson, J. and Fielding, P.E., 1972. The origins of the colours of natural yellow, blue, and green sapphires. Australian journal of chemistry, 25(7): 1371-1385.

Fritsch, E. and Rossman, G.R., 1987. An update on color in gems. Part 1: Introduction and colors caused by dispersed metal ions. Gems & gemology, 23(3): 126-139.

Fritsch, E. and Rossman, G.R., 1988. An update on color in gems. Part 2: Colors involving multiple atoms and color centers. Gems & Gemology, 24(1): 3-15.

Gübelin, E.J., 1940. Differences between Burma and Siam rubies. Gems & Gemology, 3(5): 69-72.

Gübelin, E.J., 1971. New analytical results of the inclusions in Siam rubies. Journal of Australian Gemmology, 12(7): 242-252.

Gübelin, E.J., 1973. Internal world of gemstones. Zurich, ABC Edition, pp. 234.

Gübelin, E.J. and Koivula, J.I., 1986. Photoatlas of Inclusions in Gemstones, Volume 1. Zurich, Switzerland, ABC Edition, revised Jan., 1992: German edition, 1986 (Bildatlas der Einschlusse Edelsteinen): 532.

Guo, J., Griffin, W.L. and O'Reilly, S.Y., 1994. A cobalt-rich spinel inclusion in a sapphire from Bo Ploi, Thailand. Mineralogical Magazine, 58(391): 247-258.

Guo, J., O'Reilly, S.Y. and Griffin, W.L., 1996. Corundum from basaltic terrains: a mineral inclusion approach to the enigma. Contributions to Mineralogy and Petrology, 122: 368–386.

Guo, J., Wang, F. and Yakoumelos, G., 1992. Sapphires from Changle in Shandong Province, China. Gems & Gemology, 28(4): 255-260.

Haggerty, S.E., 1991. Oxide mineralogy of the upper mantle. Reviews in Mineralogy and Geochemistry, 25(1): 355-416.

Hänni, H.A., 1994. Origin determination for gemstones: Possibilities, restrictions, and reliability. Journal of Gemmology, 24(3): 139-148.

Hughes, R.W., 1997. Ruby & sapphire. Boulder, CO, RWH Publishing.

Intasopa, S., Atichat, W. and Pisutha-Arnond, V., 1998. Inclusions in Corundum: A New Approach to the Definition of Standards for Origin Determination. Science and Technology for Gem and Jewelry Industry [in Thai] Thailand Research Fund.

Intasopa, S., Atichat, W., Pisutha-Arnond, V. and Sriprasert, B., 2002. การศึกษามลทินในพลอยคอรันดัม เพื่อการจัดแบ่งแหล่งกำเนิดและมาตรฐาน.

Intasopa, S., Atichat, W., Pisutha-Arnond, V., Sriprasert, B., Narudeesombat, N. and Phuttarat, T., 1999. Inclusions in Chanthaburi – Trat corundums: A clue to their genesis, in Thai. Proceedings of the Symposium on Mineral, Energy, and Water Resources of Thailand: Towards the Year 2000, October 28-29, 1999, Bangkok, Thailand: 471-484.

Irving, A.J., 1986. Polybaric mixing in alkalic basalts and kimberlites: Evidence from corundum, zircon and ilmenite megacrysts. Geological Society of Australia Abstracts Series. , 16: 262-264.

Joseph, D., Lal, M., Shinde, P. S., & Padalia, B. D. , 2000. Characterization of gem stones (rubies and sapphires) by energy-dispersive x-ray fluorescence spectrometry. X-Ray Spectrometry. An International Journal, 29(2): 147-150.

Khamloet, P., 2011. Mineral chemistry of inclusions in basaltic sapphires from Southeast Asia, Chulalongkorn University.

Khamloet, P., Pisutha-Arnond, V. and Sutthirat, C., 2014. Mineral inclusions in sapphire from the basalt-related deposit in Bo Phloi, Kanchanaburi, Western Thailand: indication of their genesis. Russian Geology and Geophysics, 55(9): 1087-1102.

Koivula, J.I. and Fryer, C.W., 1987. Sapphirine (not sapphire) in a ruby from Bo Rai, Thailand. Journal of Gemmology, 20(6): 369-370.

Krzemnicki, M.S., Hänni, H.A., Guggenheim, R. and Mathys, D., 1996. Investigations on sapphires from an alkali basalt, South West Rwanda. Journal of Gemmology, 25(2): 90–106.

Lavrent'ev, Y.G., Korolyuk, V., Usova, L. and Nigmatulina, E., 2015. Electron probe microanalysis of rock-forming minerals with a JXA-8100 electron probe microanalyzer. Russian Geology and Geophysics, 56(10): 1428-1436.

Levinson, A.A. and Cook, F.A., 1994. Gem corundum in alkali basalt: origin and occurrence. Gems & Gemology, 30(4): 253-262.

MacGetchin, T.R. and Silver, L.T., 1970. Compositional relations from kimberlites and related rocks in the Moses Rock Dike, San Juan County, Utah. American

Mineralogist, 55: 1738–1771.

McGee, B.M., 2005. Characteristics and origin of the Weldborough sapphire, NE Tasmania. Unpublished BSc. thesis, University of Tasmania, Hobart.

Meyer, H.O.A., 1968. Chrome pyrope: an inclusion in diamond. Science, 160: 1446–1447.

Mogmued, J., Monarumit, N., Won-in, K. and Satitkune, S., 2017. Spectroscopic properties for identifying sapphire samples from Ban Bo Kaew, Phrae Province, Thailand. Journal of Physics: Conference Series, 901.

Morimoto, N., Fabries, J., Ferguson, A.K., Ginzburg, I.V., Rose, M., Seifert, F.A., Zussman, J., Aoki, K. and Gottardi, G., 1988. Nomenclature of pyroxenes. American Mineralogist, 73: 1123-1133.

Oakes, G.M., Barron, L.M. and Lishmund, S.R., 1996. Alkali basalts and associated volcaniclastic rocks as a source of sapphire in Eastern Australia. Australian Journal of Earth Sciences, 43(3): 289-298.

Palanza, V., Di Martino, D., Paleari, A., Spinolo, G. and Prosperi, L., 2008. Micro-Raman spectroscopy applied to the study of inclusions within sapphire. Journal of Raman Spectroscopy, 39(8): 1007-1011.

Palke, A.C., Renfro, N.D. and Berg, R.B., 2016. Origin of sapphires from a lamprophyre dike at Yogo Gulch, Montana, USA: Clues from their melt inclusions. Lithos, 260: 339-344.

Pattamalai, K., 2015. Chanthaburi-Trat corundum deposits, Eastern Thailand Proceedings of the 3rd Lao-Thai Technical Conference, July 7-8,2015: 219-229.

Peucat, J.-J., Ruffault, P., Fritsch, E., Bouhnik-Le Coz, M., Simonet, C. and Lasnier, B., 2007. Ga/Mg ratio as a new geochemical tool to differentiate magmatic from metamorphic blue sapphires. Lithos, 98(1-4): 261-274.

Pisutha-Arnond, V., Wathanakul, P., Atichat, W., Sutthirat, C., Sriprasert, B., Leelawatanasuk, T. and Soomboon, C., 2007. Unusual sapphire assemblages fron the Kanchanaburi gem field, Western Thailand. Proceedings of the 30th International Gemmological Conference (IGC 2007), Mosscow.

Pisutha-Arnond, V., Wathanakul, P. and Intasopa, S., 1999. New evidences on the origin of Kanchanaburi sapphire. Proceedings of the Symposium on Mineral, Energy, and Water Resources of Thailand: Towards the year 2000, Bangkok, Thailand

(Abstract).

Promprated, P., Taylor, L.A. and Neal, C.R., 2003. Petrochemistry of mafic granulite xenoliths from the Chantaburi basaltic field: implications for the nature of the lower crust beneath Thailand. International Geology Review, 45(5): 383-406.

Saminpanya, S. and Sutherland, F.L., 2011. Different origins of Thai area sapphire and ruby, derived from mineral inclusions and co-existing minerals. European Journal of Mineralogy, 23(4): 683-694.

Saraphanchotwitthaya, S., Witienranee, R., Pattamalai, K. and Tangpong, P., 2003. A report on the exploration for gemsctones at Tha Mai, Laem Sing and Muang Chanthaburi Distrint, Chanthaburi Province. In: D.o.M.R. Bureau of Mineral Resources, Bangkok, No.11/2003 (Editor), pp. 285.

Schmetzer, K., 1987. Zur Deutung der Farbursache blauer Saphire-eine Diskussion. Neues Jahrbuch für Mineralogie Monatshefte, 8: 337-343.

Schwarz, D., Pardieu, V., Saul, J.M., Schmetzer, K., Laurs, B.M., Giuliani, G., Klemm, L., Malsy, A.-K., Erel, E. and Hauzenberger, C., 2008. Rubies and sapphires from Winza, Central Tanzania. Gems & Gemology, 44(4): 322-347.

Singbamroong, S., 2004. Spectroscopy of Lao Corundum, Chiang Mai: Graduate School Chiang Mai University, 2004, 137 pp.

Singbamroong, S. and Thanasuthipitak, T., 2004. Study of solid mineral inclusions in sapphires from Ban Huai Sai area, Laos, by Raman spectroscopy. Chiang Mai J. Sci, 31(3): 251-263.

Sirinawin, T., 1981. Geochemistry and genetic significance of gem-bearing basalt in Chantaburi-Trat area. M.Sc. Theris submitted to the Department of Geological Sciences, Chiang Mai University: 87.

Smith, C.P., Kammerling, R.C., Keller, A.S., Peretti, A., Scarratt, K., Khoa, N.D. and Repetto, S., 1995. Sapphires from Southern Vietnam. Gems & Gemology, 31: 168-186.

Sutherland, F.L., Bosshart, G., Fanning, C.M., Hoskin, P.W.O. and Coenraads, R.R., 2002. Sapphire crystallization, age and origin, Ban Huai Sai Laos: age based on zircon inclusions. Journal of Asian Earth Sciences, 20(7): 841–849.

Sutherland, F.L. and Coenraads, R.R., 1996. An unusual ruby-sapphire-sapphirine-spinel

assemblage from the Tertiary Barrington volcanic province, New South Wales, Australia. Mineralogical Magazine, 60(4): 623-638.

Sutherland, F.L., Coenraads, R.R., Schwarz, D., Raynor, L.R., Barron, B.J. and Webb, G.B., 2003. Al-rich diopside in alluvial ruby and corundum-bearing xenoliths, Australian and SE Asian basalt fields. Mineralogical Magazine, 67(4): 717-732.

Sutherland, F.L., Hoskin, P.W., Fanning, C.M. and Coenraads, R.R., 1998a. Models of corundum origin from alkali basaltic terrains: a reappraisal. Mineralogy and Petrology, 133(4): 356-372.

Sutherland, F.L., Schwarz, D., Jobbins, E.A., Coenraads, R.R. and Webb, G., 1998b. Distinctive gem corundum suits from discrete basalt fields: a comparative study of Barrington, Australia, and West Pailin, Cambodia, gemfields. Journal of Gemmology, 26(2): 65-85.

Sutthirat, C., 2001. Petrogenesis of mantle and crustal xenoliths and xenocrysts in basaltic rocks associated with corundum deposits in Thailand. Doctoral dissertation, Department of Earth Sciences, The University of Manchester, United Kingdom.

Sutthirat, C., Atichat, W., Pisutha-Arnond, V., Wathanakul, P., Sriprasert, B., Leelawatanasuk, T., Leelawatanasuk, T., Eamjamroon, K., Ruangkaew, P., Kaewprasit, T., Yodkaew, P., Promkrak, P., Khamloet, P., Buaydee, N., Swasdiwatin, P., Intamara, A., Noodam, C., Muengthai, T. and Poompang, S., 2005. โครงการข้อมูลแหล่งวัตถุดิบอัญมณีและการบ่งชี้แหล่งกำเนิดทางธรณีวิทยาที่คาบเกี่ยวกัน.

Sutthirat, C., Charusiri, P., Farrar, E. and Clark, A.H., 1994. New $^{40}Ar/^{39}Ar$ geochronology and characteristics of some Cenozoic basalts in Thailand, Proceeding of International Symposium on: Stratigraphic Correlation of Southeast Asia, 15-20 November 1994, Bangkok, Thailand, Department of Mineral Resources and IGCP 306, 1994, Bangkok, Thailand, pp. 306-321.

Sutthirat, C., Hauzenberger, C., Chualaowanich, T. and Assawincharoenkij, T., 2018. Mantle and deep crustal xenoliths in basalts from the Bo Rai ruby deposit, Eastern Thailand: Original source of basaltic ruby. Journal of Asian Earth Sciences, 164: 366-379.

Sutthirat, C., Saminpanya, S., Droop, G.T.R., Henderson, C.M.B. and Manning, D.A.C., 2001. Clinopyroxene-corundum assemblages from alkali basalt and alluvium, eastern Thailand: constraints on the origin of Thai rubies. Mineralogical Magazine, 65(2): 277-295.

Tippawan, U., Chulapakorn, T., Bootkul, D., Pangkason, C. and Intarasiri, S., 2016. Investigation on modification of ion implanted natural corundum by UV–Vis-NIR spectroscopy. Surface and Coatings Technology, 306: 358-363.

Uher, P., Giuliani, G., Szakáll, S., Fallick, A., Strunga, V., Vaculovič, T., Ozdín, D. and Gregánová, M., 2012. Sapphires related to alkali basalts from the Cerová Highlands, Western Carpathians (Southern Slovakia): composition and origin. Geologica Carpathica, 63(1): 71-82.

Upton, B.G.J., Aspen, P. and Chapman, N.A., 1983. The upper mantle and deep crust beneath the British Isles: evidence from inclusions in volcanic rocks. Journal of the Geological Society of Thailand, 140(1): 105–121.

Upton, B.G.J., Hinton, R.W., Aspen, P., Finch, A. and Valley, J.W., 1999. Megacrysts and associated xenoliths: Evidence for migration of geochemically enriched melts in the upper mantle beneath Scotland. Journal of Petrology, 40(6): 935-956.

Vichit, P., 1992. Gemstones in Thailand, In: Piencharoen, C. (ed) Proceedings of a National Conference on Geologic Resources of Thailand—Potential for Future Development: 17–24 November 1992, Bangkok, Thailand, Department of Mineral Resources, Bangkok, Thailand, pp. 124-150.

Vichit, P., Vudhichativanich, S. and Hansawek, R., 1978. The distribution and some characteristics of corundum-bearing basalts in Thailand. Journal of the Geological Society of Thailand, 3: M4–1 to M4–38.

Waltham, T., 1999. The ruby mines of Mogok. Geology Today, 15(143–149).

Wark, D.A. and Miller, C.F., 1993. Accessory mineral behavior during differentiation of a granite suite: monazite, xenotime and zircon in the Sweetwater Wash pluton, southeastern California, USA. Chemical Geology, 110(1-3): 49-67.

Yaemniyom, N. and Pongsapich, W., 1982. Petrochemistry study of corundum-bearing basalts at Bo Phloi district, Kanchanaburi Province. Unpublished MSc thesis. Department of Geology, Chulalongkorn University, Thailand: 19-52.

APPENDICES

Appendix A – Gemological properties

The gemological properties of Bo Rai ruby

Table A1 The gemological properties of ruby from Bo Rai

Item	Sample	Photo	Color	Weight (ct)	R.I.	Fluorescence	
						LWUV	SWUV
1	9TRA016		PR-RP	0.12	1.770-1.761	Moderate red	Inert
2	9TRA017		PR-RP	0.17	1.770-1.762	Weak red	Inert
3	9TRA022		pR	0.18	1.770-1.761	Inert	Inert
4	9TRA023		PR-RP	0.22	1.770-1.760	Moderate red	Inert
5	9TRA024		PR-RP	0.08	1.770-1.761	Moderate red	Inert
6	9TRA026		rP	0.13	1.770-1.762	Weak red	Inert
7	9TRA028		PR-RP	0.30	1.770-1.761	Weak red	Inert
8	9TRA029	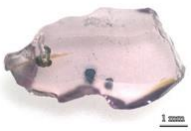	rP	0.32	1.770-1.761	Moderate red	Inert
9	9TRA031		PR-RP	0.08	1.770-1.761	Moderate red	Inert
10	9TRA033		PR-RP	0.31	1.770-1.760	Moderate red	Inert

Table A1 The gemological properties of ruby from Bo Rai

Item	Sample	Photo	Color	Weight	R.I.	Fluorescence	
11	9TRA036		rP	0.12	1.770-1.761	Weak red	Inert
12	9TRA038		PR-RP	0.09	1.770-1.760	Moderate red	Inert
13	9TRA039		PR-RP	0.11	1.770-1.760	Moderate red	Inert
14	9TRA044		PR-RP	0.22	1.770-1.760	Moderate red	Inert
15	9TRA045		PR-RP	0.11	1.770-1.760	Moderate red	Inert
16	9TRA048		PR-RP	0.15	1.770-1.760	Weak red	Inert
17	9TRA049		PR-RP	0.05	1.770-1.760	Moderate red	Inert
18	9TRA051		PR-RP	0.12	1.770-1.760	Weak red	Inert
19	9TRA052		PR-RP	0.13	1.770-1.761	Weak red	Inert
20	9TRA053		PR-RP	0.07	1.770-1.760	Moderate red	Inert
21	9TRA055		PR-RP	0.62	1.771-1.762	Moderate red	Inert
22	9TRA057		PR-RP	0.18	1.770-1.761	Moderate red	Inert
23	9TRA060		PR-RP	0.19	1.770-1.761	Weak red	Inert
24	9TRA061		PR-RP	0.06	1.771-1.761	Moderate red	Inert

Table A1 The gemological properties of ruby from Bo Rai

Item	Sample	Photo	Color	Weight	R.I.	Fluorescence	
25	9TRA062		PR-RP	0.12	1.770-1.761	Weak red	Inert
26	9TRA073		PR-RP	0.11	1.770-1.761	Weak red	Inert
27	9TRA075		pR	0.09	1.771-1.762	Weak red	Inert
28	9TRA078		PR-RP	0.11	1.770-1.761	Moderate red	Inert
29	9TRA081		PR-RP	0.14	1.771-1.762	Weak red	Inert
30	9TRA084		PR-RP	0.19	1.771-1.761	Moderate red	Inert
31	9TRA086		PR-RP	0.12	1.770-1.761	Weak red	Inert
32	9TRA088		PR-RP	0.14	1.770-1.761	Moderate red	Inert
33	9TRA090		PR-RP	0.15	1.770-1.761	Moderate red	Inert
34	9TRA092		PR-RP	0.10	1.770-1.761	Weak red	Inert
35	9TRA095		PR-RP	0.14	1.770-1.760	Moderate red	Inert
36	9TRA098		PR-RP	0.09	1.770-1.761	Moderate red	Inert
37	9TRA102		PR-RP	0.05	1.770-1.761	Moderate red	Inert
38	9TRA105		PR-RP	0.11	1.770-1.761	Moderate red	Inert

Table A1 The gemological properties of ruby from Bo Rai

Item	Sample	Photo	Color	Weight	R.I.	Fluorescence	
39	9TRA108		PR-RP	0.10	1.770-1.760	Moderate red	Inert
40	9TRA113	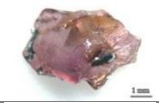	PR-RP	0.29	1.770-1.761	Moderate red	Inert
41	9TRA118		PR-RP	0.16	1.770-1.760	Moderate red	Inert
42	9TRA121		PR-RP	0.11	1.770-1.760	Weak red	Inert
43	9TRA124		PR-RP	0.14	1.770-1.760	Moderate red	Inert
44	9TRA126		PR-RP	0.09	1.770-1.760	Moderate red	Inert
45	9TRA127		PR-RP	0.22	1.770-1.761	Weak red	Inert
46	9TRA128		PR-RP	0.09	1.771-1.761	Moderate red	Inert
47	9TRA131		PR-RP	0.17	1.770-1.761	Weak red	Inert
48	9TRA132		PR-RP	0.03	1.770-1.761	Weak red	Inert
49	9TRA137		rP	0.18	1.770-1.761	Weak red	Inert
50	9TRA151		PR-RP	0.18	1.770-1.760	Weak red	Inert
51	9TRA154		PR-RP	0.06	1.770-1.762	Weak red	Inert
52	9TRA155		rP	0.16	1.770-1.760	Moderate red	Inert

Table A1 The gemological properties of ruby from Bo Rai

Item	Sample	Photo	Color	Weight	R.I.	Fluorescence	
53	9TRA156		P	0.26	1.770-1.760	Weak red	Inert
54	9TRA158		PR-RP	0.18	1.770-1.761	Weak red	Inert
55	9TRA160		PR-RP	0.15	1.770-1.760	Weak red	Inert
56	9TRA161		PR-RP	0.21	1.770-1.760	Moderate red	Inert
57	9TRA169		PR-RP	0.24	1.770-1.760	Weak red	Inert
58	9TRA171		rP	0.36	1.770-1.761	Weak red	Inert
59	9TRA176	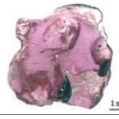	PR-RP	0.23	1.770-1.760	Weak red	Inert
60	9TRA192		PR-RP	0.05	1.770-1.760	Moderate red	Inert
61	9TRA193		rP	0.35	1.770-1.760	Weak red	Inert
62	9TRA194		PR-RP	0.07	1.770-1.760	Weak red	Inert
63	9TRA195		PR-RP	0.26	1.770-1.760	Weak red	Inert
64	9TRA196		PR-RP	0.13	1.770-1.760	Moderate red	Inert
65	9TRA197		rP	0.33	1.770-1.761	Moderate red	Inert
66	9TRA198	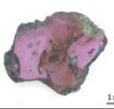	PR-RP	0.15	1.770-1.761	Weak red	Inert

Table A1 The gemological properties of ruby from Bo Rai

Item	Sample	Photo	Color	Weight	R.I.	Fluorescence	
67	9TRA199		PR-RP	0.16	1.770-1.761	Weak red	Inert
68	9TRA201		PR-RP	0.23	1.770-1.761	Weak red	Inert
69	9TRA202	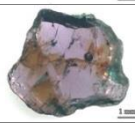	P	0.39	1.770-1.761	Weak red	Inert
70	9TRA203		PR-RP	0.09	1.770-1.761	Moderate red	Inert
71	9TRA204		PR-RP	0.07	1.770-1.761	Moderate red	Inert
72	9TRA206		PR-RP	0.09	1.770-1.760	Moderate red	Inert
73	9TRA207		PR-RP	0.15	1.770-1.760	Moderate red	Inert
74	9TRA208		PR-RP	0.06	1.770-1.761	Moderate red	Inert
75	9TRA209		PR-RP	0.05	1.770-1.760	Moderate red	Inert
76	9TRA210		rP	0.06	1.770-1.760	Weak red	Inert
77	9TRA211		rP	0.08	1.770-1.760	Moderate red	Inert
78	9TRA212		PR-RP	0.09	1.770-1.760	Weak red	Inert
79	9TRA213		PR-RP	0.10	1.770-1.760	Moderate red	Inert
80	9TRA214		PR-RP	0.13	1.770-1.761	Weak red	Inert

Table A1 The gemological properties of ruby from Bo Rai

Item	Sample	Photo	Color	Weight	R.I.	Fluorescence	
81	9TRA215		PR-RP	0.49	1.770-1.761	Weak red	Inert
82	9TRA217	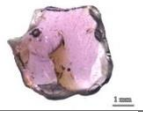	rP	0.20	1.770-1.760	Weak red	Inert
83	9TRA218		PR-RP	0.08	1.770-1.760	Moderate red	Inert
84	9TRA219	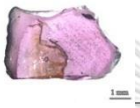	rP	0.23	1.770-1.761	Moderate red	Inert
85	9TRA223		PR-RP	0.14	1.770-1.760	Moderate red	Inert
86	9TRA228	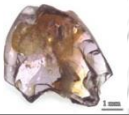	rP	0.23	1.770-1.761	Moderate red	Inert
87	9TRA231		rP	0.86	1.770-1.760	Moderate red	Inert
88	9TRA232	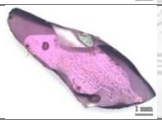	rP	0.65	1.770-1.760	Weak red	Inert

The gemological properties of Bo Welu ruby

Table A2 The gemological properties of ruby from Bo Welu

Item	Sample	Photo	Color	Weight (ct)	R.I.	Fluorescence	
						LWUV	SWUV
1	9TWL006		rP	0.41	1.770-1.760	Weak red	Inert
2	9TWL007		rP	0.41	1.770-1.761	Weak red	Inert
3	9TWL009	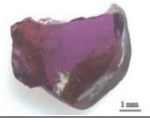	PR-RP	0.53	1.770-1.761	Weak red	Inert

Table A2 The gemological properties of ruby from Bo Welu

Item	Sample	Photo	Color	Weight (ct)	R.I.	Fluorescence	
						LWUV	SWUV
4	9TWL010		PR-RP	0.36	1.770-1.760	Weak red	Inert
5	9TWL011		pR	0.13	1.770-1.760	Weak red	Inert
6	9TWL012		rP	0.53	1.770-1.760	Weak red	Inert
7	9TWL013		pR	0.28	1.770-1.761	Weak red	Inert
8	9TWL019	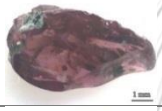	PR-RP	0.55	1.770-1.761	Weak red	Inert
9	9TWL020		PR-RP	0.43	1.770-1.760	Weak red	Inert
10	9TWL021		PR-RP	0.28	1.770-1.760	Moderate red	Inert
11	9TWL023		PR-RP	0.16	1.770-1.760	Moderate red	Inert
12	9TWL026		PR-RP	0.54	1.770-1.761	Weak red	Inert
13	9TWL029		PR-RP	0.54	1.770-1.761	Weak red	Inert
14	9TWL035		PR-RP	0.30	1.770-1.760	Moderate red	Inert
15	9TWL039		rP	0.34	1.770-1.760	Weak red	Inert
16	9TWL045		rP	0.58	1.770-1.761	Weak red	Inert

Table A2 The gemological properties of ruby from Bo Welu

Item	Sample	Photo	Color	Weight (ct)	R.I.	Fluorescence	
						LWUV	SWUV
17	9TWL046		P	0.46	1.770-1.760	Weak red	Inert
18	9TWL049		PR-RP	0.36	1.770-1.761	Moderate red	Inert
19	9TWL051		rP	0.60	1.770-1.760	Weak red	Inert
20	9TWL053		PR-RP	0.40	1.770-1.760	Weak red	Inert
21	9TWL054		rP	0.72	1.770-1.760	Weak red	Inert
22	9TWL055		rP	0.49	1.770-1.760	Weak red	Inert
23	9TWL059	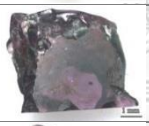	PR-RP	0.67	1.770-1.761	Weak red	Inert
24	9TWL067		PR-RP	0.46	1.770-1.761	Weak red	Inert
25	9TWL073		P	0.62	1.770-1.760	Weak red	Inert
26	9TWL077		P	0.71	1.770-1.760	Weak red	Inert
27	9TWL081		rP	0.25	1.770-1.761	Weak red	Inert
28	9TWL085		PR-RP	0.20	1.770-1.761	Weak red	Inert
29	9TWL086		rP	0.30	1.770-1.760	Weak red	Inert

Table A2 The gemological properties of ruby from Bo Welu

Item	Sample	Photo	Color	Weight (ct)	R.I.	Fluorescence	
						LWUV	SWUV
30	9TWL087	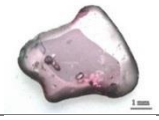	rP	0.21	1.770-1.760	Weak red	Inert
31	9TWL089		PR-RP	0.28	1.770-1.761	Moderate red	Inert
32	9TWL092		P	0.25	1.770-1.760	Weak red	Inert
33	9TWL093		PR-RP	0.50	1.770-1.761	Weak red	Inert
34	9TWL095		PR-RP	0.33	1.770-1.760	Weak red	Inert
35	9TWL096		rP	0.23	1.770-1.760	Weak red	Inert
36	9TWL099	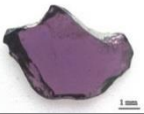	rP	0.28	1.770-1.760	Weak red	Inert
37	9TWL100	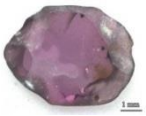	PR-RP	0.33	1.770-1.761	Weak red	Inert
38	9TWL105		rP	0.26	1.770-1.761	Weak red	Inert
39	9TWL114	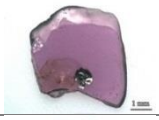	rP	0.17	1.770-1.760	Weak red	Inert
40	9TWL118		rP	0.21	1.770-1.761	Moderate red	Inert
41	9TWL122		rP	0.10	1.770-1.761	Weak red	Inert
42	9TWL131		rP	0.37	1.770-1.760	Weak red	Inert

Table A2 The gemological properties of ruby from Bo Welu

Item	Sample	Photo	Color	Weight (ct)	R.I.	Fluorescence	
						LWUV	SWUV
43	9TWL132		PR-RP	0.35	1.770-1.760	Moderate red	Inert
44	9TWL135		PR-RP	0.17	1.770-1.760	Weak red	Inert
45	9TWL136	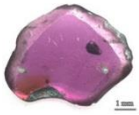	PR-RP	0.26	1.770-1.761	Moderate red	Inert
46	9TWL141	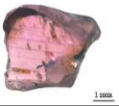	PR-RP	0.32	1.770-1.761	Weak red	Inert
47	9TWL143		rP	0.26	1.770-1.760	Weak red	Inert
48	9TWL152	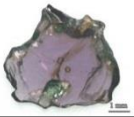	rP	0.20	1.770-1.760	Weak red	Inert
49	9TWL153		rP	0.27	1.770-1.761	Weak red	Inert
50	9TWL154	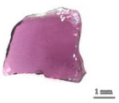	PR-RP	0.07	1.770-1.760	Weak red	Inert
51	9TWL157	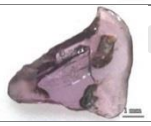	rP	0.19	1.770-1.761	Weak red	Inert
52	9TWL158		PR-RP	0.13	1.770-1.760	Moderate red	Inert
53	9TWL160		PR-RP	0.34	1.770-1.761	Weak red	Inert
54	9TWL172		PR-RP	0.10	1.770-1.761	Weak red	Inert
55	9TWL174	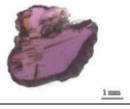	rP	0.29	1.770-1.760	Weak red	Inert

Table A2 The gemological properties of ruby from Bo Welu

Item	Sample	Photo	Color	Weight (ct)	R.I.	Fluorescence	
						LWUV	SWUV
56	9TWL176		rP	0.15	1.770-1.760	Weak red	Inert
57	9TWL178		rP	0.19	1.770-1.761	Moderate red	Inert
58	9TWL180		rP	0.26	1.770-1.760	Weak red	Inert

The gemological properties of Bo Welu sapphire

Table A3 The gemological properties of sapphire from Bo Welu

Item	Sample	Photo	Color	Weight (ct)	R.I.	Fluorescence	
						LWUV	SWUV
1	8TWL001		gB	6.87	1.770-1.760	Inert	Inert
2	8TWL002		gB	2.12	1.771-1.761	Inert	Inert
3	8TWL016		gB	0.87	1.771-1.762	Inert	Inert
4	8TWL018		gB	1.07	1.770-1.760	Inert	Inert
5	8TWL022		gB	1.45	1.770-1.760	Inert	Inert
6	8TWL023	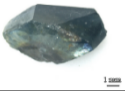	gB	1.29	1.771-1.761	Inert	Inert
7	8TWL026	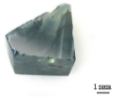	gB	1.15	1.770-1.760	Inert	Inert

Table A3 The gemological properties of sapphire from Bo Welu

Item	Sample	Photo	Color	Weight (ct)	R.I.	Fluorescence	
						LWUV	SWUV
8	8TWL028		gB	1.21	1.770-1.760	Inert	Inert
9	8TWL031		gB	0.75	1.771-1.762	Inert	Inert
10	8TWL035		gB	1.37	1.770-1.760	Inert	Inert
11	8TWL036		gB	1.35	1.770-1.760	Inert	Inert
12	8TWL040		B	1.07	1.770-1.760	Inert	Inert
13	8TWL046		gB	0.91	1.771-1.762	Inert	Inert
14	8TWL053		gB	0.20	1.771-1.762	Inert	Inert
15	8TWL059		B	0.45	1.770-1.760	Inert	Inert
16	8TWL064		B	0.68	1.770-1.760	Inert	Inert
17	8TWL067		B	0.61	1.770-1.760	Inert	Inert
18	8TWL068		B	1.52	1.770-1.760	Inert	Inert
19	8TWL074		gB	0.28	1.770-1.760	Inert	Inert
20	8TWL082		gB	0.59	1.770-1.760	Inert	Inert

Table A3 The gemological properties of sapphire from Bo Welu

Item	Sample	Photo	Color	Weight (ct)	R.I.	Fluorescence	
						LWUV	SWUV
21	8TWL083	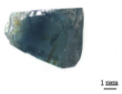	gB	1.09	1.771-1.761	Inert	Inert
22	8TWL093		gB	0.43	1.771-1.761	Inert	Inert
23	8TWL096	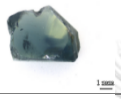	gB	0.85	1.770-1.760	Inert	Inert
24	8TWL097	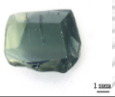	BG-GB	0.84	1.770-1.760	Inert	Inert
25	8TWL099	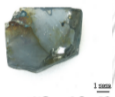	gB	0.71	1.771-1.761	Inert	Inert
26	8TWL100		gB	0.43	1.770-1.760	Inert	Inert
27	8TWL101		gB	0.90	1.770-1.760	Inert	Inert
28	8TWL102		B	1.56	1.770-1.760	Inert	Inert
29	8TWL103	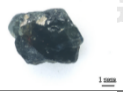	BG-GB	0.83	1.770-1.760	Inert	Inert
30	8TWL104		gB	0.56	1.771-1.761	Inert	Inert
31	8TWL105		gB	0.32	1.770-1.760	Inert	Inert
32	8TWL106		gB	1.01	1.770-1.760	Inert	Inert
33	8TWL108		gB	0.46	1.770-1.760	Inert	Inert

Table A3 The gemological properties of sapphire from Bo Welu

Item	Sample	Photo	Color	Weight (ct)	R.I.	Fluorescence	
						LWUV	SWUV
34	8TWL111	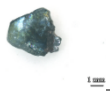	gB	0.23	1.770-1.760	Inert	Inert
35	8TWL112		B	0.77	1.770-1.760	Inert	Inert
36	8TWL113		B	0.51	1.770-1.760	Inert	Inert
37	8TWL114		B	1.40	1.771-1.761	Inert	Inert
38	8TWL116		B	1.70	1.770-1.760	Inert	Inert
39	8TWL117		gB	2.06	1.770-1.760	Inert	Inert
40	8TWL119		gB	1.16	1.770-1.760	Inert	Inert
41	8TWL120	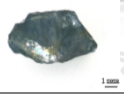	gB	0.90	1.771-1.761	Inert	Inert

Appendix B – Mineral inclusions

Mineral inclusions in Bo Rai ruby

9TRA016-in1 *9TRA022-in1* *9TRA022-in2* *9TRA023-in1*

9TRA028-in1 *9TRA033-in1* *9TRA036-in1* *9TRA038-in1*

9TRA039-in1 *9TRA044-in1* *9TRA045-in1* *9TRA048-in1*

9TRA051 -in1 *9TRA051-in2* *9TRA052-in1* *9TRA057-in1*

9TRA060-in1 *9TRA061-in1* *9TRA061-in2* *9TRA062-in1*

9TRA075-in1 *9TRA078-in1* *9TRA081-in1* *9TRA084-in1*

Figure B-1 Pyroxene inclusions in Bo Rai ruby

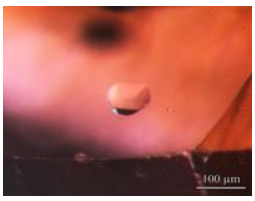
9TRA086-in1


9TRA086-in2


9TRA086-in4

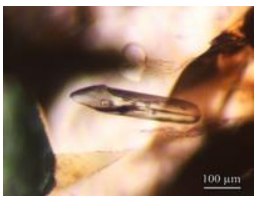
9TRA086-in5


9TRA090-in1

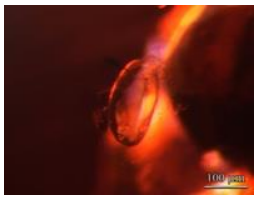
9TRA092-in1

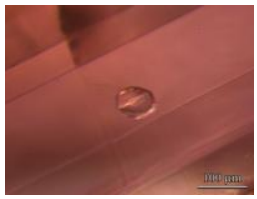
9TRA095-in1

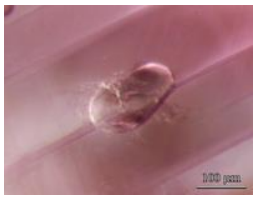
9TRA095-in2


9TRA098-in1

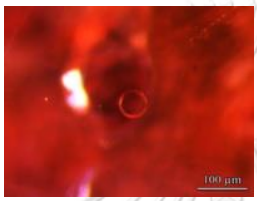
9TRA102-in1


9TRA102-in2

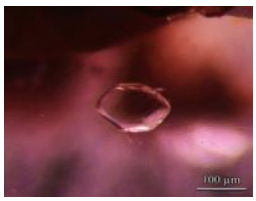
9TRA105-in1

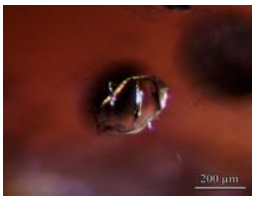
9TRA108-in1


9TRA113 -in1

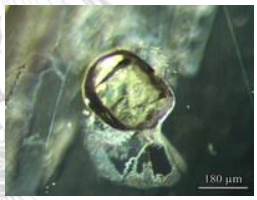
9TRA118-in1

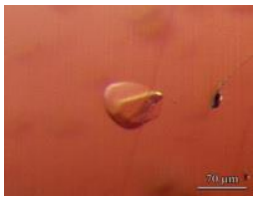
9TRA118-in2

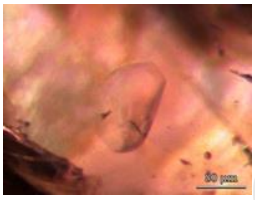
9TRA121-in1

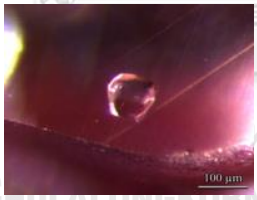
9TRA124 -in1

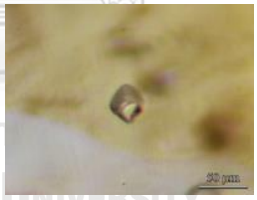
9TRA126-in1

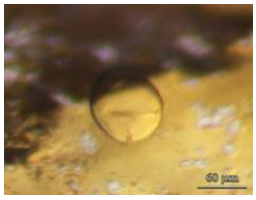
9TRA126-in2

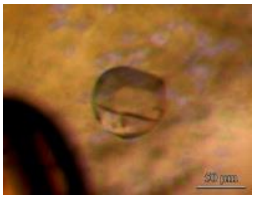
9TRA126-in3


9TRA127-in1-4

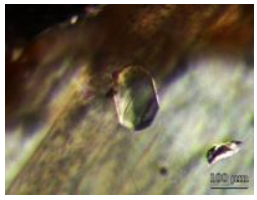
9TRA128-in1

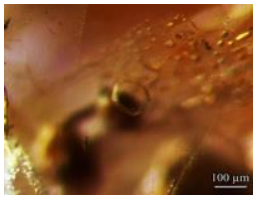
9TRA131-in1


9TRA132-in1

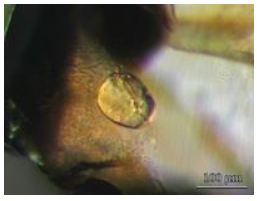
9TRA132-in2


9TRA137-in1

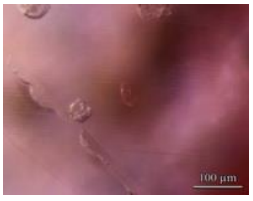
9TRA151-in2

Figure B-1 Pyroxene inclusions in Bo Rai ruby (continued)

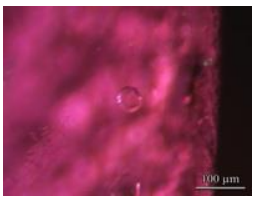
9TRA154-in1

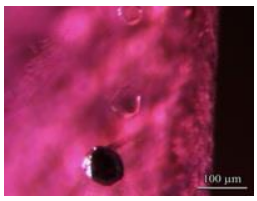
9TRA154-in2


9TRA155-in1

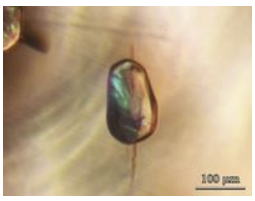
9TRA155-in2

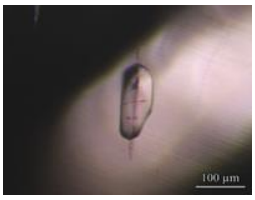
9TRA155-in3

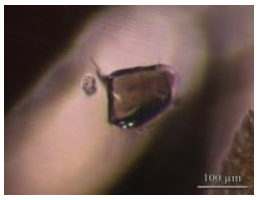
9TRA155-in4


9TRA155-in5


9TRA155-in6

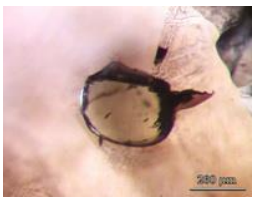
9TRA156-in1


9TRA158-in1

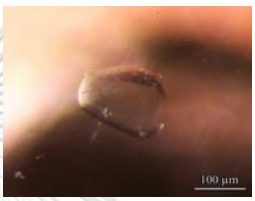
9TRA160-in2

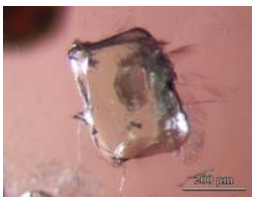
9TRA160-in3

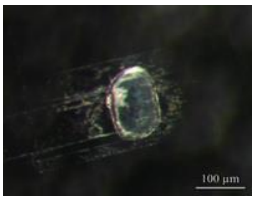
9TRA161-in1


9TRA192-in1

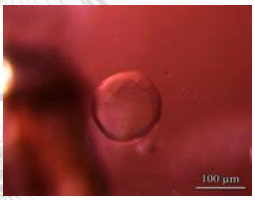
9TRA192-in2

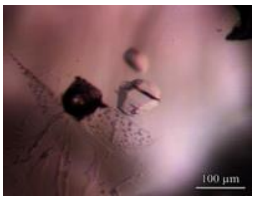
9TRA193-in1


9TRA194-in1

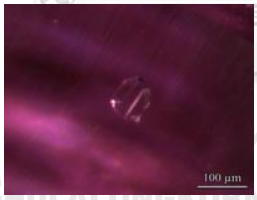
9TRA195-in1


9TRA195-in2

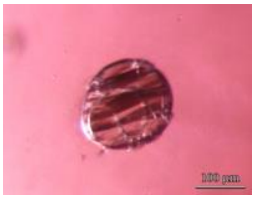
9TRA196-in1


9TRA197-in1


9TRA197-in2

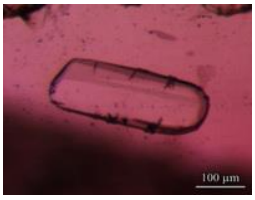
9TRA198-in1

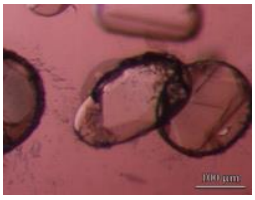
9TRA198-in2

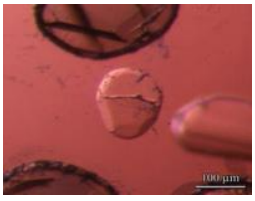
9TRA198-in3

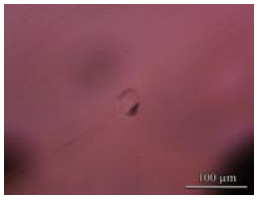
9TRA198-in4


9TRA198-in5

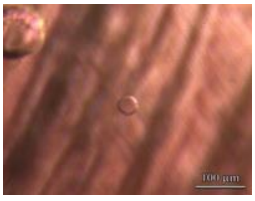
9TRA199-in1

Figure B-1 Pyroxene inclusions in Bo Rai ruby (continued)

Figure B-1 Pyroxene inclusions in Bo Rai ruby (continued)

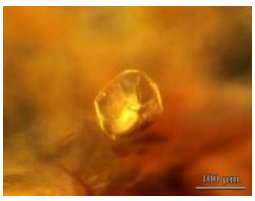

9TRA228-in2

Figure B-1 Pyroxene inclusions in Bo Rai ruby (continued)

9TRA017-in1

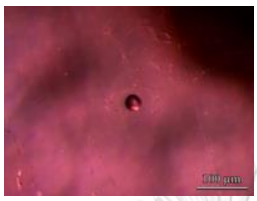

9TRA031-in1

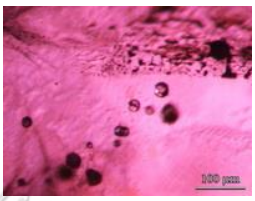

9TRA171-in8

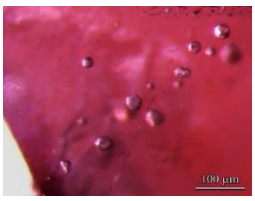

9TRA171-in9

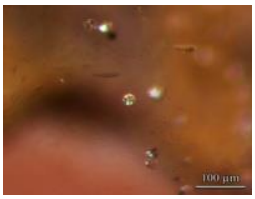

9TRA219-in2

Figure B-2 Feldspar inclusions in Bo Rai ruby

9TRA169

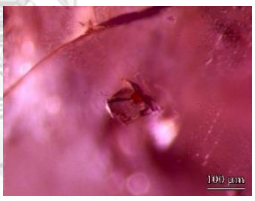

9TRA024

Figure B-3 Sillimanite inclusions in Bo Rai rubies

9TRA029-in1

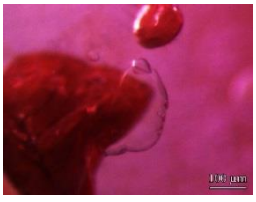

9TRA049-in1

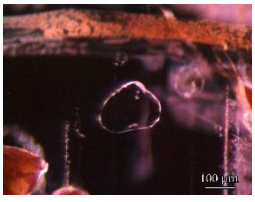

9TRA049-in2

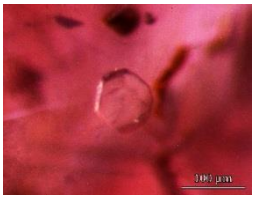

9TRA053-in1

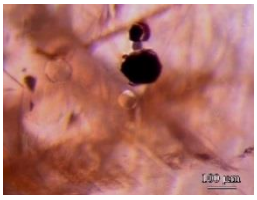

9TRA053-in2

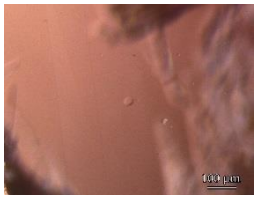

9TRA206-in3

9TRA215-in1

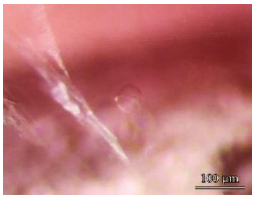

9TRA218-in1

Figure B-4 Garnet inclusions in Bo Rai ruby


9TRA055-in2

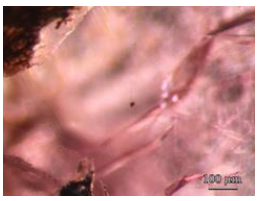
9TRA088-in1

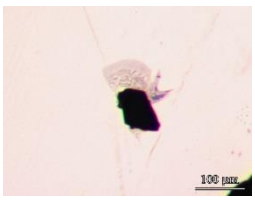
9TRA160-in1

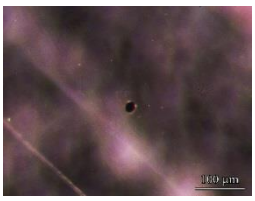
9TRA176-in1

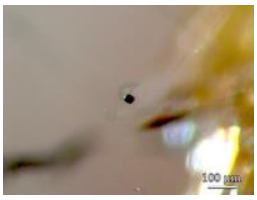
9TRA202-in1

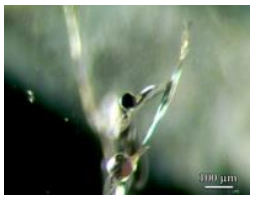
9TRA202-in2

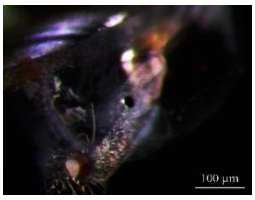
9TRA208-in1


9TRA214-in1

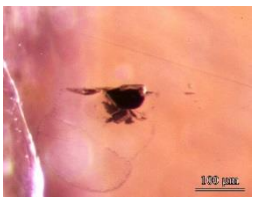
9TRA219-in1

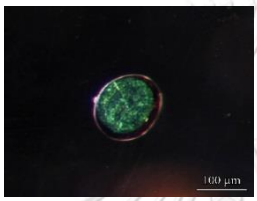
9TRA231-in1

Figure B-5 Sulphide inclusions in Bo Rai ruby

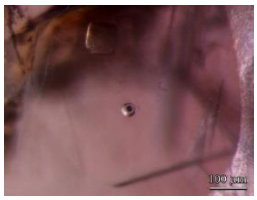
9TRA073-in1

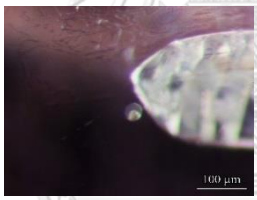
9TRA195-in3

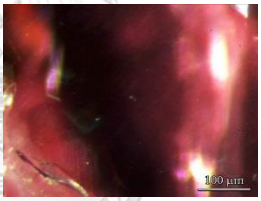
9TRA088-in2

Figure B-6 Two-phase inclusions (sample 9TRA073 and 9TRA195) and anatase (sample 9TRA088) inclusions in Bo Rai ruby

Mineral inclusions in Bo Welu ruby

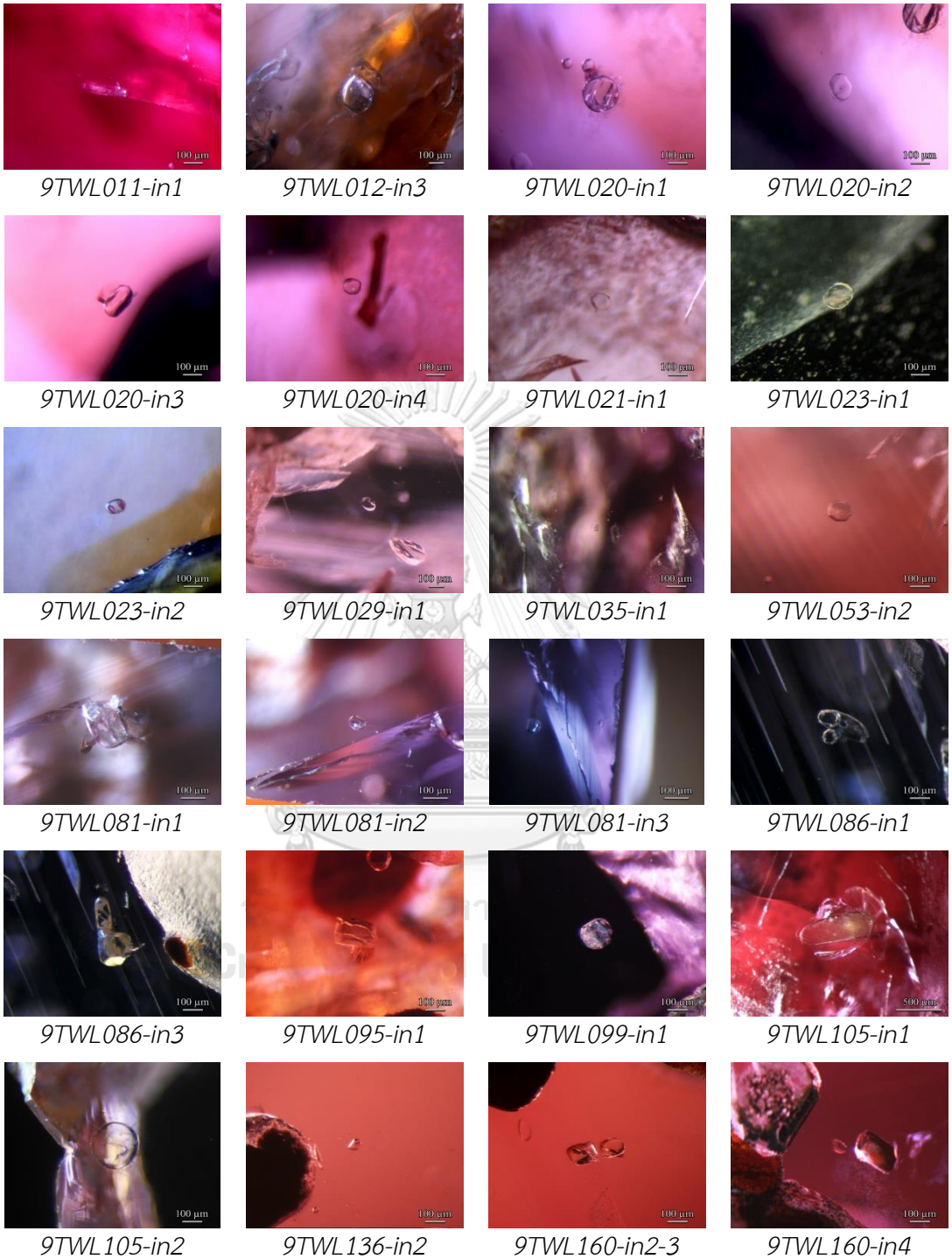

Figure B-7 Pyroxene inclusions in Bo Welu ruby

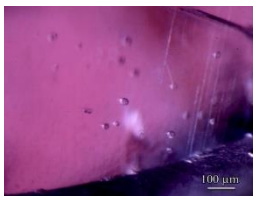
9TWL007-in1

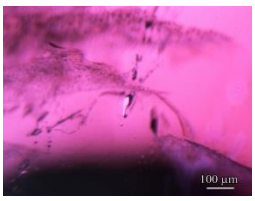
9TWL010-in1

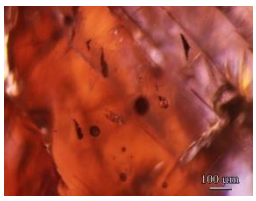
9TWL012-in2

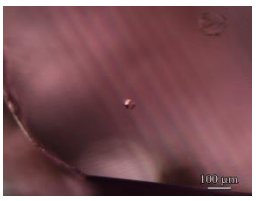
9TWL053-in1

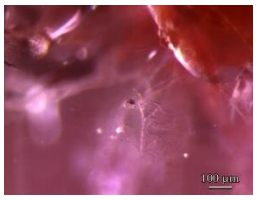
9TWL055-in1

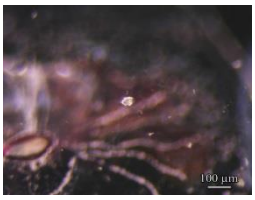
9TWL118-in1

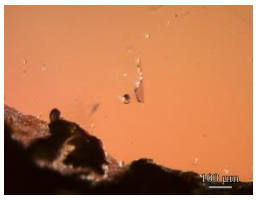
9TWL122-in3

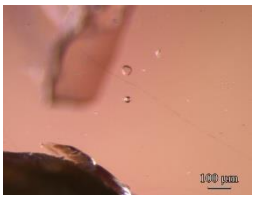
9TWL122-in4

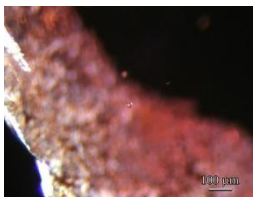
9TWL172-in1

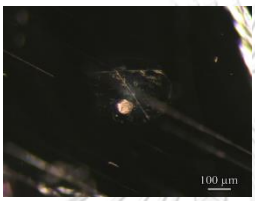
9TWL176-in1


9TWL178-in1

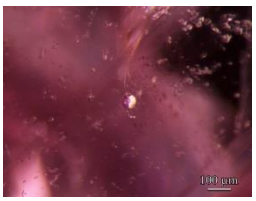
9TWL132-in1


9TWL157-in1

Figure B-8 Feldspar inclusions in Bo Welu ruby

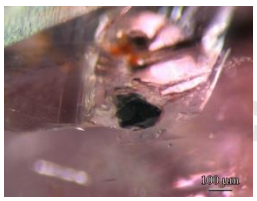
9TWL019

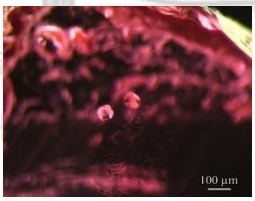
9TWL154


9TWL180-in1

Figure B-9 Feldspar-spinel inclusions in Bo Welu ruby


9TWL085-in3

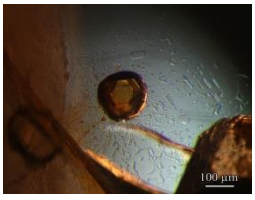
9TWL152-in1

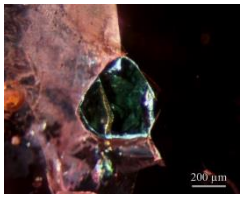
9TWL160-in1

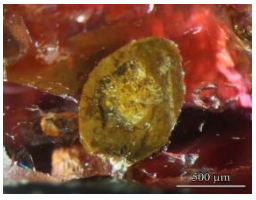
9TWL095-in2

Figure B-10 Spinel (sample 9TWL085), sillimanite (sample 9TWL152), sapphirine (sample 9TWL160), and quartz (sample 9TWL095) inclusions in Bo Welu ruby

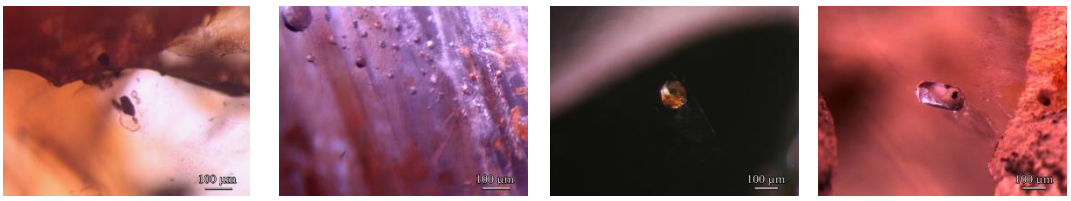

9TWL012-In1 9TWL026-in1 9TWL153-in1 9TWL096-in1-2

Figure B-11 Nepheline (sample 9TWL012, 9TWL026, and 9TWL153) and anhydrite-pyrrhotite (sample 9TWL096) inclusions in Bo Welu ruby

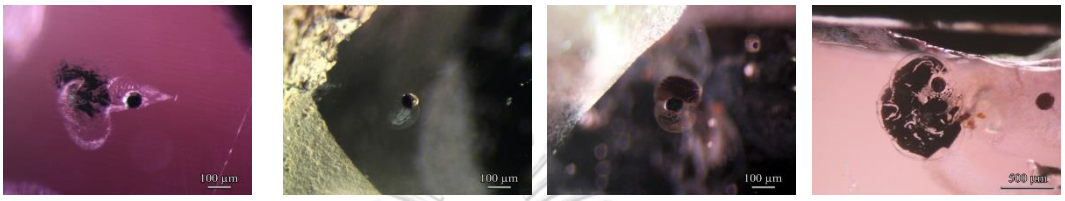

9TWL046-in1 9TWL087-in2 9TWL100-in1 9TWL114-in1

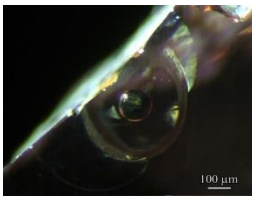

9TWL143-in1

Figure B-12 Sulphide inclusions in Bo Welu ruby

9TWL059-in1 9TWL059-in2 9TWL087-in1 9TWL089-in1

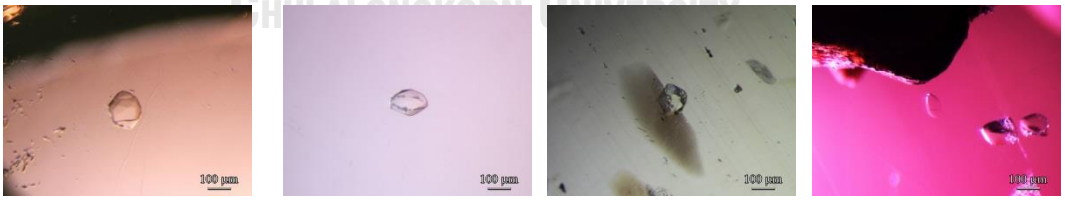

9TWL092-in1 9TWL092-in2 9TWL158-in1 9TWL160-in5

Figure B-13 Garnet inclusions in Bo Welu ruby

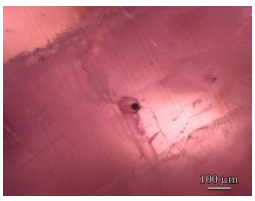
9TWL067-in1


9TWL077-in1

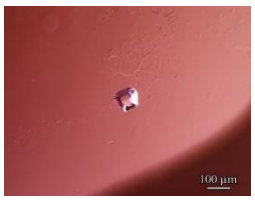
9TWL131-in1

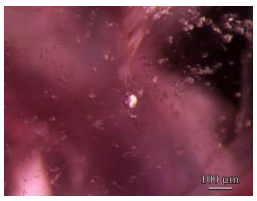
9TWL132-in1

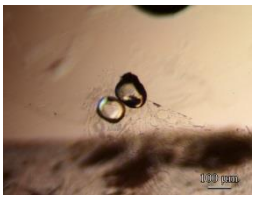
9TWL135-in1


9TWL174-in2

Figure B-14 Two-phase inclusions in Bo Welu ruby

Mineral inclusions in Bo Welu sapphire


8TWL002-in1

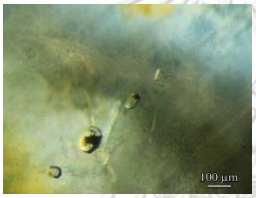
8TWL016-in1

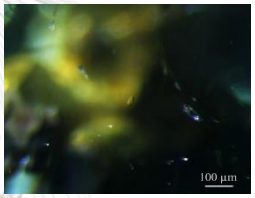
8TWL018-in1

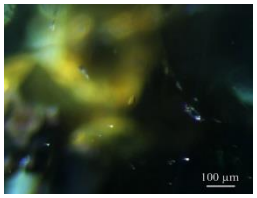
8TWL018-in2

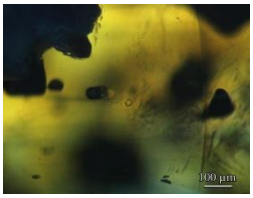
8TWL018-in3

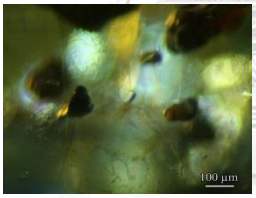
8TWL018-in4

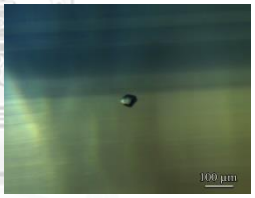
8TWL023-in1

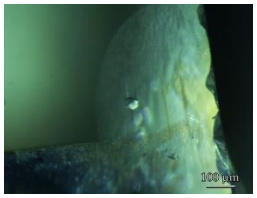
8TWL026-in2

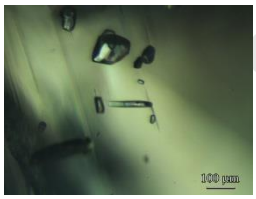
8TWL026-in3


8TWL026-in4

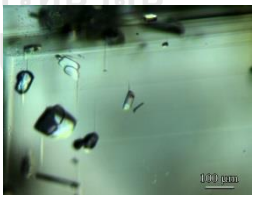
8TWL026-in5


8TWL031-in1


8TWL040-in1

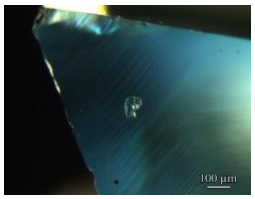
8TWL053-in2


8TWL067-in1


8TWL083-in1

Figure B-15 Feldspar inclusions in Bo Welu sapphire

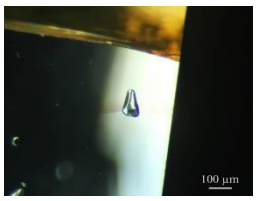

8TWL083-in2

8TWL083-in3

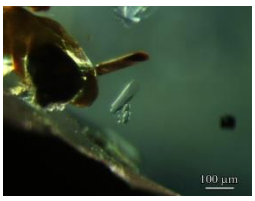

8TWL093-in4

8TWL093-in5

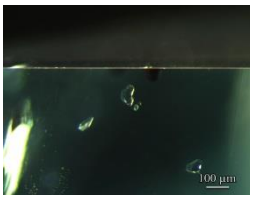

8TWL093-in7-8

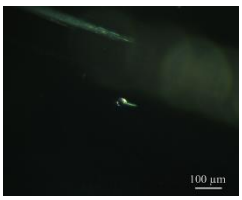

8TWL097-in1

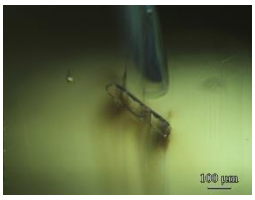

8TWL097-in2-3

8TWL097-in4-6

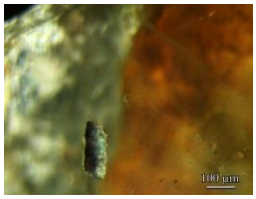

8TWL099-in1

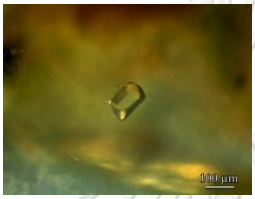

8TWL099-in2

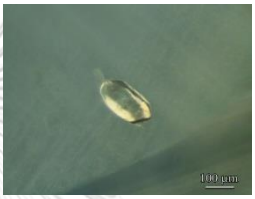

8TWL099-in3

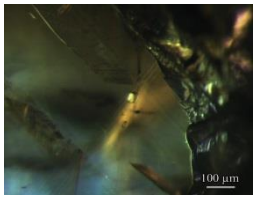

8TWL102-in1

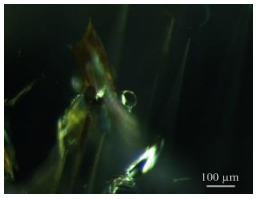

8TWL102-in2

8TWL102-in3

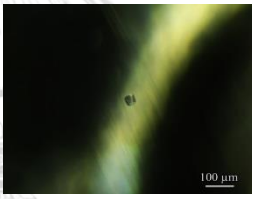

8TWL105-in1

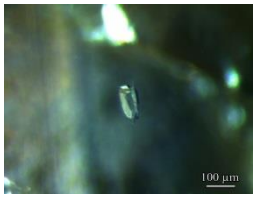

8TWL111-in1

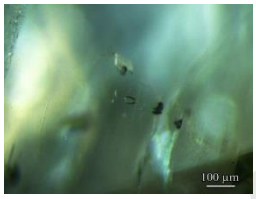

8TWL112-in1

8TWL113-in1

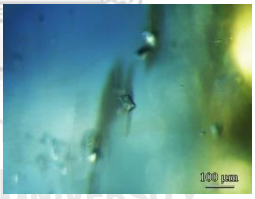

8TWL114-in1

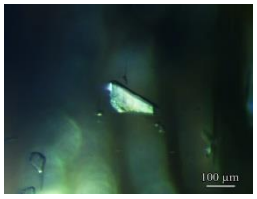

8TWL114-in2

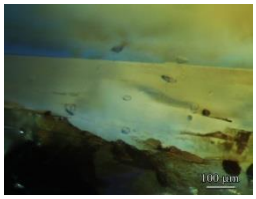

8TWL114-in4

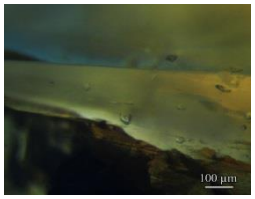

8TWL114-in5

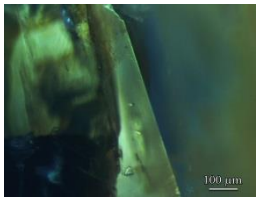

8TWL114-in6

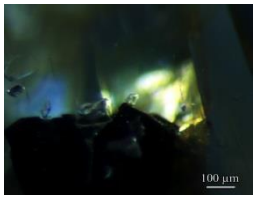

8TWL114-in8

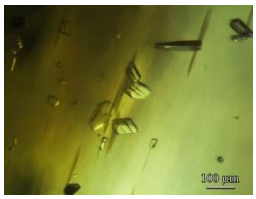

8TWL114-in12-17

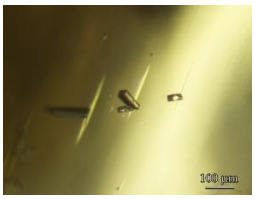

8TWL114-in18

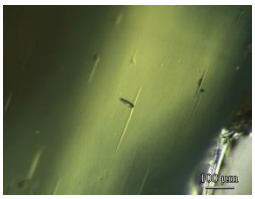

8TWL114-in19

8TWL114-in22

Figure B-15 Feldspar inclusions in Bo Welu sapphire (continued)

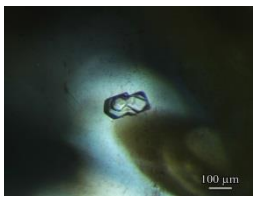
8TWL116-in1

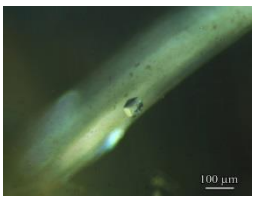
8TWL116-in2

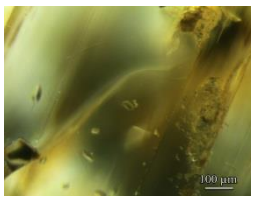
8TWL117-in1

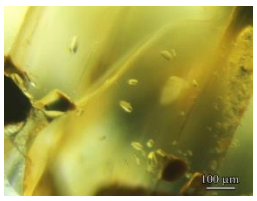
8TWL117-in2


8TWL119-in1

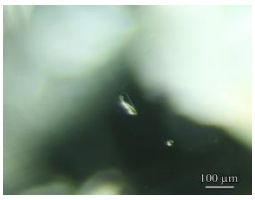
8TWL119-in3

Figure B-15 Feldspar inclusions in Bo Welu sapphire (continued)

Figure B-16 Monazite with feldspar inclusions in Bo Welu sapphire sample 8TWL114


8TWL026-in6

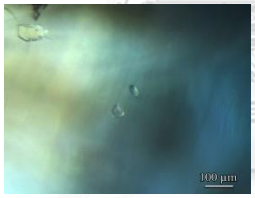
8TWL036-in3-4

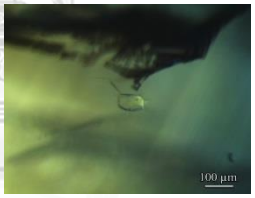
8TWL036-in5


8TWL036-in6


8TWL036-in7


8TWL040-in3

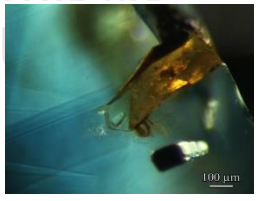
8TWL053-in1

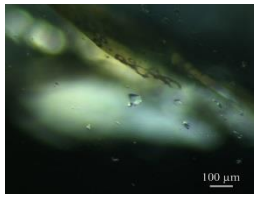
8TWL068-in1

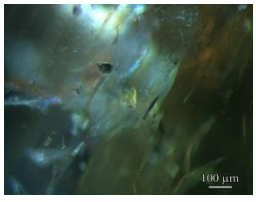
8TWL068-in2


8TWL093-in6

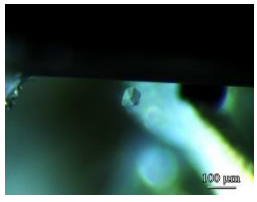
8TWL104-in3

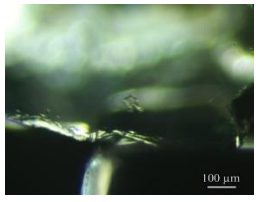
8TWL119-in2

Figure B-17 Monazite inclusions in Bo Welu sapphire

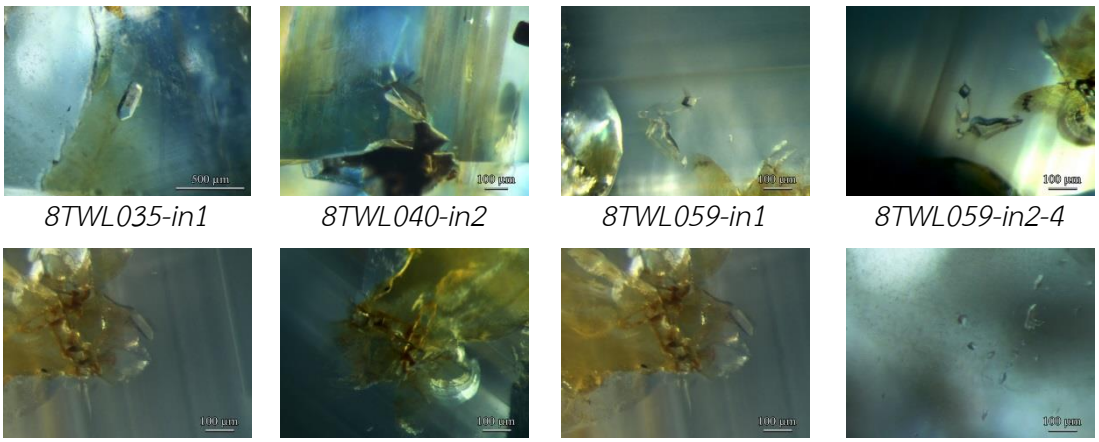

8TWL035-in1 *8TWL040-in2* *8TWL059-in1* *8TWL059-in2-4*

8TWL059-in5 *8TWL059-in6-8,9,13-14* *8TWL059-in10-12* *8TWL101-in1*

Figure B-18 Zircon inclusions in Bo Welu sapphire

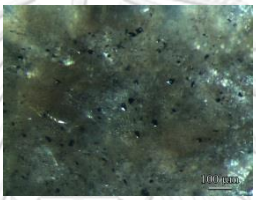

Figure B-19 Sulphide inclusions in Bo Welu sapphire sample 8TWL046

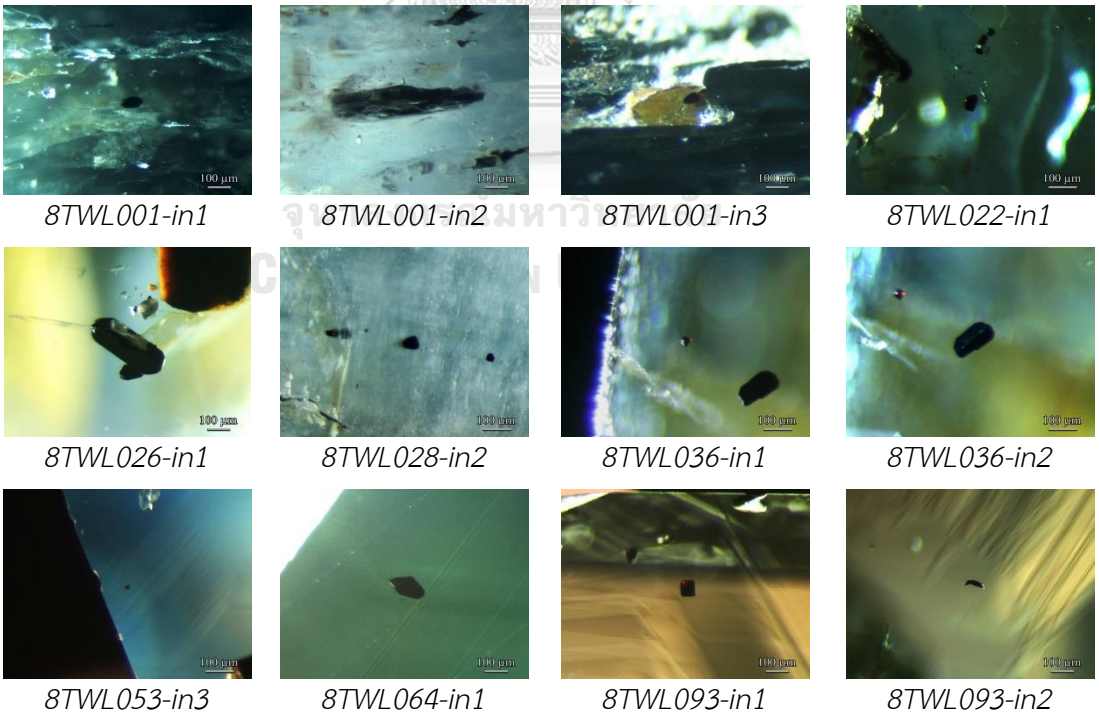

8TWL001-in1 *8TWL001-in2* *8TWL001-in3* *8TWL022-in1*

8TWL026-in1 *8TWL028-in2* *8TWL036-in1* *8TWL036-in2*

8TWL053-in3 *8TWL064-in1* *8TWL093-in1* *8TWL093-in2*

Figure B-20 Columbite inclusions in Bo Welu sapphire

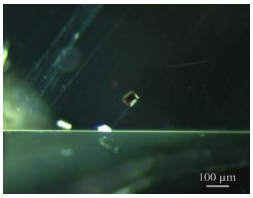

8TWL093-in3

8TWL096-in2

8TWL097-in7

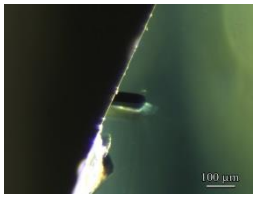

8TWL097-in8

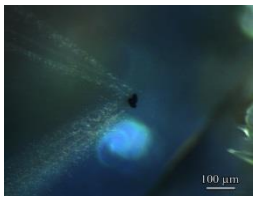

8TWL100-in1

8TWL104-in1

8TWL104-in2

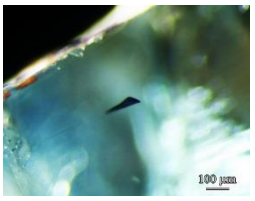

8TWL106-in1

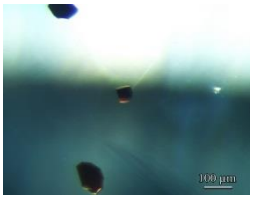

8TWL108-in1

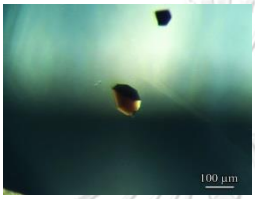

8TWL108-in2

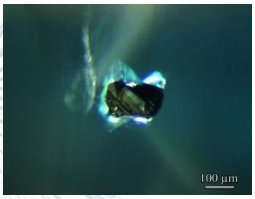

8TWL108-in3

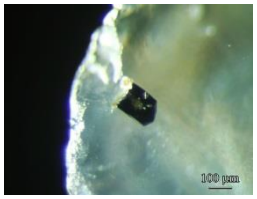

8TWL120-in1

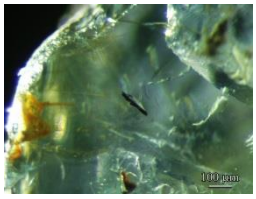

8TWL120-in2

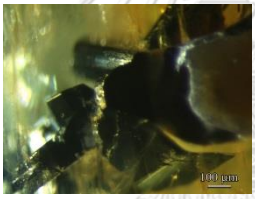

8TWL114-in22

Figure B-20 Columbite inclusions in Bo Welu sapphire (continued)

Appendix C - FIIR Spectra

Representative FIIR Spectra of Bo Rai ruby

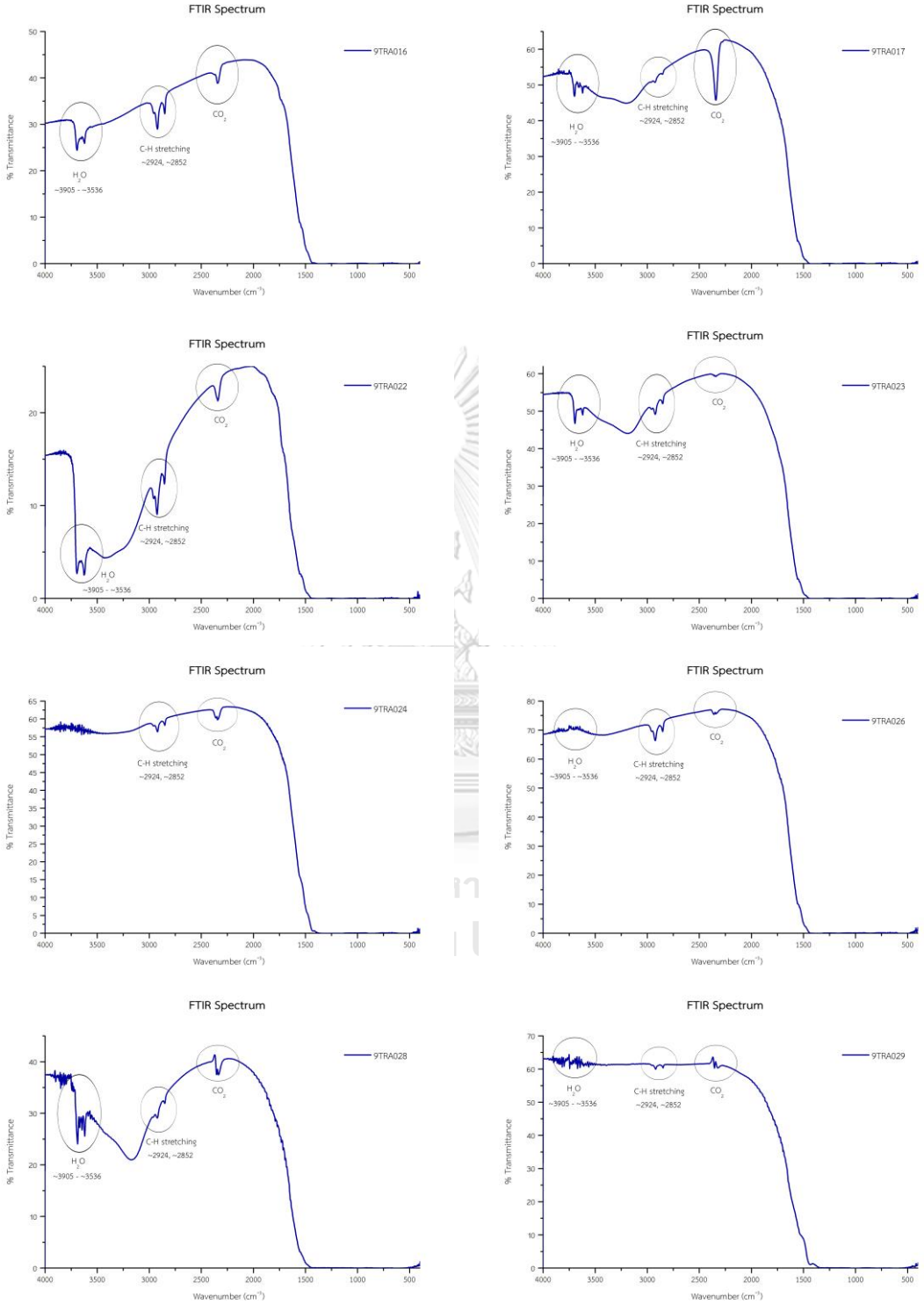

Figure C-1 Representative FIIR Spectra of Bo Rai ruby

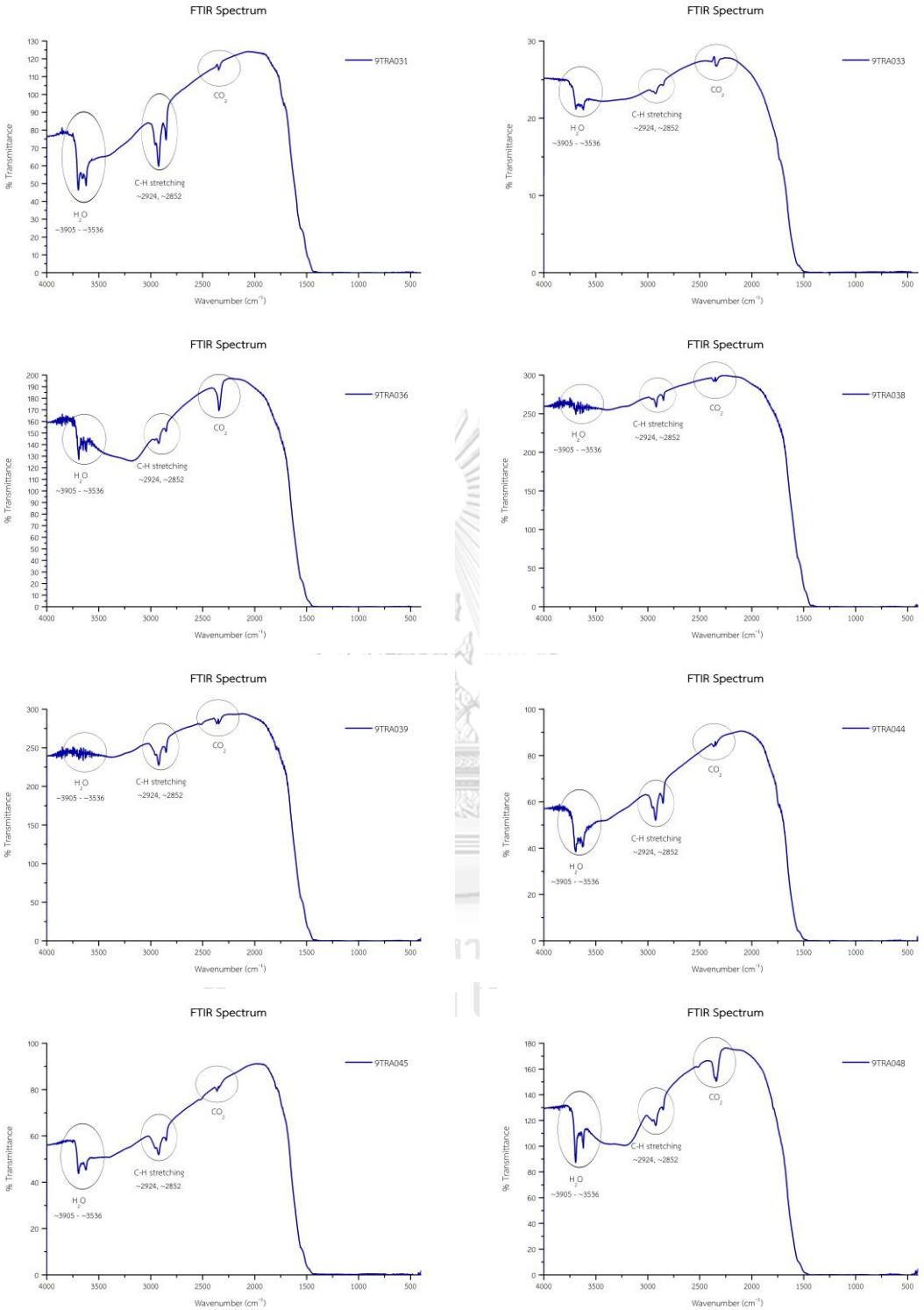

Figure C-1 Representative FIIR Spectra of Bo Rai ruby (continued)

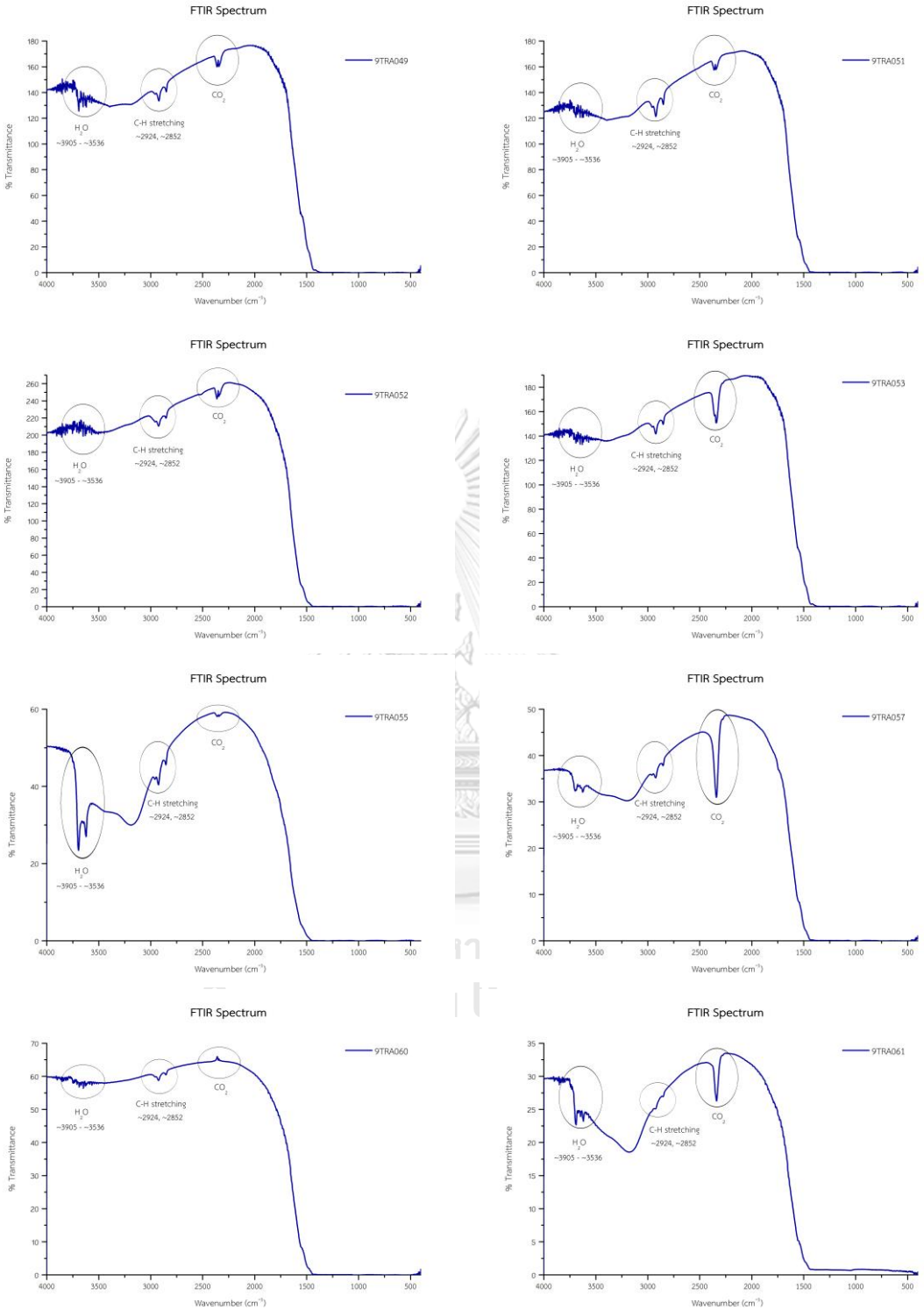

Figure C-1 Representative FIIR Spectra of Bo Rai ruby (continued)

Representative FIIR Spectra of Bo Welu ruby

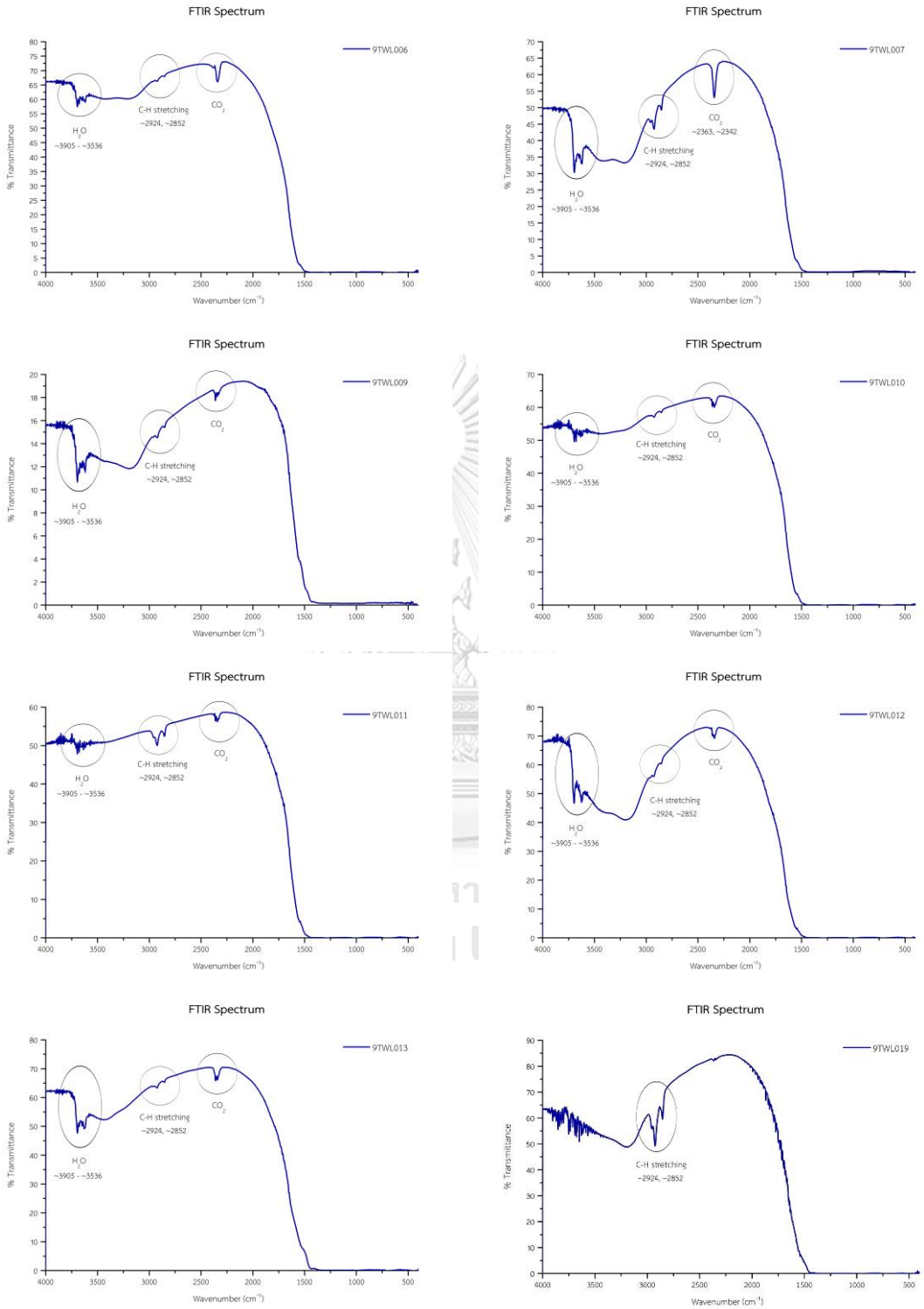

Figure C-2 Representative FIIR Spectra of Bo Welu ruby

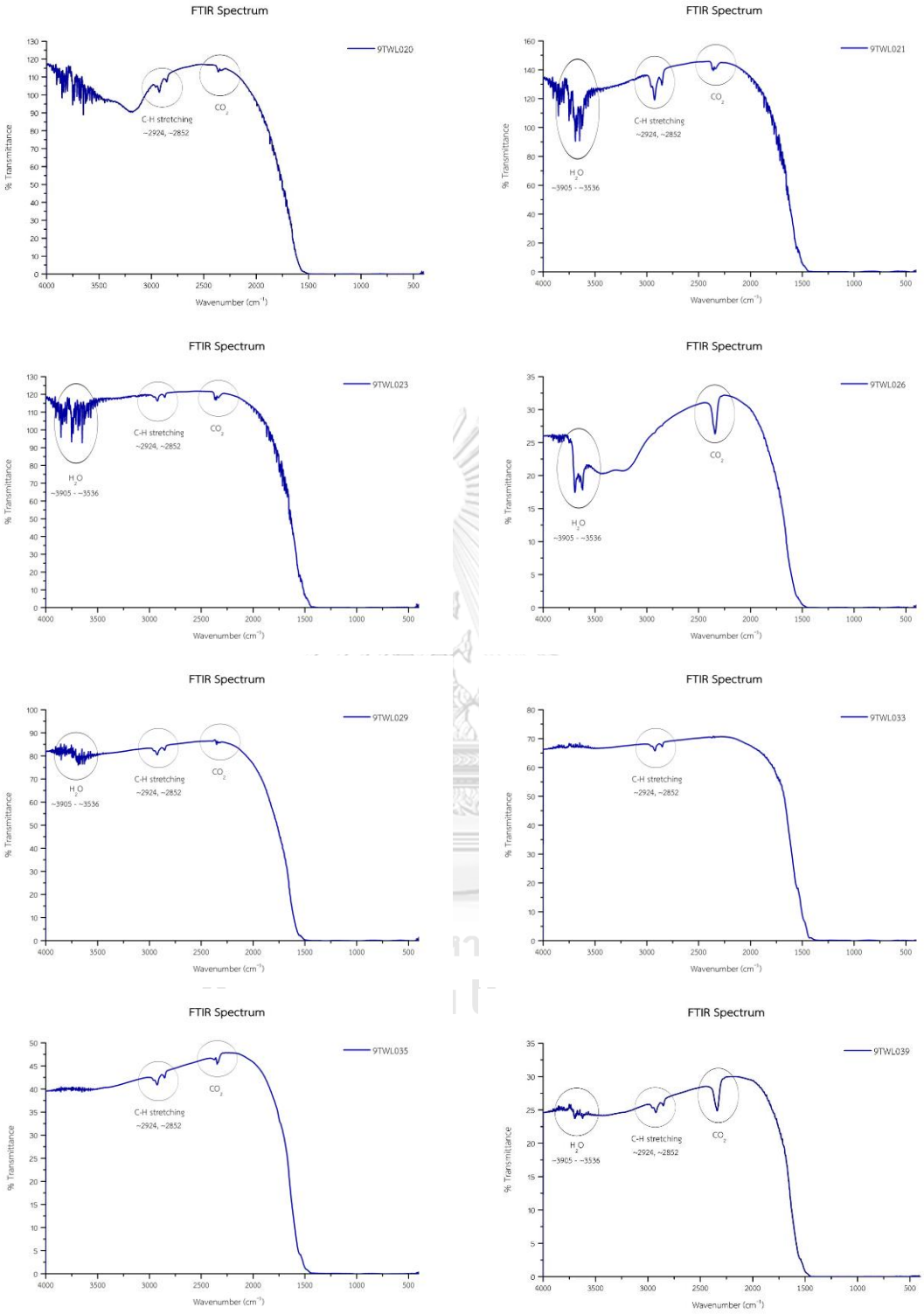

Figure C-2 Representative FIIR Spectra of Bo Welu ruby (continued)

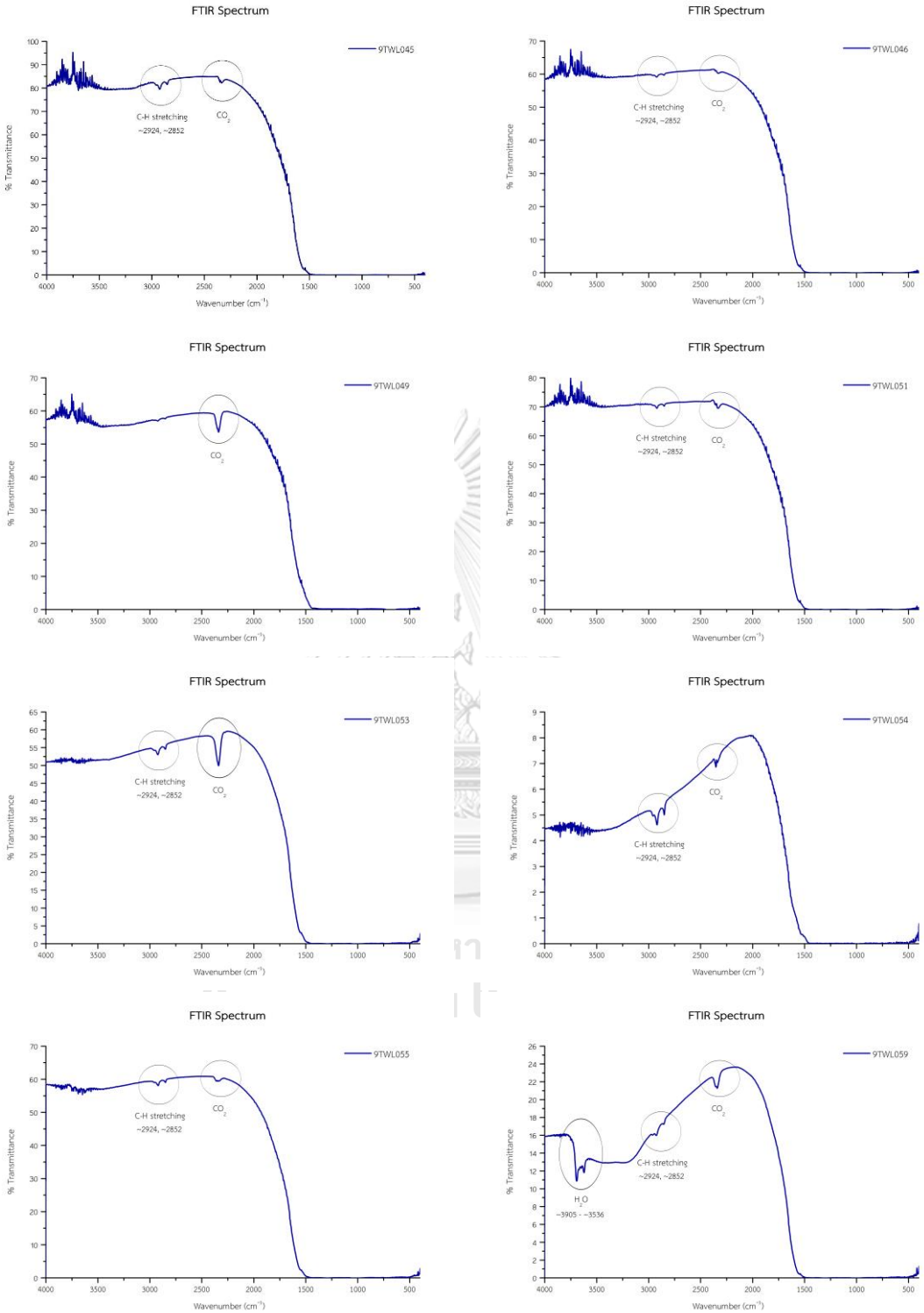

Figure C-2 Representative FIIR Spectra of Bo Welu ruby (continued)

Representative FIIR Spectra of Bo Welu sapphire

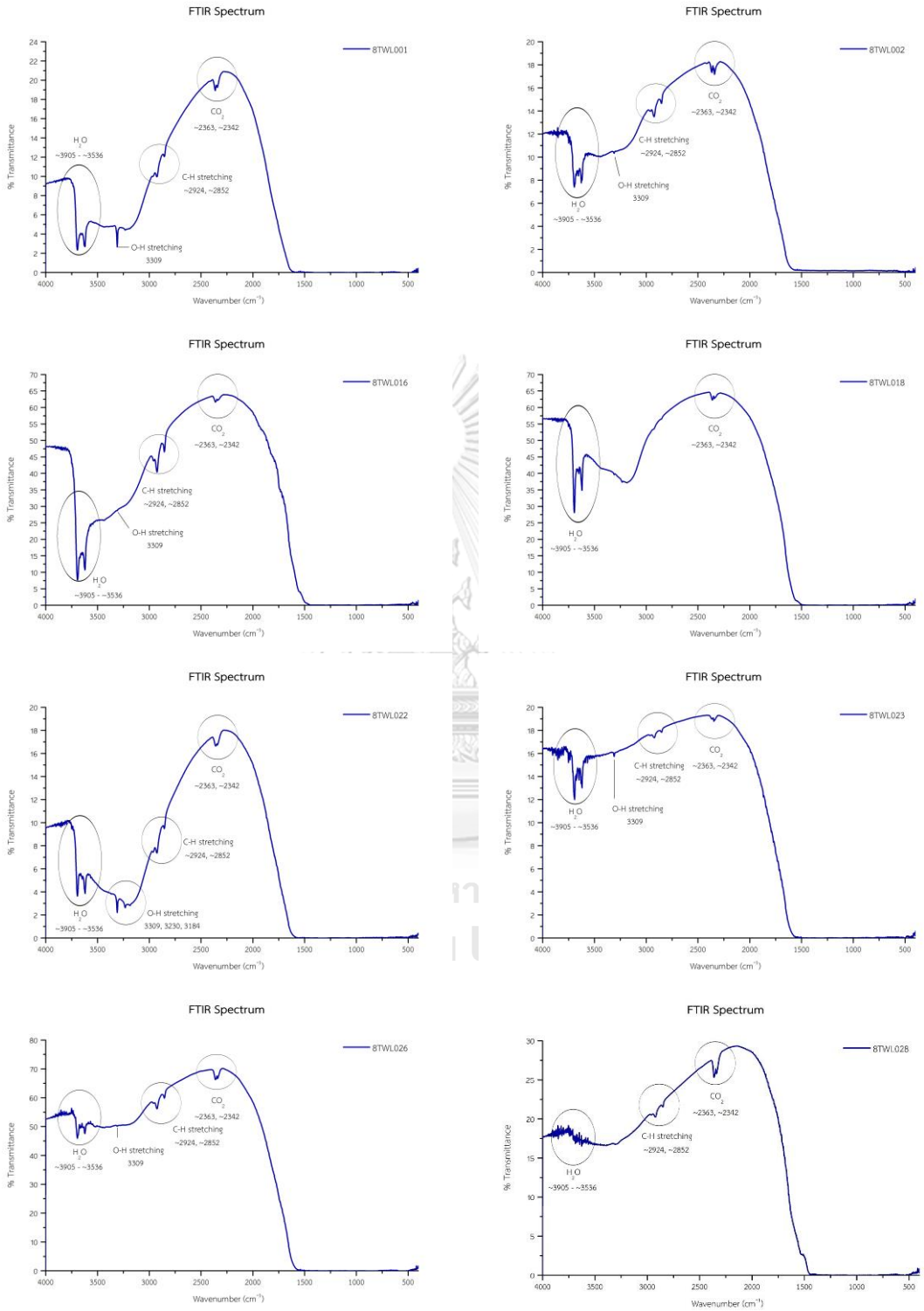

Figure C-3 Representative FIIR Spectra of Bo Welu sapphire

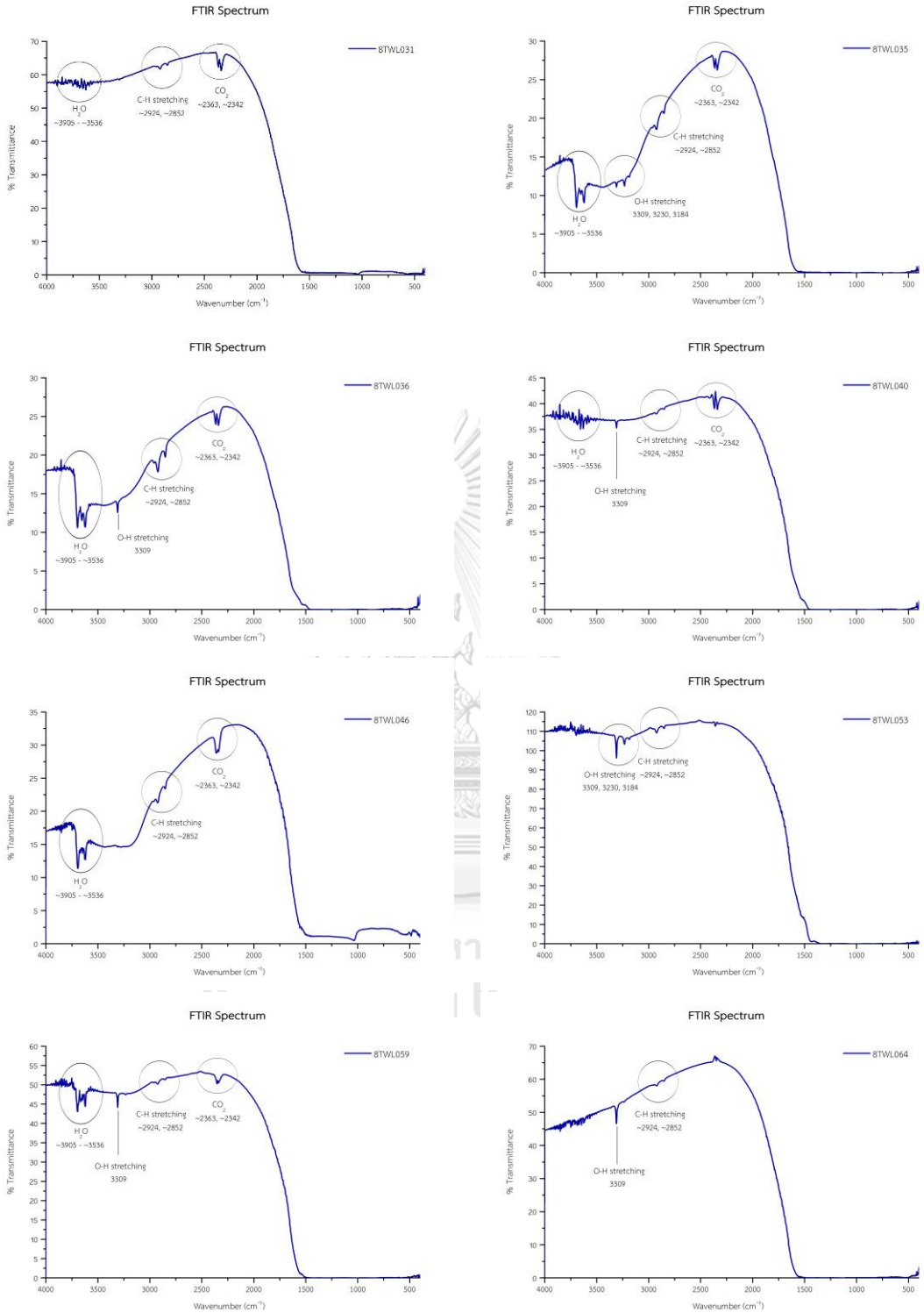

Figure C-3 Representative FIIR Spectra of Bo Welu sapphire (continued)

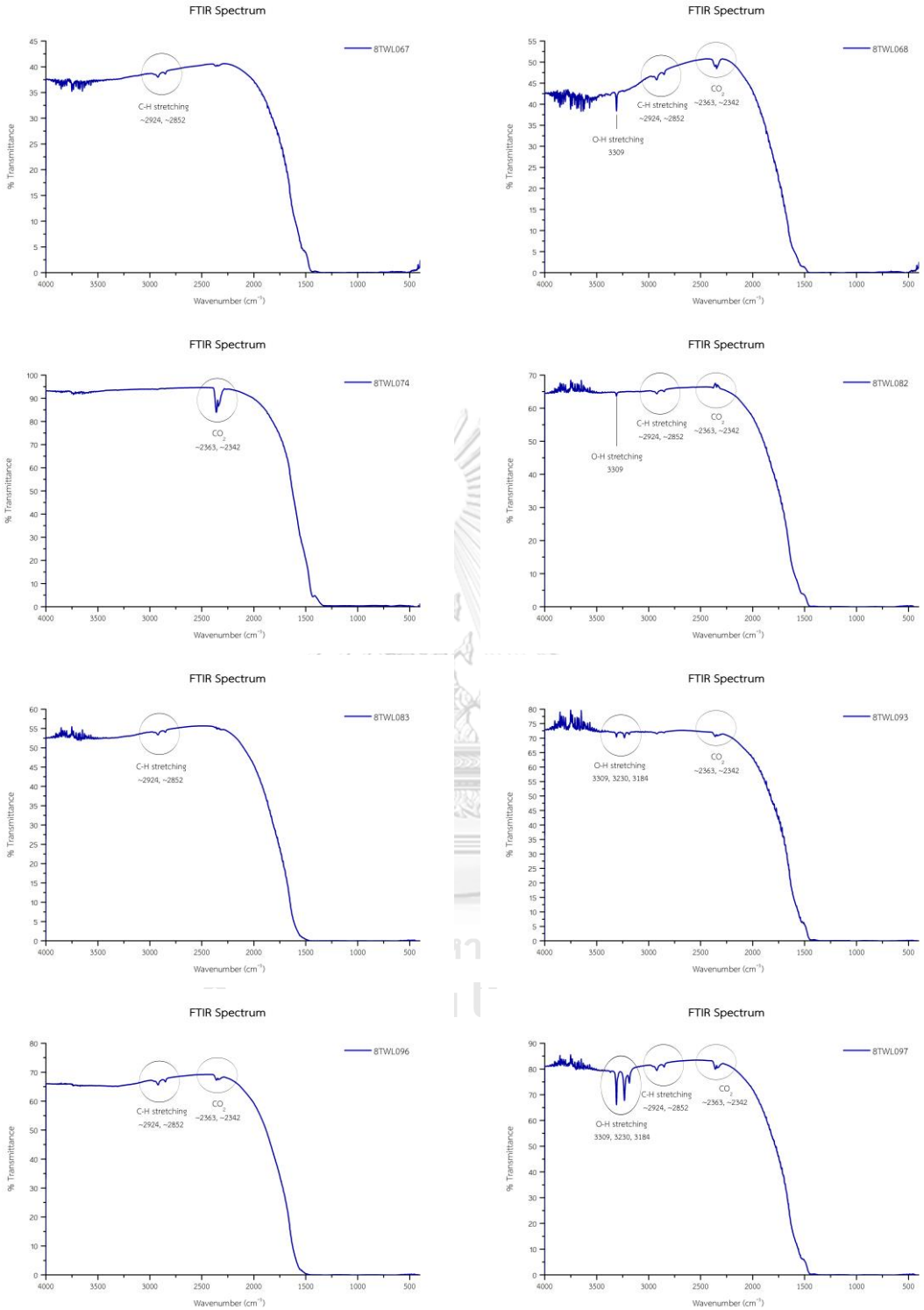

Figure C-3 Representative FIIR Spectra of Bo Welu sapphire (continued)

Appendix D - UV-vis Spectra

Representative UV-Vis-NIR absorption spectra of Bo Rai ruby

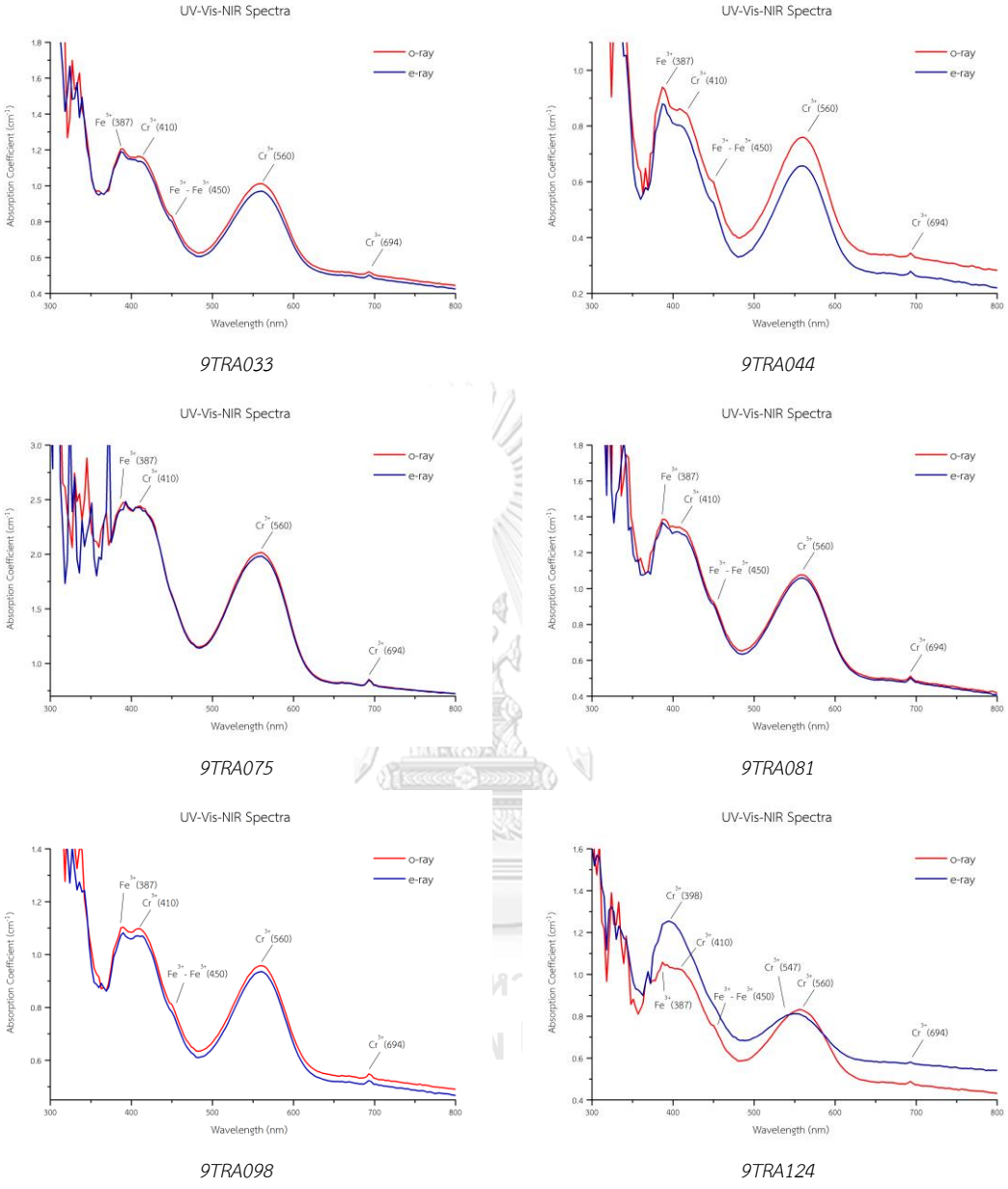

Figure D-1 Representative UV-Vis-NIR absorption spectra of Bo Rai ruby

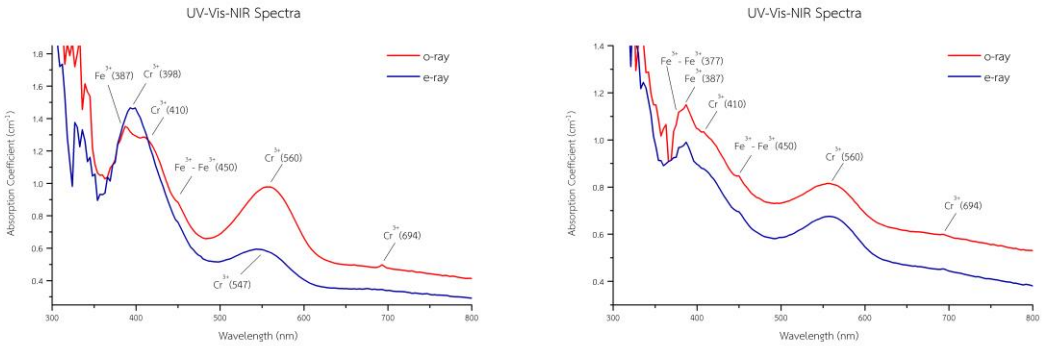

9TRA127

9TRA137

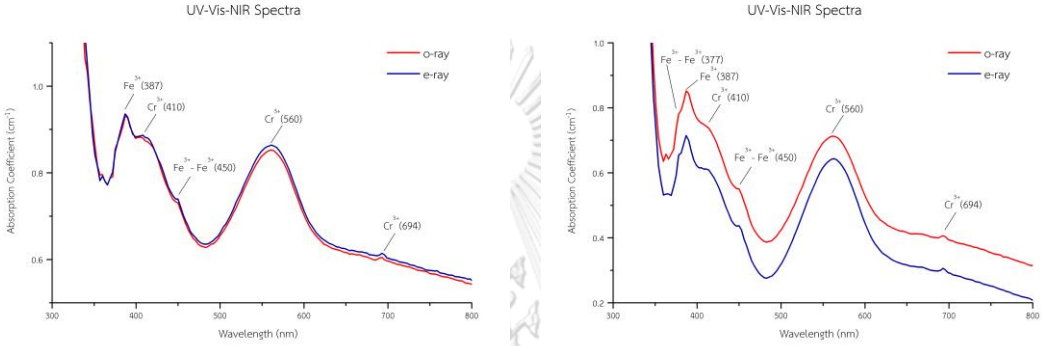

9TRA155

9TRA156

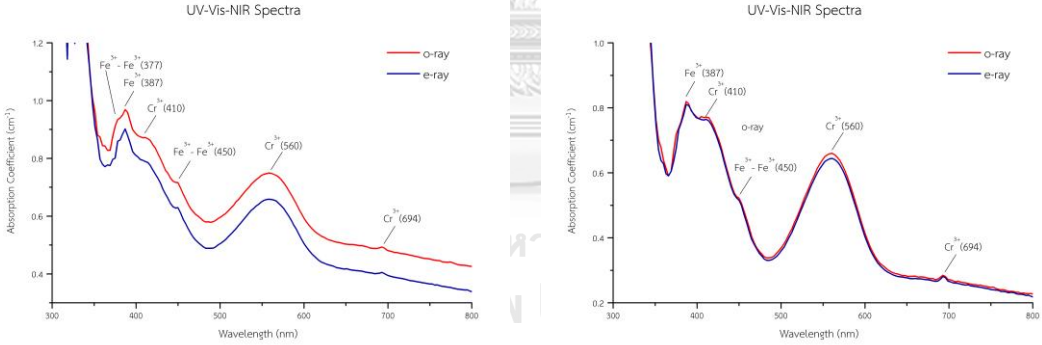

9TRA158

9TRA176

Figure D-1 Representative UV-Vis-NIR absorption spectra of Bo Rai ruby (continued)

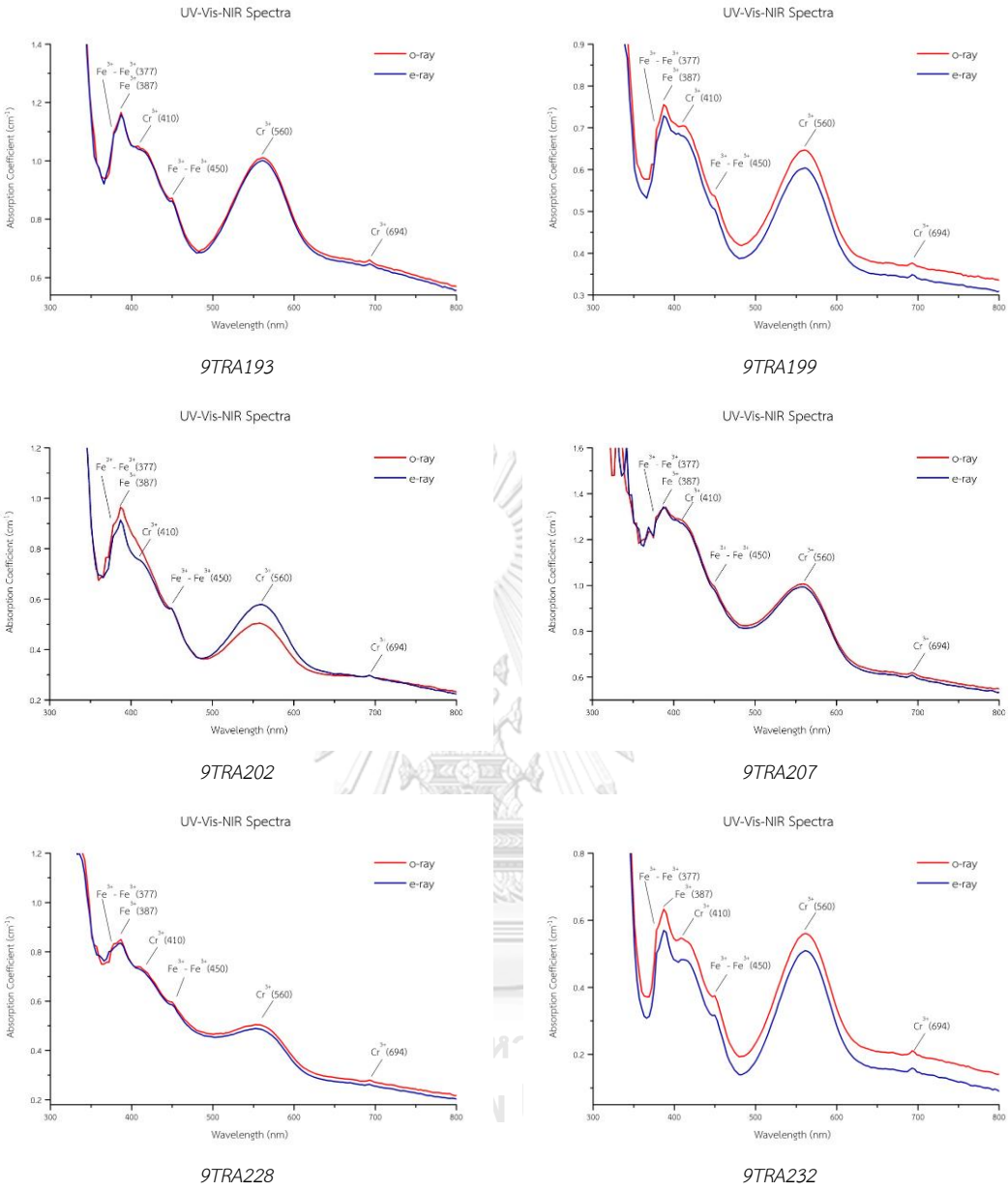

9TRA193 *9TRA199*

9TRA202 *9TRA207*

9TRA228 *9TRA232*

Figure D-1 Representative UV-Vis-NIR absorption spectra of Bo Rai ruby (continued)

Representative UV-Vis-NIR absorption spectra of Bo Welu ruby

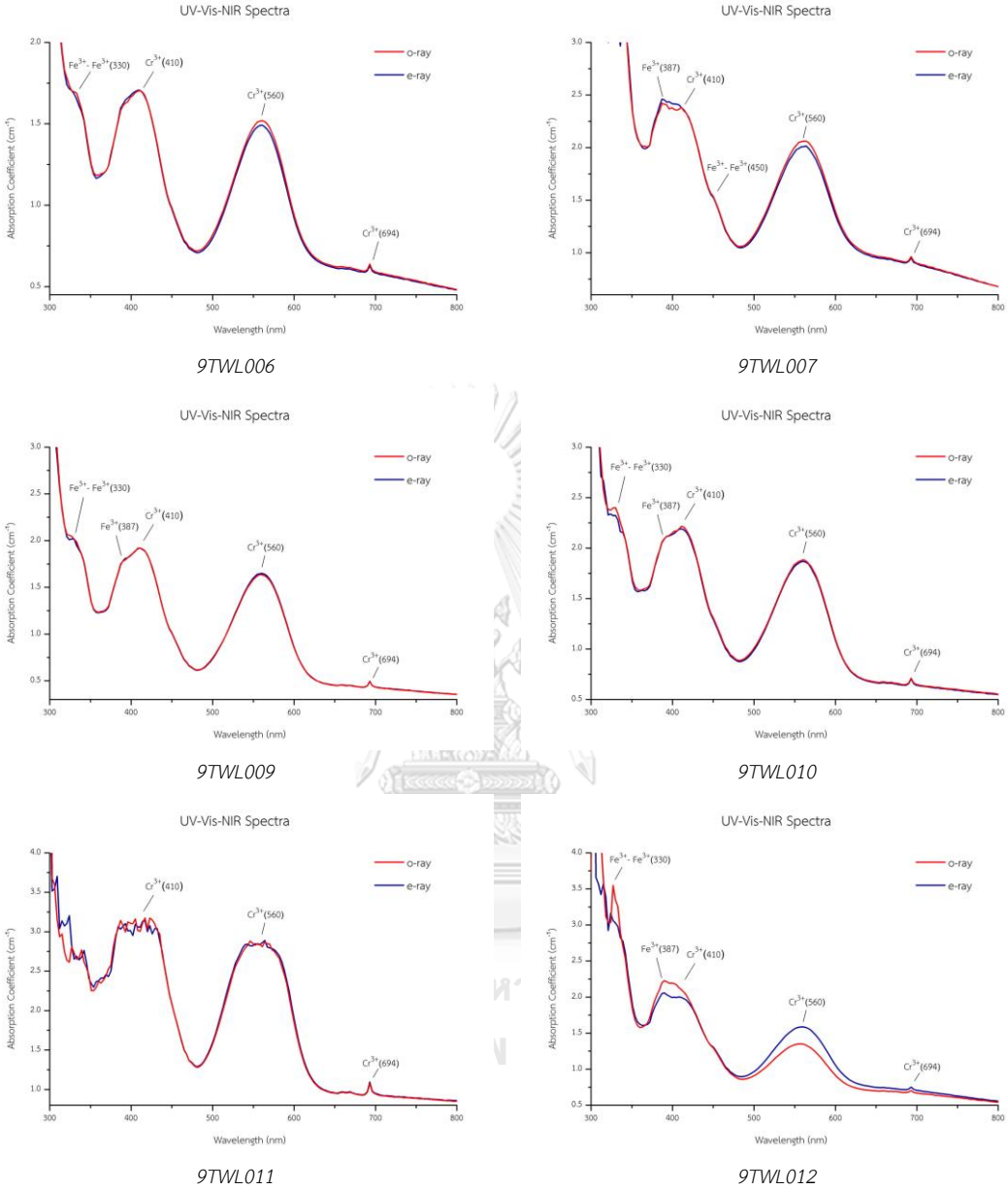

Figure D-2 Representative UV-Vis-NIR absorption spectra of Bo Welu ruby

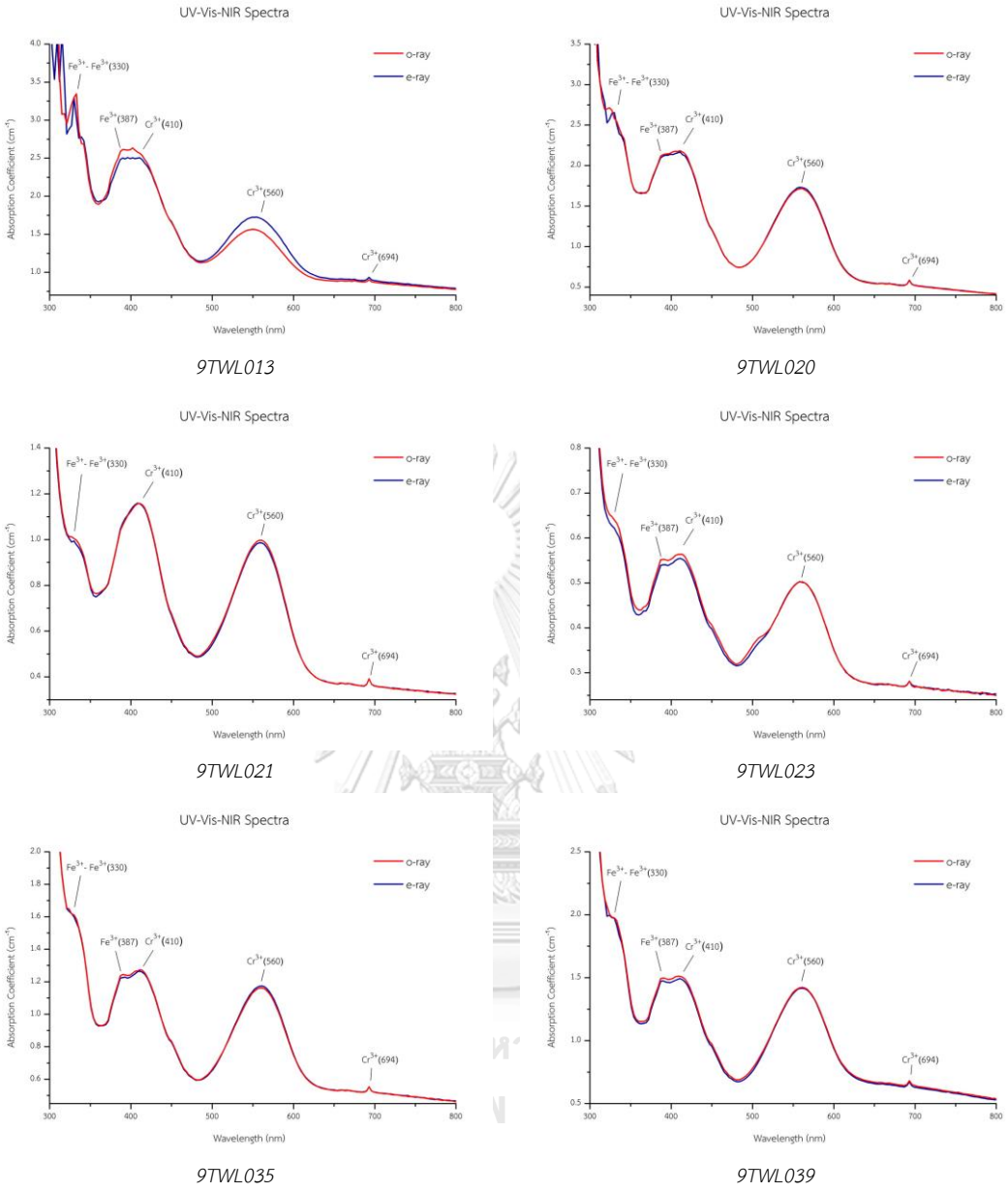

9TWL013 *9TWL020*

9TWL021 *9TWL023*

9TWL035 *9TWL039*

Figure D-2 Representative UV-Vis-NIR absorption spectra of Bo Welu ruby (continued)

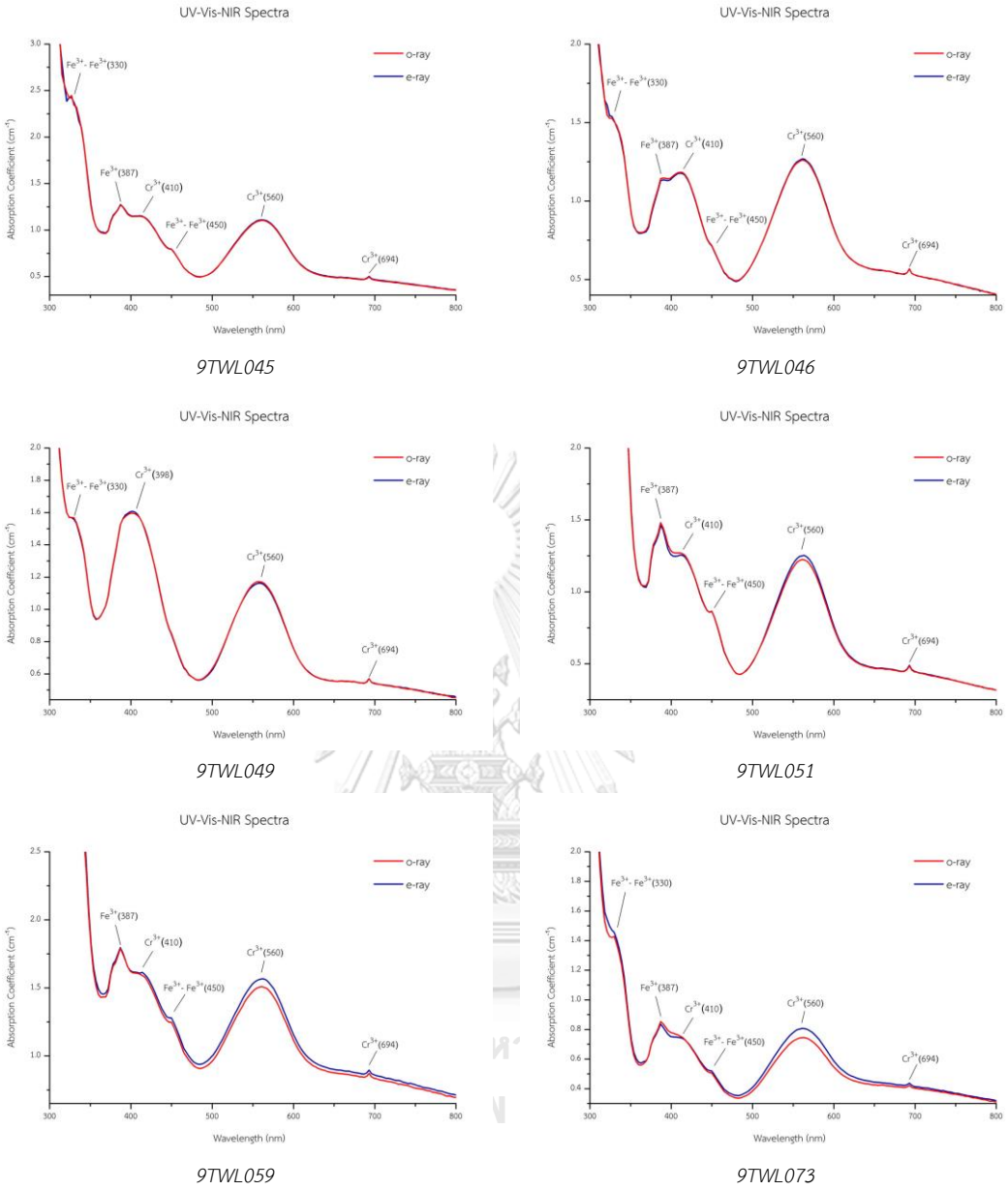

9TWL045 *9TWL046*

9TWL049 *9TWL051*

9TWL059 *9TWL073*

Figure D-2 Representative UV-Vis-NIR absorption spectra of Bo Welu ruby (continued)

Representative UV-Vis-NIR absorption spectra of Bo Welu sapphire

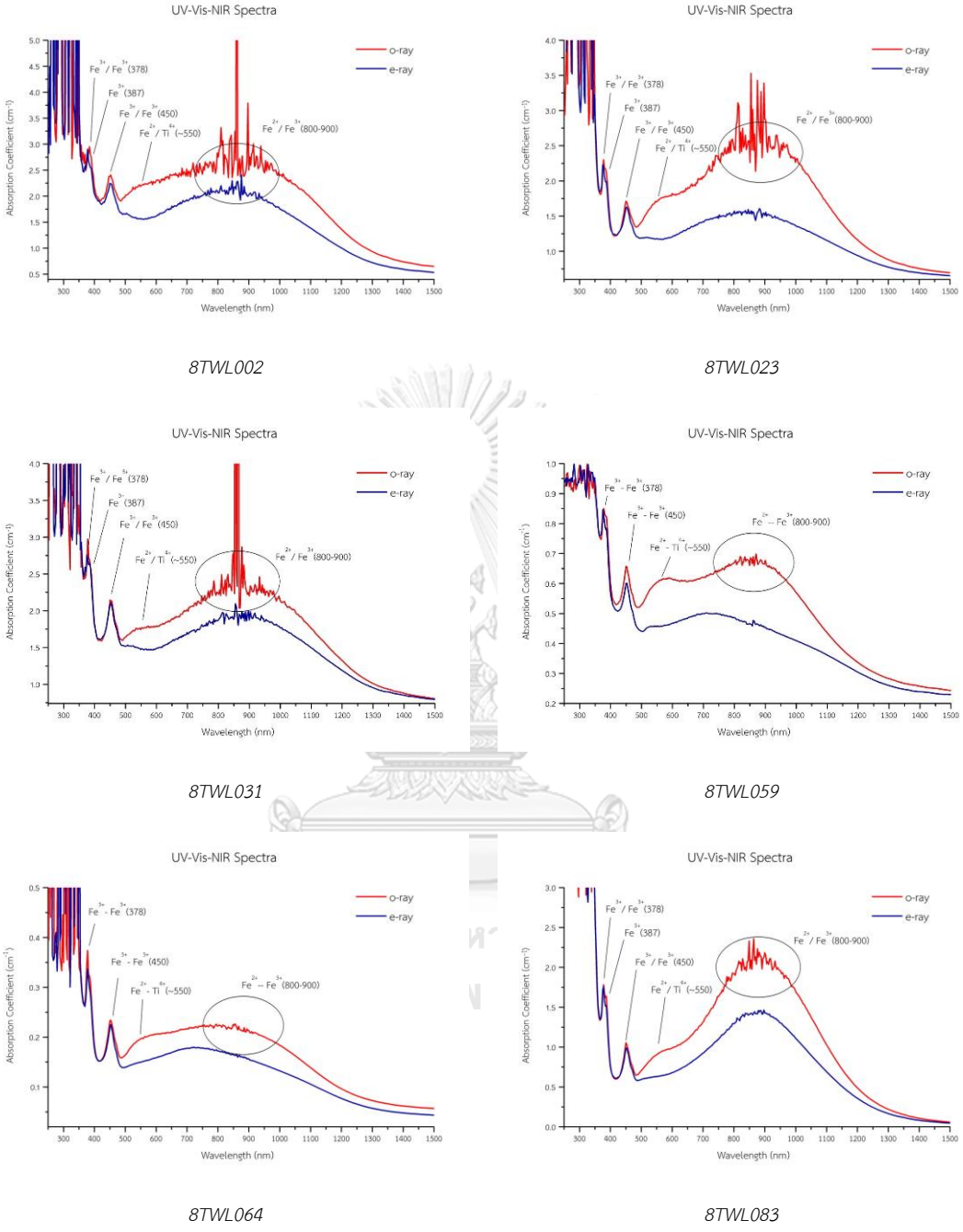

Figure D-3 Representative UV-Vis-NIR absorption spectra of Bo Welu sapphire

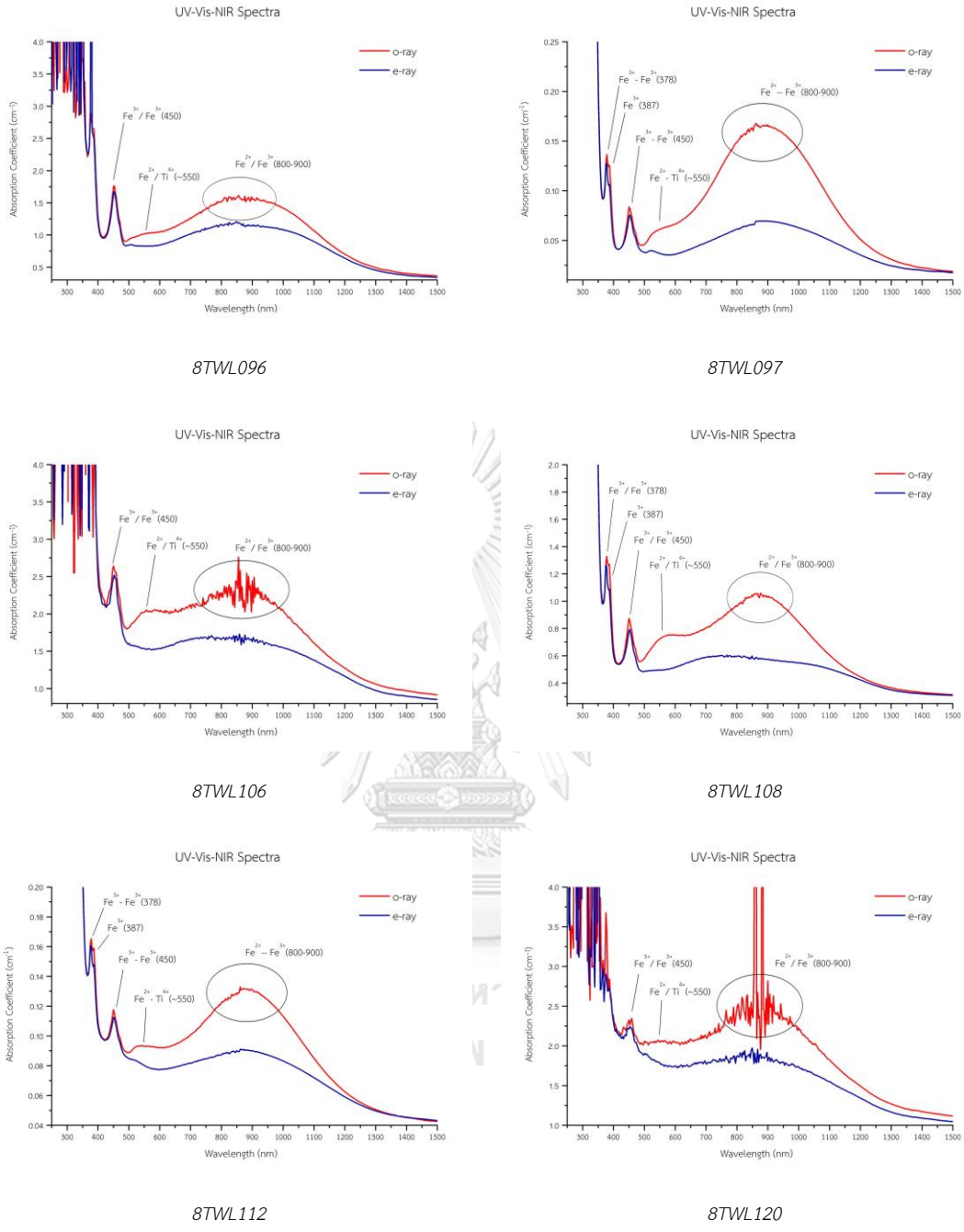

Figure D-3 Representative UV-Vis-NIR absorption spectra of Bo Welu sapphire (continued)

Appendix E - Raman spectra

Representative Raman spectra of mineral inclusions in Bo Rai ruby

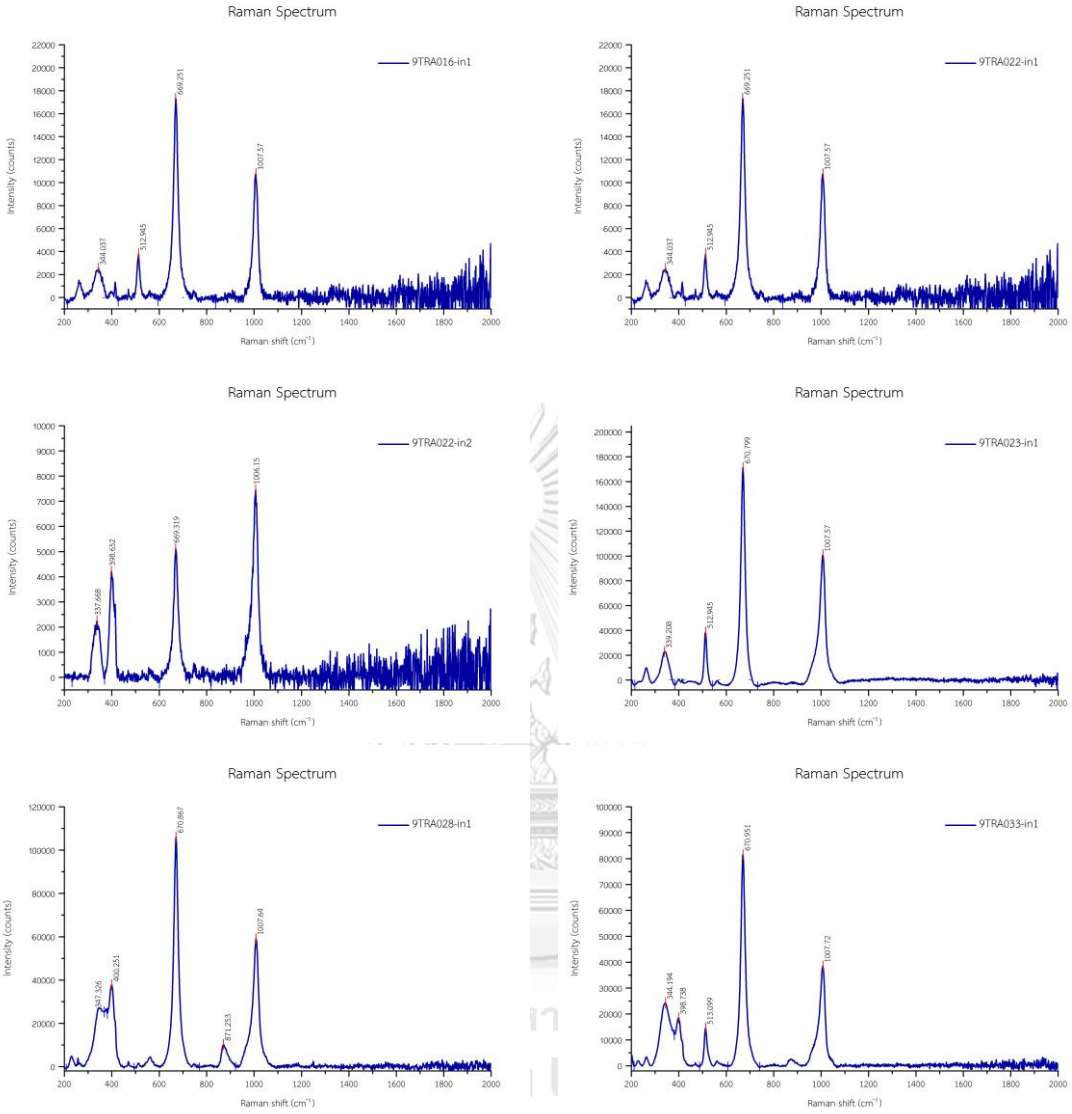

Figure E-1 Representative Raman spectra of pyroxene inclusion in Bo Rai ruby

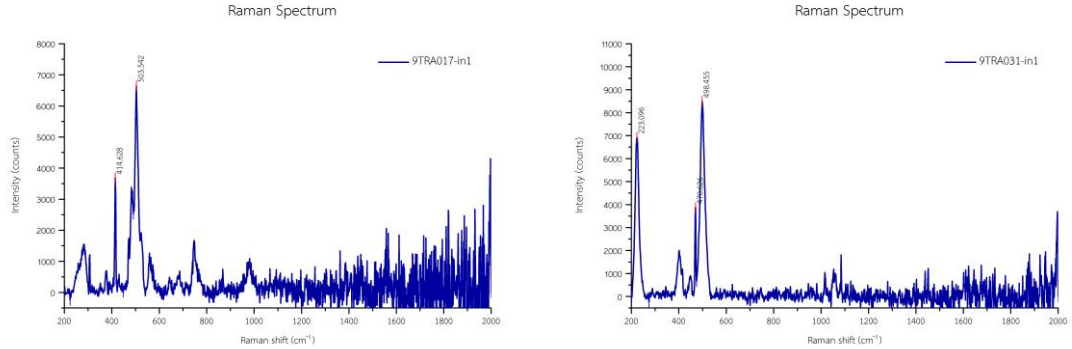

Figure E-2 Representative Raman spectra of feldspar inclusion in Bo Rai ruby

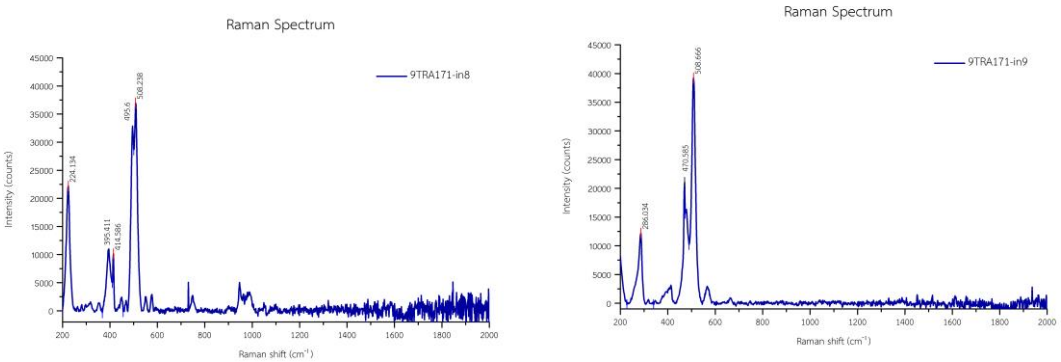

Figure E-3 Representative Raman spectra of feldspar inclusion in Bo Rai ruby (continued)

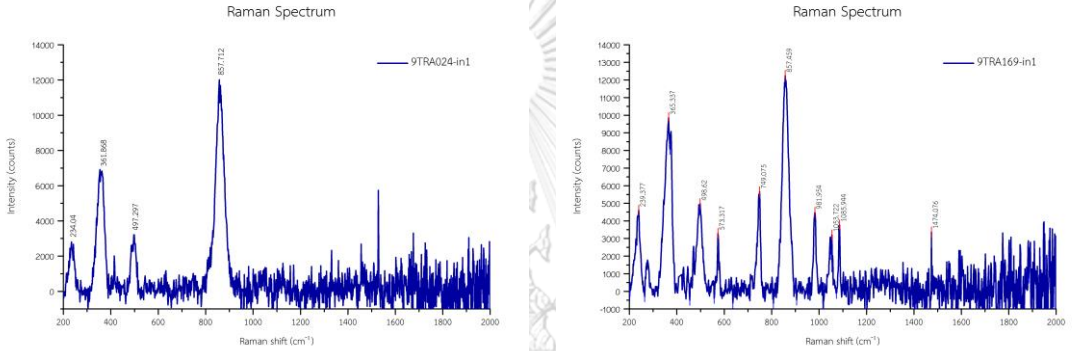

Figure E-4 Representative Raman spectra of sillimanite inclusion in Bo Rai ruby

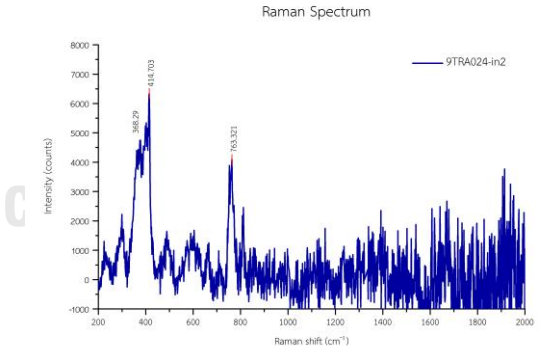

Figure E-5 Representative Raman spectrum of spinel inclusion in Bo Rai ruby sample 9TRA024

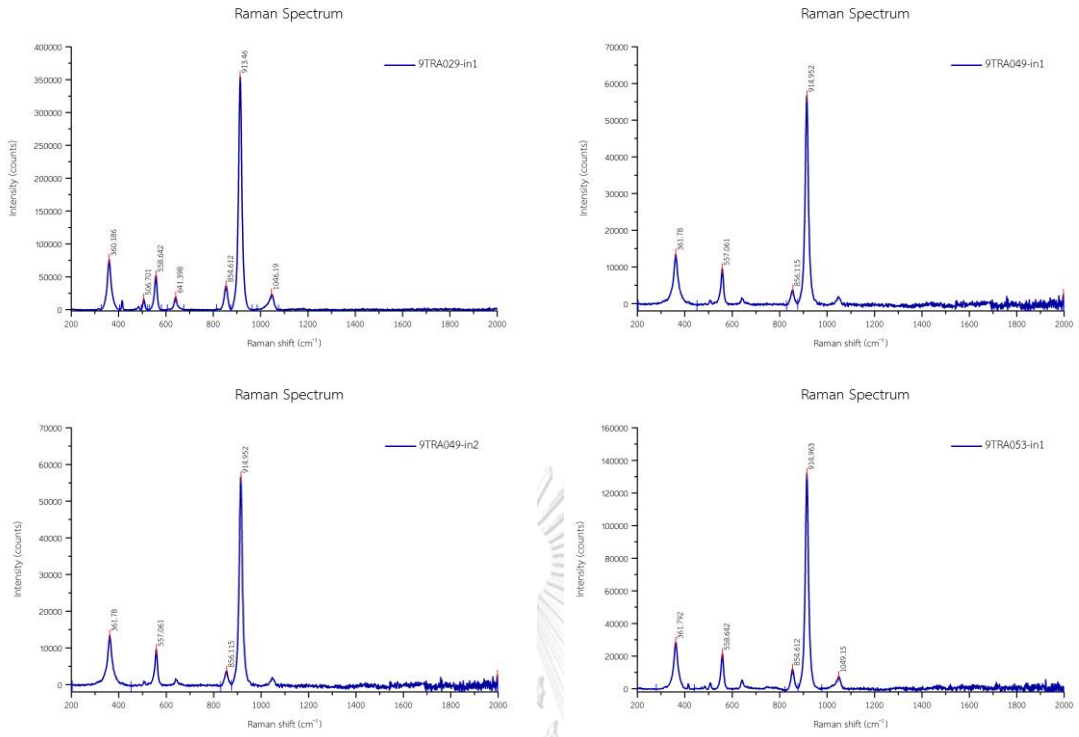

Figure E-6 Representative Raman spectra of garnet inclusions observed in Bo Rai ruby.

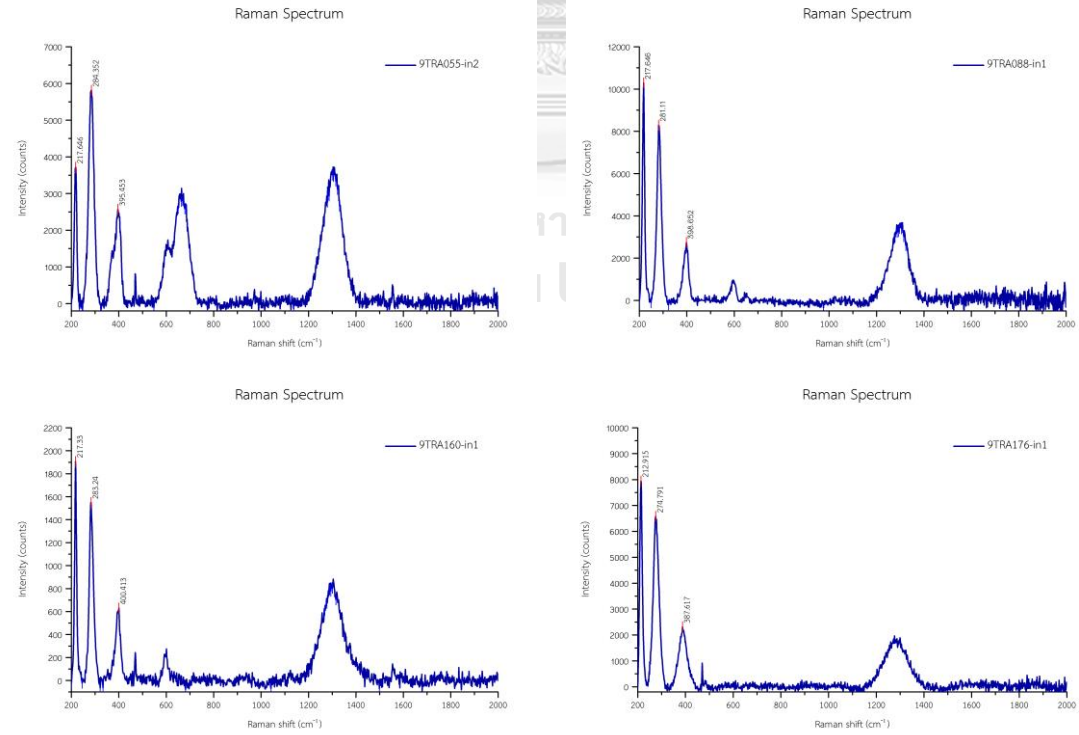

Figure E-7 Representative Raman spectra of pyrrhotite inclusions observed in Bo Rai ruby

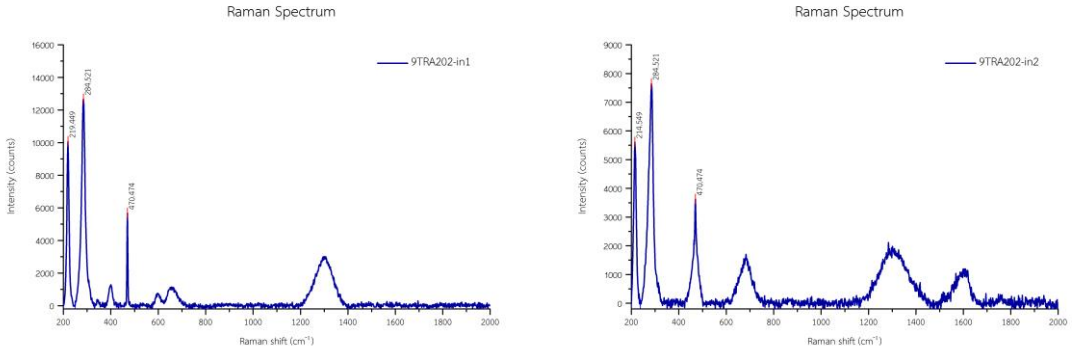

Figure E-8 Representative Raman spectra of pyrrhotite inclusions observed in Bo Rai ruby (continued)

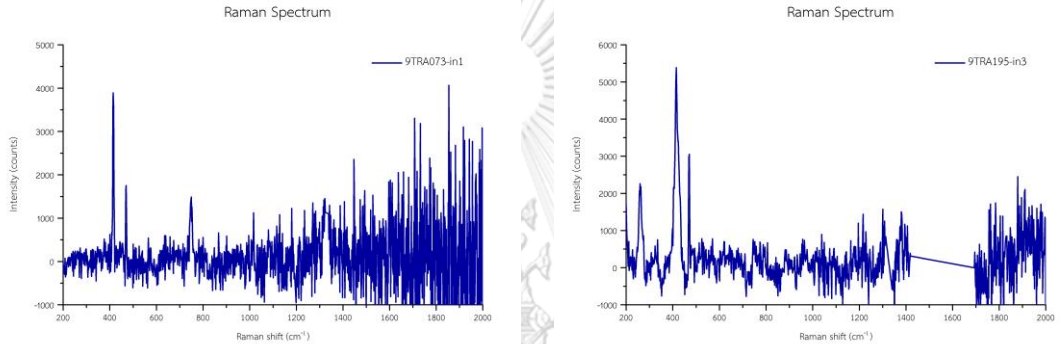

Figure E-9 Raman spectra of silicate melt inclusions observed in Bo Rai ruby

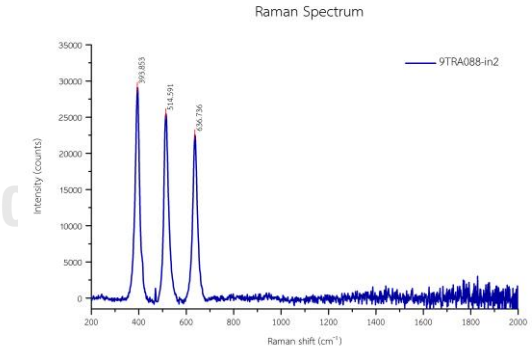

Figure E-10 Raman spectrum of anatase inclusion observed in Bo Rai ruby sample 9TRA088

Representative Raman spectra of mineral inclusions in Bo Welu ruby

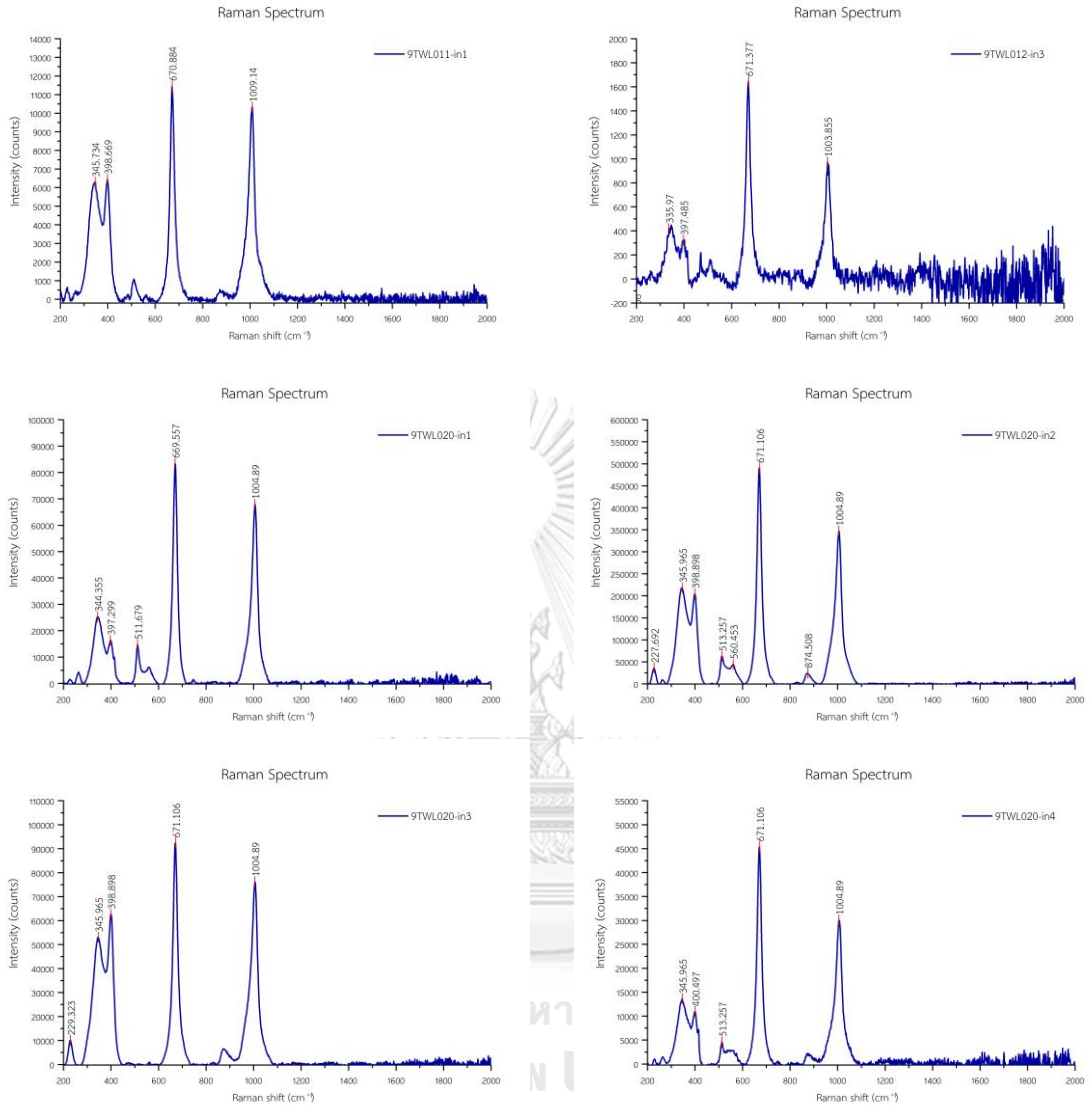

Figure E-11 Representative Raman spectra of pyroxene inclusions in Bo Welu ruby

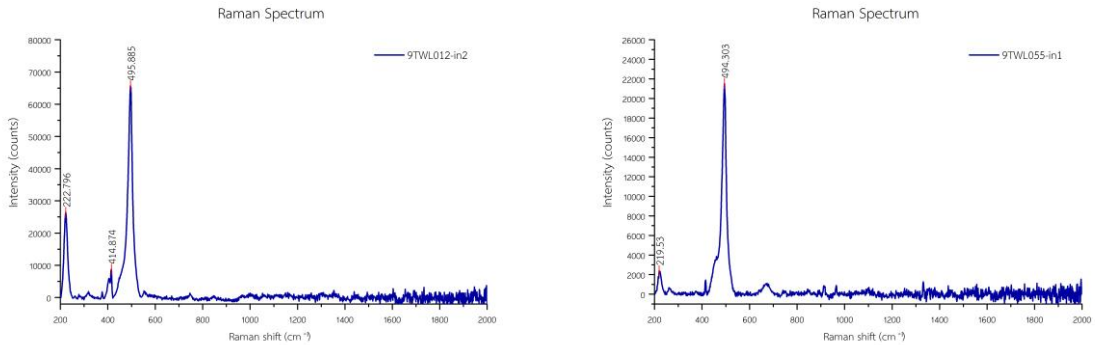

Figure E-12 Representative Raman spectra of feldspar inclusions in Bo Welu ruby

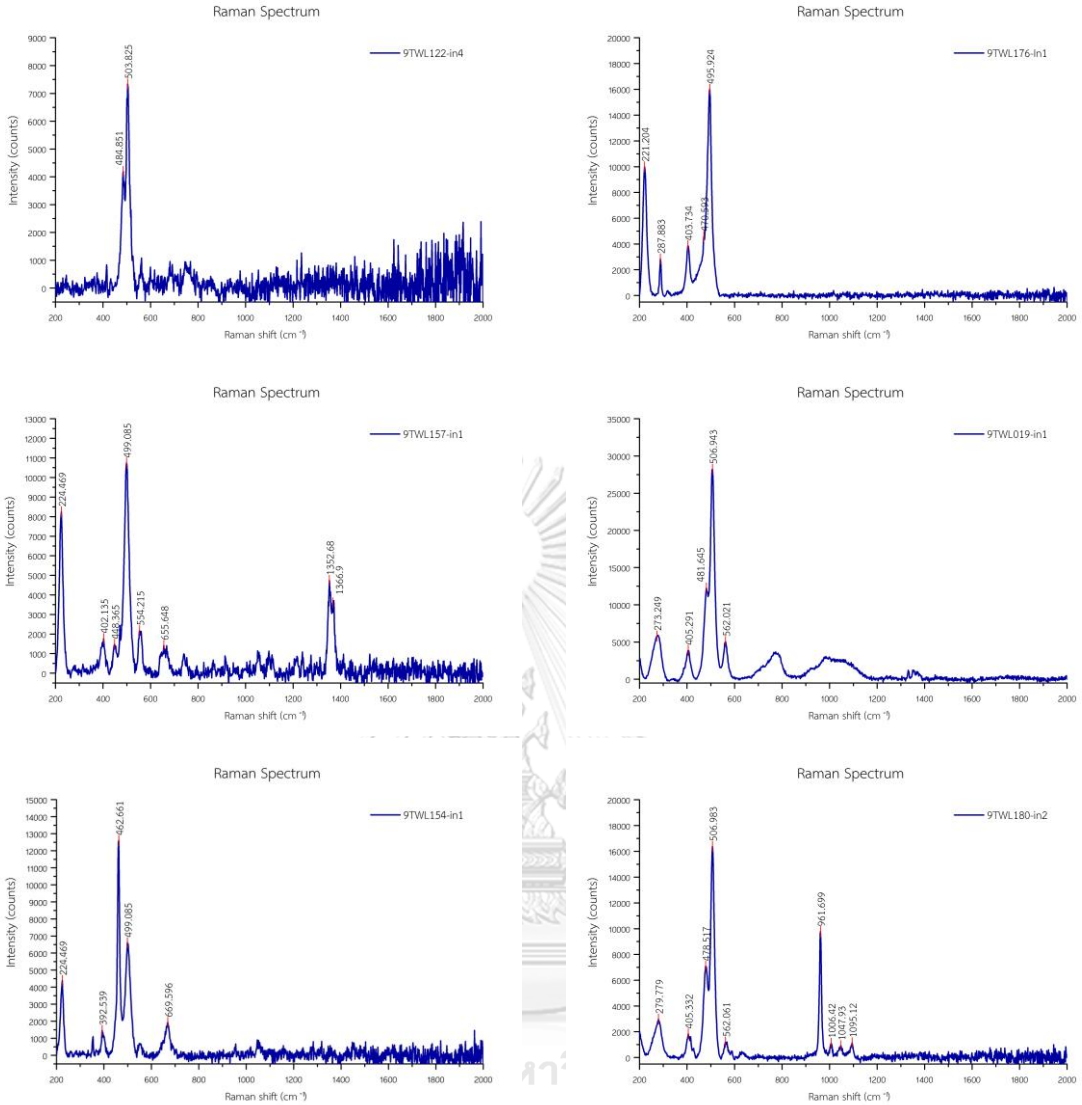

Figure E-13 Representative Raman spectra of feldspar inclusions in Bo Welu ruby (continued)

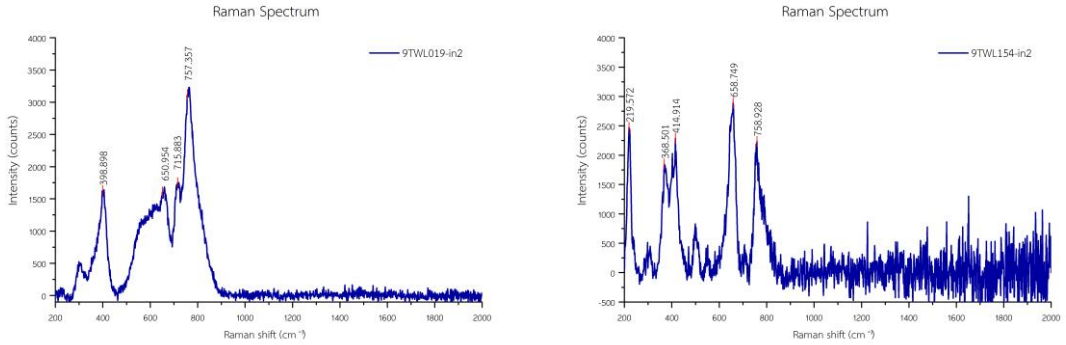

Figure E-14 Representative Raman spectra of spinel inclusions in Bo Welu ruby

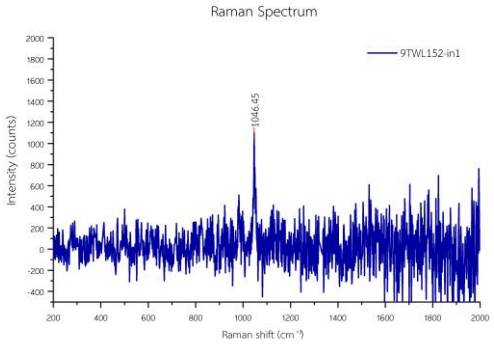

Figure E-15 Raman spectrum of sillimanite inclusion in Bo Welu ruby sample 9TWL152

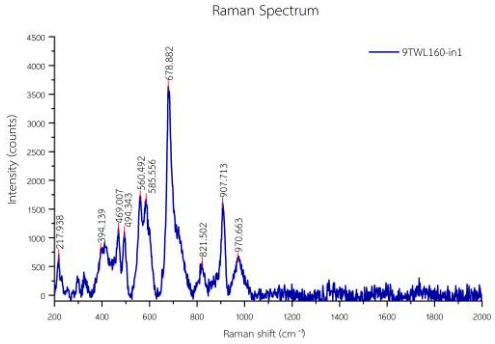

Figure E-16 Raman spectrum of sapphirine inclusion in Bo Welu ruby sample 9TWL160

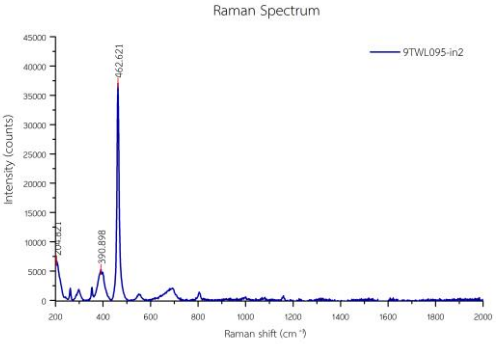

Figure E-17 Raman spectrum of quartz inclusion in Bo Welu ruby sample 9TWL095

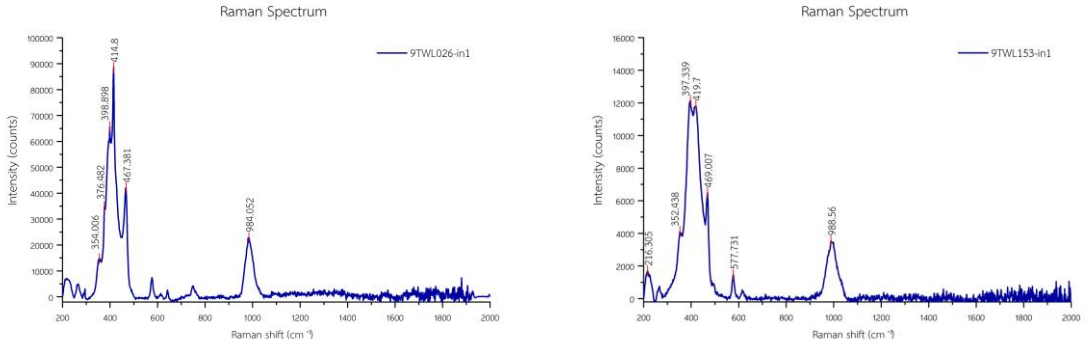

Figure E-18 Representative Raman spectra of nepheline inclusions in Bo Welu ruby

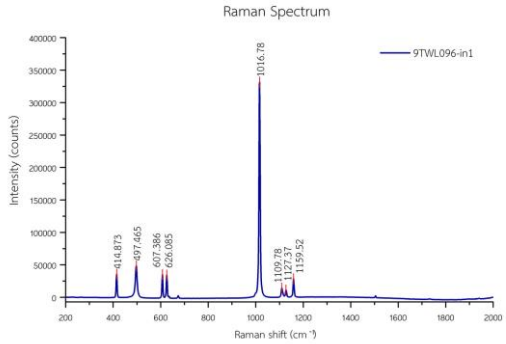

Figure E-19 Raman spectrum of anhydrite inclusion in Bo Welu ruby sample 9TWL096

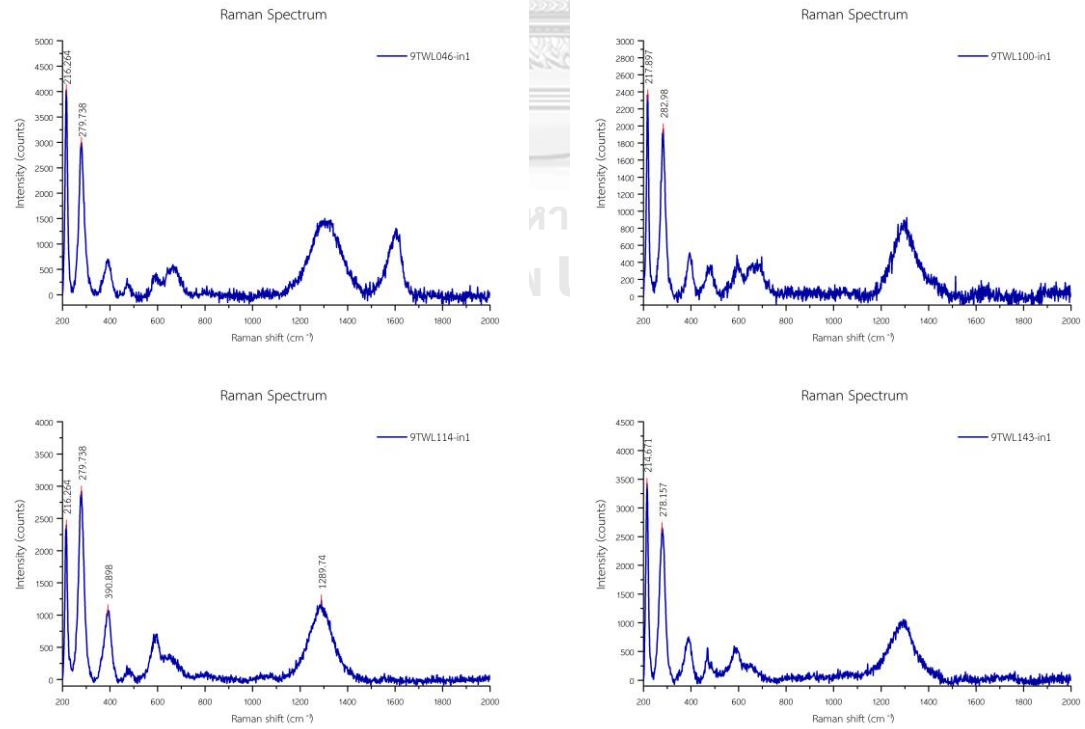

Figure E-20 Representative Raman spectra of pyrrhotite inclusions in Bo Welu ruby

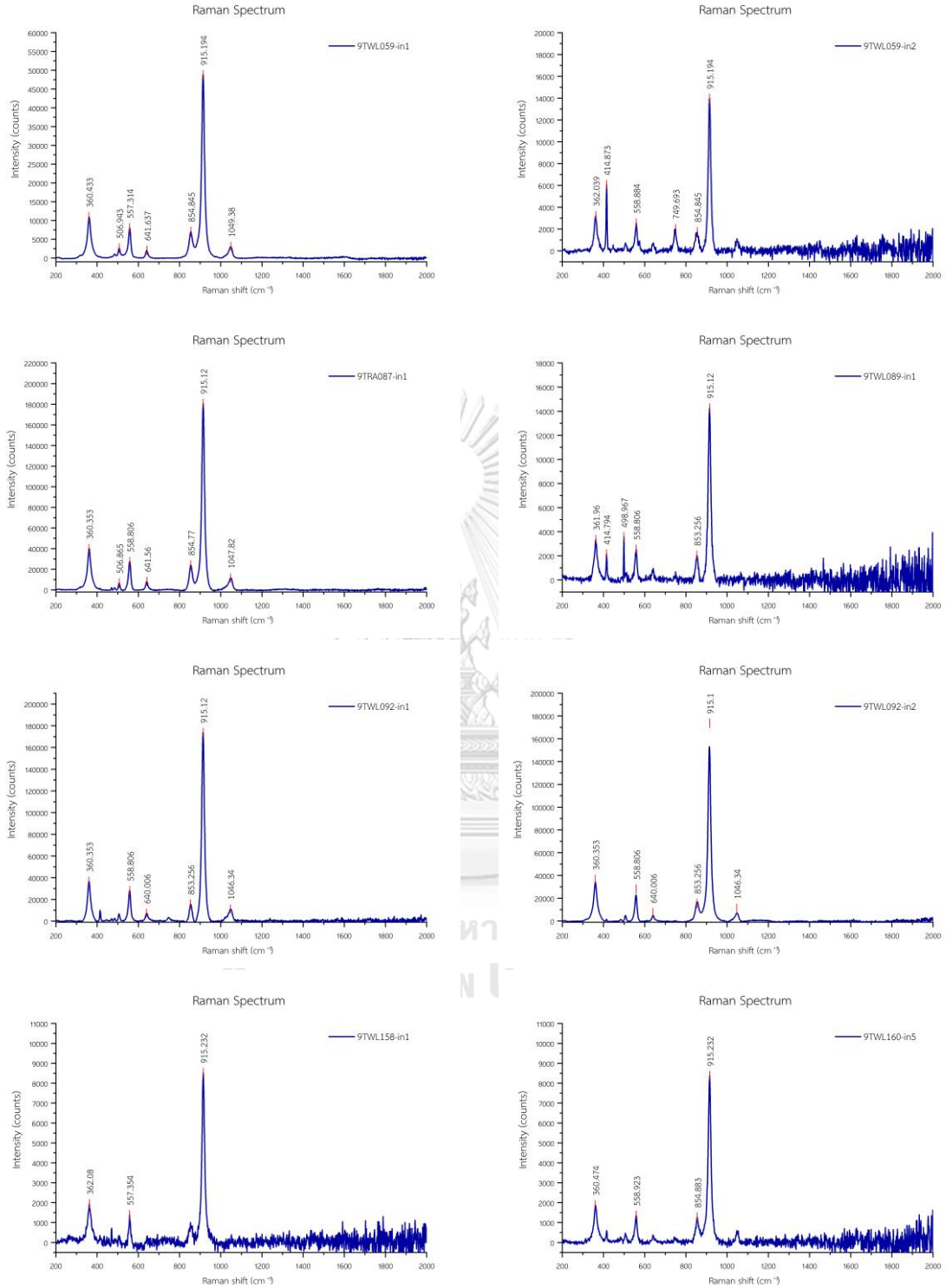

Figure E-21 Representative Raman spectra of garnet inclusions in Bo Welu ruby

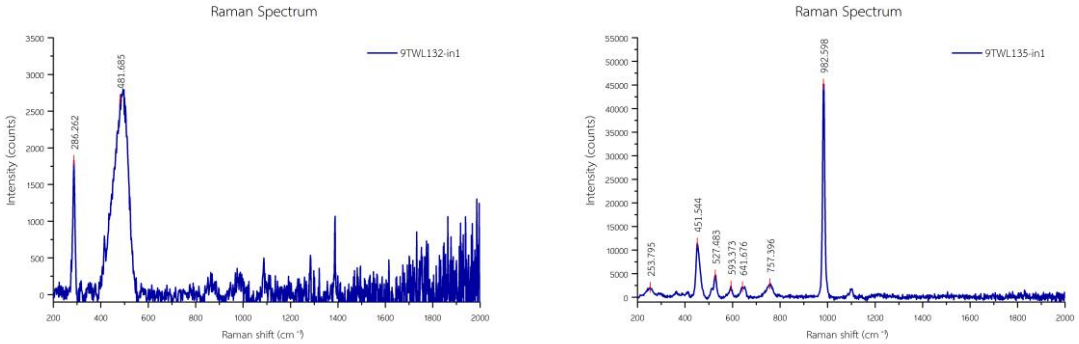

Figure E-22 Representative Raman spectra of silicate melt inclusions in Bo Welu ruby

Representative Raman spectra of mineral inclusions in Bo Welu sapphire

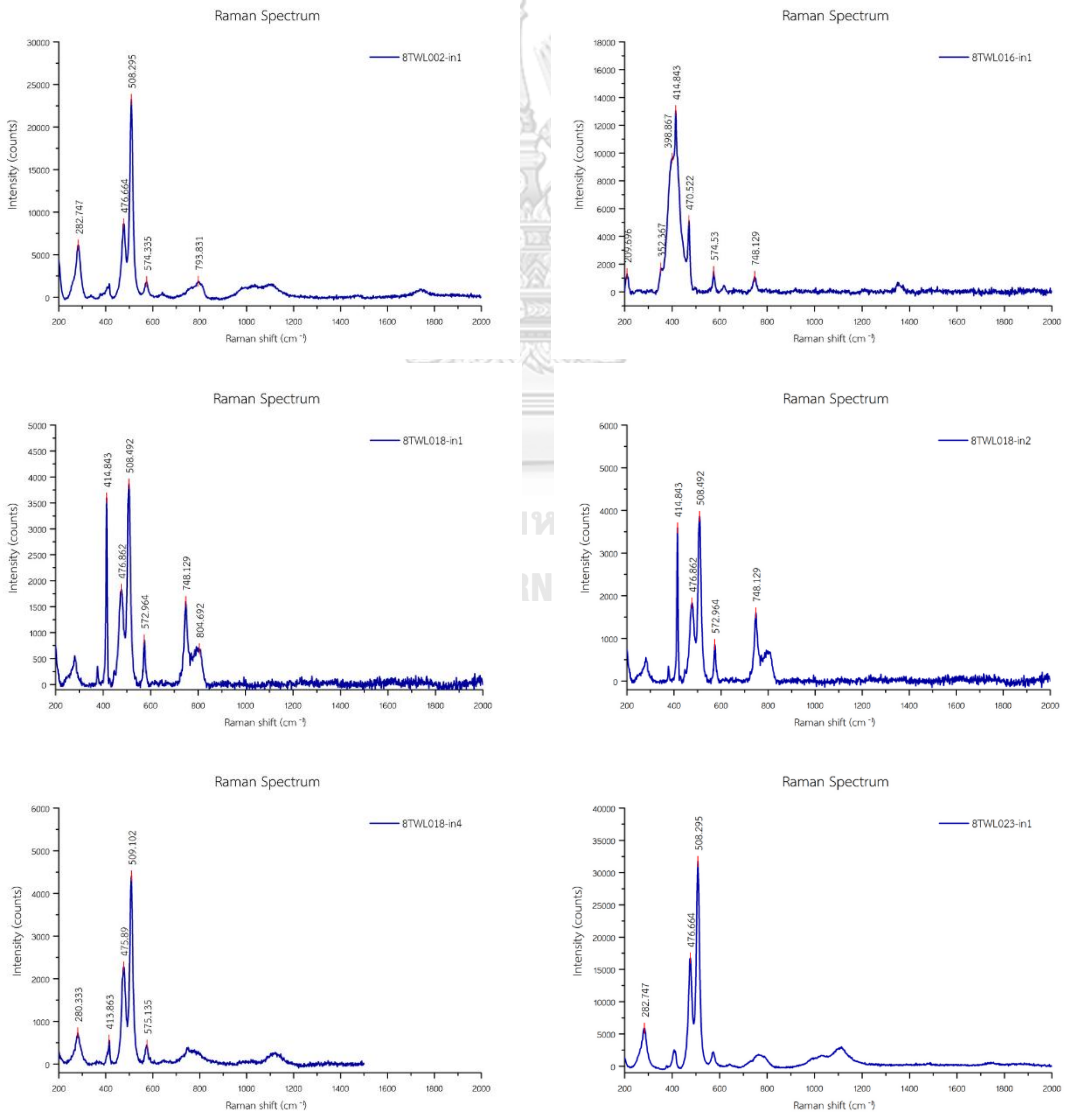

Figure E-23 Representative Raman spectra of feldspar inclusions in Bo Welu sapphire

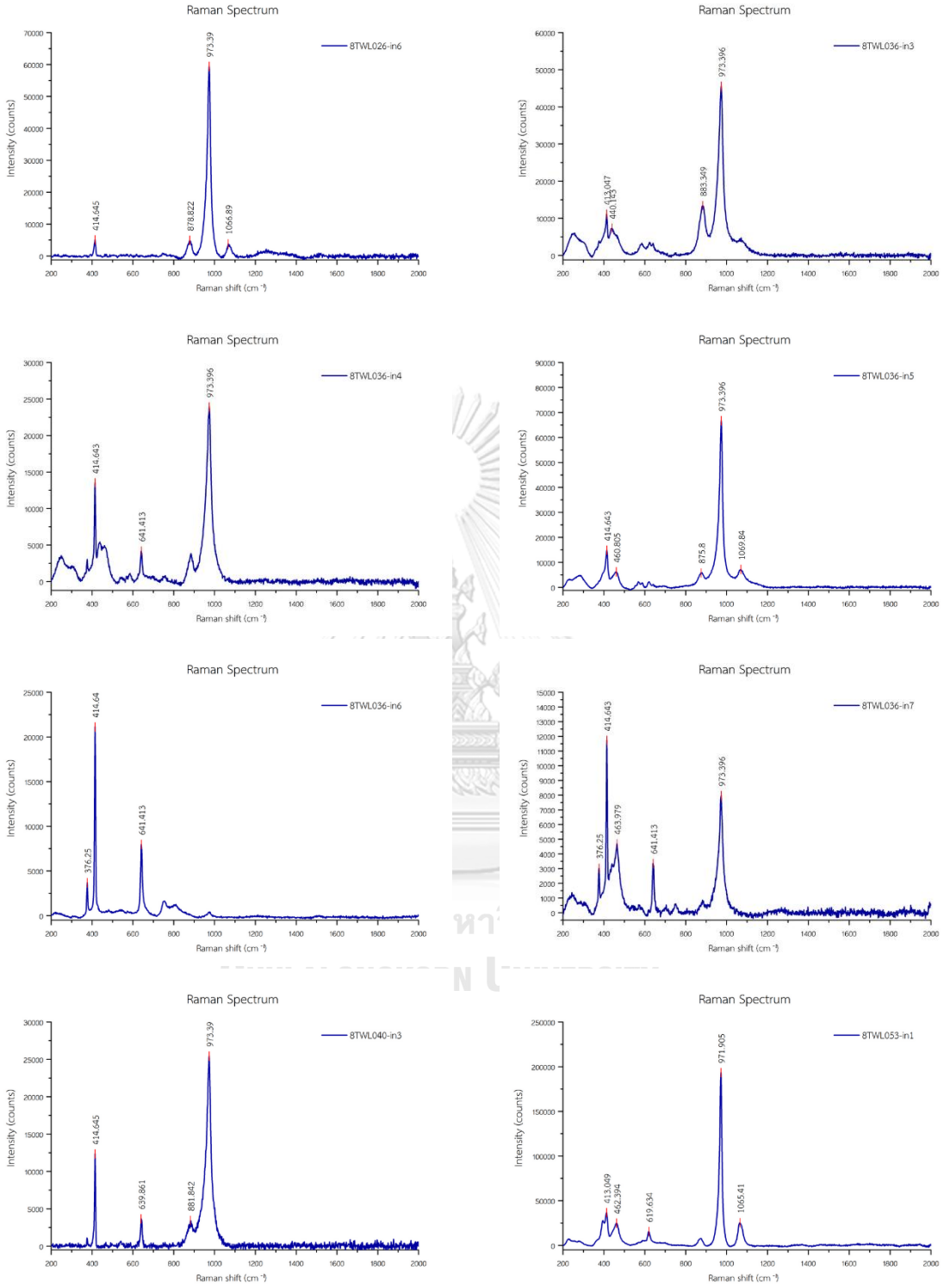

Figure E-24 Representative Raman spectra of monazite inclusions in Bo Welu sapphire

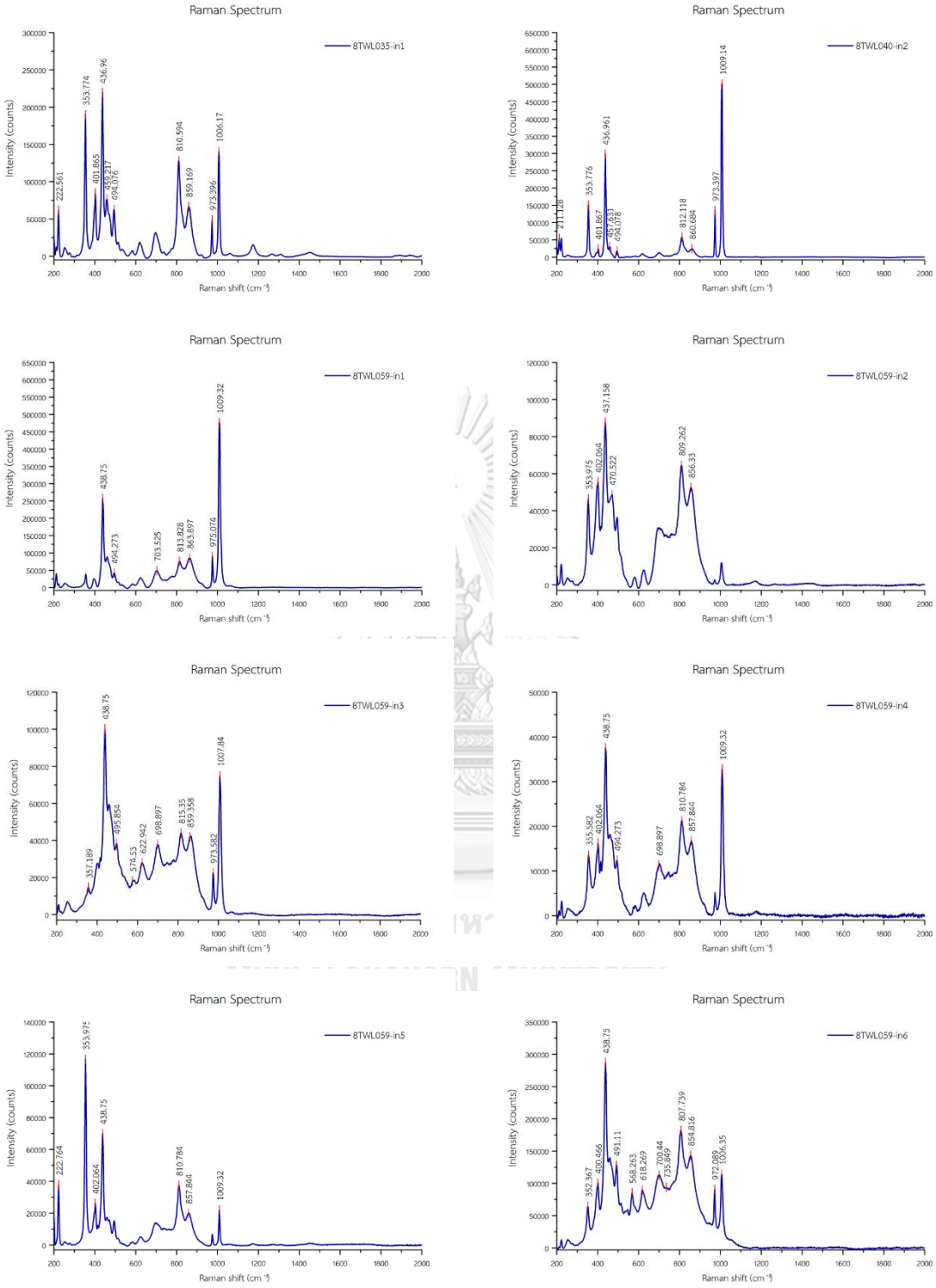

Figure E-25 Representative Raman spectra of zircon inclusions in Bo Welu sapphire

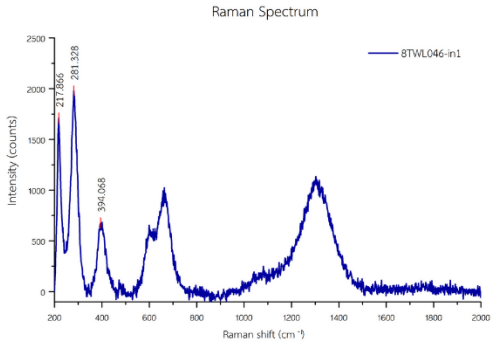

Figure E-26 Raman spectrum of Sulphide inclusion in Bo Welu sapphire sample 8TWL046

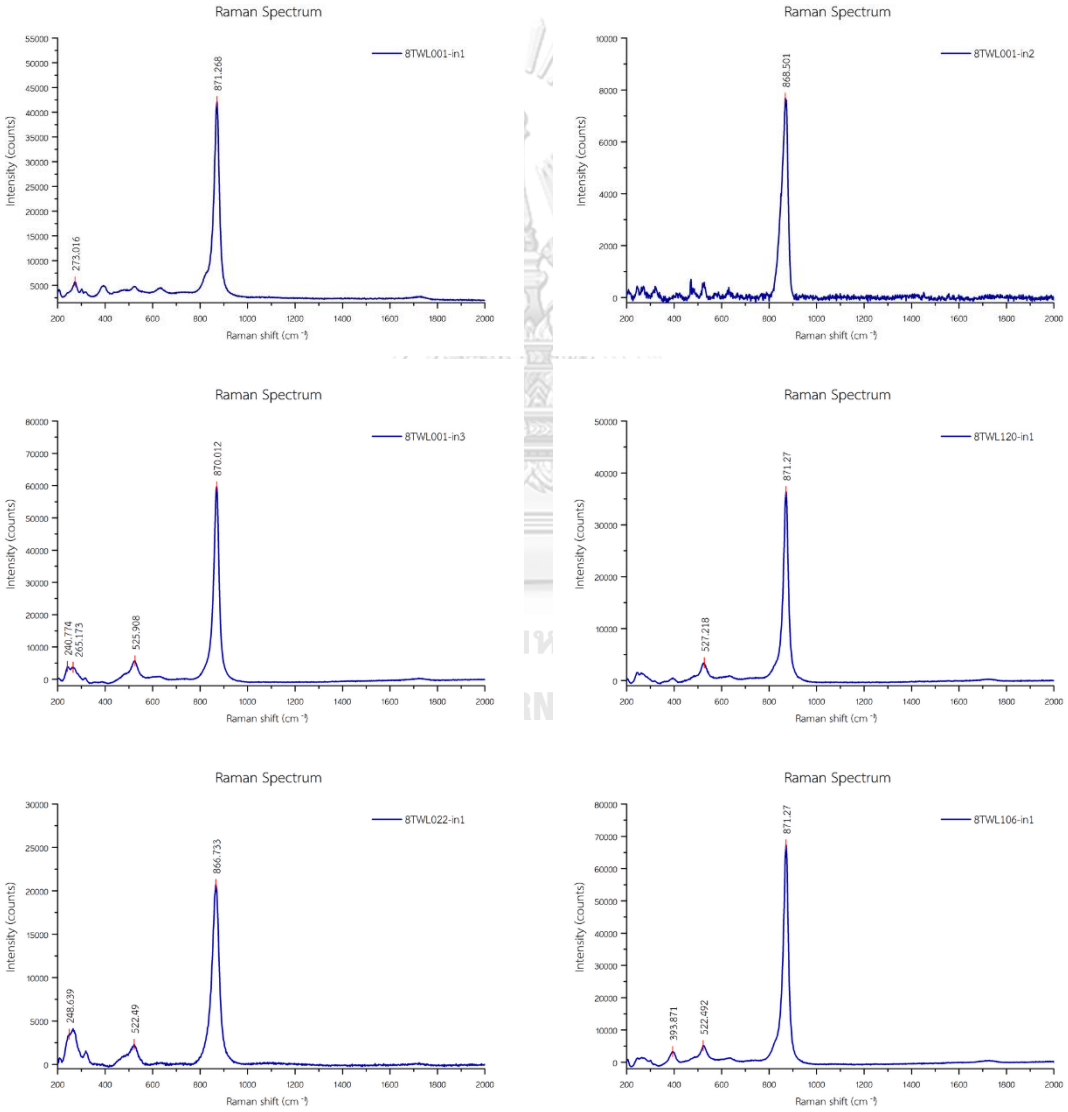

Figure E-27 Representative Raman spectra of columbite inclusions in Bo Welu sapphire

Appendix F - EDXRF analysis of corundum

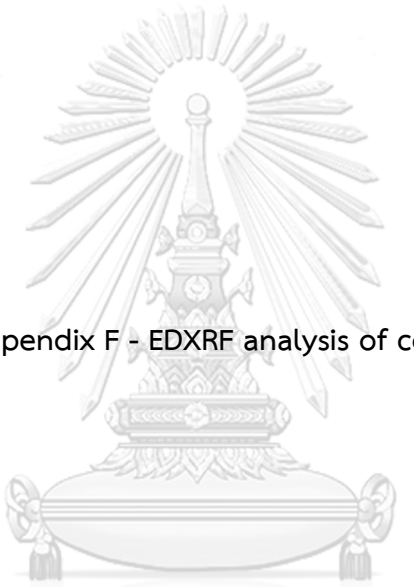

Table F-1 Representative semi-quantitative EDXRF analyses Bo Rai ruby

Element Oxides (wt.%)	9TRA016	9TRA017	9TRA023	9TRA028	9TRA029	9TRA031	9TRA033	9TRA039	9TRA044	9TRA045
V_2O_5	ND	0.0299	ND	ND	0.0031	ND	0.0049	0.0145	0.0419	ND
TiO_2	0.0575	0.1000	0.0360	0.0465	0.0222	0.1481	0.0259	0.0655	0.3302	0.1706
Al_2O_3	98.7021	98.5994	99.1005	98.5191	99.4416	98.0151	99.3779	98.5833	98.5023	98.4909
Cr_2O_3	0.5610	0.4010	0.2878	0.4004	0.0600	0.7002	0.1192	0.4203	0.1897	0.4755
Ga_2O_3	0.0181	0.0072	0.0110	0.0196	0.0091	0.0307	0.0084	0.0063	0.0058	0.0203
Fe_2O_3	0.6612	0.8626	0.5647	1.0144	0.4639	1.1059	0.4636	0.9102	0.9301	0.8426
Total	99.9999	100.0001	100.0000	100.0000	99.9999	100.0000	99.9999	100.0001	100.0000	99.9999
Fe_2O_3/TiO_2	11.50	8.63	15.69	21.82	20.90	7.47	17.90	13.90	2.82	4.94
Cr_2O_3/Ga_2O_3	30.99	55.69	26.16	20.43	6.59	22.81	14.19	66.71	32.71	23.42
TiO_2/Ga_2O_3	3.18	13.89	3.27	2.37	2.44	4.82	3.08	10.40	56.93	8.40
Fe_2O_3/Cr_2O_3	1.18	2.15	1.96	2.53	7.73	1.58	3.89	2.17	4.90	1.77

ND = not detected

Table F-1 Representative semi-quantitative EDXRF analyses Bo Rai ruby (continued)

Element Oxides (wt.%)	9TRA048	9TRA051	9TRA052	9TRA053	9TRA055	9TRA057	9TRA060	9TRA061	9TRA073	9TRA075
V_2O_5	0.0206	0.0230	0.0365	0.0229	ND	0.0110	ND	0.0241	0.0110	0.0121
TiO_2	0.0928	0.1319	0.0687	0.2611	0.0528	0.0209	0.0419	0.0862	0.0383	0.4417
Al_2O_3	98.8770	98.2628	98.6473	98.7348	98.4832	99.0886	98.7924	98.7215	98.9913	98.1592
Cr_2O_3	0.2791	0.3531	0.3402	0.1386	0.4799	0.2881	0.3644	0.5851	0.3419	0.5010
Ga_2O_3	0.0091	0.0125	0.0121	0.0252	ND	0.0053	0.0029	0.0043	0.0107	ND
Fe_2O_3	0.7214	1.2167	0.8952	0.8174	0.9841	0.5862	0.7984	0.5790	0.6067	0.8860
Total	100.0000	100.0000	100.0000	100.0000	100.0000	100.0001	100.0000	100.0002	99.9999	100.0000
Fe_2O_3/TiO_2	7.77	9.22	13.03	3.13	18.64	28.05	19.05	6.72	15.84	2.01
Cr_2O_3/Ga_2O_3	30.67	28.25	28.12	5.50	-	54.36	125.66	136.07	31.95	-
TiO_2/Ga_2O_3	10.20	10.55	5.68	10.36	-	3.94	14.45	20.05	3.58	-
Fe_2O_3/Cr_2O_3	2.58	3.45	2.63	5.90	2.05	2.03	2.19	0.99	1.77	1.77

ND = not detected

Table F-1 Representative semi-quantitative EDXRF analyses Bo Rai ruby (continued)

Element Oxides (wt.%)	9TRA078	9TRA081	9TRA084	9TRA086	9TRA088	9TRA090	9TRA095	9TRA098	9TRA102	9TRA105
V_2O_5	ND	0.0053	0.0142	0.0377	0.0266	0.0380	ND	0.0246	ND	0.0379
TiO_2	0.6732	0.0429	0.0436	0.0669	0.0349	0.0425	0.0223	0.0683	0.6005	0.0788
Al_2O_3	97.8279	98.7919	98.5734	97.9199	98.5819	98.4708	99.1743	98.8304	98.0741	97.7017
Cr_2O_3	0.4535	0.3524	0.3695	0.7325	0.4394	0.4919	0.2400	0.3472	0.7031	0.9167
Ga_2O_3	ND	0.0032	0.0187	0.0090	0.0083	0.0123	0.0062	0.0044	0.0099	0.0155
Fe_2O_3	1.0454	0.8043	0.9805	1.2341	0.9089	0.9445	0.5573	0.7251	0.6124	1.2494
Total	100.0000	100.0000	99.9999	100.0001	100.0000	100.0000	100.0001	100.0000	100.0000	100.0000
Fe_2O_3/TiO_2	1.55	18.75	22.49	18.45	26.04	22.22	24.99	10.62	1.02	15.86
Cr_2O_3/Ga_2O_3	-	110.13	19.76	81.39	52.94	39.99	38.71	78.91	71.02	59.14
TiO_2/Ga_2O_3	-	13.41	2.33	7.43	4.20	3.46	3.60	15.52	60.66	5.08
Fe_2O_3/Cr_2O_3	2.31	2.28	2.65	1.68	2.07	1.92	2.32	2.09	0.87	1.36

b ND = not detected

Table F-1 Representative semi-quantitative EDXRF analyses Bo Rai ruby (continued)

Element Oxides (wt.%)	9TRA137	9TRA154	9TRA155	9TRA156	9TRA158	9TRA160	9TRA161	9TRA169	9TRA171	9TRA176
V_2O_5	0.0357	ND	0.0117	0.0101	0.0147	0.0191	0.0204	0.0038	0.0043	0.0076
TiO_2	0.0679	0.2091	0.0764	0.0775	0.0466	0.1535	0.0861	0.0344	0.0282	0.0368
Al_2O_3	98.5421	98.4135	98.8279	98.9454	98.9437	98.1564	99.0973	99.0007	98.9220	99.0563
Cr_2O_3	0.3087	0.5875	0.1191	0.1823	0.3518	0.3918	0.1875	0.1628	0.2291	0.1831
Ga_2O_3	0.0164	0.0087	0.0142	0.0041	0.0179	0.0226	0.0073	0.0077	0.0075	0.0070
Fe_2O_3	1.0292	0.7813	0.9506	0.7805	0.6254	1.2566	0.6013	0.7906	0.8088	0.7092
Total	100.0000	100.0001	99.9999	99.9999	100.0001	100.0000	99.9999	100.0000	99.9999	100.0000
Fe_2O_3/TiO_2	15.16	3.74	12.44	10.07	13.42	8.19	6.98	22.98	28.68	19.27
Cr_2O_3/Ga_2O_3	18.82	67.53	8.39	44.46	19.65	17.34	25.68	21.14	30.55	26.16
TiO_2/Ga_2O_3	4.14	24.03	5.38	18.90	2.60	6.79	11.79	4.47	3.76	5.26
Fe_2O_3/Cr_2O_3	3.33	1.33	7.98	4.28	1.78	3.21	3.21	4.86	3.53	3.87

ND = not detected

Table F-1 Representative semi-quantitative EDXRF analyses Bo Rai ruby (continued)

Element Oxides (wt.%)	9TRA192	9TRA193	9TRA194	9TRA195	9TRA196	9TRA197	9TRA198	9TRA199	9TRA201	9TRA203
V_2O_5	0.0241	0.0111	0.0019	ND	0.0126	0.0080	0.0130	ND	0.0046	0.0167
TiO_2	0.0923	0.0611	0.0118	0.0258	0.0401	0.0200	0.0375	0.0831	0.0409	0.0398
Al_2O_3	98.6841	99.0049	99.1006	99.2097	99.0335	99.4955	98.8380	99.1560	98.9796	98.7801
Cr_2O_3	0.5233	0.1578	0.3923	0.1621	0.4247	0.1182	0.5203	0.1733	0.3141	0.4345
Ga_2O_3	ND	0.0136	0.0050	0.0088	0.0059	0.0055	0.0073	0.0107	0.0089	0.0094
Fe_2O_3	0.6762	0.7515	0.4884	0.5937	0.4832	0.3528	0.5839	0.5769	0.6518	0.7196
Total	100.0000	100.0000	100.0000	100.0001	100.0000	100.0000	100.0000	100.0000	99.9999	100.0001
Fe_2O_3/TiO_2	7.33	12.30	41.39	23.01	12.05	17.64	15.57	6.94	15.94	18.08
Cr_2O_3/Ga_2O_3	-	11.60	78.46	18.42	71.98	21.49	71.27	16.20	35.29	46.22
TiO_2/Ga_2O_3	-	4.49	2.36	2.93	6.80	3.64	5.14	7.77	4.60	4.23
Fe_2O_3/Cr_2O_3	1.29	4.76	1.24	3.66	1.14	2.98	1.12	3.33	2.08	1.66

ND = not detected

Table F-1 Representative semi-quantitative EDXRF analyses Bo Rai ruby (continued)

Element Oxides (wt.%)	9TRA204	9TRA206	9TRA207	9TRA208	9TRA209	9TRA210	9TRA211	9TRA212	9TRA213	9TRA214
V_2O_5	0.0168	0.0102	0.0046	0.0064	0.0206	0.0079	0.0210	0.0097	0.0242	0.0234
TiO_2	0.0249	0.0932	0.0402	0.0421	0.0325	0.0506	0.0656	0.0592	0.0759	0.0837
Al_2O_3	98.7606	98.7763	99.0022	99.1260	98.4085	98.9013	98.9492	99.0897	98.8195	98.3835
Cr_2O_3	0.4272	0.3804	0.2522	0.2726	0.7948	0.3376	0.3574	0.2644	0.4563	0.6047
Ga_2O_3	0.0045	0.0053	0.0113	0.0052	0.0125	0.0112	0.0083	0.0068	0.0161	0.0086
Fe_2O_3	0.7661	0.7345	0.6896	0.5477	0.7311	0.6915	0.5986	0.5702	0.6081	0.8962
Total	100.0001	99.9999	100.0001	100.0000	100.0000	100.0001	100.0001	100.0000	100.0001	100.0001
Fe_2O_3/TiO_2	30.77	7.88	17.15	13.01	22.50	13.67	9.13	9.63	8.01	10.71
Cr_2O_3/Ga_2O_3	94.93	71.77	22.32	52.42	63.58	30.14	43.06	38.88	28.34	70.31
TiO_2/Ga_2O_3	5.53	17.58	3.56	8.10	2.60	4.52	7.90	8.71	4.71	9.73
Fe_2O_3/Cr_2O_3	1.79	1.93	2.73	2.01	0.92	2.05	1.67	2.16	1.33	1.48

Table F-1 Representative semi-quantitative EDXRF analyses Bo Rai ruby (continued)

Element Oxides (wt.%)	9TRA215	9TRA217	9TRA218	9TRA219	9TRA223	9TRA228	9TRA231	9TRA232
V_2O_5	0.0065	ND	0.0218	0.0079	0.0139	0.0055	0.0016	0.0034
TiO_2	0.0327	0.0474	0.0582	0.0407	0.0490	0.0225	0.0153	0.0304
Al_2O_3	99.1941	98.9063	98.9059	99.0708	98.3699	99.2882	99.4737	99.2312
Cr_2O_3	0.1528	0.2644	0.3977	0.2392	0.3965	0.0782	0.0871	0.1015
Ga_2O_3	0.0080	0.0082	0.0075	0.0027	0.0118	0.0055	0.0034	0.0034
Fe_2O_3	0.6059	0.7737	0.6088	0.6388	1.1588	0.6001	0.4189	0.6301
Total	100.0000	100.0000	99.9999	100.0001	99.9999	100.0000	100.0000	100.0000
Fe_2O_3/TiO_2	18.53	16.32	10.46	15.70	23.65	26.67	27.38	20.73
Cr_2O_3/Ga_2O_3	19.10	32.24	53.03	88.59	33.60	14.22	25.62	29.85
TiO_2/Ga_2O_3	4.09	5.78	7.76	15.07	4.15	4.09	4.50	8.94
Fe_2O_3/Cr_2O_3	3.97	2.93	1.53	2.67	2.92	7.67	4.81	6.21

ND = not detected

Table F-2 Representative semi-quantitative EDXRF analyses Bo Welu ruby

Element Oxides (wt.%)	9TWL011	9TWL006	9TWL009	9TWL020	9TWL021	9TWL010	9TWL035	9TWL039	9TWL023	9TWL049
V_2O_5	0.0080	0.0070	0.0064	0.0018	0.0117	0.0018	0.0114	0.0050	0.0071	0.0038
TiO_2	0.0463	0.0435	0.0196	0.0282	0.0147	0.0330	0.0687	0.0623	0.0221	0.0381
Al_2O_3	98.1655	99.2787	99.3160	99.1931	99.0320	99.1188	99.1113	99.1210	99.4525	99.2964
Cr_2O_3	0.9389	0.2672	0.2463	0.2795	0.3250	0.2791	0.2620	0.2353	0.1492	0.1871
Ga_2O_3	0.0112	0.0085	0.0043	0.0056	0.0092	0.0066	0.0102	0.0111	0.0098	0.0084
Fe_2O_3	0.8301	0.3952	0.4075	0.4918	0.6074	0.5606	0.5364	0.5652	0.3593	0.4662
Total	100.0000	100.0001	100.0001	100.0000	100.0000	99.9999	100.0000	99.9999	100.0000	100.0000
Fe_2O_3/TiO_2	17.93	9.09	20.79	17.44	41.32	16.99	7.81	9.07	16.26	12.24
Cr_2O_3/Ga_2O_3	83.83	31.44	57.28	49.91	35.33	42.29	25.69	21.20	15.22	22.27
TiO_2/Ga_2O_3	4.13	5.12	4.56	5.04	1.60	5.00	6.74	5.61	2.26	4.54
Fe_2O_3/Cr_2O_3	0.88	1.48	1.65	1.76	1.87	2.01	2.05	2.40	2.41	2.49

Table F-2 Representative semi-quantitative EDXRF analyses Bo Welu ruby (continued).

Element Oxides (wt.%)	9TWL046	9TWL013	9TWL007	9TWL012	9TWL067	9TWL019	9TWL026	9TWL045	9TWL053	9TWL081
V_2O_5	0.0090	0.0088	0.0056	0.0105	0.0074	ND	0.0041	0.0091	0.0022	0.0117
TiO_2	0.0342	0.0564	0.0716	0.0469	0.0402	0.0251	0.0359	0.0418	0.0256	0.0459
Al_2O_3	99.3448	98.9346	99.0744	99.1316	99.2736	99.2458	99.2014	99.1858	99.3198	99.1504
Cr_2O_3	0.1699	0.2749	0.2300	0.2041	0.1458	0.1552	0.1505	0.1402	0.1156	0.1389
Ga_2O_3	0.0086	0.0061	0.0105	0.0108	0.0054	0.0073	0.0066	0.0078	0.0037	0.0065
Fe_2O_3	0.4335	0.7193	0.6080	0.5961	0.5275	0.5667	0.6016	0.6154	0.5331	0.6465
Total	100.0000	100.0001	100.0001	100.0000	99.9999	100.0001	100.0001	100.0001	100.0000	99.9999
Fe_2O_3/TiO_2	12.68	12.75	8.49	12.71	13.12	22.58	16.76	14.72	20.82	14.08
Cr_2O_3/Ga_2O_3	19.76	45.07	21.90	18.90	27.00	21.26	22.80	17.97	31.24	21.37
TiO_2/Ga_2O_3	3.98	9.25	6.82	4.34	7.44	3.44	5.44	5.36	6.92	7.06
Fe_2O_3/Cr_2O_3	2.55	2.62	2.64	2.92	3.62	3.65	4.00	4.39	4.61	4.65

ND = not detected

Table F-2 Representative semi-quantitative EDXRF analyses Bo Welu ruby (continued).

Element Oxides (wt.%)	9TWL055	9TWL054	9TWL051	9TWL059	9TWL029	9TWL077	9TWL073	9TWL092
V_2O_5	0.0060	0.0027	0.0064	0.0049	0.0066	0.0051	0.0037	0.0366
TiO_2	0.0304	0.0385	0.0371	0.0385	0.1211	0.0497	0.0514	0.0699
Al_2O_3	99.2628	99.2114	99.0788	99.2400	98.8173	99.2404	99.3978	98.5241
Cr_2O_3	0.1180	0.1248	0.1288	0.1032	0.1461	0.0950	0.0610	0.518
Ga_2O_3	0.0116	0.0090	0.0080	0.0054	0.0155	0.0087	0.0049	0.0369
Fe_2O_3	0.5712	0.6136	0.7409	0.6081	0.8935	0.6011	0.4812	0.8144
Total	100.0000	100.0000	100.0000	100.0001	100.0001	100.0000	100.0000	99.9999
Fe_2O_3/TiO_2	18.79	15.94	19.97	15.79	7.38	12.09	9.36	11.65
Cr_2O_3/Ga_2O_3	10.17	13.87	16.10	19.11	9.43	10.92	12.45	14.04
TiO_2/Ga_2O_3	2.62	4.28	4.64	7.13	7.81	5.71	10.49	1.89
Fe_2O_3/Cr_2O_3	4.84	4.92	5.75	5.89	6.12	6.33	7.89	1.57

Table F-3 Representative semi-quantitative EDXRF analyses Bo Welu sapphire

Element Oxides (wt.%)	8TWL001	8TWL002	8TWL016	8TWL018	8TWL022	8TWL023	8TWL026	8TWL028	8TWL031	8TWL036
V_2O_5	0.0027	0.0026	0.0059	ND	0.0021	0.0053	0.0031	0.0091	0.0031	0.0025
TiO_2	0.0296	0.0106	0.0285	0.0159	0.0271	0.0268	0.0324	0.0231	0.0344	0.0215
Al_2O_3	98.9498	99.0226	99.3806	98.9225	98.8462	98.9493	98.9550	98.8947	98.7154	98.7711
Cr_2O_3	0.0087	0.0049	0.0077	0.0030	0.0058	0.0055	0.0041	0.0115	0.0040	0.0042
Ga_2O_3	0.0317	0.0226	0.0195	0.0316	0.0288	0.0265	0.0339	0.0297	0.0309	0.0241
Fe_2O_3	0.9775	0.9367	0.5578	1.0270	1.0900	0.9866	0.9714	1.0319	1.2122	1.1767
Total	100.0000	100.0000	100.0000	100.0000	100.0000	100.0000	99.9999	100.0000	100.0000	100.0001
Fe_2O_3/TiO_2	33.02	88.37	19.57	64.59	40.22	36.81	29.98	44.67	35.24	54.73
Cr_2O_3/Ga_2O_3	0.27	0.22	0.39	0.09	0.20	0.21	0.12	0.39	0.13	0.17
TiO_2/Ga_2O_3	0.93	0.47	1.46	0.50	0.94	1.01	0.96	0.78	1.11	0.89
Fe_2O_3/Cr_2O_3	112.36	191.16	72.44	342.33	187.93	179.38	236.93	89.73	303.05	280.17

ND = not detected

Table F-3 Representative semi-quantitative EDXRF analyses Bo Welu sapphire (continued).

Element Oxides (wt.%)	8TWL040	8TWL046	8TWL053	8TWL059	8TWL064	8TWL067	8TWL068	8TWL074	8TWL082
V_2O_5	0.0052	0.0040	ND	0.0058	0.0077	0.0040	0.0034	0.0136	ND
TiO_2	0.0164	0.0310	0.0208	0.0178	0.0232	0.0126	0.0050	0.0472	0.0144
Al_2O_3	99.2969	98.8401	98.7569	99.1308	98.5909	99.2093	99.2844	99.0377	98.9966
Cr_2O_3	0.0075	0.0038	0.0019	0.0063	0.0025	0.0046	0.0042	0.0104	0.0042
Ga_2O_3	0.0215	0.0304	0.0378	0.0354	0.0485	0.0258	0.0346	0.0141	0.0238
Fe_2O_3	0.6525	1.0906	1.1826	0.8039	1.3273	0.7438	0.6686	0.8769	0.9609
Total	100.0000	99.9999	100.0000	100.0000	100.0001	100.0001	100.0002	99.9999	99.9999
Fe_2O_3/TiO_2	39.79	35.18	56.86	45.16	57.21	59.03	133.72	18.58	66.73
Cr_2O_3/Ga_2O_3	0.35	0.13	0.05	0.18	0.05	0.18	0.12	0.74	0.18
TiO_2/Ga_2O_3	0.76	1.02	0.55	0.50	0.48	0.49	0.14	3.35	0.61
Fe_2O_3/Cr_2O_3	87.00	287.00	622.42	127.60	530.92	161.70	159.19	84.32	228.79

ND = not detected

Table F-3 Representative semi-quantitative EDXRF analyses Bo Welu sapphire (continued).

Element Oxides (wt.%)	8TWL083	8TWL093	8TWL096	8TWL097	8TWL099	8TWL100	8TWL101	8TWL102	8TWL103	8TWL104
V_2O_5	ND	0.0020	0.0103	ND	0.0031	0.0106	0.0136	0.0034	0.0072	0.0046
TiO_2	0.0244	0.0210	0.0186	0.0101	0.0241	0.0584	0.0250	0.0131	0.0354	0.0279
Al_2O_3	99.0621	99.0184	98.8804	99.0217	99.4917	98.9523	98.9314	98.9666	98.6803	99.4723
Cr_2O_3	0.0032	0.0051	0.0071	0.0024	0.0042	0.0084	0.0077	0.0019	ND	0.0069
Ga_2O_3	0.0263	0.0333	0.0376	0.0289	0.0185	0.0438	0.0370	0.0296	0.0506	0.0394
Fe_2O_3	0.8841	0.9202	1.0460	0.9369	0.4584	0.9264	0.9852	0.9855	1.2266	0.4489
Total	100.0001	100.0000	100.0000	100.0000	100.0000	99.9999	99.9999	100.0001	100.0001	100.0000
Fe_2O_3/TiO_2	36.23	43.82	56.24	92.76	19.02	15.86	39.41	75.23	34.65	16.09
Cr_2O_3/Ga_2O_3	0.12	0.15	0.19	0.08	0.23	0.19	0.21	0.06	-	0.18
TiO_2/Ga_2O_3	0.93	0.63	0.49	0.35	1.30	1.33	0.68	0.44	0.70	0.71
Fe_2O_3/Cr_2O_3	276.28	180.43	147.32	390.38	109.14	110.29	127.95	518.68	-	65.06

ND = not detected

Table F-3 Representative semi-quantitative EDXRF analyses Bo Welu sapphire (continued).

Element Oxides (wt.%)	8TWL105	8TWL106	8TWL108	8TWL111	8TWL112	8TWL113	8TWL114	8TWL116	8TWL117	8TWL119	8TWL120
V_2O_5	0.0047	0.0106	0.0044	0.0024	0.0046	ND	0.0046	ND	0.0017	0.0027	ND
TiO_2	0.0192	0.0916	0.0109	0.0190	0.0148	0.0165	0.0488	0.0053	0.0107	0.0219	0.0175
Al_2O_3	98.8486	98.6721	99.1121	98.9593	99.3015	98.5656	99.3335	98.8105	99.1741	99.3502	99.0889
Cr_2O_3	0.0058	ND	0.0018	0.0028	0.0021	0.0044	0.0083	0.0090	0.0018	0.0075	0.0035
Ga_2O_3	0.0262	0.0359	0.0538	0.0352	0.0297	0.0300	0.0345	0.0272	0.0238	0.0271	0.0374
Fe_2O_3	1.0955	1.1898	0.8171	0.9813	0.6473	1.3835	0.5703	1.1480	0.7879	0.5908	0.8526
Total	100.0000	100.0000	100.0001	100.0000	100.0000	100.0000	100.0000	100.0000	100.0000	100.0002	99.9999
Fe_2O_3/TiO_2	57.06	12.99	74.96	51.65	43.74	83.85	11.69	216.60	73.64	26.98	48.72
Cr_2O_3/Ga_2O_3	0.22	0.00	0.03	0.08	0.07	0.15	0.24	0.33	0.08	0.28	0.09
TiO_2/Ga_2O_3	0.73	2.55	0.20	0.54	0.50	0.55	1.41	0.19	0.45	0.81	0.47
Fe_2O_3/Cr_2O_3	188.88	-	453.94	350.46	308.24	314.43	68.71	127.56	437.72	78.77	243.60

ND = not detected

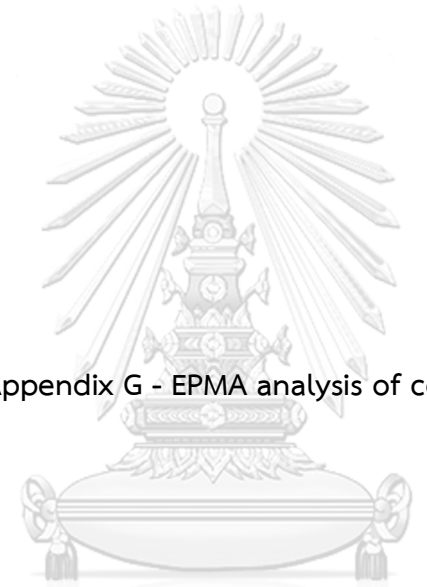

Appendix G - EPMA analysis of corundum

Table G-1 Representative EPMA analyses of Bo Rai ruby

Element Oxides (wt.%)	9TRA016-1	9TRA016-2	9TRA017-1	9TRA017-2	9TRA017-3	9TRA023-1	9TRA023-2	9TRA024-1	9TRA024-2	9TRA024-3	9TRA029-1	9TRA029-2
SiO_2	0.094	0.003	0.028	0.034	0.040	0.046	0.088	0.045	0.087	0.071	0.021	0.003
TiO_2	0.018	0.019	0.048	0.056	0.060	ND	0.009	ND	0.023	0.039	ND	ND
Al_2O_3	98.920	98.920	99.001	98.826	98.853	99.486	98.008	98.435	98.619	98.856	98.158	98.090
Cr_2O_3	0.083	0.238	0.237	0.310	0.296	0.146	0.204	0.482	0.361	0.313	0.153	0.086
Ga_2O_3	0.014	0.013	ND	0.015	0.042	0.034	ND	0.072	0.012	0.022	ND	ND
V_2O_3	0.003	0.003	ND	ND	0.009	0.009	0.002	ND	0.009	0.003	0.012	0.002
FeO total	0.392	0.362	0.636	0.686	0.622	0.328	0.374	0.404	0.444	0.381	0.434	0.466
MnO	ND	0.041	ND	0.025	ND	ND	ND	0.023	0.014	ND	ND	ND
MgO	0.020	0.024	0.012	0.011	0.014	0.030	0.024	0.055	0.051	0.023	0.010	0.001
Total	99.544	99.623	99.962	99.963	99.936	100.079	98.709	99.516	99.620	99.708	98.788	98.648
Fe_2O_3/TiO_2	21.78	19.05	13.25	12.25	10.37	-	41.56	-	19.30	9.77	-	-
Cr_2O_3/Ga_2O_3	5.93	18.31	-	20.67	7.05	4.29	-	6.69	30.08	14.23	-	-
TiO_2/Ga_2O_3	1.29	1.46	-	3.73	1.43	-	-	-	1.92	1.77	-	-
Fe_2O_3/Cr_2O_3	4.72	1.52	2.68	2.21	2.10	2.25	1.83	0.84	1.23	1.22	2.84	5.42
Ga_2O_3/MgO	0.70	0.54	-	1.36	3.00	1.13	-	1.31	0.24	0.96	-	-
Fe_2O_3/Ga_2O_3	19.60	15.08	53.00	62.36	44.43	10.93	15.58	7.35	8.71	16.57	43.40	466.00
3 (O)												
Si	0.002	0.000	0.001	0.001	0.001	0.001	0.002	0.001	0.002	0.001	0.000	0.000
Ti	0.000	0.000	0.001	0.001	0.001	0.000	0.000	0.000	0.000	0.001	0.000	0.000
Al	1.992	1.992	1.989	1.987	1.987	1.993	1.991	1.987	1.987	1.989	1.993	1.994
Cr	0.001	0.003	0.003	0.004	0.004	0.002	0.003	0.006	0.005	0.004	0.002	0.001
Ga	0.000	0.000	0.000	0.000	0.000	0.000	0.000	0.001	0.000	0.000	0.000	0.000
V	0.000	0.000	0.000	0.000	0.000	0.000	0.000	0.000	0.000	0.000	0.000	0.000
Fe^{3+}	0.004	0.005	0.008	0.009	0.008	0.005	0.004	0.006	0.006	0.004	0.006	0.007
Fe^{2+}	0.001	0.000	0.001	0.001	0.001	0.000	0.001	0.000	0.000	0.001	0.000	0.000
Mn	0.000	0.001	0.000	0.000	0.000	0.000	0.000	0.000	0.000	0.000	0.000	0.000
Mg	0.001	0.001	0.000	0.000	0.000	0.001	0.001	0.002	0.001	0.001	0.000	0.000
Total*	2.001	2.002	2.003	2.003	2.003	2.002	2.001	2.002	2.002	2.001	2.002	2.002

ND = not detected

Table G-1 Representative EPMA analyses of Bo Rai ruby (continued)

Element Oxides (wt.%)	9TRA036-1	9TRA036-2	9TRA038-1	9TRA038-2	9TRA039-1	9TRA039-2	9TRA045-1	9TRA045-2	9TRA048-1	9TRA048-2	9TRA049-1
SiO_2	0.051	0.051	0.063	0.074	0.031	0.040	0.017	0.074	0.065	0.026	0.013
TiO_2	ND	0.036	0.015	ND	0.032	0.010	0.015	0.005	ND	0.057	0.011
Al_2O_3	99.445	99.114	98.515	99.258	98.739	98.063	98.360	99.119	98.883	99.831	98.922
Cr_2O_3	0.083	0.096	0.125	0.150	0.224	0.265	0.266	0.212	0.187	0.175	0.527
Ga_2O_3	0.009	0.034	0.015	ND	0.006	0.023	0.016	ND	ND	ND	ND
V_2O_3	ND	0.007	0.004	0.017	ND	ND	ND	0.012	0.002	ND	0.007
FeO total	0.435	0.449	0.4 25	0.442	0.499	0.485	0.357	0.466	0.452	0.412	0.382
MnO	ND	0.037	ND	0.031	ND	ND	0.009	0.022	ND	ND	ND
MgO	0.013	0.014	0.000	0.021	0.028	0.011	0.020	0.020	0.016	0.035	0.010
Total	100.036	99.838	99.162	99.993	99.559	98.897	99.060	99.930	99.605	100.536	99.872
Fe_2O_3/TiO_2	-	12.47	28.33	-	15.59	48.50	23.80	93.20	-	7.23	34.73
Cr_2O_3/Ga_2O_3	9.22	2.82	8.33	-	37.33	11.52	16.63	-	-	-	-
TiO_2/Ga_2O_3	-	1.06	1.00	-	5.33	0.43	0.94	-	-	-	-
Fe_2O_3/Cr_2O_3	5.24	4.68	3.40	2.95	2.23	1.83	1.34	2.20	2.42	2.35	0.72
Ga_2O_3/MgO	0.69	2.43	-	-	0.21	2.09	0.80	-	-	-	-
Fe_2O_3/Ga_2O_3	33.46	32.07	-	21.05	17.82	44.09	17.85	23.30	28.25	11.77	38.20
3 (O)											
Si	0.001	0.001	0.001	0.001	0.001	0.001	0.000	0.000	0.001	0.001	0.000
Ti	0.000	0.001	0.000	0.000	0.000	0.000	0.000	0.000	0.000	0.001	0.000
Al	1.993	1.992	1.992	1.991	1.990	1.990	1.991	1.991	1.991	1.991	1.989
Cr	0.001	0.001	0.002	0.002	0.003	0.004	0.004	0.004	0.003	0.002	0.007
Ga	0.000	0.000	0.000	0.000	0.000	0.000	0.000	0.000	0.000	0.000	0.000
V	0.000	0.000	0.000	0.000	0.000	0.000	0.000	0.000	0.000	0.000	0.000
Fe^{3+}	0.006	0.006	0.005	0.006	0.007	0.006	0.005	0.005	0.006	0.006	0.005
Fe^{2+}	0.001	0.001	0.001	0.000	0.000	0.001	0.000	0.000	0.001	0.000	0.000
Mn	0.000	0.001	0.000	0.000	0.000	0.000	0.000	0.000	0.000	0.000	0.000
Mg	0.000	0.000	0.000	0.001	0.001	0.000	0.001	0.001	0.001	0.001	0.000
Total*	2.002	2.002	2.002	2.002	2.002	2.002	2.002	2.002	2.002	2.002	2.002

ND = not detected

Table G-1 Representative EPMA analyses of Bo Rai ruby (continued)

Element Oxides (wt.%)	9TRA051-1	9TRA051-2	9TRA052-2	9TRA053-1	9TRA053-2	9TRA057-1	9TRA057-2	9TRA061-2	9TRA073-1	9TRA073-2	9TRA073-3
SiO_2	0.065	0.034	0.048	0.080	0.024	0.043	0.014	0.055	0.096	0.093	0.047
TiO_2	0.044	0.044	ND	ND	ND	0.008	0.055	0.006	0.052	0.021	0.036
Al_2O_3	98.762	98.010	98.110	98.320	98.752	98.323	98.531	99.280	98.901	98.879	99.030
Cr_2O_3	0.229	0.199	0.237	0.346	0.314	0.228	0.224	0.281	0.194	0.245	0.210
Ga_2O_3	0.060	0.095	0.024	ND	0.005	ND	ND	0.005	ND	0.020	ND
V_2O_3	0.001	ND	ND	0.010	0.009	0.022	0.015	0.015	0.003	0.005	0.028
FeO total	0.582	0.628	0.652	0.383	0.307	0.469	0.553	0.427	0.486	0.454	0.447
MnO	0.019	0.028	0.012	ND	0.024	ND	0.037	0.050	ND	ND	ND
MgO	0.018	0.006	ND	0.022	0.010	0.022	0.005	0.028	0.013	0.027	0.034
Total	99.780	99.044	99.083	99.161	99.445	99.115	99.434	100.147	99.745	99.744	99.832
Fe_2O_3/TiO_2	13.23	14.27	-	-	-	58.63	10.05	71.17	9.35	21.62	12.42
Cr_2O_3/Ga_2O_3	3.82	2.09	9.88	-	62.80	-	-	56.20	-	12.25	-
TiO_2/Ga_2O_3	0.73	0.46	-	-	-	-	-	1.20	-	1.05	-
Fe_2O_3/Cr_2O_3	2.54	3.16	2.75	1.11	0.98	2.06	2.47	1.52	2.51	1.85	2.13
Ga_2O_3/MgO	3.33	15.83	-	-	0.50	-	-	0.18	-	0.74	-
Fe_2O_3/Ga_2O_3	32.33	104.67	-	17.41	30.70	21.32	110.60	15.25	37.38	16.81	13.15
3 (O)											
Si	0.001	0.001	0.000	0.001	0.001	0.000	0.001	0.000	0.001	0.002	0.001
Ti	0.001	0.001	0.000	0.000	0.000	0.000	0.000	0.001	0.000	0.001	0.001
Al	1.988	1.988	1.989	1.989	1.989	1.992	1.991	1.990	1.989	1.989	1.990
Cr	0.003	0.003	0.004	0.003	0.005	0.004	0.003	0.003	0.004	0.003	0.003
Ga	0.001	0.001	0.000	0.000	0.000	0.000	0.000	0.000	0.000	0.000	0.000
V	0.000	0.000	0.000	0.000	0.000	0.000	0.000	0.000	0.000	0.000	0.000
Fe^{3+}	0.007	0.009	0.010	0.009	0.005	0.004	0.006	0.008	0.006	0.005	0.006
Fe^{2+}	0.001	0.000	0.000	0.001	0.001	0.000	0.000	0.000	0.000	0.002	0.001
Mn	0.000	0.000	0.000	0.000	0.000	0.000	0.000	0.001	0.001	0.000	0.000
Mg	0.001	0.000	0.001	0.000	0.001	0.000	0.001	0.000	0.001	0.000	0.001
Total*	2.002	2.003	2.003	2.003	2.002	2.002	2.002	2.003	2.002	2.002	2.002

ND = not detected

Table G-1 Representative EPMA analyses of Bo Rai ruby (continued)

Element Oxides (wt.%)	9TRA051-1	9TRA051-2	9TRA052-2	9TRA053-1	9TRA053-2	9TRA057-1	9TRA057-2	9TRA061-2	9TRA073-1	9TRA073-2	9TRA073-3
SiO_2	0.065	0.034	0.048	0.080	0.024	0.043	0.014	0.055	0.096	0.093	0.047
TiO_2	0.044	0.044	ND	ND	ND	0.008	0.055	0.006	0.052	0.021	0.036
Al_2O_3	98.762	98.010	98.110	98.320	98.752	98.323	98.531	99.280	98.901	98.879	99.030
Cr_2O_3	0.229	0.199	0.237	0.346	0.314	0.228	0.224	0.281	0.194	0.245	0.210
Ga_2O_3	0.060	0.095	0.024	ND	0.005	ND	ND	0.005	ND	0.020	ND
V_2O_3	0.001	ND	ND	0.010	0.009	0.022	0.015	0.015	0.003	0.005	0.028
FeO total	0.582	0.628	0.652	0.383	0.307	0.469	0.553	0.427	0.486	0.454	0.447
MnO	0.019	0.028	0.012	ND	0.024	ND	0.037	0.050	ND	ND	ND
MgO	0.018	0.006	ND	0.022	0.010	0.022	0.005	0.028	0.013	0.027	0.034
Total	99.780	99.044	99.083	99.161	99.445	99.115	99.434	100.147	99.745	99.744	99.832
Fe_2O_3/TiO_2	13.23	14.27	-	-	-	58.63	10.05	71.17	9.35	21.62	12.42
Cr_2O_3/Ga_2O_3	3.82	2.09	9.88	-	62.80	-	-	56.20	-	12.25	-
TiO_2/Ga_2O_3	0.73	0.46	-	-	-	-	-	1.20	-	1.05	-
Fe_2O_3/Cr_2O_3	2.54	3.16	2.75	1.11	0.98	2.06	2.47	1.52	2.51	1.85	2.13
Ga_2O_3/MgO	3.33	15.83	-	-	0.50	-	-	0.18	-	0.74	-
Fe_2O_3/Ga_2O_3	32.33	104.67	-	17.41	30.70	21.32	110.60	15.25	37.38	16.81	13.15
3 (O)											
Si	0.001	0.001	0.000	0.001	0.001	0.000	0.001	0.000	0.001	0.002	0.001
Ti	0.001	0.001	0.000	0.000	0.000	0.000	0.000	0.001	0.000	0.001	0.001
Al	1.988	1.988	1.989	1.989	1.989	1.992	1.991	1.990	1.989	1.989	1.990
Cr	0.003	0.003	0.004	0.003	0.005	0.004	0.003	0.003	0.004	0.003	0.003
Ga	0.001	0.001	0.000	0.000	0.000	0.000	0.000	0.000	0.000	0.000	0.000
V	0.000	0.000	0.000	0.000	0.000	0.000	0.000	0.000	0.000	0.000	0.000
Fe^{3+}	0.007	0.009	0.010	0.009	0.005	0.004	0.006	0.008	0.006	0.005	0.006
Fe^{2+}	0.001	0.000	0.000	0.001	0.001	0.000	0.000	0.000	0.000	0.002	0.001
Mn	0.000	0.000	0.000	0.000	0.000	0.000	0.000	0.001	0.001	0.000	0.000
Mg	0.001	0.000	0.001	0.000	0.001	0.000	0.001	0.000	0.001	0.000	0.001
Total*	2.002	2.003	2.003	2.003	2.002	2.002	2.002	2.003	2.002	2.002	2.002

ND = not detected

Table G-1 Representative EPMA analyses of Bo Rai ruby (continued)

Element Oxides (wt.%)	9TRA081-1	9TRA086-1	9TRA086-2	9TRA090-1	9TRA090-2	9TRA108-1	9TRA108-2	9TRA113-1	9TRA113-2	9TRA118-1	9TRA124-1
SiO_2	0.065	0.062	ND	0.026	0.068	0.040	0.065	0.088	0.082	0.045	0.014
TiO_2	0.043	0.048	0.044	0.041	0.013	ND	0.039	ND	0.076	0.016	ND
Al_2O_3	99.328	98.736	98.602	98.238	98.199	98.639	98.248	98.552	98.960	98.317	99.075
Cr_2O_3	0.361	0.467	0.125	0.108	0.191	0.091	0.245	0.091	0.100	0.091	0.228
Ga_2O_3	0.032	ND	ND	ND	ND	ND	0.004	0.011	ND	ND	0.002
V_2O_3	ND	0.001	ND	ND	0.006	ND	ND	0.011	0.002	ND	ND
FeO total	0.559	0.590	0.215	0.589	0.569	0.323	0.452	0.505	0.532	0.430	0.519
MnO	0.025	0.003	ND	ND	ND	0.075	ND	0.034	0.006	ND	ND
MgO	0.029	0.015	0.010	0.012	0.009	0.044	0.034	0.006	0.006	0.016	0.014
Total	100.442	99.922	98.996	99.014	99.055	99.212	99.087	99.298	99.764	98.915	99.852
Fe_2O_3/TiO_2	13.00	12.29	4.89	14.37	43.77	-	11.59	-	7.00	26.88	-
Cr_2O_3/Ga_2O_3	11.28	-	-	-	-	-	61.25	8.27	-	-	114.00
TiO_2/Ga_2O_3	1.34	-	-	-	-	-	9.75	-	-	-	-
Fe_2O_3/Cr_2O_3	1.55	1.26	1.72	5.45	2.98	3.55	1.84	5.55	5.32	4.73	2.28
Ga_2O_3/MgO	1.10	-	-	-	-	-	0.12	1.83	-	-	0.14
Fe_2O_3/Ga_2O_3	19.28	39.33	21.50	49.08	63.22	7.34	13.29	84.17	88.67	26.88	37.07
3 (O)											
Si	0.001	0.001	0.000	0.001	0.001	0.001	0.001	0.002	0.001	0.001	0.000
Ti	0.001	0.001	0.001	0.001	0.000	0.000	0.001	0.000	0.001	0.000	0.000
Al	1.986	1.985	1.995	1.991	1.990	1.993	1.989	1.991	1.990	1.993	1.992
Cr	0.005	0.006	0.002	0.001	0.003	0.001	0.003	0.001	0.001	0.001	0.003
Ga	0.000	0.000	0.000	0.000	0.000	0.000	0.000	0.000	0.000	0.000	0.000
V	0.000	0.000	0.000	0.000	0.000	0.000	0.000	0.000	0.000	0.000	0.000
Fe^{3+}	0.007	0.007	0.003	0.008	0.007	0.005	0.006	0.006	0.006	0.006	0.007
Fe^{2+}	0.001	0.001	0.000	0.001	0.001	0.000	0.001	0.001	0.002	0.001	0.000
Mn	0.000	0.000	0.000	0.000	0.000	0.001	0.000	0.000	0.000	0.000	0.000
Mg	0.001	0.001	0.000	0.000	0.000	0.001	0.001	0.000	0.000	0.001	0.000
Total*	2.002	2.002	2.001	2.003	2.002	2.002	2.002	2.002	2.002	2.002	2.003

ND = not detected

Table G-2 Representative EPMA analyses of Bo Welu ruby

Element Oxides (wt.%)	9TWL011-2	9TWL019-1	9TWL029-1	9TWL029-2	9TWL046-1	9TWL095-1	9TWL095-2	9TWL099-1	9TWL100-1	9TWL100-2	9TWL105-1
SiO_2	0.028	0.100	ND	0.079	0.045	0.079	0.089	0.057	0.058	0.058	0.069
TiO_2	0.019	0.010	0.025	0.012	0.042	0.036	0.029	0.036	0.036	0.024	0.031
Al_2O_3	97.205	97.500	97.730	97.970	97.810	98.098	97.899	98.003	97.587	97.796	98.551
Cr_2O_3	1.084	0.230	0.180	0.171	0.228	0.167	0.202	0.231	0.286	0.295	0.076
Ga_2O_3	0.070	0.010	0.072	0.044	0.180	ND	0.047	ND	ND	0.058	0.013
V_2O_3	ND	0.010	0.024	0.008	0.012	0.003	0.008	0.003	ND	ND	0.002
FeO total	0.513	0.780	0.559	0.559	0.517	0.514	0.599	0.554	0.615	0.652	0.507
MnO	ND	ND	0.044	0.035	ND	0.036	ND	0.027	ND	ND	0.031
MgO	0.017	0.020	0.033	0.016	0.046	0.041	0.026	0.032	0.013	0.022	0.026
Total	98.936	98.660	98.667	98.894	98.880	98.974	98.899	98.943	98.595	98.905	99.306
Fe_2O_3/TiO_2	27.00	78.00	22.36	46.58	12.31	14.28	20.66	15.39	17.08	27.17	16.35
Cr_2O_3/Ga_2O_3	15.49	23.00	2.50	3.89	1.27	-	4.30	-	-	5.09	5.85
TiO_2/Ga_2O_3	0.27	1.00	0.35	0.27	0.23	-	0.62	-	-	0.41	2.38
Fe_2O_3/Cr_2O_3	0.47	3.39	3.11	3.27	2.27	3.08	2.97	2.40	2.15	2.21	6.67
Ga_2O_3/MgO	4.12	0.50	2.18	2.75	3.91	-	1.81	-	-	2.64	0.50
Fe_2O_3/Ga_2O_3	30.18	39.00	16.94	34.94	11.24	12.54	23.04	17.31	47.31	29.64	19.50
3 (O)											
Si	0.002	0.002	0.002	0.002	0.002	0.002	0.003	0.001	0.001	0.002	0.002
Ti	0.000	0.000	0.000	0.000	0.001	0.001	0.000	0.001	0.001	0.000	0.000
Al	1.977	1.986	1.987	1.988	1.986	1.989	1.986	1.988	1.988	1.986	1.990
Cr	0.015	0.003	0.002	0.002	0.003	0.002	0.003	0.003	0.004	0.004	0.001
Ga	0.001	0.000	0.001	0.000	0.002	0.000	0.001	0.000	0.000	0.001	0.000
V	0.000	0.000	0.000	0.000	0.000	0.000	0.000	0.000	0.000	0.000	0.000
Fe^{3+}	0.006	0.010	0.007	0.007	0.006	0.007	0.006	0.007	0.008	0.008	0.006
Fe^{2+}	0.002	0.002	0.001	0.001	0.002	0.000	0.003	0.001	0.001	0.002	0.001
Mn	0.000	0.000	0.000	0.000	0.001	0.001	0.000	0.000	0.000	0.000	0.000
Mg	0.000	0.000	0.001	0.001	0.000	0.001	0.000	0.001	0.000	0.000	0.001
Total*	2.002	2.003	2.002	2.002	2.002	2.002	2.002	2.002	2.003	2.003	2.002

ND = not detected

Table G-2 Representative EPMA analyses of Bo Welu ruby (continued)

Element Oxides (wt.%)	9TWL105-2	9TWL114-1	9TWL114-2	9TWL118-1	9TWL122-2	9TWL131-1	9TWL132-1	9TWL132-2	9TWL135-1	9TWL135-2	9TWL136-1
SiO_2	0.057	0.125	0.114	0.047	0.008	0.039	0.043	0.035	0.070	0.059	0.050
TiO_2	0.026	0.030	0.042	0.038	0.041	0.041	0.036	0.027	0.019	0.026	0.030
Al_2O_3	97.841	97.406	97.642	97.876	97.791	99.779	97.978	97.633	98.082	98.083	99.030
Cr_2O_3	0.031	0.224	0.174	0.316	0.200	0.276	0.254	0.259	0.131	0.184	0.340
Ga_2O_3	0.005	0.086	0.014	0.002	ND	0.041	0.082	0.098	0.098	ND	0.030
V_2O_3	ND	ND	ND	0.007	0.004	0.005	ND	0.008	ND	0.011	ND
FeO total	0.538	0.533	0.503	0.401	0.470	0.604	0.293	0.377	0.654	0.597	0.450
MnO	0.044	ND	0.053	ND	ND	ND	ND	ND	ND	ND	ND
MgO	0.045	0.021	0.030	0.034	0.026	0.037	0.002	0.026	0.030	0.022	0.010
Total	98.587	98.425	98.572	98.721	98.540	100.822	98.688	98.463	99.084	98.982	99.940
Fe_2O_3/TiO_2	20.69	17.77	11.98	10.55	11.46	14.73	8.14	13.96	34.42	22.96	15.00
Cr_2O_3/Ga_2O_3	6.20	2.60	12.43	158.00	-	6.73	3.10	2.64	1.34	-	11.33
TiO_2/Ga_2O_3	5.20	0.35	3.00	19.00	-	1.00	0.44	0.28	0.19	-	1.00
Fe_2O_3/Cr_2O_3	17.35	2.38	2.89	1.27	2.35	2.19	1.15	1.46	4.99	3.24	1.32
Ga_2O_3/MgO	0.11	4.10	0.47	0.06	-	1.11	41.00	3.77	3.27	-	3.00
Fe_2O_3/Ga_2O_3	11.96	25.38	16.77	11.79	18.08	16.32	146.50	14.50	21.80	27.14	45.00
3 (O)											
Si	0.001	0.003	0.004	0.002	0.001	0.002	0.001	0.001	0.002	0.003	0.001
Ti	0.000	0.000	0.001	0.001	0.001	0.001	0.001	0.000	0.000	0.000	0.000
Al	1.991	1.987	1.986	1.989	1.991	1.987	1.990	1.989	1.988	1.988	1.989
Cr	0.000	0.003	0.002	0.004	0.003	0.004	0.003	0.004	0.002	0.002	0.005
Ga	0.000	0.001	0.000	0.000	0.000	0.000	0.001	0.001	0.001	0.000	0.000
V	0.000	0.000	0.000	0.000	0.000	0.000	0.000	0.000	0.000	0.000	0.000
Fe^{3+}	0.008	0.005	0.004	0.004	0.006	0.007	0.002	0.004	0.008	0.006	0.005
Fe^{2+}	0.000	0.003	0.003	0.002	0.001	0.002	0.002	0.001	0.001	0.003	0.001
Mn	0.001	0.000	0.000	0.000	0.000	0.001	0.000	0.000	0.000	0.000	0.000
Mg	0.001	0.000	0.001	0.000	0.000	0.000	0.000	0.000	0.000	0.000	0.000
Total*	2.003	2.002	2.001	2.001	2.002	2.002	2.001	2.001	2.003	2.002	2.002

ND = not detected

Table G-2 Representative EPMA analyses of Bo Welu ruby (continued)

Element Oxides (wt.%)	9TWL136-2	9TWL143-1	9TWL143-2	9TWL152-1	9TWL152-2	9TWL153-1	9TWL153-2	9TWL154-2	9TWL157-1	9TWL158-1	9TWL158-2
SiO_2	0.020	0.150	0.092	0.011	0.036	0.045	0.008	0.078	0.053	0.030	0.070
TiO_2	0.010	0.040	0.062	0.041	0.030	0.071	0.069	0.012	0.011	0.020	0.020
Al_2O_3	99.100	97.700	97.886	97.457	97.755	97.569	97.527	97.743	97.823	99.140	99.120
Cr_2O_3	0.370	0.130	0.162	0.137	0.145	0.096	0.146	0.762	0.154	0.220	0.230
Ga_2O_3	0.010	0.120	ND	0.021	0.083	0.119	0.153	ND	0.074	0.110	ND
V_2O_3	ND	0.010	0.011	0.018	0.005	0.016	ND	0.010	0.008	ND	ND
FeO total	0.440	0.700	0.698	0.765	0.758	0.550	0.572	0.477	0.458	0.430	0.480
MnO	ND	0.040	ND	ND	ND	0.022	0.006	ND	0.047	ND	0.020
MgO	ND	0.030	0.009	0.024	0.010	0.041	0.034	0.047	0.016	0.030	0.020
Total	99.950	98.920	98.920	98.474	98.822	98.529	98.515	99.129	98.644	99.980	99.960
Fe_2O_3/TiO_2	44.00	17.50	11.26	18.66	25.27	7.75	8.29	39.75	41.64	21.50	24.00
Cr_2O_3/Ga_2O_3	37.00	1.08	-	6.52	1.75	0.81	0.95	-	2.08	2.00	-
TiO_2/Ga_2O_3	1.00	0.33	-	1.95	0.36	0.60	0.45	-	0.15	0.18	-
Fe_2O_3/Cr_2O_3	1.19	5.38	4.31	5.58	5.23	5.73	3.92	0.63	2.97	1.95	2.09
Ga_2O_3/MgO	-	4.00	-	0.88	8.30	2.90	4.50	-	4.63	3.67	-
Fe_2O_3/Ga_2O_3	-	23.33	77.56	31.88	75.80	13.41	16.82	10.15	28.63	14.33	24.00
3 (O)											
Si	0.000	0.003	0.002	0.001	0.003	0.002	0.001	0.002	0.002	0.001	0.001
Ti	0.000	0.001	0.001	0.001	0.000	0.001	0.001	0.000	0.000	0.000	0.000
Al	1.990	1.985	1.987	1.988	1.985	1.987	1.987	1.982	1.989	1.990	1.990
Cr	0.005	0.002	0.002	0.002	0.002	0.001	0.002	0.010	0.002	0.003	0.003
Ga	0.000	0.001	0.000	0.000	0.001	0.001	0.002	0.000	0.001	0.001	0.000
V	0.000	0.000	0.000	0.000	0.000	0.000	0.000	0.000	0.000	0.000	0.000
Fe^{3+}	0.006	0.008	0.007	0.010	0.008	0.006	0.007	0.005	0.006	0.006	0.006
Fe^{2+}	0.000	0.002	0.003	0.001	0.003	0.002	0.001	0.001	0.000	0.000	0.001
Mn	0.000	0.000	0.000	0.000	0.000	0.001	0.000	0.001	0.000	0.000	0.000
Mg	0.000	0.001	0.000	0.000	0.000	0.001	0.000	0.000	0.001	0.000	0.001
Total*	2.002	2.003	2.002	2.003	2.003	2.002	2.002	2.002	2.002	2.002	2.002

ND = not detected

Table G-2 Representative EPMA analyses of Bo Welu ruby (continued)

Element Oxides (wt.%)	9TWL160-1	9TWL172-1	9TWL172-2	9TWL174-1	9TWL176-2	9TWL178-1	9TWL178-2	9TWL180-1	9TWL180-2
SiO_2	0.036	0.025	0.008	0.014	ND	0.033	0.025	0.033	ND
TiO_2	0.032	0.057	0.041	0.096	0.041	0.030	0.015	0.059	0.060
Al_2O_3	97.484	97.303	97.521	98.602	97.976	99.786	99.370	99.466	99.772
Cr_2O_3	0.406	0.490	0.453	0.251	0.150	0.170	0.150	0.228	0.220
Ga_2O_3	0.067	0.153	ND	0.014	0.072	ND	0.134	0.069	ND
V_2O_3	0.006	ND	0.018	ND	0.013	0.019	0.001	0.004	ND
FeO total	0.741	0.602	0.599	0.644	0.492	0.423	0.419	0.593	0.652
MnO	0.006	ND	ND	ND	0.009	0.034	ND	ND	ND
MgO	0.031	0.034	0.002	0.065	0.015	0.013	0.010	0.028	0.051
Total	98.809	98.664	98.642	99.686	98.768	100.508	100.124	100.480	100.755
Fe_2O_3/TiO_2	23.16	10.56	14.61	6.71	12.00	14.10	27.93	10.05	10.87
Cr_2O_3/Ga_2O_3	6.06	3.20	-	17.93	2.08	-	1.12	3.30	-
TiO_2/Ga_2O_3	0.48	0.37	-	6.86	0.57	-	0.11	0.86	-
Fe_2O_3/Cr_2O_3	1.83	1.23	1.32	2.57	3.28	2.49	2.79	2.60	2.96
Ga_2O_3/MgO	2.16	4.50	-	0.22	4.80	-	13.40	2.46	-
Fe_2O_3/Ga_2O_3	23.90	17.71	299.50	9.91	32.80	32.54	41.90	21.18	12.78
3 (O)									
Si	0.002	0.001	0.001	0.001	0.001	0.001	0.003	0.002	0.000
Ti	0.000	0.001	0.001	0.001	0.001	0.000	0.000	0.001	0.001
Al	1.982	1.983	1.986	1.987	1.990	1.991	1.989	1.986	1.989
Cr	0.006	0.007	0.006	0.003	0.002	0.002	0.002	0.003	0.003
Ga	0.001	0.002	0.000	0.000	0.001	0.000	0.001	0.001	0.000
V	0.000	0.000	0.000	0.000	0.000	0.000	0.000	0.000	0.000
Fe^{3+}	0.009	0.007	0.007	0.008	0.006	0.005	0.003	0.006	0.009
Fe^{2+}	0.002	0.002	0.001	0.001	0.001	0.001	0.003	0.003	0.000
Mn	0.000	0.000	0.000	0.001	0.000	0.000	0.000	0.000	0.001
Mg	0.000	0.000	0.000	0.000	0.000	0.001	0.000	0.000	0.000
Total*	2.003	2.002	2.002	2.003	2.002	2.002	2.001	2.002	2.003

ND = not detected

Table G-3 Representative EPMA analyses of Bo Welu sapphire.

Element Oxides (wt.%)	8TWL001-1	8TWL001-2	8TWL001-3	8TWL002-1	8TWL002-2	8TWL002-3	8TWL016-1	8TWL016-2	8TWL018-1	8TWL018-2	8TWL018-3
SiO_2	0.066	ND	0.019	ND	0.017	ND	0.006	0.011	0.025	ND	ND
TiO_2	0.022	ND	0.037	0.079	0.003	ND	0.025	0.048	0.006	0.030	0.007
Al_2O_3	98.544	98.558	98.375	99.287	98.175	98.499	99.156	97.877	98.261	98.252	99.100
Cr_2O_3	ND	ND	ND	ND	0.011	ND	ND	ND	0.034	0.008	0.011
Ga_2O_3	0.040	0.073	0.141	ND	0.108	0.043	0.147	0.007	0.023	ND	ND
V_2O_3	ND	ND	0.001	0.009	0.004	ND	0.005	ND	0.004	ND	ND
FeO total	0.975	0.846	1.143	1.342	1.140	1.094	0.711	0.685	1.205	1.129	1.112
MnO	0.003	ND	ND	ND	ND	0.014	ND	ND	0.034	0.031	ND
MgO	0.001	ND	ND	ND	ND	ND	ND	ND	ND	ND	ND
Total	99.651	99.477	99.716	100.717	99.458	99.650	100.050	98.628	99.592	99.450	100.230
Fe_2O_3/TiO_2	44.32	-	30.89	16.99	380.00	-	28.44	14.27	200.83	37.63	158.86
Cr_2O_3/Ga_2O_3	-	-	-	-	0.10	-	-	-	1.48	-	-
TiO_2/Ga_2O_3	0.55	-	0.26	-	0.03	-	0.17	6.86	0.26	-	-
Fe_2O_3/Cr_2O_3	-	-	-	-	103.64	-	-	-	35.44	141.13	101.09
Ga_2O_3/MgO	40.00	-	-	-	-	-	-	-	-	-	-
Fe_2O_3/Ga_2O_3	975.00	-	-	-	-	-	-	-	-	-	-
3 (O)											
Si	0.001	0.000	0.000	0.000	0.001	0.000	0.000	0.000	0.001	0.000	0.000
Ti	0.000	0.000	0.001	0.001	0.000	0.000	0.000	0.001	0.000	0.000	0.000
Al	1.988	1.991	1.986	1.986	1.987	1.989	1.991	1.992	1.986	1.988	1.989
Cr	0.000	0.000	0.000	0.000	0.000	0.000	0.000	0.000	0.000	0.000	0.000
Ga	0.000	0.001	0.002	0.000	0.001	0.000	0.002	0.000	0.000	0.000	0.000
V	0.000	0.000	0.000	0.000	0.000	0.000	0.000	0.000	0.000	0.000	0.000
Fe^{3+}	0.012	0.012	0.015	0.018	0.016	0.015	0.010	0.009	0.017	0.016	0.015
Fe^{2+}	0.002	0.000	0.001	0.001	0.001	0.000	0.000	0.001	0.000	0.000	0.000
Mn	0.000	0.000	0.000	0.000	0.000	0.000	0.000	0.000	0.000	0.000	0.000
Mg	0.000	0.000	0.000	0.000	0.000	0.000	0.000	0.000	0.000	0.000	0.000
Total*	2.004	2.004	2.005	2.006	2.005	2.005	2.003	2.003	2.006	2.005	2.005

ND = not detected

Table G-3 Representative EPMA analyses of Bo Welu sapphire (continued).

Element Oxides (wt.%)	8TWL022-1	8TWL022-2	8TWL022-3	8TWL023-1	8TWL023-2	8TWL023-3	8TWL026-1	8TWL026-2	8TWL028-1	8TWL028-2	8TWL028-3
SiO_2	0.000	0.044	0.000	0.025	0.000	0.000	0.000	0.014	0.008	0.008	0.077
TiO_2	0.000	0.044	0.029	0.107	0.032	0.047	0.027	0.055	0.018	0.009	0.042
Al_2O_3	98.007	98.049	98.930	99.110	99.577	98.640	98.778	97.686	98.027	98.015	98.517
Cr_2O_3	0.000	0.019	0.034	0.034	0.030	0.000	0.000	0.000	0.026	0.004	0.004
Ga_2O_3	0.071	0.023	0.182	0.166	0.063	0.000	0.071	0.038	0.053	0.013	0.066
V_2O_3	0.000	0.000	0.000	0.000	0.003	0.010	0.001	0.000	0.034	0.000	0.001
FeO total	0.957	0.997	1.058	1.233	1.101	1.191	1.176	1.138	1.041	1.600	1.104
MnO	0.000	0.000	0.000	0.014	0.040	0.000	0.006	0.003	0.023	0.006	0.000
MgO	0.000	0.000	0.000	0.004	0.000	0.002	0.000	0.000	0.000	0.000	0.000
Total	99.035	99.176	100.233	100.693	100.846	99.890	100.059	98.934	99.230	99.655	99.811
Fe_2O_3/TiO_2	-	22.66	36.48	11.52	34.41	25.34	43.56	20.69	57.83	177.78	26.29
Cr_2O_3/Ga_2O_3	0.00	0.83	0.19	0.20	0.48	-	0.00	0.00	0.49	0.31	0.06
TiO_2/Ga_2O_3	0.00	1.91	0.16	0.64	0.51	-	0.38	1.45	0.34	0.69	0.64
Fe_2O_3/Cr_2O_3	-	52.47	31.12	36.26	36.70	-	-	-	40.04	400.00	276.00
Ga_2O_3/MgO	-	-	-	41.50	-	0.00	-	-	-	-	-
Fe_2O_3/Ga_2O_3	-	-	-	308.25	-	595.50	-	-	-	-	-
Formula 3(O)											
Si	0.000	0.001	0.000	0.001	0.000	0.000	0.000	0.000	0.000	0.000	0.002
Ti	0.000	0.001	0.000	0.001	0.000	0.001	0.000	0.001	0.000	0.000	0.001
Al	1.990	1.988	1.987	1.983	1.988	1.988	1.987	1.987	1.988	1.984	1.986
Cr	0.000	0.000	0.000	0.000	0.000	0.000	0.000	0.000	0.000	0.000	0.000
Ga	0.001	0.000	0.002	0.002	0.001	0.000	0.001	0.000	0.001	0.000	0.001
V	0.000	0.000	0.000	0.000	0.000	0.000	0.000	0.000	0.000	0.000	0.000
Fe^{3+}	0.014	0.013	0.015	0.016	0.016	0.016	0.016	0.015	0.015	0.023	0.014
Fe^{2+}	0.000	0.001	0.001	0.002	0.000	0.001	0.000	0.001	0.000	0.000	0.002
Mn	0.000	0.000	0.000	0.000	0.001	0.000	0.000	0.000	0.000	0.000	0.000
Mg	0.000	0.000	0.000	0.000	0.000	0.000	0.000	0.000	0.000	0.000	0.000
Total*	2.005	2.004	2.005	2.005	2.005	2.005	2.006	2.005	2.005	2.008	2.005

Table G-3 Representative EPMA analyses of Bo Welu sapphire (continued).

Element Oxides (wt.%)	8TWL031-1	8TWL031-2	8TWL031-3	8TWL035-1	8TWL035-2	8TWL035-3	8TWL036-1	8TWL036-2	8TWL036-3	8TWL040-1	8TWL040-2
SiO_2	0.017	ND	0.028	ND	0.022	0.014	0.014	0.003	ND	0.041	ND
TiO_2	0.039	0.006	0.021	0.015	0.074	0.044	0.028	ND	0.031	0.027	0.006
Al_2O_3	99.619	98.978	99.364	98.903	98.389	98.308	99.078	98.499	97.512	98.155	98.459
Cr_2O_3	ND	ND	ND	ND	0.008	0.004	ND	ND	0.030	ND	0.026
Ga_2O_3	0.023	0.033	ND	ND	0.091	0.071	0.134	0.048	0.189	0.005	ND
V_2O_3	ND	0.001	ND	0.013	ND	ND	ND	0.026	ND	0.007	0.007
FeO total	1.302	1.187	1.264	0.899	1.057	1.025	1.119	1.167	1.193	0.732	0.753
MnO	0.020	0.029	0.017	0.040	ND	0.014	ND	ND	ND	0.003	0.026
MgO	ND	ND	ND	0.001	ND	ND	ND	ND	ND	ND	ND
Total	101.020	100.234	100.694	99.871	99.641	99.480	100.373	99.743	98.955	98.970	99.277
Fe_2O_3/TiO_2	33.38	197.83	60.19	59.93	14.28	23.30	39.96	-	38.48	27.11	125.50
Cr_2O_3/Ga_2O_3	-	-	-	-	0.09	0.06	-	-	0.16	-	-
TiO_2/Ga_2O_3	1.70	0.18	-	-	0.81	0.62	0.21	-	0.16	5.40	-
Fe_2O_3/Cr_2O_3	-	-	-	-	132.13	256.25	-	-	39.77	-	28.96
Ga_2O_3/MgO	-	-	-	-	-	-	-	-	-	-	-
Fe_2O_3/Ga_2O_3	-	-	-	899.00	-	-	-	-	-	-	-
3 (O)											
Si	0.000	0.000	0.001	0.000	0.001	0.000	0.000	0.000	0.000	0.001	0.000
Ti	0.001	0.000	0.000	0.000	0.001	0.001	0.000	0.000	0.000	0.000	0.000
Al	1.986	1.988	1.987	1.991	1.986	1.988	1.987	1.988	1.986	1.991	1.992
Cr	0.000	0.000	0.000	0.000	0.000	0.000	0.000	0.000	0.000	0.000	0.000
Ga	0.000	0.000	0.000	0.000	0.001	0.001	0.001	0.001	0.002	0.000	0.000
V	0.000	0.000	0.000	0.000	0.000	0.000	0.000	0.000	0.000	0.000	0.000
Fe^{3+}	0.018	0.017	0.017	0.013	0.013	0.014	0.015	0.017	0.017	0.009	0.011
Fe^{2+}	0.001	0.000	0.001	0.000	0.002	0.001	0.001	0.000	0.000	0.002	0.000
Mn	0.000	0.000	0.000	0.001	0.000	0.000	0.000	0.000	0.000	0.000	0.000
Mg	0.000	0.000	0.000	0.000	0.000	0.000	0.000	0.000	0.000	0.000	0.000
Total*	2.006	2.006	2.006	2.004	2.004	2.005	2.005	2.006	2.006	2.003	2.004

ND = not detected

Table G-3 Representative EPMA analyses of Bo Welu sapphire (continued).

Element Oxides (wt.%)	8TWL040-3	8TWL046-1	8TWL046-2	8TWL046-3	8TWL053-1	8TWL053-2	8TWL053-3	8TWL059-1
SiO_2	ND	ND	0.025	0.006	0.022	0.047	0.019	0.036
TiO_2	0.035	0.009	ND	0.019	0.037	0.048	0.065	0.103
Al_2O_3	98.950	98.241	98.633	98.400	98.498	98.413	98.562	98.916
Cr_2O_3	0.023	0.004	0.023	ND	0.008	ND	0.015	ND
Ga_2O_3	0.005	0.260	0.091	0.076	0.038	0.058	0.081	ND
V_2O_3	ND	0.014	ND	ND	0.009	ND	ND	ND
FeO total	0.953	1.647	1.218	1.134	0.999	1.165	1.079	1.049
MnO	ND	ND	ND	ND	0.054	ND	0.029	ND
MgO	ND	ND	ND	ND	ND	ND	ND	0.007
Total	99.966	100.175	99.990	99.635	99.665	99.731	99.850	100.111
Fe_2O_3/TiO_2	27.23	183.00	-	59.68	27.00	24.27	16.60	10.18
Cr_2O_3/Ga_2O_3	4.60	0.02	0.25	-	0.21	-	0.19	-
TiO_2/Ga_2O_3	7.00	0.03	-	0.25	0.97	0.83	0.80	-
Fe_2O_3/Cr_2O_3	41.43	411.75	52.96	-	124.88	-	71.93	-
Ga_2O_3/MgO	-	-	-	-	-	-	-	-
Fe_2O_3/Ga_2O_3	-	-	-	-	-	-	-	149.86
3 (O)								
Si	0.000	0.000	0.001	0.000	0.001	0.001	0.001	0.001
Ti	0.001	0.000	0.000	0.000	0.001	0.001	0.001	0.001
Al	1.990	1.981	1.986	1.988	1.988	1.986	1.986	1.987
Cr	0.000	0.000	0.000	0.000	0.000	0.000	0.000	0.000
Ga	0.000	0.003	0.001	0.001	0.000	0.001	0.001	0.000
V	0.000	0.000	0.000	0.000	0.000	0.000	0.000	0.000
Fe^{3+}	0.013	0.023	0.017	0.016	0.014	0.015	0.014	0.013
Fe^{2+}	0.001	0.000	0.001	0.001	0.000	0.002	0.001	0.002
Mn	0.000	0.000	0.000	0.000	0.001	0.000	0.000	0.000
Mg	0.000	0.000	0.000	0.000	0.000	0.000	0.000	0.000
Total*	2.004	2.008	2.006	2.005	2.005	2.005	2.005	2.004

ND = not detected

Table G-3 Representative EPMA analyses of Bo Welu sapphire (continued).

Element Oxides (wt.%)	8TWL059-2	8TWL059-3	8TWL064-1	8TWL064-2	8TWL064-3	8TWL067-1	8TWL067-2	8TWL067-3	8TWL068-1	8TWL068-2	8TWL068-3
SiO_2	ND	0.025	0.033	0.041	0.030	0.030	0.044	0.033	ND	ND	0.003
TiO_2	0.003	ND	0.036	0.003	0.034	ND	ND	0.030	0.006	ND	ND
Al_2O_3	98.967	98.656	98.490	98.603	98.639	98.231	98.653	98.499	98.850	98.814	99.190
Cr_2O_3	ND	ND	ND	0.026	0.026	ND	ND	0.019	ND	0.004	ND
Ga_2O_3	ND	0.098	0.015	0.023	0.126	0.101	0.058	0.058	0.020	0.043	0.086
V_2O_3	ND	ND	0.016	0.010	0.005	ND	0.006	0.008	ND	0.016	ND
FeO total	0.951	0.926	1.676	1.806	1.526	0.786	0.921	0.742	0.787	0.765	0.684
MnO	ND	0.046	ND	ND	ND	ND	ND	ND	ND	ND	0.011
MgO	0.001	ND	ND	0.019	ND	ND	0.013	ND	ND	ND	ND
Total	99.922	99.751	100.266	100.531	100.386	99.148	99.695	99.389	99.663	99.642	99.974
Fe_2O_3/TiO_2	317.00	-	46.56	602.00	44.88	-	-	24.73	131.17	-	-
Cr_2O_3/Ga_2O_3	-	-	-	1.13	0.21	-	-	0.33	-	0.09	-
TiO_2/Ga_2O_3	-	-	2.40	0.13	0.27	-	-	0.52	0.30	-	-
Fe_2O_3/Cr_2O_3	-	-	-	69.46	58.69	-	-	39.05	-	191.25	-
Ga_2O_3/MgO	-	-	-	1.21	-	-	4.46	-	-	-	-
Fe_2O_3/Ga_2O_3	951.00	-	-	95.05	-	-	70.85	-	-	-	-
3 (O)											
Si	0.000	0.001	0.001	0.001	0.001	0.001	0.001	0.001	0.000	0.000	0.000
Ti	0.000	0.000	0.001	0.000	0.000	0.000	0.000	0.000	0.000	0.000	0.000
Al	1.991	1.989	1.982	1.981	1.982	1.991	1.989	1.990	1.992	1.992	1.992
Cr	0.000	0.000	0.000	0.000	0.000	0.000	0.000	0.000	0.000	0.000	0.000
Ga	0.000	0.001	0.000	0.000	0.001	0.001	0.001	0.001	0.000	0.000	0.001
V	0.000	0.000	0.000	0.000	0.000	0.000	0.000	0.000	0.000	0.000	0.000
Fe^{3+}	0.014	0.013	0.023	0.025	0.021	0.011	0.013	0.009	0.011	0.011	0.010
Fe^{2+}	0.000	0.000	0.001	0.000	0.001	0.001	0.000	0.001	0.000	0.000	0.000
Mn	0.000	0.001	0.000	0.000	0.000	0.000	0.000	0.000	0.000	0.000	0.000
Mg	0.000	0.000	0.000	0.001	0.000	0.000	0.000	0.000	0.000	0.000	0.000
Total*	2.005	2.005	2.008	2.008	2.007	2.004	2.004	2.003	2.004	2.004	2.003

ND = not detected

Table G-3 Representative EPMA analyses of Bo Welu sapphire (continued).

Element Oxides (wt.%)	8TWL074-1	8TWL074-2	8TWL074-3	8TWL082-1	8TWL082-2	8TWL082-3	8TWL083-1	8TWL083-2	8TWL083-3	8TWL093-1	8TWL093-2
SiO_2	0.014	0.055	0.011	0.033	0.069	ND	0.050	ND	0.041	0.019	ND
TiO_2	0.077	0.015	0.039	ND	ND	ND	0.031	0.061	0.070	0.005	0.012
Al_2O_3	98.323	99.736	98.092	98.945	98.956	98.293	98.316	98.825	98.124	98.391	98.834
Cr_2O_3	0.042	0.049	0.015	0.057	ND	0.026	ND	0.004	0.008	0.042	0.068
Ga_2O_3	0.076	0.008	0.144	0.083	0.008	0.197	0.098	ND	0.048	ND	ND
V_2O_3	0.011	0.015	0.027	0.006	0.003	ND	ND	ND	ND	ND	ND
FeO total	0.964	0.889	0.865	1.176	1.103	1.170	0.916	1.052	1.023	1.297	1.153
MnO	0.031	ND	0.014	ND	0.017	0.006	0.003	ND	0.009	ND	ND
MgO	0.014	0.017	0.004	ND	ND	ND	ND	ND	ND	ND	0.003
Total	99.552	100.784	99.211	100.300	100.156	99.692	99.414	99.942	99.323	99.754	100.070
Fe_2O_3/TiO_2	12.52	59.27	22.18	-	-	-	29.55	17.25	14.61	259.40	96.08
Cr_2O_3/Ga_2O_3	0.55	6.13	0.10	0.69	-	0.13	-	-	0.17	-	-
TiO_2/Ga_2O_3	1.01	1.88	0.27	-	-	-	0.32	-	1.46	-	-
Fe_2O_3/Cr_2O_3	22.95	18.14	57.67	20.63	-	45.00	-	263.00	127.88	30.88	16.96
Ga_2O_3/MgO	5.43	0.47	36.00	-	-	-	-	-	-	-	-
Fe_2O_3/Ga_2O_3	68.86	52.29	216.25	-	-	-	-	-	-	-	384.33
3 (O)											
Si	0.000	0.001	0.001	0.001	0.001	0.000	0.001	0.000	0.001	0.000	0.000
Ti	0.001	0.000	0.001	0.000	0.000	0.000	0.000	0.001	0.001	0.000	0.000
Al	1.987	1.989	1.988	1.986	1.988	1.986	1.988	1.989	1.987	1.986	1.988
Cr	0.001	0.001	0.000	0.001	0.000	0.000	0.000	0.000	0.000	0.001	0.001
Ga	0.001	0.000	0.002	0.001	0.000	0.002	0.001	0.000	0.001	0.000	0.000
V	0.000	0.000	0.000	0.000	0.000	0.000	0.000	0.000	0.000	0.000	0.000
Fe^{3+}	0.013	0.012	0.012	0.016	0.015	0.017	0.012	0.014	0.013	0.018	0.016
Fe^{2+}	0.001	0.001	0.001	0.001	0.001	0.000	0.001	0.001	0.001	0.001	0.000
Mn	0.000	0.000	0.000	0.000	0.000	0.000	0.000	0.000	0.000	0.000	0.000
Mg	0.000	0.001	0.000	0.000	0.000	0.000	0.000	0.000	0.000	0.000	0.000
Total*	2.004	2.004	2.004	2.005	2.005	2.006	2.004	2.005	2.004	2.006	2.005

ND = not detected

Table G-3 Representative EPMA analyses of Bo Welu sapphire (continued).

Element Oxides (wt.%)	8TWL093-3	8TWL096-1	8TWL096-2	8TWL096-3	8TWL097-1	8TWL097-2	8TWL097-3	8TWL099-1	8TWL099-2	8TWL099-3	8TWL100-1
SiO_2	0.011	0.028	0.008	0.008	0.003	ND	ND	0.030	0.058	0.017	ND
TiO_2	0.018	0.040	ND	0.009	0.021	0.029	0.038	0.024	ND	0.032	0.022
Al_2O_3	98.688	98.835	98.957	98.593	98.429	99.237	98.433	98.704	98.817	98.496	99.088
Cr_2O_3	ND	ND	ND	ND	ND	ND	0.057	0.019	0.027	ND	ND
Ga_2O_3	0.058	0.091	0.159	0.040	0.025	ND	0.045	0.020	0.174	0.141	0.020
V_2O_3	ND	ND	ND	0.022	ND	0.001	0.003	ND	0.018	0.006	ND
FeO total	1.310	1.130	1.265	1.132	1.492	1.375	1.337	0.545	0.519	0.512	1.010
MnO	ND	0.009	0.003	0.020	0.029	0.017	0.009	ND	ND	ND	0.003
MgO	ND	ND	0.003	ND	ND	ND	ND	ND	ND	0.001	ND
Total	100.085	100.133	100.395	99.824	99.999	100.659	99.922	99.342	99.613	99.205	100.143
Fe_2O_3/TiO_2	72.78	28.25	-	125.78	71.05	47.41	35.18	22.71	-	16.00	45.91
Cr_2O_3/Ga_2O_3	-	-	-	-	-	-	1.27	0.95	0.16	-	-
TiO_2/Ga_2O_3	0.31	0.44	-	0.23	0.84	-	0.84	1.20	-	0.23	1.10
Fe_2O_3/Cr_2O_3	-	-	-	-	-	-	23.46	28.68	19.22	-	-
Ga_2O_3/MgO	-	-	53.00	-	-	-	-	-	-	141.00	-
Fe_2O_3/Ga_2O_3	-	-	421.67	-	-	-	-	-	-	512.00	-
3 (O)											
Si	0.001	0.001	0.000	0.000	0.001	0.000	0.001	0.001	0.001	0.001	0.000
Ti	0.000	0.001	0.000	0.000	0.000	0.000	0.001	0.000	0.000	0.000	0.000
Al	1.986	1.987	1.986	1.988	1.984	1.986	1.984	1.993	1.991	1.992	1.990
Cr	0.000	0.000	0.000	0.000	0.000	0.000	0.001	0.000	0.000	0.000	0.000
Ga	0.001	0.001	0.002	0.000	0.000	0.000	0.001	0.000	0.002	0.002	0.000
V	0.000	0.000	0.000	0.000	0.000	0.000	0.000	0.000	0.000	0.000	0.000
Fe^{3+}	0.018	0.015	0.018	0.016	0.021	0.019	0.018	0.007	0.006	0.006	0.014
Fe^{2+}	0.001	0.001	0.000	0.000	0.000	0.000	0.001	0.001	0.001	0.001	0.000
Mn	0.000	0.000	0.000	0.000	0.000	0.000	0.000	0.000	0.000	0.000	0.000
Mg	0.000	0.000	0.000	0.000	0.000	0.000	0.000	0.000	0.000	0.000	0.000
Total*	2.006	2.005	2.006	2.005	2.007	2.006	2.006	2.002	2.002	2.002	2.005

ND = not detected

Table G-3 Representative EPMA analyses of Bo Welu sapphire (continued).

Element Oxides (wt.%)	8TWL100-2	8TWL100-3	8TWL101-1	8TWL101-2	8TWL101-3	8TWL102-1	8TWL102-2	8TWL102-3	8TWL103-1	8TWL103-2	8TWL103-3
SiO_2	0.006	ND	0.028	ND	0.022	0.033	ND	0.028	ND	0.052	ND
TiO_2	0.083	0.009	0.001	0.015	0.020	0.020	0.003	ND	ND	0.012	0.041
Al_2O_3	98.970	98.297	98.850	98.166	98.518	98.095	98.814	98.962	98.150	98.798	99.927
Cr_2O_3	ND	ND	ND	0.030	ND	0.034	0.026	0.004	ND	ND	ND
Ga_2O_3	0.023	0.045	0.033	0.083	0.083	ND	0.013	0.073	ND	ND	0.028
V_2O_3	0.006	0.013	ND	ND	0.009	0.002	0.012	ND	0.003	0.003	0.018
FeO total	1.237	0.628	1.015	1.025	1.055	1.065	1.078	1.081	1.363	1.320	1.339
MnO	ND	0.048	0.026	ND	0.046	ND	ND	ND	ND	ND	ND
MgO	0.002	ND	ND	ND	ND	ND	ND	ND	ND	0.013	ND
Total	100.327	99.040	99.953	99.319	99.753	99.249	99.946	100.148	99.516	100.198	101.353
Fe_2O_3/TiO_2	14.90	69.78	1015.00	68.33	52.75	53.25	359.33	-	-	110.00	32.66
Cr_2O_3/Ga_2O_3	-	-	-	0.36	-	-	2.00	0.05	-	-	-
TiO_2/Ga_2O_3	3.61	0.20	0.03	0.18	0.24	-	0.23	-	-	-	1.46
Fe_2O_3/Cr_2O_3	-	-	-	34.17	-	31.32	41.46	270.25	-	-	-
Ga_2O_3/MgO	11.50	-	-	-	-	-	-	-	-	-	-
Fe_2O_3/Ga_2O_3	618.50	-	-	-	-	-	-	-	-	101.54	-
3 (O)											
Si	0.001	0.000	0.001	0.000	0.000	0.001	0.000	0.001	0.000	0.001	0.000
Ti	0.001	0.000	0.000	0.000	0.000	0.000	0.000	0.000	0.000	0.000	0.001
Al	1.986	1.992	1.989	1.988	1.988	1.988	1.989	1.988	1.987	1.986	1.986
Cr	0.000	0.000	0.000	0.000	0.000	0.000	0.000	0.000	0.000	0.000	0.000
Ga	0.000	0.001	0.000	0.001	0.001	0.000	0.000	0.001	0.000	0.000	0.000
V	0.000	0.000	0.000	0.000	0.000	0.000	0.000	0.000	0.000	0.000	0.000
Fe^{3+}	0.016	0.009	0.014	0.014	0.015	0.014	0.015	0.015	0.019	0.018	0.018
Fe^{2+}	0.002	0.000	0.000	0.000	0.000	0.001	0.000	0.001	0.000	0.001	0.001
Mn	0.000	0.001	0.000	0.000	0.001	0.000	0.000	0.000	0.000	0.000	0.000
Mg	0.000	0.000	0.000	0.000	0.000	0.000	0.000	0.000	0.000	0.000	0.000
Total*	2.005	2.003	2.005	2.005	2.005	2.005	2.005	2.005	2.006	2.006	2.006

ND = not detected

Table G-3 Representative EPMA analyses of Bo Welu sapphire (continued).

Element Oxides (wt.%)	8TWL105-1	8TWL105-2	8TWL105-3	8TWL106-1	8TWL106-2	8TWL106-3	8TWL108-1	8TWL108-2	8TWL108-3	8TWL111-1	8TWL111-2
SiO_2	ND	ND	0.025	ND	0.003	0.022	0.025	0.003	0.030	0.022	ND
TiO_2	0.032	0.058	0.053	0.091	0.128	0.227	0.009	ND	0.010	0.022	0.033
Al_2O_3	98.850	99.881	98.844	98.503	98.765	98.205	98.048	98.465	98.519	98.771	98.622
Cr_2O_3	ND	0.045	ND	0.004	ND	ND	ND	ND	0.053	0.011	ND
Ga_2O_3	0.015	0.008	0.028	0.161	0.129	0.164	0.154	0.096	0.096	0.088	0.088
V_2O_3	0.013	ND	ND	ND	0.002	ND	0.007	ND	0.007	ND	0.007
FeO total	1.362	1.356	1.301	1.464	1.392	1.440	0.929	0.756	0.850	1.110	1.292
MnO	ND	ND	0.037	ND	ND	0.006	0.003	ND	ND	ND	ND
MgO	ND	ND	ND	ND	ND	ND	ND	ND	ND	ND	ND
Total	100.272	101.348	100.288	100.223	100.419	100.064	99.175	99.320	99.565	100.024	100.042
Fe_2O_3/TiO_2	42.56	23.38	24.55	16.09	10.88	6.34	103.22	-	85.00	50.45	39.15
Cr_2O_3/Ga_2O_3	-	5.63	-	0.02	-	-	-	-	0.55	0.13	-
TiO_2/Ga_2O_3	2.13	7.25	1.89	0.57	0.99	1.38	0.06	-	0.10	0.25	0.38
Fe_2O_3/Cr_2O_3	-	30.13	-	366.00	-	-	-	-	16.04	100.91	-
Ga_2O_3/MgO	-	-	-	-	-	-	-	-	-	-	-
Fe_2O_3/Ga_2O_3	-	-	-	-	-	-	-	-	-	-	-
3 (O)											
Si	0.000	0.000	0.001	0.000	0.000	0.000	0.001	0.000	0.001	0.001	0.000
Ti	0.000	0.001	0.001	0.001	0.002	0.003	0.000	0.000	0.000	0.000	0.000
Al	1.986	1.985	1.985	1.983	1.983	1.980	1.988	1.992	1.989	1.987	1.986
Cr	0.000	0.001	0.000	0.000	0.000	0.000	0.000	0.000	0.001	0.000	0.000
Ga	0.000	0.000	0.000	0.002	0.001	0.002	0.002	0.001	0.001	0.001	0.001
V	0.000	0.000	0.000	0.000	0.000	0.000	0.000	0.000	0.000	0.000	0.000
Fe^{3+}	0.019	0.018	0.018	0.019	0.018	0.017	0.013	0.011	0.012	0.015	0.018
Fe^{2+}	0.001	0.001	0.001	0.001	0.002	0.003	0.001	0.000	0.001	0.001	0.001
Mn	0.000	0.000	0.001	0.000	0.000	0.000	0.000	0.000	0.000	0.000	0.000
Mg	0.000	0.000	0.000	0.000	0.000	0.000	0.000	0.000	0.000	0.000	0.000
Total*	2.006	2.006	2.006	2.007	2.006	2.006	2.004	2.004	2.004	2.005	2.006

ND = not detected

Table G-3 Representative EPMA analyses of Bo Welu sapphire (continued).

Element Oxides (wt.%)	8TWL111-3	8TWL112-1	8TWL113-1	8TWL113-2	8TWL113-3	8TWL114-1	8TWL114-2	8TWL114-3	8TWL116-1	8TWL116-2	8TWL116-3
SiO_2	0.033	0.044	0.028	0.069	0.003	0.047	0.036	0.028	0.044	0.052	0.028
TiO_2	0.010	0.045	0.019	0.054	0.021	0.014	0.012	ND	ND	0.023	0.003
Al_2O_3	98.873	97.741	98.718	99.171	99.224	98.419	98.069	98.583	98.722	98.529	99.805
Cr_2O_3	0.004	ND	0.008	ND	0.030	0.023	0.019	ND	0.026	ND	0.042
Ga_2O_3	ND	ND	0.068	0.154	ND	ND	0.103	ND	0.144	ND	0.055
V_2O_3	0.025	ND	0.009	ND	ND	ND	ND	0.005	0.016	ND	ND
FeO total	1.202	0.760	1.649	1.889	1.916	0.645	0.740	0.692	1.498	1.434	1.263
MnO	ND	ND	0.003	ND	ND	ND	0.040	0.040	ND	0.031	0.023
MgO	ND	0.019	ND	ND	ND	ND	ND	ND	ND	ND	ND
Total	100.147	98.609	100.502	101.337	101.194	99.148	99.019	99.348	100.450	100.069	101.219
Fe_2O_3/TiO_2	120.20	16.89	86.79	34.98	91.24	46.07	61.67	-	-	62.35	421.00
Cr_2O_3/Ga_2O_3	-	-	0.12	-	-	-	0.18	-	0.18	-	0.76
TiO_2/Ga_2O_3	-	-	0.28	0.35	-	-	0.12	-	-	-	0.05
Fe_2O_3/Cr_2O_3	300.50	-	206.13	-	63.87	28.04	38.95	-	57.62	-	30.07
Ga_2O_3/MgO	-	-	-	-	-	-	-	-	-	-	-
Fe_2O_3/Ga_2O_3	-	40.00	-	-	-	-	-	-	-	-	-
3 (O)											
Si	0.001	0.001	0.001	0.001	0.000	0.001	0.001	0.001	0.001	0.001	0.001
Ti	0.000	0.001	0.000	0.001	0.000	0.000	0.000	0.000	0.000	0.000	0.000
Al	1.987	1.990	1.982	1.978	1.981	1.992	1.990	1.992	1.983	1.984	1.986
Cr	0.000	0.000	0.000	0.000	0.000	0.000	0.000	0.000	0.000	0.000	0.001
Ga	0.000	0.000	0.001	0.002	0.000	0.000	0.001	0.000	0.002	0.000	0.001
V	0.000	0.000	0.000	0.000	0.000	0.000	0.000	0.000	0.000	0.000	0.000
Fe^{3+}	0.016	0.010	0.022	0.025	0.027	0.008	0.010	0.010	0.021	0.020	0.017
Fe^{2+}	0.001	0.001	0.001	0.002	0.000	0.001	0.001	0.000	0.001	0.001	0.000
Mn	0.000	0.000	0.000	0.000	0.000	0.000	0.001	0.001	0.000	0.000	0.000
Mg	0.000	0.001	0.000	0.000	0.000	0.000	0.000	0.000	0.000	0.000	0.000
Total*	2.005	2.003	2.008	2.008	2.009	2.003	2.003	2.003	2.007	2.007	2.006

ND = not detected

Table G-3 Representative EPMA analyses of Bo Welu sapphire (continued).

Element Oxides (wt.%)	8TWL117-1	8TWL117-2	8TWL117-3	8TWL119-1	8TWL119-2	8TWL119-3	8TWL120-1	8TWL120-2	8TWL120-3
SiO_2	0.030	0.003	0.025	0.017	0.036	ND	0.008	ND	0.019
TiO_2	0.016	0.046	0.010	0.002	0.010	0.044	0.031	0.021	ND
Al_2O_3	98.903	98.673	98.763	98.065	98.543	98.711	98.438	98.954	98.449
Cr_2O_3	0.026	0.030	0.015	ND	ND	0.026	ND	ND	0.011
Ga_2O_3	0.025	0.040	0.096	0.015	0.116	0.040	0.035	0.111	0.035
V_2O_3	0.029	0.002	0.016	ND	ND	0.008	0.007	ND	0.018
FeO total	0.941	1.121	0.896	0.736	0.814	0.958	1.043	1.043	0.948
MnO	ND	ND	ND	ND	ND	ND	ND	ND	ND
MgO	ND	ND	ND	ND	ND	0.014	ND	0.003	ND
Total	99.970	99.915	99.821	98.835	99.519	99.801	99.562	100.132	99.480
Fe_2O_3/TiO_2	58.81	24.37	89.60	368.00	81.40	21.77	33.65	49.67	-
Cr_2O_3/Ga_2O_3	1.04	0.75	0.16	-	-	0.65	-	-	0.31
TiO_2/Ga_2O_3	0.64	1.15	0.10	0.13	0.09	1.10	0.89	0.19	-
Fe_2O_3/Cr_2O_3	36.19	37.37	59.73	-	-	36.85	-	-	86.18
Ga_2O_3/MgO	-	-	-	-	-	2.86	-	37.00	-
Fe_2O_3/Ga_2O_3	-	-	-	-	-	68.43	-	347.67	-
3 (O)									
Si	0.001	0.000	0.001	0.000	0.001	0.000	0.001	0.000	0.001
Ti	0.000	0.001	0.000	0.000	0.000	0.001	0.000	0.000	0.000
Al	1.989	1.987	1.989	1.992	1.990	1.989	1.988	1.988	1.989
Cr	0.000	0.000	0.000	0.000	0.000	0.000	0.000	0.000	0.000
Ga	0.000	0.000	0.001	0.000	0.001	0.000	0.000	0.001	0.000
V	0.000	0.000	0.000	0.000	0.000	0.000	0.000	0.000	0.000
Fe^{3+}	0.012	0.015	0.012	0.010	0.011	0.013	0.014	0.014	0.013
Fe^{2+}	0.001	0.001	0.001	0.000	0.001	0.000	0.001	0.001	0.001
Mn	0.000	0.000	0.000	0.000	0.000	0.000	0.000	0.000	0.000
Mg	0.000	0.000	0.000	0.000	0.000	0.000	0.000	0.000	0.000
Total*	2.004	2.005	2.004	2.003	2.004	2.004	2.005	2.005	2.004

ND = not detected

Appendix H - EPMA analysis of mineral inclusions

Table H-1 EPMA analyses of pyroxene inclusions in Bo Rai ruby

Mineral phase analysis (wt%)	9TRA016-in1		9TRA023-in1		9TRA036-in1			9TRA038-in1			9TRA039-in1		9TRA048-in1		9TRA051-in1		9TRA051-in2	
SiO_2	46.51	46.93	47.10	46.73	46.55	45.89	46.96	47.02	47.02	46.21	47.13	47.90	46.94	47.17	47.17	46.99	46.72	47.30
TiO_2	0.14	0.17	0.04	0.02	0.11	0.13	0.14	0.13	0.08	0.12	0.35	0.30	0.33	0.36	0.18	0.27	0.36	0.22
Al_2O_3	14.68	14.49	14.69	14.93	13.88	14.86	14.11	15.62	15.91	16.29	14.88	14.04	14.94	14.92	13.78	13.64	13.85	13.94
Cr_2O_3	0.14	0.15	0.08	0.05	0.04	0.03	0.02	0.02	0.11	0.04	0.15	0.09	0.14	0.12	0.09	0.15	0.11	0.06
FeO total	2.25	2.21	2.25	2.18	2.67	2.69	2.53	2.63	2.52	2.61	2.26	2.60	2.37	2.40	3.31	3.37	4.00	3.31
MnO	ND	0.01	0.04	0.02	0.01	ND	0.01	0.04	ND	0.03	0.04	0.05	0.01	ND	ND	0.01	0.05	0.04
MgO	11.93	11.97	11.65	11.65	13.32	12.83	12.41	11.70	11.64	11.61	12.08	12.18	11.58	11.50	11.25	11.31	11.10	11.41
CaO	22.09	21.70	21.76	21.83	21.34	21.47	21.92	20.66	20.71	20.87	21.55	21.76	21.66	21.84	21.84	21.81	21.42	21.63
K_2O	0.01	0.01	0.01	0.01	0.01	0.02	0.01	ND	0.01	0.03	0.02	0.02	0.01	0.02	0.01	0.01	0.03	0.01
Na_2O	1.02	1.01	1.20	1.18	0.97	0.95	0.60	1.17	1.12	1.11	1.16	1.15	0.92	0.88	1.07	1.07	1.00	1.06
Total	98.f76	98.66	98.81	98.56	98.89	98.88	98.71	99.00	99.13	98.91	99.60	100.09	98.92	99.22	98.69	98.66	98.66	98.96
6 (O)																		
Si	1.705	1.718	1.722	1.713	1.706	1.683	1.720	1.712	1.708	1.686	1.709	1.731	1.714	1.717	1.736	1.732	1.725	1.734
Ti	0.004	0.005	0.001	0.001	0.003	0.004	0.004	0.004	0.002	0.003	0.010	0.008	0.009	0.010	0.005	0.007	0.010	0.006
Al	0.634	0.625	0.633	0.645	0.599	0.642	0.609	0.670	0.681	0.701	0.636	0.598	0.643	0.640	0.598	0.593	0.603	0.602
Cr	0.004	0.004	0.002	0.001	0.001	0.001	0.001	0.001	0.003	0.001	0.004	0.003	0.004	0.003	0.003	0.004	0.003	0.002
Fe^{3+}	0.025	0.000	0.005	0.015	0.077	0.077	0.000	0.000	0.000	0.000	0.006	0.003	0.000	0.000	0.000	0.001	0.000	0.000
Fe^{2+}	0.044	0.068	0.063	0.052	0.005	0.005	0.078	0.080	0.077	0.080	0.062	0.076	0.072	0.073	0.102	0.104	0.124	0.101
Mn	0.000	0.000	0.001	0.001	0.000	0.000	0.000	0.001	0.000	0.001	0.001	0.002	0.000	0.000	0.000	0.000	0.002	0.001
Mg	0.652	0.653	0.635	0.636	0.727	0.702	0.678	0.635	0.630	0.632	0.653	0.656	0.630	0.624	0.617	0.621	0.611	0.624
Ca	0.868	0.852	0.853	0.857	0.838	0.843	0.860	0.806	0.806	0.816	0.837	0.843	0.847	0.852	0.861	0.861	0.848	0.850
K	0.000	0.001	0.001	0.000	0.001	0.001	0.000	0.000	0.000	0.001	0.001	0.001	0.000	0.001	0.000	0.000	0.001	0.000
Na	0.073	0.072	0.085	0.084	0.069	0.068	0.043	0.083	0.079	0.078	0.082	0.081	0.065	0.062	0.076	0.076	0.072	0.075
Total*	4.008	3.998	4.002	4.005	4.026	4.026	3.993	3.991	3.987	3.999	4.002	4.001	3.986	3.983	3.998	4.000	3.998	3.996
% Ca	55.50	54.16	55.00	55.47	53.38	54.39	53.22	52.99	53.27	53.40	53.93	53.52	54.68	55.00	54.49	54.29	53.57	53.97
% Mg	41.69	41.51	40.94	41.17	46.31	45.29	41.96	41.75	41.64	41.36	42.07	41.65	40.67	40.28	39.05	39.16	38.60	39.62
% Fe	2.81	4.32	4.06	3.37	0.32	0.32	4.83	5.26	5.09	5.24	3.99	4.83	4.65	4.71	6.46	6.56	7.83	6.41
Total**	100.00	100.00	100.00	100.00	100.00	100.00	100.00	100.00	100.00	100.00	100.00	100.00	100.00	100.00	100.00	100.00	100.00	100.00

Diopside formula = $Ca(Mg,Fe^{2+},Fe^{3+},Al)[(Si,Al)_2O_6]$, Fe^{2+} and Fe^{3+} recalculated from total FeO after the method of Droop (1987) and assigned using ideal cation sum

ND = not detected

Table H-1 EPMA analyses of pyroxene inclusions in Bo Rai ruby (continued)

Mineral phase analysis (wt%)	9TRA052-in1		9TRA057-in1		9TRA061-in1		9TRA061-in2		9TRA086-in1		9TRA086-in2		9TRA113-in1			9TRA118-in1		
SiO_2	47.46	47.53	46.58	46.58	47.01	46.77	46.76	47.12	46.97	46.75	46.97	46.75	46.16	46.80	46.52	47.60	47.60	47.60
TiO_2	0.34	0.36	0.05	0.05	0.06	0.08	0.12	0.10	0.21	0.28	0.21	0.28	0.01	0.06	0.05	0.02	0.02	0.02
Al_2O_3	13.41	13.34	15.22	15.22	14.79	15.79	14.83	14.87	14.81	14.28	14.81	14.28	14.59	14.78	14.93	14.96	14.96	14.96
Cr_2O_3	0.05	0.11	0.07	0.07	0.19	0.09	0.24	0.13	0.23	0.38	0.23	0.38	0.01	0.06	0.03	0.08	0.08	0.08
FeO total	3.32	3.29	2.68	2.68	2.32	2.40	2.48	2.45	2.94	3.01	2.94	3.01	2.81	3.03	2.98	2.94	2.94	2.94
MnO	0.04	0.04	0.04	0.04	0.01	ND	0.05	0.04	0.03	0.05	0.03	0.05	0.06	0.06	0.14	ND	ND	ND
MgO	11.69	11.60	12.35	12.35	11.64	11.96	11.42	11.45	11.67	11.84	11.67	11.84	11.85	11.94	11.96	11.82	11.82	11.82
CaO	21.67	21.63	20.38	20.38	21.43	20.98	21.58	21.77	21.59	21.25	21.59	21.25	21.81	21.00	21.03	20.80	20.80	20.80
K_2O	0.01	0.01	ND	ND	ND	0.02	ND	0.02	0.02	0.02	0.02	0.02	0.02	0.02	0.02	0.01	0.01	0.01
Na_2O	1.14	1.09	1.61	1.61	1.07	1.08	1.03	1.07	1.17	1.17	1.17	1.17	1.24	1.29	1.28	1.46	1.46	1.46
Total	99.14	99.01	98.99	98.99	98.51	99.16	98.52	98.99	99.65	99.08	99.65	99.08	98.60	99.03	98.94	99.71	99.71	99.71
6 (O)																		
Si	1.739	1.743	1.701	1.701	1.722	1.700	1.716	1.720	1.709	1.713	1.709	1.713	1.701	1.712	1.704	1.725	1.725	1.725
Ti	0.009	0.010	0.001	0.001	0.002	0.002	0.003	0.003	0.006	0.008	0.006	0.008	0.000	0.002	0.001	0.001	0.001	0.001
Al	0.579	0.576	0.655	0.655	0.639	0.676	0.642	0.640	0.635	0.617	0.635	0.617	0.634	0.637	0.645	0.639	0.639	0.639
Cr	0.001	0.003	0.002	0.002	0.006	0.003	0.007	0.004	0.007	0.011	0.007	0.011	0.000	0.002	0.001	0.002	0.002	0.002
Fe^{3+}	0.007	0.000	0.078	0.078	0.000	0.000	0.000	0.000	0.017	0.022	0.017	0.022	0.078	0.040	0.052	0.016	0.016	0.016
Fe^{2+}	0.095	0.101	0.004	0.004	0.071	0.073	0.076	0.075	0.072	0.070	0.072	0.070	0.009	0.053	0.039	0.073	0.073	0.073
Mn	0.001	0.001	0.001	0.001	0.000	0.000	0.002	0.001	0.001	0.002	0.001	0.002	0.002	0.002	0.004	0.000	0.000	0.000
Mg	0.638	0.634	0.672	0.672	0.636	0.648	0.625	0.623	0.633	0.647	0.633	0.647	0.651	0.651	0.653	0.639	0.639	0.639
Ca	0.851	0.850	0.797	0.797	0.841	0.817	0.849	0.852	0.842	0.834	0.842	0.834	0.861	0.823	0.826	0.808	0.808	0.808
K	0.000	0.000	0.000	0.000	0.000	0.001	0.000	0.001	0.001	0.001	0.001	0.001	0.001	0.001	0.001	0.000	0.000	0.000
Na	0.081	0.077	0.114	0.114	0.076	0.076	0.073	0.076	0.083	0.083	0.083	0.083	0.089	0.091	0.091	0.103	0.103	0.103
Total*	4.002	3.996	4.026	4.026	3.992	3.997	3.993	3.994	4.006	4.007	4.006	4.007	4.026	4.013	4.017	4.005	4.005	4.005
% Ca	53.72	53.63	54.11	54.11	54.33	53.12	54.77	54.97	54.43	53.77	54.43	53.77	56.61	53.90	54.41	53.16	53.16	53.16
% Mg	40.28	40.00	45.62	45.62	41.09	42.13	40.32	40.19	40.92	41.72	40.92	41.72	42.80	42.63	43.02	42.04	42.04	42.04
% Fe	6.00	6.37	0.27	0.27	4.59	4.75	4.90	4.84	4.65	4.51	4.65	4.51	0.59	3.47	2.57	4.80	4.80	4.80
Total**	100.00	100.00	100.00	100.00	100.00	100.00	100.00	100.00	100.00	100.00	100.00	100.00	100.00	100.00	100.00	100.00	100.00	100.00

Diopside formula = $Ca(Mg,Fe^{2+},Fe^{3+},Al)[(Si,Al)_2O_6]$, Fe^{2+} and Fe^{3+} recalculated from total FeO after the method of Droop (1987) and assigned using ideal cation sum
ND = not detected

Table H-1 EPMA analyses of pyroxene inclusions in Bo Rai ruby (continued)

Mineral phase analysis (wt%)	9TRA118-in2		9TRA124-in1		9TRA126-in1		9TRA126-in2			9TRA126-in3			9TRA156-in1			9TRA195-in1		9TRA218-in2
SiO_2	46.85	46.89	46.16	45.86	47.79	47.05	47.48	48.37	48.62	48.14	47.60	48.36	46.80	47.21	47.56	47.41	46.47	47.08
TiO_2	0.03	0.04	0.08	0.09	ND	0.07	0.06	0.04	ND	0.06	0.03	0.09	0.61	0.57	0.60	0.02	0.12	0.11
Al_2O_3	14.50	15.13	15.81	15.90	14.37	16.71	14.31	14.25	14.23	14.10	14.24	14.25	14.58	14.38	14.15	14.96	14.84	14.63
Cr_2O_3	0.04	0.06	0.13	0.05	0.05	0.09	0.05	0.02	0.17	0.07	0.08	0.06	0.08	0.06	0.07	0.09	0.05	0.08
FeO	3.39	2.98	2.79	2.89	2.12	2.06	2.23	2.07	2.21	2.18	2.30	2.10	3.45	3.55	3.51	2.80	2.70	2.28
MnO	0.08	ND	0.02	0.06	0.04	ND	ND	0.04	0.01	0.06	ND	0.02	0.02	0.09	0.05	ND	0.04	0.05
MgO	11.97	11.81	11.10	11.27	11.75	12.95	12.91	11.87	12.68	12.53	12.47	12.36	11.08	11.04	11.01	11.51	11.43	11.87
CaO	20.98	20.46	22.24	21.84	21.55	20.97	21.19	21.19	21.13	21.50	21.00	21.34	21.81	21.66	21.47	21.90	21.94	21.97
K_2O	0.01	0.02	0.02	0.02	0.03	0.01	0.01	0.02	0.02	ND	0.02	0.02	0.03	ND	ND	0.01	0.01	0.01
Na_2O	1.44	1.44	0.87	0.84	1.01	0.98	1.05	1.09	1.03	1.08	1.05	1.04	1.35	1.36	1.41	0.90	0.88	0.97
Total	99.29	98.82	99.21	98.82	98.75	100.91	99.29	98.95	100.09	99.71	98.82	99.68	99.80	99.91	99.81	99.63	98.51	99.05
6 (O)																		
Si	1.713	1.715	1.687	1.683	1.744	1.677	1.724	1.756	1.747	1.740	1.736	1.746	1.707	1.719	1.731	1.721	1.709	1.718
Ti	0.001	0.001	0.002	0.002	0.000	0.002	0.002	0.001	0.000	0.002	0.001	0.002	0.017	0.016	0.016	0.001	0.003	0.003
Al	0.625	0.652	0.681	0.688	0.618	0.702	0.612	0.610	0.603	0.601	0.612	0.606	0.627	0.617	0.607	0.640	0.643	0.629
Cr	0.001	0.002	0.004	0.001	0.001	0.003	0.001	0.001	0.005	0.002	0.002	0.002	0.002	0.002	0.002	0.003	0.001	0.002
Fe^{3+}	0.071	0.027	0.000	0.002	0.000	0.008	0.014	0.000	0.000	0.000	0.000	0.000	0.031	0.013	0.000	0.000	0.000	0.000
Fe^{2+}	0.032	0.064	0.085	0.087	0.065	0.054	0.054	0.063	0.066	0.066	0.070	0.063	0.075	0.096	0.107	0.085	0.083	0.070
Mn	0.002	0.000	0.001	0.002	0.001	0.000	0.000	0.001	0.000	0.002	0.000	0.001	0.001	0.003	0.002	0.000	0.001	0.002
Mg	0.653	0.644	0.605	0.616	0.639	0.688	0.699	0.642	0.679	0.675	0.678	0.665	0.602	0.599	0.597	0.623	0.627	0.646
Ca	0.822	0.802	0.871	0.859	0.842	0.801	0.824	0.824	0.813	0.833	0.820	0.825	0.852	0.845	0.837	0.852	0.865	0.859
K	0.000	0.001	0.001	0.001	0.001	0.000	0.000	0.001	0.001	0.000	0.001	0.001	0.001	0.000	0.000	0.000	0.000	0.000
Na	0.102	0.102	0.062	0.060	0.071	0.068	0.074	0.077	0.072	0.076	0.074	0.073	0.095	0.096	0.099	0.063	0.063	0.069
Total*	4.024	4.009	3.999	4.001	3.983	4.003	4.005	3.976	3.986	3.995	3.994	3.985	4.010	4.004	3.998	3.989	3.997	3.998
% Ca	54.55	53.11	55.80	54.99	54.46	51.91	52.25	53.89	52.18	52.92	52.30	53.12	55.72	54.87	54.32	54.62	54.92	54.54
% Mg	43.33	42.65	38.76	39.44	41.33	44.59	44.32	41.99	43.58	42.88	43.24	42.82	39.37	38.90	38.74	39.94	39.81	41.02
% Fe	2.12	4.24	5.45	5.57	4.20	3.50	3.42	4.12	4.24	4.19	4.46	4.06	4.91	6.23	6.94	5.45	5.27	4.44
Total**	100.00	100.00	100.00	100.00	100.00	100.00	100.00	100.00	100.00	100.00	100.00	100.00	100.00	100.00	100.00	100.00	100.00	100.00

Diopside formula = $Ca(Mg,Fe^{2+},Fe^{3+},Al)[(Si,Al)_2O_6]$, Fe^{2+} and Fe^{3+} recalculated from total FeO after the method of Droop (1987) and assigned using ideal cation sum
ND = not detected

Table H-2 EPMA analyses of feldspar inclusions in Bo Rai ruby

Mineral phase analysis (wt%)	9TRA017-in1			9TRA171-in8		9TRA219-in2		9TRA031-in1	
SiO_2	47.20	47.03	46.78	45.11	45.34	46.31	49.76	57.43	58.17
TiO_2	ND	ND	0.01	0.02	0.01	ND	0.02	0.05	0.08
Al_2O_3	33.36	33.34	33.62	34.05	33.87	34.47	31.49	24.86	24.72
Cr_2O_3	0.04	ND	0.03	0.01	ND	ND	0.01	0.05	ND
Ga_2O_3	ND	0.03	ND	ND	0.02	ND	0.03	0.05	ND
V2O3	ND	0.03	ND	ND	0.01	0.01	ND	0.02	0.01
FeO	0.13	0.14	0.18	0.42	0.42	0.22	0.71	0.31	0.46
MnO	ND	ND	0.01	0.06	0.03	ND	0.03	ND	0.02
MgO	0.01	0.04	0.03	ND	ND	0.07	0.21	0.06	0.64
CaO	17.52	17.60	17.58	18.26	18.13	17.02	14.15	7.86	7.52
K_2O	0.02	0.03	0.01	0.02	0.02	0.03	0.12	1.05	1.05
Na_2O	1.68	1.71	1.69	1.53	1.48	1.14	2.33	6.74	6.02
Total	99.95	99.95	99.94	99.49	99.31	99.27	98.86	98.47	98.68
8(O)									
Si	2.171	2.165	2.154	2.099	2.111	2.139	2.292	2.626	2.643
Ti	0.000	0.000	0.000	0.001	0.000	0.000	0.001	0.002	0.003
Al	1.808	1.809	1.825	1.867	1.858	1.876	1.709	1.339	1.324
Cr	0.001	0.000	0.001	0.000	0.000	0.000	0.000	0.002	0.000
Ga	0.000	0.001	0.000	0.000	0.001	0.000	0.001	0.002	0.000
V	0.000	0.001	0.000	0.000	0.000	0.000	0.000	0.001	0.000
Fe	0.005	0.006	0.007	0.016	0.016	0.008	0.027	0.012	0.017
Mn	0.000	0.000	0.000	0.002	0.001	0.000	0.001	0.000	0.001
Mg	0.001	0.003	0.002	0.000	0.000	0.005	0.014	0.004	0.043
Ca	0.863	0.868	0.867	0.910	0.905	0.842	0.698	0.385	0.366
K	0.001	0.002	0.001	0.001	0.001	0.002	0.007	0.061	0.061
Na	0.149	0.153	0.151	0.138	0.134	0.102	0.208	0.597	0.530
Total*	5.000	5.007	5.009	5.036	5.027	4.975	4.960	5.030	4.988
Atomic%									
Ca	85.19	84.85	85.08	86.75	87.02	89.01	76.45	36.91	38.24
K	0.10	0.20	0.10	0.10	0.10	0.21	0.77	5.85	6.37
Na	14.71	14.96	14.82	13.16	12.88	10.78	22.78	57.24	55.38
Total**	100.00	100.00	100.00	100.00	100.00	100.00	100.00	100.0	100.00

ND = not detected

Table H-3 EPMA analyses of sillimanite with spinel inclusions in Bo Rai ruby

Mineral phase analysis (wt%)	Sillimanite			
	9TRA169-in1		9TRA024-in1	
SiO_2	31.49	36.60	36.49	36.37
TiO_2	0.04	ND	ND	ND
Al_2O_3	66.68	62.42	62.24	62.27
Cr_2O_3	0.05	0.02	0.21	0.23
Ga_2O_3	0.07	0.01	ND	0.07
V_2O_3	ND	0.02	0.01	0.04
FeO	0.48	0.39	0.73	0.78
MnO	ND	ND	0.01	ND
MgO	0.06	0.07	0.12	0.07
CaO	0.15	0.27	0.16	0.14
K_2O	0.19	0.18	0.08	0.07
Na_2O	0.01	0.03	0.03	ND
Total	99.20	100.00	100.08	100.05
20 (O)				
Si	3.801	3.968	3.959	3.950
Ti	0.083	0.000	0.000	0.000
Al	7.949	7.977	7.959	7.970
Cr	0.006	0.002	0.018	0.020
Ga	0.015	0.001	0.000	0.005
V	0.000	0.001	0.001	0.003
Fe	0.059	0.035	0.066	0.071
Mn	0.000	0.000	0.001	0.000
Mg	0.007	0.011	0.019	0.011
Ca	0.201	0.031	0.019	0.016
K	0.011	0.025	0.011	0.010
Na	0.009	0.005	0.006	0.000
Total*	12.141	12.057	12.060	12.056

ND = not detected

Mineral phase analysis (wt%)	Spinel		
	9TRA024-in2		
SiO_2	0.09	0.72	0.01
TiO_2	ND	ND	0.26
Al_2O_3	67.59	68.52	64.96
Cr_2O_3	1.41	0.66	0.40
Ga_2O_3	0.04	0.03	ND
V_2O_3	0.02	ND	0.02
FeO total	8.12	7.56	13.55
MnO	0.03	0.01	ND
MgO	22.59	22.25	20.38
CaO	ND	0.16	0.04
ZnO	NA	NA	0.04
K_2O	0.01	0.03	0.02
Na_2O	0.01	0.06	0.01
Total	99.92	99.99	99.68
4 (O)			
Si	0.002	0.018	0.000
Ti	0.000	0.000	0.005
Al	1.968	1.980	2.151
Cr	0.028	0.013	0.009
Ga	0.001	0.000	0.000
V	0.000	0.000	0.000
Fe^{3+}	0.000	0.000	0.235
Fe^{2+}	0.168	0.155	0.323
Mn	0.001	0.000	0.000
Mg	0.832	0.813	0.423
Zn	0.000	0.000	0.001
Ca	0.000	0.004	-0.234
K	0.000	0.001	0.001
Na	0.000	0.003	0.001
Total*	3.000	2.988	2.915

NA = not analyzed, ND = not detected

Table H-4 EPMA analyses of garnet inclusions in Bo Rai ruby

Mineral phase analysis (wt%)	9TRA029-in1			9TRA049-in1			9TRA053-in1		9TRA053-in2		9TRA206-in3		9TRA215-in1			9TRA218-in1	
SiO_2	41.58	41.78	41.45	41.77	42.16	42.68	42.56	42.39	42.50	41.94	41.88	41.62	41.95	42.17	42.07	41.43	42.03
TiO_2	0.03	0.03	0.05	0.02	0.04	0.04	0.01	0.03	ND	0.03	0.01	0.01	0.05	0.07	0.05	0.02	0.01
Al_2O_3	23.04	22.99	23.09	23.01	23.44	23.26	23.30	23.29	23.26	23.32	22.65	23.01	23.30	23.10	23.39	24.12	23.31
Cr_2O_3	ND	ND	0.02	0.18	0.18	0.12	0.06	0.03	0.08	0.10	0.05	0.07	0.08	0.04	0.09	0.10	0.06
FeO total	11.07	10.99	11.29	6.55	6.71	6.64	7.09	7.20	7.02	7.05	7.21	7.28	9.50	9.59	9.27	6.29	6.32
MnO	0.19	0.11	0.23	0.20	0.09	0.17	0.22	0.18	0.18	0.16	0.20	0.25	0.19	0.21	0.19	0.12	0.15
MgO	15.67	15.27	15.65	18.33	18.23	18.38	17.97	18.05	18.50	18.27	17.21	17.08	15.69	15.67	15.69	18.71	18.08
CaO	8.33	8.65	8.58	8.78	8.57	8.78	8.48	8.56	8.39	8.35	9.43	9.58	9.45	9.38	9.33	9.90	8.64
K_2O	ND	ND	0.01	ND	ND	ND	ND	0.01	ND	ND	ND	ND	0.01	ND	ND	ND	ND
Na_2O	ND	0.02	ND	0.02	ND	0.01	0.02	ND	ND	0.02	ND	ND	ND	ND	ND	ND	0.02
Total	99.91	99.83	100.36	98.85	99.41	100.07	99.70	99.73	99.73	99.73	99.73	99.73	100.22	100.23	100.07	99.73	99.73
12 (O)																	
Si	3.012	3.028	2.997	3.004	3.010	3.028	3.033	3.022	3.021	3.005	3.030	3.008	3.016	3.031	3.023	2.933	3.020
Ti	0.002	0.002	0.003	0.001	0.002	0.002	0.001	0.002	0.000	0.002	0.001	0.000	0.003	0.004	0.003	0.001	0.001
Al	1.967	1.964	1.967	1.950	1.973	1.944	1.957	1.958	1.948	1.969	1.932	1.960	1.975	1.957	1.981	2.012	1.974
Cr	0.000	0.000	0.001	0.010	0.010	0.007	0.004	0.002	0.005	0.006	0.003	0.004	0.005	0.002	0.005	0.006	0.003
Fe^{3+}	0.008	0.000	0.051	0.048	0.000	0.000	0.000	0.000	0.007	0.023	0.005	0.030	0.000	0.000	0.000	0.169	0.000
Fe^{2+}	0.663	0.666	0.631	0.346	0.400	0.394	0.422	0.429	0.411	0.399	0.432	0.410	0.571	0.577	0.557	0.203	0.380
Mn	0.011	0.007	0.014	0.012	0.006	0.010	0.013	0.011	0.011	0.010	0.012	0.016	0.012	0.013	0.012	0.007	0.009
Mg	1.693	1.650	1.687	1.965	1.941	1.943	1.908	1.919	1.960	1.951	1.856	1.841	1.682	1.679	1.681	1.974	1.937
Ca	0.646	0.672	0.665	0.677	0.655	0.668	0.647	0.654	0.639	0.641	0.731	0.742	0.728	0.722	0.718	0.751	0.665
K	0.000	0.000	0.001	0.000	0.000	0.000	0.000	0.001	0.000	0.000	0.000	0.000	0.001	0.000	0.000	0.000	0.000
Na	0.000	0.002	0.000	0.003	0.000	0.001	0.002	0.000	0.000	0.003	0.000	0.000	0.000	0.000	0.000	0.000	0.003
Total*	8.003	7.990	8.017	8.016	7.997	7.996	7.987	7.997	8.002	8.008	8.002	8.010	7.992	7.985	7.981	8.057	7.992
ΣR^{2+}	3.013	2.995	2.997	3.000	3.002	3.015	2.991	3.013	3.021	3.001	3.031	3.008	2.993	2.991	2.968	2.935	2.991
ΣR^{3+}	1.977	1.965	2.022	2.009	1.985	1.952	1.961	1.961	1.960	2.000	1.940	1.994	1.982	1.963	1.989	2.188	1.978
Mg/(Mg+Fe^{2+})	0.719	0.712	0.728	0.850	0.829	0.831	0.819	0.817	0.827	0.830	0.811	0.818	0.746	0.744	0.751	0.907	0.836
Alm% (Fe^{2+})	22.00	22.24	21.05	11.53	13.32	13.07	14.11	14.24	13.60	13.30	14.25	13.63	19.08	19.29	18.77	6.92	12.70
Pyr% (Mg)	56.19	55.09	56.29	65.50	64.66	64.44	63.81	63.69	64.88	65.01	61.23	61.18	56.20	56.14	56.64	67.26	64.76
Gro% (Ca)	21.33	22.41	21.59	21.90	21.69	22.05	21.58	21.66	21.02	21.03	24.01	24.24	24.23	24.07	24.09	23.53	22.19
Sps% (Mn)	0.37	0.23	0.47	0.40	0.20	0.33	0.43	0.37	0.36	0.33	0.40	0.53	0.40	0.43	0.40	0.24	0.30
Uv%	0.00	0.00	0.01	0.11	0.11	0.08	0.04	0.02	0.05	0.06	0.04	0.05	0.06	0.02	0.06	0.07	0.03
And%	0.09	0.00	0.56	0.54	0.00	0.00	0.00	0.00	0.08	0.25	0.06	0.37	0.00	0.00	0.00	1.98	0.00
Ca-Ti Gt	0.02	0.02	0.03	0.01	0.02	0.02	0.01	0.02	0.00	0.02	0.01	0.00	0.04	0.05	0.04	0.01	0.01

ΣR^{2+}= Fe^{2+}+Mn+Mg+Ca , ΣR^{3+}= Fe^{3+}+Ti+Al+Cr
ND = not detected

Table H-5 EPMA analyses of pyrrhotite inclusions in Bo Rai ruby

Mineral phase analysis (wt%)	9TRA214-in1		9TRA160-in1		9TRA176-in1		9TRA202-in1		9TRA208-in1		9TRA055-in1		9TRA231-in1	
Tl	0.29	ND	ND	ND	0.04	ND	0.14	0.30	0.21	0.27	0.32	0.37	0.29	0.18
Al	0.09	0.03	0.05	0.04	0.06	0.29	0.03	0.03	0.05	0.02	0.03	0.04	0.07	0.11
In	0.01	ND	ND	ND	ND	ND	ND	ND	0.05	ND	ND	ND	0.01	ND
Ba	0.28	0.23	0.35	0.35	0.27	0.18	ND	0.11	0.22	0.14	ND	ND	ND	ND
Fe	9.39	9.15	11.65	9.19	9.21	8.65	29.58	31.21	21.61	21.12	33.76	34.68	45.74	42.42
S	18.71	17.96	19.66	19.35	14.93	15.15	25.16	26.49	22.12	22.14	27.67	27.72	21.49	25.34
As	ND	ND	ND	NA	ND	0.03	0.02	ND	ND	ND	NA	NA	NA	NA
Pb	ND	ND	NA	ND	ND	ND	ND	ND	ND	ND	ND	ND	ND	ND
Cu	62.17	61.49	57.79	64.39	51.69	48.16	15.35	18.32	42.88	42.00	ND	0.03	0.47	1.05
Ni	0.06	0.12	0.02	0.06	4.59	4.22	15.82	11.67	0.14	0.08	23.22	22.63	4.42	4.58
Mo	0.23	0.36	0.28	0.39	0.43	0.26	0.59	0.45	0.44	0.40	0.56	0.42	0.24	0.44
Pt	ND	0.01	ND	ND	ND	ND	ND	0.04	ND	ND	0.10	0.02	ND	0.14
Sn	ND	ND	0.01	NA	ND	ND	ND	ND	ND	0.02	NA	NA	NA	NA
Zn	ND	ND	ND	NA	ND	0.29	ND	ND	ND	ND	NA	NA	NA	NA
Co	ND	ND	ND	NA	ND	ND	ND	ND	ND	ND	NA	NA	NA	NA
Total*	91.24	89.35	89.81	93.78	81.22	77.21	86.69	88.63	87.71	86.195	85.64	85.90	72.74	74.25
Formula														
Tl	0.008	0.000	0.000	0.000	0.001	0.000	0.001	0.003	0.003	0.003	0.014	0.017	0.002	0.001
Al	0.020	0.006	0.015	0.012	0.014	0.068	0.002	0.002	0.004	0.002	0.010	0.013	0.003	0.005
In	0.001	0.000	0.000	0.000	0.000	0.000	0.000	0.000	0.001	0.000	0.000	0.000	0.000	0.000
Ba	0.012	0.010	0.021	0.021	0.012	0.008	0.000	0.001	0.004	0.003	0.000	0.000	0.000	0.000
Fe	1.000	1.000	1.702	1.364	1.000	1.000	1.000	1.000	1.000	1.000	5.604	5.747	1.000	1.000
S	3.472	3.421	5.000	5.000	2.824	3.051	1.481	1.478	1.782	1.826	8.000	8.000	0.818	1.040
As	0.000	0.000	0.000	0.000	0.000	0.003	0.001	0.000	0.000	0.000	0.000	0.000	NA	NA
Pb	0.000	0.000	0.000	0.000	0.000	0.000	0.000	0.000	0.000	0.000	0.000	0.000	0.000	0.000
Cu	5.821	5.909	7.417	8.395	4.933	4.895	0.456	0.516	1.744	1.748	0.000	0.004	0.009	0.022
Ni	0.006	0.012	0.003	0.008	0.474	0.464	0.509	0.356	0.006	0.004	3.667	3.568	0.092	0.103
Mo	0.014	0.023	0.024	0.033	0.027	0.018	0.012	0.008	0.012	0.011	0.054	0.040	0.003	0.006
Pt	0.000	0.000	0.000	0.000	0.000	0.000	0.000	0.000	0.000	0.000	0.005	0.001	0.000	0.001
Sn	0.000	0.000	0.001	0.000	0.000	0.000	0.000	0.000	0.000	0.000	0.002	0.002	NA	NA
Zn	0.000	0.000	0.000	0.000	0.000	0.028	0.000	0.000	0.000	0.000	0.000	0.000	NA	NA
Co	0.000	0.000	0.000	0.000	0.000	0.000	0.000	0.000	0.000	0.000	0.000	0.000	NA	NA
Total**	10.354	10.382	14.183	14.833	9.285	9.535	3.462	3.365	4.556	4.597	17.354	17.390	1.928	2.178

NA = not analyzed, ND = not detected

Table H-6 EPMA analyses of two-phase inclusions in Bo Rai ruby.

Mineral phase analysis (wt%)	9TRA073-in1	9TRA195-in3
SiO_2	56.51	48.54
TiO_2	0.10	0.07
Al_2O_3	26.44	31.86
Cr_2O_3	0.03	0.01
FeO	2.00	1.55
MnO	0.02	0.03
MgO	3.19	2.96
CaO	9.65	11.09
K_2O	0.44	1.26
Na_2O	0.75	1.37
Total	99.13	98.74
Formula		
Si	0.941	0.808
Ti	0.001	0.001
Al	0.519	0.625
Cr	0.000	0.000
Fe	0.028	0.022
Mn	0.000	0.000
Mg	0.079	0.073
Ca	0.172	0.198
K	0.009	0.027
Na	0.024	0.044
Total*	1.773	1.798

Table H-7 EPMA analyses of pyroxene inclusions in Bo Welu ruby

Mineral phase analysis (wt%)	9TWL011-in1		9TWL020-in1			9TWL020-in2			9TWL020-in3		9TWL021-in1		9TWL023-in1		9TWL029-in1		9TWL035-in1	
SiO_2	45.92	46.09	47.58	47.84	47.85	47.47	48.17	47.72	48.42	46.81	46.55	46.05	48.39	48.51	44.85	44.70	49.28	50.02
TiO_2	0.13	0.61	0.38	0.39	0.30	0.27	0.35	0.34	0.39	0.32	0.14	0.18	0.11	0.12	0.24	0.22	0.75	0.72
Al_2O_3	14.78	14.32	15.23	15.41	15.42	15.12	15.20	15.02	15.38	14.85	15.98	16.29	14.69	14.73	16.50	15.51	8.82	9.00
Cr_2O_3	0.51	0.51	0.29	0.21	0.15	0.19	0.15	0.20	0.06	0.15	0.18	0.25	0.13	0.09	0.17	0.16	0.13	0.09
FeO	2.86	3.48	3.59	3.69	3.74	3.51	3.70	3.59	3.33	3.32	2.99	3.09	2.39	2.46	3.04	2.97	3.28	3.28
MnO	0.06	ND	0.01	0.01	ND	0.06	0.03	0.05	0.03	0.03	0.10	0.09	0.08	0.01	ND	ND	0.01	0.02
MgO	11.95	10.78	10.28	9.98	9.08	9.42	9.55	9.86	9.29	9.10	9.48	10.71	10.54	10.52	11.41	11.72	12.88	12.81
CaO	22.11	22.71	21.30	21.20	21.77	22.51	21.50	21.65	21.45	23.18	22.11	21.97	22.39	22.45	22.52	23.05	23.99	23.30
K_2O	0.01	ND	0.02	ND	0.02	ND	0.02	0.01	0.01	0.01	ND	0.01	ND	0.02	0.02	ND	ND	0.01
Na_2O	1.57	1.27	1.23	1.26	1.65	1.40	1.31	1.27	1.54	1.22	1.13	1.66	1.07	0.98	1.11	1.19	0.76	0.74
Total	99.90	99.76	99.90	99.98	99.99	99.95	99.97	99.70	99.90	99.00	98.66	100.29	99.80	99.90	99.85	99.53	99.90	100.00
6 (O)																		
Si	1.678	1.691	1.727	1.733	1.738	1.728	1.745	1.736	1.752	1.724	1.711	1.672	1.750	1.752	1.639	1.644	1.805	1.822
Ti	0.003	0.017	0.010	0.011	0.008	0.007	0.009	0.009	0.011	0.009	0.004	0.005	0.003	0.003	0.006	0.006	0.021	0.020
Al	0.636	0.619	0.651	0.658	0.660	0.649	0.649	0.644	0.656	0.645	0.692	0.697	0.626	0.627	0.711	0.672	0.381	0.386
Cr	0.015	0.015	0.008	0.006	0.004	0.005	0.004	0.006	0.002	0.004	0.005	0.007	0.004	0.003	0.005	0.005	0.004	0.003
Fe^{3+}	0.147	0.062	0.000	0.000	0.000	0.000	0.000	0.000	0.000	0.000	0.000	0.088	0.000	0.000	0.110	0.160	0.027	0.000
Fe^{2+}	0.000	0.045	0.109	0.112	0.114	0.107	0.112	0.109	0.101	0.102	0.092	0.006	0.072	0.074	0.000	0.000	0.073	0.100
Mn	0.002	0.000	0.000	0.000	0.000	0.002	0.001	0.002	0.001	0.001	0.003	0.003	0.002	0.000	0.000	0.000	0.000	0.001
Mg	0.651	0.589	0.556	0.539	0.492	0.512	0.516	0.535	0.501	0.500	0.520	0.580	0.568	0.566	0.622	0.642	0.703	0.696
Ca	0.865	0.893	0.828	0.823	0.847	0.878	0.835	0.844	0.831	0.915	0.870	0.855	0.868	0.869	0.882	0.908	0.942	0.910
K	0.001	0.000	0.001	0.000	0.001	0.000	0.001	0.000	0.000	0.001	0.000	0.001	0.000	0.001	0.001	0.000	0.000	0.001
Na	0.111	0.091	0.087	0.088	0.116	0.099	0.092	0.090	0.108	0.087	0.080	0.117	0.075	0.069	0.079	0.085	0.054	0.052
Total*	4.049	4.021	3.977	3.969	3.980	3.987	3.965	3.975	3.963	3.987	3.977	4.030	3.969	3.965	4.037	4.054	4.009	3.990
% Ca	57.06	58.48	55.46	55.83	58.29	58.65	57.07	56.72	57.99	60.32	58.70	59.33	57.56	57.59	58.64	58.58	54.83	53.34
% Mg	42.94	38.57	37.24	36.57	33.86	34.20	35.27	35.95	34.96	32.96	35.09	40.25	37.67	37.51	41.36	41.42	40.92	40.80
% Fe	0.00	2.95	7.30	7.60	7.85	7.15	7.66	7.33	7.05	6.72	6.21	0.42	4.77	4.90	0.00	0.00	4.25	5.86
Total**	100.00	100.00	100.00	100.00	100.00	100.00	100.00	100.00	100.00	100.00	100.00	100.00	100.00	100.00	100.00	100.00	100.00	100.00

Diopside formula = $Ca(Mg,Fe^{2+},Fe^{3+},Al)[(Si,Al)_2O_6]$, Fe^{2+} and Fe^{3+} recalculated from total FeO after the method of Droop (1987) and assigned using ideal cation sum
ND = not detected

Table H-7 EPMA analyses of pyroxene inclusions in Bo Welu ruby (continued)

Mineral phase analysis (wt%)	9TWL053-in2		9TWL086-in1		9TWL086-in2		9TWL086-in3		9TWL095-in1		9TWL099-in1		9TWL105-in1		9TWL105-in2	
SiO_2	46.75	46.71	47.27	47.43	47.08	46.85	46.56	47.14	45.98	45.57	46.33	46.25	45.36	45.17	44.72	44.82
TiO_2	0.16	0.19	0.83	0.85	0.86	0.83	0.76	0.70	0.25	0.25	0.24	0.25	0.19	0.19	0.22	0.21
Al_2O_3	15.44	15.90	13.64	13.50	13.31	13.16	13.34	13.27	15.31	15.38	14.40	14.31	15.83	16.05	16.15	16.16
Cr_2O_3	0.04	0.07	0.02	0.04	0.01	0.13	0.05	0.07	0.12	0.14	0.11	0.12	0.10	0.06	0.09	0.07
FeO total	2.93	3.14	3.31	3.41	3.37	3.30	3.38	3.17	2.88	2.87	3.53	3.56	3.17	3.18	3.13	3.23
MnO	ND	0.04	0.05	0.01	ND	0.05	0.02	0.02	0.01	0.06	0.05	0.04	ND	0.07	0.07	0.07
MgO	10.45	10.14	11.58	11.46	11.21	11.27	11.45	11.11	11.64	11.34	11.41	11.58	11.36	11.38	11.44	11.38
CaO	22.06	21.54	22.06	22.09	21.88	21.80	22.03	21.92	22.10	22.16	22.33	22.30	22.80	22.89	23.07	22.97
K_2O	0.01	0.01	ND	ND	ND	ND	ND	ND	ND	ND	0.02	0.02	ND	ND	ND	0.03
Na_2O	1.22	1.25	1.21	1.19	1.20	1.17	1.17	1.17	1.66	1.62	1.49	1.50	0.95	0.93	0.98	0.99
Total	99.07	99.00	99.97	99.99	98.90	98.54	98.76	98.57	99.95	99.39	99.90	99.93	99.76	99.92	99.88	99.91
6 (O)																
Si	1.711	1.709	1.721	1.726	1.732	1.731	1.719	1.738	1.676	1.672	1.695	1.693	1.659	1.651	1.638	1.641
Ti	0.004	0.005	0.023	0.023	0.024	0.023	0.021	0.019	0.007	0.007	0.007	0.007	0.005	0.005	0.006	0.006
Al	0.666	0.686	0.585	0.579	0.577	0.573	0.580	0.577	0.658	0.665	0.621	0.617	0.682	0.691	0.697	0.697
Cr	0.001	0.002	0.001	0.001	0.000	0.004	0.001	0.002	0.003	0.004	0.003	0.004	0.003	0.002	0.003	0.002
Fe^{3+}	0.000	0.000	0.018	0.006	0.000	0.001	0.035	0.000	0.134	0.131	0.116	0.130	0.081	0.091	0.123	0.119
Fe^{2+}	0.090	0.096	0.083	0.098	0.104	0.101	0.070	0.098	0.000	0.000	0.000	0.000	0.016	0.006	0.000	0.000
Mn	0.000	0.001	0.001	0.000	0.000	0.001	0.001	0.001	0.000	0.002	0.002	0.001	0.000	0.002	0.002	0.002
Mg	0.570	0.553	0.629	0.622	0.614	0.620	0.630	0.611	0.632	0.620	0.622	0.632	0.620	0.620	0.625	0.621
Ca	0.865	0.845	0.860	0.861	0.862	0.863	0.871	0.866	0.863	0.871	0.875	0.874	0.893	0.896	0.905	0.901
K	0.001	0.001	0.000	0.000	0.000	0.000	0.000	0.000	0.000	0.000	0.001	0.001	0.000	0.000	0.000	0.002
Na	0.087	0.089	0.085	0.084	0.086	0.084	0.084	0.083	0.118	0.115	0.105	0.106	0.068	0.066	0.070	0.070
Total*	3.995	3.986	4.006	4.002	3.999	4.000	4.012	3.995	4.045	4.044	4.039	4.044	4.027	4.031	4.041	4.040
% Ca	56.72	56.56	54.71	54.46	54.56	54.48	55.44	54.98	57.73	58.42	58.45	58.03	58.40	58.87	59.15	59.20
% Mg	37.38	37.01	40.01	39.34	38.86	39.14	40.10	38.79	42.27	41.58	41.55	41.97	40.55	40.74	40.85	40.80
% Fe	5.90	6.43	5.28	6.20	6.58	6.38	4.46	6.22	0.00	0.00	0.00	0.00	1.05	0.39	0.00	0.00
Total**	100.00	100.00	100.00	100.00	100.00	100.00	100.00	100.00	100.00	100.00	100.00	100.00	100.00	100.00	100.00	100.00

Diopside formula = $Ca(Mg,Fe^{2+},Fe^{3+},Al)[(Si,Al)_2O_6]$, Fe2+ and Fe3+ recalculated from total FeO after the method of Droop (1987) and assigned using ideal cation

ND = not detected

Table H-8 EPMA analyses of feldspar inclusions in Bo Welu ruby

Mineral phase analysis (wt%)	9TWL007 -In1	9TWL118- in1	9TWL122-in3		9TWL122-in4		9TWL012-in2		9TWL053 -in1	9TWL055 -in1	9TWL176 -in1	9TWL178 -in1	9TWL154 -in1*	9TWL019-in1*		9TWL180-in1*	
SiO_2	53.31	51.61	49.18	49.27	48.61	48.86	64.91	65.42	58.21	58.02	61.34	60.45	55.99	54.1	54.63	52.0	52.16
TiO_2	0.04	0.17	ND	0.02	ND	ND	0.03	0.15	0.09	0.04	0.07	0.02	0.03	ND	0.01	ND	ND
Al_2O_3	28.84	29.54	31.71	31.48	32.46	32.41	21.54	21.15	26.30	26.36	23.67	24.72	26.97	29.1	28.49	30.7	29.91
Cr_2O_3	0.05	0.05	0.06	ND	ND	ND	0.05	0.05	ND	ND	ND	ND	0.03	0.01	0.05	0.12	0.07
Ga_2O_3	0.04	0.04	0.04	0.03	ND	0.01	0.01	ND	ND	ND	ND	0.01	0.05	ND	0.04	0.02	0.12
V_2O_3	0.02	0.01	0.01	ND	ND	ND	ND	0.04	ND	0.04	ND	ND	0.02	ND	ND	ND	0.05
FeO	0.13	0.09	0.12	0.14	0.07	0.11	0.12	0.33	0.01	0.09	0.46	0.23	0.25	0.24	0.23	0.39	0.87
MnO	ND	ND	0.02	ND	0.03	ND	0.01	ND	ND	0.04	ND	0.01	ND	0.04	0.04	0.09	0.13
MgO	ND	ND	0.02	0.14	0.03	0.03	ND	0.02	0.27	0.05	0.20	ND	0.03	ND	0.03	0.02	0.08
CaO	12.08	11.16	16.45	16.35	16.51	16.32	1.48	1.96	7.38	7.30	6.29	8.83	11.04	10.6	10.24	12.0	12.02
K_2O	0.47	3.50	0.01	0.01	0.12	0.09	3.08	3.08	1.22	1.35	0.07	0.04	0.02	0.17	0.27	ND	ND
Na_2O	4.97	3.59	2.31	2.32	2.14	2.16	7.71	7.65	6.69	6.66	7.76	5.64	5.51	5.60	5.96	4.00	4.04
Total	99.95	99.76	99.94	99.77	99.96	99.98	98.95	99.84	100.17	99.95	99.87	99.93	99.94	99.9	99.99	99.4	99.44
8 (O)																	
Si	2.424	2.379	2.254	2.261	2.228	2.236	2.899	2.902	2.607	2.606	2.732	2.690	2.527	2.44	2.470	2.36	2.382
Ti	0.001	0.006	0.000	0.001	0.000	0.000	0.001	0.005	0.003	0.001	0.002	0.001	0.001	0.00	0.000	0.00	0.000
Al	1.545	1.605	1.713	1.702	1.753	1.748	1.134	1.106	1.388	1.396	1.243	1.296	1.435	1.55	1.518	1.64	1.609
Cr	0.002	0.002	0.002	0.000	0.000	0.000	0.002	0.002	0.000	0.000	0.000	0.000	0.001	0.00	0.002	0.00	0.003
Ga	0.001	0.001	0.001	0.001	0.000	0.000	0.000	0.000	0.000	0.000	0.000	0.000	0.001	0.00	0.001	0.00	0.003
V	0.001	0.000	0.000	0.000	0.000	0.000	0.000	0.001	0.000	0.001	0.000	0.000	0.001	0.00	0.000	0.00	0.002
Fe	0.005	0.003	0.005	0.006	0.003	0.004	0.004	0.012	0.000	0.004	0.017	0.009	0.010	0.00	0.009	0.01	0.033
Mn	0.000	0.000	0.001	0.000	0.001	0.000	0.000	0.000	0.000	0.002	0.000	0.000	0.000	0.00	0.001	0.00	0.005
Mg	0.000	0.000	0.001	0.010	0.002	0.002	0.000	0.001	0.018	0.003	0.013	0.000	0.002	0.00	0.002	0.00	0.005
Ca	0.588	0.551	0.808	0.804	0.811	0.800	0.071	0.093	0.354	0.352	0.300	0.421	0.534	0.51	0.496	0.58	0.588
K	0.027	0.206	0.001	0.001	0.007	0.005	0.175	0.174	0.070	0.077	0.004	0.002	0.001	0.01	0.015	0.00	0.000
Na	0.438	0.321	0.205	0.206	0.190	0.191	0.668	0.658	0.580	0.580	0.670	0.486	0.482	0.49	0.522	0.35	0.357
Total*	5.033	5.075	4.991	4.990	4.994	4.988	4.954	4.955	5.021	5.022	4.982	4.905	4.995	5.02	5.038	4.98	4.988
Atomic%																	
Ca	55.84	51.12	79.67	79.54	80.47	80.30	7.74	10.04	35.25	34.86	30.82	46.30	52.46	50.6	48.00	62.4	62.20
K	2.58	19.11	0.07	0.06	0.67	0.52	19.18	18.86	6.96	7.66	0.41	0.22	0.12	0.97	1.48	0.01	0.00
Na	41.58	29.78	20.26	20.40	18.85	19.19	73.08	71.10	57.79	57.49	68.77	53.48	47.42	48.4	50.52	37.5	37.80
Total**	100.00	100.00	100.0	100.0	100.0	100.0	100.0	100.0	100.00	100.00	100.00	100.00	100.00	100.	100.00	100.	100.0

*Feldspar assemblage with spinel inclusion
ND = not detected

Table H-9 Representative EPMA analyses of spinel inclusions in Bo Welu ruby.

Mineral phase analysis (wt%)	9TWL154-In2*				9TWL019-in2*				9TWL180-in1*			9TWL085-in2	
SiO_2	0.21	0.10	ND	0.12	0.09	0.05	ND	0.04	0.08	0.06	0.03	0.08	0.09
TiO_2	2.23	2.51	ND	ND	0.03	0.02	ND	0.43	0.02	1.09	ND	ND	ND
Al_2O_3	63.95	63.37	63.89	63.61	66.50	65.61	64.46	64.71	66.07	64.25	64.68	66.48	67.46
Cr_2O_3	1.41	1.67	1.49	1.66	0.26	0.20	0.28	0.25	0.11	0.13	0.07	0.45	0.38
Ga_2O_3	ND	ND	0.05	ND	ND	0.06	0.10	ND	ND	0.08	0.04	ND	ND
V_2O_3	0.03	ND	ND	0.01	ND	0.01	ND	ND	0.01	ND	0.03	ND	ND
FeO total	10.25	10.61	10.50	10.89	12.92	13.43	13.20	13.11	13.39	13.50	13.58	11.46	11.81
MnO	0.21	0.24	0.18	0.21	0.08	0.09	0.11	0.09	0.11	0.10	0.08	0.26	0.27
MgO	20.47	20.59	22.98	22.51	19.89	19.71	20.79	20.19	21.08	20.56	20.81	21.26	19.96
ZnO	0.01	0.04	NA	NA	NA	NA	0.03	0.09	NA	0.04	0.07	NA	NA
CaO	0.05	0.01	0.02	0.08	0.07	ND	ND	ND	0.01	0.04	ND	0.04	0.03
K_2O	ND	ND	ND	0.01	0.01	ND	0.01	ND	0.01	0.02	ND	0.02	ND
Na_2O	0.05	ND	0.01	0.01	0.02	0.01	ND	ND	ND	0.03	0.05	ND	ND
Total	98.86	99.13	99.12	99.11	99.87	99.19	98.99	98.91	100.8	99.90	99.43	100.05	99.99
4 (O)													
Si	0.005	0.002	0.000	0.003	0.002	0.001	0.000	0.001	0.002	0.002	0.001	0.002	0.002
Ti	0.043	0.048	0.000	0.000	0.001	0.000	0.000	0.008	0.000	0.021	0.000	0.000	0.000
Al	1.909	1.893	1.906	1.903	1.975	1.969	1.941	1.948	1.948	1.921	1.941	1.962	1.990
Cr	0.028	0.033	0.030	0.033	0.005	0.004	0.006	0.005	0.002	0.003	0.001	0.009	0.007
Ga	0.000	0.000	0.000	0.000	0.000	0.001	0.002	0.000	0.000	0.001	0.001	0.000	0.000
V	0.001	0.000	0.000	0.000	0.000	0.000	0.000	0.000	0.000	0.000	0.001	0.000	0.000
Fe^{3+}	0.000	0.000	0.084	0.078	0.020	0.032	0.068	0.038	0.059	0.044	0.076	0.035	0.000
Fe^{2+}	0.217	0.225	0.138	0.154	0.252	0.254	0.214	0.242	0.221	0.242	0.213	0.205	0.247
Mn	0.005	0.005	0.004	0.005	0.002	0.002	0.002	0.002	0.002	0.002	0.002	0.005	0.006
Mg	0.773	0.778	0.868	0.852	0.747	0.748	0.792	0.769	0.786	0.777	0.790	0.793	0.745
Zn	0.000	0.001	0.000	0.000	0.000	0.000	0.001	0.002	0.000	0.001	0.001	0.000	0.000
Ca	0.001	0.000	0.001	0.002	0.002	0.000	0.000	0.000	0.000	0.001	0.000	0.001	0.001
K	0.000	0.000	0.000	0.000	0.000	0.000	0.000	0.000	0.000	0.001	0.000	0.001	0.000
Na	0.002	0.000	0.000	0.000	0.001	0.001	0.000	0.000	0.000	0.001	0.002	0.000	0.000
Total*	2.984	2.986	3.032	3.029	3.007	3.012	3.026	3.014	3.022	3.017	3.029	3.013	2.999

*Feldspar assemblage with spinel inclusion
NA = not analyzed, ND = not detected

Table H-10 EPMA analyses of sillimanite, quartz and sapphirine inclusions in Bo Welu ruby.

Mineral phase	sillimanite		quartz		sapphirine	
analysis (wt%)	9TWL152-in1		9TWL095-in2		9TWL160-in1	
SiO_2	36.38	36.97	99.61	99.54	13.38	13.97
TiO_2	0.01	ND	ND	ND	ND	ND
Al_2O_3	61.62	61.06	0.05	0.02	61.62	61.06
Cr_2O_3	ND	0.01	ND	ND	0.40	0.31
Ga_2O_3	ND	0.14	0.06	0.06	0.01	0.01
V_2O_3	0.02	0.03	ND	0.01	0.01	0.03
FeO total	1.43	1.32	0.28	0.27	3.43	3.32
MnO	ND	0.03	ND	0.01	ND	0.03
MgO	0.50	0.62	ND	ND	19.50	19.62
NiO	NA	NA	NA	NA	0.13	0.41
CaO	0.15	0.14	0.01	ND	0.15	0.14
K_2O	0.01	0.11	ND	ND	0.01	0.02
Na_2O	ND	0.13	ND	0.01	0.07	ND
Total	100.13	100.56	100.01	99.92	98.73	98.91
	20 (O)		2 (O)		20 (O)	
Si	3.958	4.008	0.998	0.998	1.588	1.655
Ti	0.001	0.000	0.000	0.000	0.000	0.000
Al	7.901	7.803	0.001	0.000	8.621	8.525
Cr	0.000	0.001	0.000	0.000	0.038	0.029
Ga	0.000	0.010	0.000	0.000	0.001	0.001
V	0.002	0.003	0.000	0.000	0.001	0.003
Fe^{3+}	0.000	0.000	0.000	0.006	0.258	0.195
Fe^{2+}	0.130	0.120	0.002	-0.004	0.083	0.134
Mn	0.000	0.003	0.000	0.000	0.000	0.003
Mg	0.081	0.100	0.000	0.000	3.451	3.465
NiO	-	-	-	-	0.012	0.039
Ca	0.017	0.016	0.000	0.000	0.019	0.017
K	0.001	0.016	0.000	0.000	0.002	0.003
Na	0.000	0.026	0.000	0.000	0.016	0.000
Total*	12.091	12.105	1.001	1.001	14.091	14.069

NA = not analyzed, ND = not detected

Table H-11 EPMA analyses of garnet inclusions in Bo Welu ruby

Mineral phase analysis (wt%)	9TWL059-in1			9TWL087-in1			9TWL089-in1		9TWL092-in1			9TWL092-in2	
SiO_2	42.71	41.06	42.03	42.47	41.53	42.40	43.16	42.74	41.80	41.92	42.14	42.57	42.40
TiO_2	0.07	0.08	0.07	0.04	0.03	0.02	0.01	0.02	0.08	0.09	0.08	0.10	0.05
Al_2O_3	23.44	22.33	23.26	23.20	22.77	23.32	23.62	23.48	23.07	22.92	22.81	23.17	23.32
Cr_2O_3	0.04	0.02	0.02	ND	ND	0.10	0.11	0.08	0.02	0.06	0.10	0.05	0.11
FeO total	9.70	9.30	9.71	8.67	8.59	8.70	6.59	6.59	10.24	10.16	10.28	10.33	10.14
MnO	0.07	0.26	0.20	0.18	0.17	0.16	0.17	0.16	0.19	0.26	0.25	0.19	0.18
MgO	15.05	18.29	15.82	16.34	16.36	15.86	17.53	17.27	15.61	15.27	15.49	15.21	15.71
CaO	8.78	8.63	8.85	8.21	9.70	8.04	8.76	8.98	8.51	8.15	8.29	8.17	8.31
K_2O	ND	0.01	0.01	ND	0.01	0.01	ND	0.01	ND	ND	ND	0.02	ND
Na_2O	0.05	0.01	ND	ND	0.01	ND	0.01	0.02	0.03	ND	0.04	0.02	ND
Total	99.90	99.99	99.98	99.10	99.17	98.60	99.96	99.34	99.54	98.84	99.47	99.82	100.21
12 (O)													
Si	3.068	2.964	3.026	3.060	3.012	3.068	3.057	3.050	3.028	3.053	3.053	3.067	3.043
Ti	0.004	0.005	0.004	0.002	0.001	0.001	0.001	0.001	0.004	0.005	0.004	0.005	0.003
Al	1.984	1.899	1.974	1.970	1.946	1.989	1.972	1.975	1.969	1.967	1.947	1.967	1.973
Cr	0.002	0.001	0.001	0.000	0.000	0.006	0.006	0.005	0.001	0.003	0.006	0.003	0.006
Fe^{3+}	0.000	0.246	0.000	0.000	0.045	0.000	0.000	0.000	0.000	0.000	0.000	0.000	0.000
Fe^{2+}	0.583	0.316	0.584	0.522	0.476	0.527	0.390	0.393	0.620	0.619	0.623	0.622	0.608
Mn	0.004	0.016	0.012	0.011	0.011	0.009	0.010	0.010	0.012	0.016	0.015	0.012	0.011
Mg	1.611	1.968	1.698	1.755	1.768	1.710	1.851	1.838	1.685	1.658	1.673	1.633	1.681
Ca	0.676	0.667	0.683	0.633	0.753	0.624	0.665	0.686	0.661	0.636	0.643	0.631	0.639
K	0.000	0.001	0.001	0.000	0.001	0.001	0.000	0.001	0.000	0.000	0.000	0.002	0.000
Na	0.006	0.001	0.000	0.000	0.002	0.000	0.001	0.002	0.004	0.000	0.005	0.003	0.001
Total*	7.938	8.083	7.983	7.953	8.015	7.934	7.954	7.961	7.984	7.957	7.969	7.945	7.965
ΣR^{2+}	2.874	2.966	2.977	2.922	3.008	2.870	2.916	2.927	2.978	2.928	2.954	2.898	2.939
ΣR^{3+}	1.990	2.151	1.979	1.972	1.993	1.996	1.979	1.980	1.975	1.976	1.957	1.975	1.982
$Mg/(Mg+Fe^{2+})$	0.734	0.862	0.744	0.771	0.788	0.765	0.826	0.824	0.731	0.728	0.729	0.724	0.734
Alm% (Fe^{2+})	20.29	10.65	19.62	17.87	15.82	18.36	13.37	13.43	20.82	21.13	21.09	21.46	20.69
Pyr% (Mg)	56.05	66.33	57.04	60.08	58.78	59.58	63.48	62.79	56.58	56.61	56.64	56.35	57.20
Gro% (Ca)	23.45	19.85	22.88	21.65	24.46	21.67	22.72	23.37	22.14	21.63	21.66	21.69	21.64
Sps% (Mn)	0.14	0.54	0.40	0.38	0.37	0.31	0.34	0.34	0.40	0.55	0.51	0.41	0.37
Uv%	0.02	0.01	0.01	0.00	0.00	0.07	0.07	0.06	0.01	0.03	0.07	0.03	0.07
And%	0.00	2.57	0.00	0.00	0.57	0.00	0.00	0.00	0.00	0.00	0.00	0.00	0.00
Ca-Ti Gt	0.05	0.05	0.05	0.02	0.01	0.01	0.01	0.01	0.04	0.05	0.04	0.06	0.03

ΣR^{2+}= Fe^{2+}+Mn+Mg+Ca , ΣR^{3+}= Fe^{3+}+Ti+Al+Cr
ND = not detected

Table H-12 EPMA analyses of anhydrite with pyrrhotite inclusions in Bo Welu ruby

Mineral phase analysis (wt%)	Anhydrite			Pyrrhotite	
	9TWL096-in1			9TWL096-in2	
SO_3	55.98	54.80	55.62	53.72	54.17
SiO_2	0.01	ND	0.03	0.02	ND
TiO_2	0.02	0.01	ND	0.01	ND
Al_2O_3	ND	0.02	0.03	0.03	ND
Cr_2O_3	ND	0.03	ND	0.09	ND
FeO	0.02	ND	0.02	44.97	45.48
MnO	ND	0.02	0.06	ND	0.05
MgO	ND	0.02	0.01	0.01	ND
CaO	42.57	44.02	44.23	1.12	0.59
K_2O	ND	ND	ND	0.02	0.01
Na_2O	ND	0.01	0.02	ND	ND
Total	98.60	98.92	100.00	99.99	100.30
4 (O)					
S	0.979	0.964	0.966	1.008	1.012
Si	0.000	0.000	0.001	0.000	0.000
Ti	0.000	0.000	0.000	0.000	0.000
Al	0.000	0.001	0.001	0.001	0.000
Cr	0.000	0.000	0.000	0.002	0.000
Fe	0.000	0.000	0.000	0.940	0.947
Mn	0.000	0.000	0.001	0.000	0.001
Mg	0.000	0.001	0.000	0.001	0.000
Ca	1.062	1.105	1.097	0.030	0.016
K	0.000	0.000	0.000	0.001	0.000
Na	0.000	0.000	0.001	0.000	0.000
Total*	2.042	2.072	2.067	1.982	1.976

ND = not detected

Table H-13 EPMA analyses of nepheline inclusions in Bo Welu ruby

Mineral phase analysis (wt%)	9TWL012-in1		9TWL026-in1		9TWL153-in1		
SiO_2	47.61	45.62	43.54	43.06	47.07	45.99	46.68
TiO_2	ND	0.70	0.02	0.03	0.02	0.07	ND
Al_2O_3	30.79	29.58	35.61	35.72	33.57	34.02	32.89
Cr_2O_3	ND	0.10	ND	0.04	ND	ND	0.05
Ga_2O_3	ND	ND	0.14	0.10	0.07	ND	0.02
V2O3	ND	ND	0.02	0.02	0.06	ND	0.04
FeO	0.22	1.80	0.27	0.20	0.11	0.15	0.13
MnO	ND	0.05	ND	ND	ND	ND	0.01
MgO	0.20	0.20	ND	ND	0.02	0.05	ND
CaO	4.67	3.21	4.29	4.45	2.64	3.09	3.11
K_2O	1.32	3.64	3.33	3.37	1.58	1.84	1.89
Na_2O	15.10	14.26	12.82	11.57	14.84	14.80	15.15
Total	99.91	99.15	100.04	98.56	99.97	100.00	99.97
4 (O)							
Si	1.116	1.098	1.027	1.027	1.095	1.074	1.092
Ti	0.000	0.013	0.000	0.001	0.000	0.001	0.000
Al	0.851	0.839	0.990	1.004	0.920	0.936	0.907
Cr	0.000	0.002	0.000	0.001	0.000	0.000	0.001
Ga	0.000	0.000	0.002	0.002	0.001	0.000	0.000
V	0.000	0.000	0.000	0.000	0.001	0.000	0.001
Fe	0.004	0.036	0.005	0.004	0.002	0.003	0.002
Mn	0.000	0.001	0.000	0.000	0.000	0.000	0.000
Mg	0.007	0.007	0.000	0.000	0.001	0.002	0.000
Ca	0.117	0.083	0.108	0.114	0.066	0.077	0.078
K	0.039	0.112	0.100	0.102	0.047	0.055	0.056
Na	0.686	0.666	0.586	0.535	0.669	0.670	0.687
Total*	2.821	2.857	2.820	2.788	2.802	2.819	2.825

ND = not detected

Table H-14 EPMA analyses of pyrrhotite inclusions in Bo Welu ruby

Mineral phase analysis (wt%)	9TWL046-in1		9TWL100-in1		9TWL114-in1		9TWL143-in1	
Tl	0.23	0.39	0.18	0.15	0.40	0.17	0.21	0.07
Al	0.01	0.04	0.04	0.02	0.01	0.01	0.03	0.04
In	ND	ND	ND	ND	ND	0.01	0.01	ND
Ba	0.02	ND	0.13	ND	ND	0.09	0.12	0.14
Fe	50.65	48.83	25.39	22.50	56.86	57.19	33.80	33.51
S	27.56	27.48	22.73	24.06	27.69	27.66	23.78	24.74
As	ND	ND	ND	ND	0.01	ND	ND	0.05
Pb	ND	ND	ND	ND	ND	ND	ND	ND
Cu	0.04	0.07	40.98	3.64	0.01	ND	29.89	29.32
Ni	8.74	10.01	0.18	32.37	4.25	4.14	ND	0.79
Mo	0.61	0.47	0.48	0.37	0.56	0.47	0.45	0.43
Pt	ND	ND	ND	0.03	ND	0.09	0.01	ND
Sn	0.02	ND	0.01	0.02	ND	ND	ND	0.01
Zn	ND	0.01	ND	ND	0.05	0.04	ND	ND
Co	ND	ND	ND	ND	ND	ND	ND	ND
Total*	87.88	87.31	90.12	83.15	89.84	89.85	88.30	89.11
Formula								
Tl	0.001	0.002	0.002	0.002	0.002	0.001	0.002	0.001
Al	0.001	0.002	0.004	0.002	0.001	0.000	0.002	0.002
In	0.000	0.000	0.000	0.000	0.000	0.000	0.000	0.000
Ba	0.000	0.000	0.002	0.000	0.000	0.001	0.001	0.002
Fe	1.000	1.000	1.000	1.000	1.000	1.000	1.000	1.000
S	0.948	0.980	1.559	1.862	0.848	0.842	1.225	1.286
As	0.000	0.000	0.000	0.000	0.000	0.000	0.000	0.001
Pb	0.000	0.000	0.000	0.000	0.000	0.000	0.000	0.000
Cu	0.001	0.001	1.418	0.142	0.000	0.000	0.777	0.769
Ni	0.164	0.195	0.007	1.369	0.071	0.069	0.000	0.023
Mo	0.007	0.006	0.011	0.010	0.006	0.005	0.008	0.007
Pt	0.000	0.000	0.000	0.000	0.000	0.000	0.000	0.000
Sn	0.000	0.000	0.000	0.000	0.000	0.000	0.000	0.000
Zn	0.000	0.000	0.000	0.000	0.001	0.001	0.000	0.000
Co	0.000	0.000	0.000	0.000	0.000	0.000	0.000	0.000
Total**	2.122	2.186	4.003	4.387	1.928	1.919	3.016	3.091

Table H-15 EPMA analyses of two-phase inclusions in Bo Welu ruby.

Mineral phase analysis (wt%)	9TWLf067-in1	9TWL077-in1	9TWL131-in1	9TWL132-in1		9TWL135-in1	9TWL174-in2
SO_3	NA	0.03	0.25	0.04	ND	6.50	NA
SiO_2	43.56	46.13	61.74	59.28	60.26	45.06	55.66
TiO_2	0.54	0.79	0.23	0.07	0.03	0.02	0.83
Al_2O_3	30.43	34.96	25.52	25.63	24.70	26.46	27.96
Cr_2O_3	0.01	0.01	ND	0.04	ND	0.09	ND
Ga_2O_3	NA	0.04	0.06	ND	0.11	ND	0.05
V_2O_3	NA	0.01	0.01	0.04	0.01	0.01	ND
CaO	20.59	5.94	5.73	3.59	3.45	18.07	5.73
FeO	1.70	2.04	1.59	0.88	0.86	0.11	2.49
MnO	ND	0.01	ND	0.01	0.04	ND	0.08
MgO	2.10	3.38	1.65	1.44	1.41	0.21	2.05
K_2O	0.01	0.03	0.12	5.44	5.44	0.02	0.41
Na_2O	1.14	5.59	2.68	3.35	3.41	3.21	4.20
Total	100.08	98.95	99.57	99.80	99.72	99.76	99.45
Formula							
S	0.000	0.000	0.003	0.001	0.000	0.081	0.000
Si	0.725	0.768	1.028	0.987	1.003	0.750	0.926
Ti	0.007	0.010	0.003	0.001	0.000	0.000	0.010
Al	0.597	0.686	0.501	0.503	0.484	0.519	0.548
Cr	0.000	0.000	0.000	0.000	0.000	0.001	0.000
Ga	0.000	0.000	0.001	0.000	0.001	0.000	0.001
V	0.000	0.000	0.000	0.000	0.000	0.000	0.000
Ca	0.367	0.106	0.102	0.064	0.062	0.322	0.102
Fe	0.024	0.028	0.022	0.012	0.012	0.002	0.035
Mn	0.000	0.000	0.000	0.000	0.000	0.000	0.001
Mg	0.052	0.084	0.041	0.036	0.035	0.005	0.051
K	0.000	0.001	0.003	0.116	0.116	0.000	0.009
Na	0.037	0.180	0.086	0.108	0.110	0.104	0.136
Total*	1.809	1.863	1.790	1.820	1.823	1.784	1.819

ND = not detected

Table H-16 EPMA analyses of feldspar inclusions in Bo Welu sapphire.

Mineral phase analysis (wt%)	8TWL002-in1		8TWL018-in2	8TWL018-in3		8TWL026-in4		8TWL026-in5	8TWL031-in1	8TWL067-in1		8TWL083-in2		8TWL093-in4	
SiO_2	66.70	66.93	66.65	66.97	66.60	65.55	65.21	65.39	66.36	66.59	66.64	66.19	65.52	66.82	66.26
TiO_2	ND	0.01	ND	0.02	0.07	ND	0.01	ND	0.06	ND	ND	ND	0.03	ND	ND
Al_2O_3	21.32	21.31	20.57	21.40	21.17	21.41	23.19	21.15	21.87	20.61	21.10	20.85	20.89	20.99	20.58
Cr_2O_3	ND	ND	ND	ND	0.03	ND	0.03	ND	ND	ND	ND	ND	ND	0.02	0.03
Ga_2O_3	0.10	0.05	ND	ND	0.07	0.01	0.08	0.09	0.04	ND	ND	0.02	0.03	0.07	0.17
V2O3	0.01	0.02	ND	0.02	ND	ND	0.03	0.02	ND	0.01	0.02	ND	ND	ND	ND
FeO	0.07	0.06	0.10	0.65	0.64	0.11	0.10	0.13	0.09	0.07	0.05	0.08	0.08	0.09	0.11
MnO	0.01	0.01	ND	0.04	0.04	0.01	0.01	0.06	ND	ND	ND	ND	ND	ND	0.03
MgO	0.01	ND	ND	ND	ND	ND	0.02	ND	0.01	ND	0.03	ND	ND	ND	ND
CaO	1.58	1.60	1.50	0.73	0.72	1.60	1.50	1.75	1.78	1.46	1.62	2.50	2.49	1.80	1.83
K_2O	1.58	1.69	1.18	2.69	2.70	1.67	1.43	1.55	1.42	1.46	1.38	1.07	1.09	1.40	1.43
Na_2O	8.92	8.73	9.62	8.47	8.68	8.74	9.33	8.66	9.05	9.70	9.36	8.54	8.47	9.11	9.16
Total	100.30	100.4	99.63	101.00	100.7	99.09	100.93	98.80	100.68	99.90	100.20	99.24	98.60	100.29	99.59
8 (O)															
Si	2.922	2.927	2.939	2.925	2.923	2.908	2.847	2.911	2.898	2.934	2.923	2.926	2.917	2.928	2.929
Ti	0.000	0.000	0.000	0.001	0.002	0.000	0.000	0.000	0.002	0.000	0.000	0.000	0.001	0.000	0.000
Al	1.101	1.098	1.069	1.102	1.095	1.119	1.193	1.110	1.126	1.070	1.091	1.086	1.096	1.084	1.072
Cr	0.000	0.000	0.000	0.000	0.001	0.000	0.001	0.000	0.000	0.000	0.000	0.000	0.000	0.001	0.001
Ga	0.003	0.001	0.000	0.000	0.002	0.000	0.002	0.003	0.001	0.000	0.000	0.000	0.001	0.002	0.005
V	0.000	0.001	0.000	0.001	0.000	0.000	0.001	0.001	0.000	0.000	0.001	0.000	0.000	0.000	0.000
Fe	0.003	0.002	0.004	0.024	0.023	0.004	0.004	0.005	0.003	0.003	0.002	0.003	0.003	0.003	0.004
Mn	0.000	0.000	0.000	0.001	0.001	0.000	0.000	0.002	0.000	0.000	0.000	0.000	0.000	0.000	0.001
Mg	0.000	0.000	0.000	0.000	0.000	0.000	0.001	0.000	0.001	0.000	0.002	0.000	0.000	0.000	0.000
Ca	0.074	0.075	0.071	0.034	0.034	0.076	0.070	0.083	0.083	0.069	0.076	0.118	0.119	0.084	0.087
K	0.089	0.094	0.066	0.150	0.151	0.094	0.080	0.088	0.079	0.082	0.077	0.060	0.062	0.078	0.081
Na	0.758	0.740	0.822	0.718	0.738	0.752	0.790	0.747	0.766	0.829	0.796	0.732	0.731	0.774	0.785
Total*	4.949	4.939	4.971	4.956	4.971	4.955	4.989	4.950	4.959	4.986	4.968	4.926	4.930	4.954	4.965
Atomic%															
Ca	8.06	8.22	7.39	3.79	3.67	8.26	7.47	9.08	8.97	7.02	8.04	13.01	13.02	9.01	9.10
K	9.62	10.35	6.91	16.62	16.36	10.22	8.46	9.58	8.52	8.38	8.12	6.62	6.76	8.35	8.48
Na	82.32	81.43	85.70	79.60	79.96	81.52	84.07	81.34	82.51	84.61	83.85	80.37	80.22	82.64	82.43
Total**	100.00	100.0	100.00	100.00	100.0	100.0	100.00	100.00	100.00	100.00	100.00	100.00	100.00	100.00	100.00

ND = not detected

Table H-16 EPMA analyses of feldspar inclusions in Bo Welu sapphire (continued).

Mineral phase analysis (wt%)	8TWL093-in5	8TWL097-in2		8TWL097-in3		8TWL097-in4	8TWL097-in5		8TWL099-in1		8TWL099-in2		8TWL099-in3		8TWL102-in1
SiO_2	69.26	67.24	65.26	66.23	66.63	64.88	68.48	67.21	66.00	66.02	65.59	65.75	66.00	66.00	65.56
TiO_2	0.06	ND	0.01	ND	0.01	0.01	0.01	ND	0.02	0.02	0.03	0.06	0.02	0.02	0.03
Al_2O_3	16.47	19.70	20.80	20.88	20.95	22.62	17.95	19.55	20.91	21.49	22.14	22.64	22.65	22.65	21.36
Cr_2O_3	0.02	ND	0.07	ND	ND	0.01	0.02	0.05	ND	ND	ND	ND	ND	ND	0.01
Ga_2O_3	0.07	ND	0.14	ND	ND	ND	0.07	0.10	0.03	ND	0.05	0.11	0.05	0.05	ND
V2O3	ND	ND	ND	ND	ND	ND	ND	ND	0.03	0.03	ND	0.02	0.05	0.05	ND
FeO	0.31	0.09	0.09	0.12	0.09	0.23	0.11	0.07	0.01	0.07	0.05	0.09	0.04	0.04	0.10
MnO	ND	0.01	0.01	ND	ND	0.01	0.01	ND	ND	ND	ND	ND	0.01	0.01	ND
MgO	ND	ND	0.01	ND	ND	ND	0.01	0.01	0.01	ND	ND	ND	ND	ND	ND
CaO	0.14	2.13	1.79	1.90	1.92	1.82	2.06	1.88	0.38	1.20	1.83	1.91	1.73	1.73	1.80
K_2O	7.43	1.20	1.28	1.30	1.29	1.46	1.34	1.37	1.74	1.02	1.43	1.47	1.48	1.48	1.48
Na_2O	6.25	9.74	9.24	8.80	9.31	9.35	9.85	9.81	9.68	9.84	8.88	9.19	8.84	8.74	8.76
Total	100.00	100.1	98.72	99.23	100.2	100.40	99.90	100.05	98.81	99.68	99.99	101.2	100.88	100.7	99.11
8 (O)															
Si	3.095	2.958	2.911	2.929	2.924	2.853	3.018	2.961	2.934	2.908	2.884	2.863	2.876	2.877	2.908
Ti	0.002	0.000	0.000	0.000	0.000	0.000	0.000	0.000	0.001	0.001	0.001	0.002	0.001	0.001	0.001
Al	0.868	1.021	1.094	1.088	1.083	1.172	0.932	1.015	1.095	1.116	1.148	1.162	1.163	1.164	1.116
Cr	0.001	0.000	0.002	0.000	0.000	0.000	0.001	0.002	0.000	0.000	0.000	0.000	0.000	0.000	0.000
Ga	0.002	0.000	0.004	0.000	0.000	0.000	0.002	0.003	0.001	0.000	0.001	0.003	0.001	0.001	0.000
V	0.000	0.000	0.000	0.000	0.000	0.000	0.000	0.000	0.001	0.001	0.000	0.001	0.002	0.002	0.000
Fe	0.011	0.003	0.003	0.004	0.003	0.009	0.004	0.003	0.000	0.002	0.002	0.003	0.001	0.001	0.004
Mn	0.000	0.000	0.000	0.000	0.000	0.000	0.000	0.000	0.000	0.000	0.000	0.000	0.001	0.001	0.000
Mg	0.000	0.000	0.001	0.000	0.000	0.000	0.001	0.001	0.001	0.000	0.000	0.000	0.000	0.000	0.000
Ca	0.007	0.100	0.086	0.090	0.090	0.086	0.097	0.089	0.018	0.057	0.086	0.089	0.081	0.081	0.086
K	0.424	0.067	0.073	0.073	0.072	0.082	0.076	0.077	0.099	0.057	0.080	0.082	0.082	0.082	0.084
Na	0.542	0.831	0.799	0.755	0.792	0.797	0.841	0.838	0.834	0.840	0.757	0.776	0.747	0.739	0.753
Total*	4.951	4.981	4.974	4.940	4.966	5.000	4.973	4.987	4.984	4.982	4.959	4.981	4.955	4.949	4.952
Atomic%															
Ca	0.69	10.04	8.93	9.80	9.46	8.87	9.61	8.84	1.88	5.93	9.32	9.40	8.89	8.97	9.28
K	43.58	6.73	7.61	7.96	7.57	8.51	7.45	7.68	10.40	6.02	8.70	8.62	9.03	9.12	9.09
Na	55.72	83.24	83.46	82.23	82.97	82.62	82.94	83.48	87.72	88.05	81.98	81.97	82.08	81.91	81.63
Total**	100.00	100.0	100.0	100.00	100.0	100.00	100.00	100.00	100.0	100.0	100.00	100.0	100.00	100.0	100.00

ND = not detected

Table H-16 EPMA analyses of feldspar inclusions in Bo Welu sapphire.

Mineral phase analysis (wt%)	8TWL102-in2		8TWL105-in1		8TWL116-in1		8TWL117 -in2	8TWL119 -in1	8TWL114 -in25
SiO_2	66.50	66.40	66.92	66.12	66.88	66.18	66.92	66.34	66.47
TiO_2	ND	0.01	ND	0.03	0.04	ND	0.02	0.01	0.01
Al_2O_3	21.57	20.37	21.30	20.74	20.11	20.47	20.61	21.57	20.92
Cr_2O_3	0.01	ND	0.04	0.05	0.04	ND	ND	ND	ND
Ga_2O_3	0.05	0.07	0.07	0.06	0.02	0.06	0.13	0.01	0.09
V2O3	ND	ND	0.03	ND	0.01	ND	ND	ND	ND
FeO	0.03	0.05	0.11	0.04	0.05	0.04	0.09	0.05	0.59
MnO	0.02	ND	ND	ND	ND	ND	ND	0.03	0.04
MgO	0.01	ND	ND	ND	ND	ND	ND	ND	0.02
CaO	1.85	1.89	1.71	1.75	1.83	1.78	1.37	1.07	0.02
K_2O	1.67	1.67	1.67	1.67	1.27	1.28	1.30	1.14	1.40
Na_2O	8.82	8.82	8.89	8.80	9.14	9.06	9.25	9.34	9.45
Total	100.53	99.28	100.74	99.26	99.39	98.88	99.69	99.55	99.00
8 (O)									
Si	2.910	2.942	2.921	2.929	2.954	2.939	2.945	2.919	2.944
Ti	0.000	0.000	0.000	0.001	0.001	0.000	0.001	0.000	0.000
Al	1.112	1.063	1.096	1.083	1.047	1.071	1.069	1.119	1.092
Cr	0.000	0.000	0.001	0.002	0.001	0.000	0.000	0.000	0.000
Ga	0.001	0.002	0.002	0.002	0.001	0.002	0.004	0.000	0.003
V	0.000	0.000	0.001	0.000	0.000	0.000	0.000	0.000	0.000
Fe	0.001	0.002	0.004	0.002	0.002	0.002	0.003	0.002	0.022
Mn	0.001	0.000	0.000	0.000	0.000	0.000	0.000	0.001	0.001
Mg	0.001	0.000	0.000	0.000	0.000	0.000	0.000	0.000	0.001
Ca	0.087	0.090	0.080	0.083	0.086	0.085	0.064	0.050	0.001
K	0.093	0.095	0.093	0.095	0.071	0.073	0.073	0.064	0.079
Na	0.748	0.757	0.752	0.756	0.783	0.780	0.789	0.796	0.811
Total*	4.954	4.951	4.951	4.952	4.947	4.951	4.949	4.952	4.954
Atomic%									
Ca	9.35	9.54	8.65	8.90	9.18	9.05	6.94	5.52	0.10
K	10.03	10.04	10.06	10.13	7.59	7.75	7.90	7.05	8.89
Na	80.62	80.42	81.29	80.97	83.23	83.20	85.16	87.43	91.01
Total**	100.00	100.00	100.00	100.00	100.00	100.00	100.00	100.00	100.00

ND = not detected

Table H-17 EPMA analyses of columbite inclusions in Bo Welu sapphire.

Mineral phase analysis (wt%)	8TWL001-in1	8TWL001-in2	8TWL001-in3	8TWL120-in1	8TWL022-in1	8TWL106-in1	8TWL036-in2	8TWL097-in7	8TWL097-in8
Nb_2O_5	74.32	75.23	76.53	75.36	72.63	75.01	74.39	74.57	72.44
Ta_2O_5	0.46	0.54	0.57	0.42	0.54	0.30	0.31	0.16	0.21
ThO_2	ND	0.21	ND	0.03	ND	ND	0.87	0.11	0.30
TiO_2	1.11	1.31	0.93	0.85	1.54	1.13	0.37	0.40	0.40
UO_2	0.02	0.05	0.05	ND	ND	0.01	3.45	2.10	2.59
ZrO_2	0.57	0.54	0.28	0.04	0.94	0.62	0.57	0.83	0.81
Al_2O_3	0.08	0.08	0.03	ND	0.13	0.15	0.15	0.14	0.14
Ce_2O_3	ND	0.10	0.08	ND	ND	0.13	1.27	1.85	1.59
Nd_2O_3	0.02	ND	0.03	0.01	ND	0.07	1.46	1.93	1.80
Sm_2O_3	ND	ND	ND	0.01	0.02	ND	0.76	0.77	0.70
Y_2O_3	ND	ND	ND	ND	ND	ND	3.19	3.46	3.33
FeO	12.52	12.84	11.99	12.60	14.26	11.37	10.37	10.45	10.38
MnO	5.95	6.01	6.51	6.53	3.61	7.37	1.48	1.24	1.31
MgO	0.73	0.62	0.49	0.41	1.00	0.36	0.09	0.16	0.12
CaO	0.05	0.13	0.10	0.08	0.05	0.10	0.47	0.81	0.70
Na_2O	ND	ND	ND	ND	ND	ND	ND	ND	ND
Total	95.84	97.65	97.59	96.33	94.72	96.63	99.18	98.97	96.80
6 (O)									
Nb	1.950	1.942	1.976	1.974	1.923	1.955	1.967	1.961	1.955
Ta	0.007	0.008	0.009	0.007	0.009	0.005	0.005	0.003	0.003
Th	0.000	0.003	0.000	0.000	0.000	0.000	0.012	0.001	0.004
Ti	0.049	0.056	0.040	0.037	0.068	0.049	0.016	0.018	0.018
U	0.000	0.001	0.001	0.000	0.000	0.000	0.045	0.027	0.034
Zr	0.016	0.015	0.008	0.001	0.027	0.017	0.016	0.023	0.023
Al	0.005	0.005	0.002	0.000	0.009	0.010	0.010	0.010	0.010
Ce	0.000	0.002	0.002	0.000	0.000	0.003	0.027	0.039	0.035
Nd	0.000	0.000	0.001	0.000	0.000	0.001	0.030	0.040	0.038
Sm	0.000	0.000	0.000	0.000	0.000	0.000	0.015	0.015	0.014
Y	0.000	0.000	0.000	0.000	0.000	0.000	0.099	0.107	0.106
Fe	0.608	0.613	0.573	0.610	0.698	0.548	0.507	0.508	0.518
Mn	0.293	0.291	0.315	0.321	0.179	0.360	0.073	0.061	0.066
Mg	0.063	0.053	0.042	0.035	0.087	0.031	0.008	0.014	0.011
Ca	0.003	0.008	0.006	0.005	0.003	0.006	0.030	0.051	0.045
Na	0.000	0.000	0.000	0.000	0.000	0.000	0.000	0.000	0.000
Total*	2.996	2.996	2.973	2.991	3.003	2.986	2.861	2.879	2.881

ND = not detected

Table H-17 Representative EPMA analyses of columbite inclusions in Bo Welu sapphire (continued).

Mineral phase analysis (wt%)	8TWL108-in3	8TWL096-in2	8TWL064-in1	8TWL120-in2	8TWL036-in1	8TWL028-in2	8TWL108-in1	8TWL108-in2-	8TWL100-in1
Nb_2O_5	74.95	76.74	74.37	73.48	75.86	78.10	76.99	77.66	76.40
Ta_2O_5	0.51	0.34	0.25	0.31	0.88	1.10	1.03	0.58	0.79
ThO_2	0.71	0.16	0.85	0.04	1.02	0.54	0.59	0.44	0.57
TiO_2	0.47	0.30	0.43	0.35	3.10	2.92	2.56	2.34	2.86
UO_2	0.81	0.82	3.50	3.58	0.62	0.73	0.57	0.70	0.48
ZrO_2	1.10	1.33	0.78	0.93	ND	0.10	0.08	ND	0.11
Al_2O_3	0.22	0.12	0.29	0.13	0.69	0.58	0.75	0.70	0.53
Ce_2O_3	0.66	0.89	1.36	0.73	0.97	0.72	0.80	0.82	0.79
Nd_2O_3	0.98	1.28	1.42	1.25	0.28	0.25	0.12	0.13	0.23
Sm_2O_3	0.60	0.60	0.72	0.61	0.03	0.01	0.05	ND	ND
Y_2O_3	3.96	3.60	2.76	3.77	ND	ND	ND	ND	ND
FeO	9.71	9.95	9.79	10.23	1.25	1.22	1.25	1.24	1.40
MnO	1.45	1.56	1.58	1.15	0.15	0.11	0.18	0.11	0.23
MgO	0.18	0.20	0.08	0.15	ND	ND	ND	0.01	ND
CaO	0.67	0.42	0.42	0.52	5.20	5.46	5.37	5.21	5.19
Na_2O	ND	ND	ND	ND	7.07	7.50	6.99	7.15	ND
Total	96.97	98.30	98.61	97.23	97.12	99.32	97.34	97.09	89.59
6 (O)									
Nb	1.981	2.000	1.973	1.969	1.919	1.928	1.938	1.957	2.068
Ta	0.008	0.005	0.004	0.005	0.013	0.016	0.016	0.009	0.013
Th	0.009	0.002	0.011	0.001	0.013	0.007	0.007	0.006	0.008
Ti	0.021	0.013	0.019	0.016	0.130	0.120	0.107	0.098	0.129
U	0.010	0.010	0.046	0.047	0.008	0.009	0.007	0.009	0.006
Zr	0.031	0.037	0.022	0.027	0.000	0.003	0.002	0.000	0.003
Al	0.015	0.008	0.020	0.009	0.045	0.037	0.049	0.046	0.038
Ce	0.014	0.019	0.029	0.016	0.020	0.014	0.016	0.017	0.017
Nd	0.021	0.026	0.030	0.026	0.005	0.005	0.002	0.003	0.005
Sm	0.012	0.012	0.015	0.012	0.001	0.000	0.001	0.000	0.000
Y	0.123	0.110	0.086	0.119	0.000	0.000	0.000	0.000	0.000
Fe	0.475	0.480	0.481	0.507	0.059	0.056	0.058	0.058	0.070
Mn	0.072	0.076	0.079	0.058	0.007	0.005	0.008	0.005	0.012
Mg	0.016	0.017	0.007	0.013	0.000	0.000	0.000	0.001	0.000
Ca	0.042	0.026	0.026	0.033	0.312	0.320	0.321	0.311	0.333
Na	0.000	0.000	0.000	0.000	0.767	0.794	0.754	0.772	0.000
Total*	2.851	2.842	2.847	2.858	3.298	3.314	3.288	3.291	2.702

ND = not detected

Table H-18 EPMA analyses of pyrrhotite inclusions in Bo Welu sapphire.

Mineral phase analysis (wt%)	8TWL046-in1	
Tl	ND	ND
Al	3.98	3.84
In	ND	0.01
Fe	58.30	58.26
S	36.22	37.22
As	0.01	ND
Pb	0.13	0.25
Cu	ND	0.03
Ni	0.01	ND
Mo	ND	ND
Pt	0.05	0.01
Sn	ND	ND
Co	ND	ND
Total*	98.71	99.63
Formula		
Tl	0.00	0.00
Al	0.14	0.14
In	0.00	0.00
Fe	1.00	1.00
S	1.08	1.11
As	0.00	0.00
Pb	0.00	0.00
Cu	0.00	0.00
Ni	0.00	0.00
Mo	0.00	0.00
Pt	0.00	0.00
Sn	0.00	0.00
Co	0.00	0.00
Total**	2.22	2.25

ND = not detected

Table H-19 Representative EPMA analyses of monazite inclusions in Bo Welu sapphire.

Mineral phase analysis (wt%)	B		gB						
	8TWL068-in2	8TWL114-in24*	8TWL036-in3	8TWL036-in4	8TWL036-in5	8TWL036-in7	8TWL082-in7	8TWL104-in3	8TWL119-in2
P_2O_5	17.69	18.14	16.13	15.81	21.09	21.62	18.72	16.49	16.36
Ta_2O_5	NA	0.41	NA	NA	0.20	0.51	0.15	NA	NA
HfO_2	NA	0.28	NA	NA	ND	0.13	ND	NA	NA
SiO_2	4.28	4.80	4.86	3.71	4.53	4.59	5.31	4.77	3.05
ThO_2	39.59	38.14	44.42	46.46	36.30	35.15	45.12	37.82	46.08
UO_2	0.94	0.05	1.06	0.95	ND	ND	ND	0.86	1.08
ZrO_2	NA	ND	NA	NA	0.12	0.02	ND	NA	NA
Al_2O_3	0.04	ND	0.08	0.07	ND	ND	ND	0.04	0.07
Ce_2O_3	21.31	24.30	21.24	19.28	23.26	24.32	15.38	21.26	17.42
Dy_2O_3	0.52	0.07	0.65	0.60	0.14	0.06	0.22	0.72	0.59
Gd_2O_3	1.18	0.71	1.02	1.14	0.84	0.57	0.92	1.70	1.75
La_2O_3	1.23	ND	0.69	1.04	ND	ND	ND	1.68	1.63
Nd_2O_3	5.40	6.41	3.81	5.33	7.81	6.94	7.33	6.42	5.70
Pr_2O_3	4.10	4.80	4.56	3.04	3.63	4.50	2.80	3.37	3.71
Sm_2O_3	1.16	0.12	0.89	0.80	0.09	0.24	0.20	1.24	1.03
Y_2O_3	0.21	0.48	0.24	0.08	0.22	0.22	0.99	0.76	0.44
FeO	0.05	ND	0.08	0.09	ND	0.20	0.07	0.02	0.04
CaO	0.75	1.70	0.30	0.24	1.14	0.24	2.19	1.64	1.29
Total	98.45	100.39	100.03	98.64	99.36	99.28	99.38	98.79	100.24
4 (O)									
P	0.709	0.699	0.657	0.669	0.782	0.795	0.715	0.662	0.680
Ta	-	0.005	-	-	0.002	0.006	0.002	-	-
Hf	-	0.004	-	-	0.000	0.002	0.000	-	-
Si	0.203	0.219	0.234	0.186	0.198	0.199	0.240	0.226	0.150
Th	0.426	0.395	0.486	0.529	0.362	0.347	0.463	0.408	0.515
U	0.010	0.000	0.011	0.011	0.000	0.000	0.000	0.009	0.012
Zr	-	0.000	-	-	0.003	0.000	0.000	-	-
Al	0.002	0.000	0.005	0.004	0.000	0.000	0.000	0.002	0.004
Ce	0.369	0.405	0.374	0.353	0.373	0.387	0.254	0.369	0.313
Dy	0.008	0.001	0.010	0.010	0.002	0.001	0.003	0.011	0.009
Gd	0.018	0.011	0.016	0.019	0.012	0.008	0.014	0.027	0.028
La	0.021	0.000	0.012	0.019	0.000	0.000	0.000	0.029	0.029
Nd	0.091	0.104	0.065	0.095	0.122	0.108	0.118	0.109	0.100
Pr	0.071	0.080	0.080	0.055	0.058	0.071	0.046	0.058	0.066
Sm	0.019	0.002	0.015	0.014	0.001	0.004	0.003	0.020	0.017
Y	0.005	0.012	0.006	0.002	0.005	0.005	0.024	0.019	0.011
Fe	0.002	0.000	0.003	0.004	0.000	0.007	0.003	0.001	0.002
Ca	0.038	0.083	0.015	0.013	0.054	0.011	0.106	0.083	0.068
Total**	1.992	2.019	1.989	1.983	1.973	1.952	1.990	2.033	2.004

NA = not analyzed, ND = not detected

Table H-20 Representative EPMA analyses of zircon inclusions in Bo Welu sapphire.

Mineral phase analysis (wt%)	8TWL 035-in1	8TWL 040-in2	8TWL 059-in1	8TWL 059-in2	8TWL 059-in3	8TWL 059-in4	8TWL 059-in5	8TWL 059-in6	8TWL 059-in7	8TWL 059-in8	8TWL 059-in10	8TWL 059-in12	8TWL 101-in1
P_2O_5	0.12	ND	ND	0.48	0.49	0.41	0.09	0.57	0.44	ND	0.20	0.40	ND
HfO_2	2.12	2.09	2.72	2.62	2.64	2.77	2.63	2.80	2.80	2.53	2.06	2.58	2.23
SiO_2	33.56	34.78	34.26	33.63	32.95	33.51	32.99	33.86	33.32	33.17	32.88	32.09	33.15
ThO_2	1.19	0.07	0.06	1.21	0.59	0.37	0.08	0.47	0.62	ND	0.01	0.50	0.01
UO_2	0.70	0.24	0.30	1.13	0.76	0.62	0.53	0.75	0.91	0.23	0.28	0.66	0.07
ZrO_2	61.81	61.13	62.18	59.39	60.24	59.95	61.32	60.66	60.17	62.81	61.55	61.96	62.54
Al_2O_3	0.02	0.07	ND	0.01	0.11	0.02	ND	ND	ND	ND	0.02	ND	0.09
Dy_2O_3	0.06	ND	ND	0.09	0.08	0.07	ND	0.12	0.14	0.02	0.01	0.09	ND
Er_2O_3	0.11	0.04	ND	0.15	0.20	0.18	0.03	0.18	0.08	0.02	0.01	0.01	ND
Lu_2O_3	0.18	0.10	ND	ND	0.10	0.15	0.06	0.06	0.27	0.07	0.11	0.08	ND
Nd_2O_3	ND	0.02	ND	ND	0.02	0.06	0.07	ND	ND	ND	0.03	ND	0.01
Pr_2O_3	ND	ND	ND	ND	0.09	ND	1.17	0.97	0.29	ND	0.91	0.46	0.26
Y_2O_3	0.37	0.17	0.05	0.85	0.80	0.74	0.11	0.81	0.74	0.04	0.16	0.82	0.06
FeO	0.02	0.08	0.05	0.07	0.09	0.08	0.06	0.08	0.10	0.04	0.05	0.07	0.11
PbO	0.15	ND	ND	0.79	ND	ND	ND	0.04	ND	ND	ND	ND	ND
Total	100.41	98.79	99.62	100.42	99.16	98.93	99.14	101.37	99.88	98.93	98.28	99.72	98.53
4 (O)													
P	0.003	0.000	0.000	0.013	0.013	0.011	0.002	0.015	0.011	0.000	0.005	0.011	0.000
Hf	0.019	0.018	0.024	0.023	0.023	0.024	0.023	0.024	0.025	0.022	0.018	0.023	0.020
Si	1.030	1.062	1.046	1.035	1.021	1.036	1.026	1.027	1.027	1.026	1.024	0.997	1.027
Th	0.008	0.000	0.000	0.008	0.004	0.003	0.001	0.003	0.004	0.000	0.000	0.004	0.000
U	0.005	0.002	0.002	0.008	0.005	0.004	0.004	0.005	0.006	0.002	0.002	0.005	0.000
Zr	0.925	0.910	0.926	0.891	0.910	0.903	0.930	0.897	0.904	0.948	0.935	0.939	0.945
Al	0.001	0.003	0.000	0.000	0.004	0.001	0.000	0.000	0.000	0.000	0.001	0.000	0.003
Dy	0.001	0.000	0.000	0.001	0.001	0.001	0.000	0.001	0.001	0.000	0.000	0.001	0.000
Er	0.001	0.000	0.000	0.001	0.002	0.002	0.000	0.002	0.001	0.000	0.000	0.000	0.000
Lu	0.002	0.001	0.000	0.000	0.001	0.001	0.001	0.001	0.002	0.001	0.001	0.001	0.000
Nd	0.000	0.000	0.000	0.000	0.000	0.001	0.001	0.000	0.000	0.000	0.000	0.000	0.000
Pr	0.000	0.000	0.000	0.000	0.001	0.000	0.013	0.011	0.003	0.000	0.010	0.005	0.003
Y	0.006	0.003	0.001	0.014	0.013	0.012	0.002	0.013	0.012	0.001	0.003	0.014	0.001
Fe	0.001	0.002	0.001	0.002	0.002	0.002	0.002	0.002	0.003	0.001	0.001	0.002	0.003
Pb	0.001	0.000	0.000	0.007	0.000	0.000	0.000	0.000	0.000	0.000	0.000	0.000	0.000
Total**	2.003	2.001	2.000	2.003	2.000	2.001	2.005	2.001	1.999	2.001	2.000	2.002	2.002
Atomic%													
Hf	0.94	0.92	1.19	1.18	1.20	1.24	1.18	1.25	1.26	1.12	0.93	1.17	0.99
Si	52.19	53.36	52.42	53.10	52.24	52.74	51.84	52.71	52.51	51.41	51.79	50.90	51.57
Zr	46.87	45.73	46.39	45.72	46.57	46.01	46.98	46.04	46.23	47.47	47.28	47.93	47.44
Total**	100.00	100.00	100.00	100.00	100.00	100.00	100.00	100.00	100.00	100.00	100.00	100.00	100.00

ND = not detected

VITA

NAME	Supparat Promwongnan
DATE OF BIRTH	20 Jan 1981
PLACE OF BIRTH	Phuket
HOME ADDRESS	78/156 Moo 6 Phetkasem 106 Nongkheam Bangkok 10160